CHARLES UNIVERSITY IN PRAGUE

Faculty of Science

Developmental and Cell Biology

Functional analysis of the piRNA pathway in golden hamsters

Ph.D. Dissertation

Zuzana Loubalová

Supervisor: Petr Svoboda, Ph.D.

Laboratory of Epigenetic Regulations,

Institute of Molecular Genetics of the Czech Academy of Sciences,

Prague, 2022

Declaration

I declare that I wrote the thesis independently and that I cited all the information sources and literature. This work will not be presented to obtain another academic degree or equivalent.

Prague, 2022 Zuzana Loubalová

"They didn't know it was impossible so they did it." Mark Twain

Acknowledgments

I would first like to thank Petr for being an exceptional mentor. I am very grateful for having the opportunity to be a PhD student in your lab and for all the time you have invested in me to grow as a scientist. Thank you for challenging me to see things from a different perspective. I am also thankful for your inspiring enthusiasm and especially for making the lab such a fun place to work!

Radek, thank you for being always there and for inspiring me to get things done. Thank you for your patience, daily interest and insightful feedback. I will always look for more control samples in everything I will do in life. Most of all, thank you for being ready to help me at any time. I will miss our lunchtimes.

I would like to thank all the members of Lab 28 for all the support and discussions. It was a pleasure to work with such talented and nice people. Thank you also for all the moments full of fun, coffee, laughter and crazy parties. Guys, you made my PhD time unforgettable. Thank you for being my second family.

My friends in Prague, thank you for all the nice moments full of fun. Special thanks go to Shubha, Diego and Pepa for being great friends who I could always count on.

Kamarádi moji, Valašsku věrni, díky že tu pro mňa dycky jste, hlavně když mňa neco dožere.

Větříku, tobě krom jiného, děkuji za tvůj pohodový pohled na svět, který mě toho hodně naučil a naplnil můj život smíchem.

Velké poděkování patří mé rodině. Mami, tati, děkuji Vám za veškerou podporu ve všem, co dělám, ač kolikrát nevíte, proč to vlastně dělám. Nejvíc však děkuji za to, že tu pro mě jste, když je potřeba. Mami, tobě patří speciální dík za každodenní telefonáty zakončené větou: „A čo škrečky?“, bez kterých si svá rána už ani neumím představit. Luci, díky za tu věčnou argumentaci vedenou nad sebemenšími maličkostmi, která mi přináší nový pohled na svět. Díky za tvůj humor, který mi pomáhá v nejtežších chvílích a hlavně za to, že mi vždycky kryješ záda, ségra.

Table of Contents

List of Abbreviations

1U-bias	Uracil at the first position
A	Adenine
AGO	Argonaute
DGCR8	DiGeorge syndrome critical region 8
Dpp	Days *post-partum*
dsDNA	Double-stranded DNA
dsRNA	Double-stranded RNA
E	Embryonic day
FACS	Fluorescence-activated cell sorting
FLI	Full-length intact
GV	Germinal vesicle
hCG	Human chorionic gonadotropin
KO	Knock-out
LINE1	Long interspersed nuclear element 1
LTR	Long terminal repeat
MaLR	Mammalian apparent LTR Retrotransposons
MII	Metaphase stage of second meiotic division
miRNA	Micro RNA
mRNA	Messenger RNA
MTC	Mouse Transcript type C
MuERVL	Mouse Endogenous Retrovirus type-L
MuLV	Mouse Leukemia Virus
NGS	Next-generation sequencing

Nt	Nucleotide
ORF	Open reading frame
PAZ	Piwi-Argonaute-Zwille
PEG	Polyethylene glycol
PGCs	Primordial germ cells
piRNA	PIWI-interacting RNA
PMSG	Pregnant mare´s serum gonadotropin
Pol II	RNA Polymerase II
RISC	RNA-induced silencing complex
RNA	Ribonucleic acid
RNAi	RNA interference
RNA-seq	RNA sequencing
RPM	Reads per million
RPKM	Reads per kilobase per million
RT-PCR	Reverse transcription polymerase chain reaction
SINE	Short interspersed nuclear elements
siRNA	Small-interfering RNA
TE	Transposable element
U	Uracil
UTR	Untranslated region
WT	Wild type
ZGA	Zygotic genome activation

Abstract

The piRNA pathway is a highly conserved mechanism that regulates gene and retrotransposon expression at transcriptional and post-transcriptional levels. Defects in the piRNA pathway impair germ cell development in animals from invertebrates to mammals. In mammals, the current knowledge of the piRNA pathway has been mainly built from mouse model studies. The mouse model suggests that the piRNA pathway is dispensable for mammalian female germline. However, mouse differs from other mammals in several important aspects. It lacks PIWIL3, one of four PIWI proteins found in other mammals, and has a highly active RNA interference in mouse oocytes, which points towards a unique combination of small RNA pathways in the mouse female germline. These specific modifications of small RNA pathways in mice could obscure the biological significance of the mammalian piRNA pathway.

My Ph.D. project aimed at investigating the importance of the piRNA pathway in mammals and analyzing conserved and derived aspects of this pathway. As golden hamsters encode all mammalian PIWI proteins and likely lack highly active RNA interference in oocytes, they represent mammalian small RNA pathways closer than mice. Therefore, we generated a golden hamster knock-out of MOV10L1 helicase, an essential factor in piRNA biogenesis. We observed sterility in both sexes of *Mov10l1* golden hamster mutants, arguing that female fertility of piRNA pathway mutants is not a common mammalian feature. We showed that *Mov10l1*$^{-/-}$ golden hamster oocytes can be fertilized and undergo meiosis, but do not support development beyond the 2-cell stage. Male hamster *Mov10l1* mutants are sterile due to germ cell loss during spermatogonia formation. In both cases, sterility is associated with disturbed transcriptome and retrotransposon derepression. In males, sterility appears to be related to derepression of MYSERV, a young family of retrotransposons, and full-length intact IAP and LINE1 elements capable of retrotransposition. Furthermore, we show an adaptive nature of the piRNA pathway that appears to respond rapidly to emerging genomic threats in different stages of development.

Overall, my thesis demonstrates that the piRNA pathway is essential for both, male and female germlines in mammals. It therefore refutes a long-held assumption that piRNAs are only necessary for mammalian male germline, as originally proposed by the mouse model. Equally important, the emergence of MYSERV element, whose expression appears to be hamster-specific, was recognized and independent evolution of ancestral retrotransposons was described.

Abstrakt

piRNA dráha je vysoce konzervovaný mechanismus, který reguluje expresi genů a retrotranspozonů na transkripční a post-transkripční úrovni. Defekty v piRNA dráze narušují normální vývoj zárodečných buněk u zvířat od bezobratlých po savce. Současná znalost piRNA dráhy u savců je založena na studiích myšího modelu. Ten navrhuje, že piRNA dráha je postradatelná pro savčí samičí zárodečnou linii. Myš se však od ostatních savců liší v několika důležitých aspektech. Myši nemají PIWIL3, jeden ze čtyř PIWI proteinů nalezených u jiných savců, a mají vysoce aktivní RNA interferenci ve svých oocytech, což poukazuje na jedinečnou kombinaci drah malých RNA v samičí zárodečné linii myší. Tyto specifické modifikace drah malých RNA u myší mohou zakrývat biologický význam piRNA dráhy u savců.

Můj PhD projekt je zaměřený na zkoumání významu piRNA dráhy u savců a analýzu konzervovaných a odvozených aspektů této dráhy. Jelikož křeček zlatý kóduje všechny savčí PIWI proteiny a pravděpodobně postrádá vysoce aktivní RNA interferenci v oocytech, jsou jeho dráhy malých RNA podobnější jiným savcům než ta myší. Proto jsme u křečka zlatého vytvořili knock-out helikázy MOV10L1, což je základní faktor piRNA biogeneze. Obě pohlaví *Mov10l1* mutantů křečka zlatého vykazovala sterilitu, což naznačuje, že samičí fertilita mutantů piRNA dráhy není běžným znakem savců. Ukázali jsme, že *Mov10l1*$^{-/-}$ oocyty křečka zlatého mohou být oplodněny a dokončit meiózu, ale nepodporují vývoj dále než do 2-buněčného stádia. Samčí *Mov10l1* mutanti křečků jsou sterilní kvůli ztrátě zárodečných buněk během tvorby spermatogonií. V obou případech je sterilita spojena s narušeným transkriptomem a derepresí retrotranspozonů. V případě samců se zdá, že sterilita souvisí s derepresí MYSERV, mladé rodiny retrotranspozonů, a kompletních neporušených IAP a LINE1 elementů schopných retrotranspozice. Navíc zde ukazujeme adaptivní povahu piRNA dráhy, která, jak se zdá, rychle reaguje na vznikající genomové hrozby v různých stádiích vývoje.

Dohromady vzato má práce ukazuje, že piRNA dráha je u savců nezbytná pro zárodečné linie samců i samic. Vyvrací proto dlouho zažitý předpoklad, že piRNA jsou nezbytné pouze pro samčí zárodečnou linii u savců, jak původně navrhoval myší model. Neméně důležité je také rozpoznání MYSERV elementu, jehož exprese se zdá být specifická pro křečky, a popsání nezávislé evoluce ancestrálních retrotranspozonů.

1 Introduction

Small ribonucleic acid (RNA) silencing pathways are important post-transcriptional control mechanisms that use small non-coding RNAs as regulatory factors. Three small RNA silencing pathways have been described in mammals: RNA interference (RNAi), microRNA (miRNA), and PIWI-interacting small RNA (piRNA) pathway. This work focuses mainly on the piRNA pathway, whose regulatory function is important for normal germ cell development. Small RNA pathways have been extensively studied in mice, and therefore the introduction focuses on the known background of small RNA pathways and their biological significance as was characterized predominantly in mice (reviewed in (Burgos, Hurtado et al. 2021)). This work uses the golden hamster as a model system to analyze the significance of the piRNA pathway in mammals. Given differences in germ cell small RNA pathways between mice and other mammals, the golden hamster surpasses the mouse model in specific aspects of biology of small RNAs in terms of similarity with other mammals. In order to understand the concept of this work in more detail, I will outline a general view of the biology of small RNA pathways and their link to gametogenesis. I will first discuss similarities and differences between individual small RNA silencing pathways in mammals, followed by a detailed description of the piRNA pathway. In the following section, I will explore the biology of retrotransposons, whose activity is regulated by the piRNA pathway and I will conclude the introductory part with a description of gametogenesis and biological role of the piRNA pathway in animal germline.

1.1 Small RNAs in RNA silencing in mammals

Small RNA silencing pathways have evolved to mediate gene regulation and provide defense against parasitic elements such as viruses or transposable elements (TEs). They are essential to many biological and evolutionary processes (reviewed in (Zhang 2009)). In mice, the most frequently used mammalian model organism, the place of action differs for individual small RNA pathways. miRNAs are ubiquitously expressed, while the pathway lost its function in oocytes and during the oocyte-to-embryo transition, apparently due to the reduced concentration of miRNAs in progressively growing oocytes (Ma, Flemr et al. 2010, Suh, Baehner et al. 2010, Kataruka, Modrak et al. 2020). In contrast, the RNAi pathway has been described as the only essential small RNA pathway in mouse oocytes and its function appears to be insignificant elsewhere (Murchison, Stein et al. 2007, Watanabe, Totoki et al. 2008, Nejepinska, Malik et al. 2012, Flemr, Malik et al. 2013). piRNA expression is typical for germ

cells and the pathway is critical for murine spermatogenesis, where it ensures normal germ cell development, but interestingly, its function appears to be insignificant in mouse oocytes (Deng and Lin 2002, Kuramochi-Miyagawa, Kimura et al. 2004, Carmell, Girard et al. 2007, Frost, Hamra et al. 2010, Zheng, Xiol et al. 2010, Cheng, Kang et al. 2014).

Although small RNA pathways differ in many respects, they all use the same concept. When a small regulatory RNA is formed, it is loaded on a protein from the Argonaute family and, through sequence complementarity, mediates repressive effects on the target (Hock and Meister 2008, Ender and Meister 2010). The miRNA and RNAi pathways utilize Dicer, an RNaseIII endonuclease, to produce small RNA molecules from RNA precursors (Bernstein, Caudy et al. 2001). Dicer, along with Argonaute and other associated proteins, is a part of the multiprotein RNA-induced silencing complex (RISC), which exerts post-transcriptional control (Gregory, Chendrimada et al. 2005). The miRNA and RNAi pathways share components downstream of the Dicer cleavage and differ in their mechanism upstream of the Dicer cleavage. In contrast, the piRNA pathway is Dicer-independent and uses a discrete subfamily of Argonaute proteins, called PIWI (Aravin, Gaidatzis et al. 2006, Girard, Sachidanandam et al. 2006, Grivna, Beyret et al. 2006).

1.1.1 Argonaute proteins

The Argonaute proteins belong to a well-conserved family of proteins that play a key role in RNA silencing in eukaryotes and can be divided into subfamilies, including AGO and PIWI (reviewed in (Meister 2013, Muller, Fazi et al. 2019)). They are structurally similar and contain four domains: the N-terminal domain, which helps with loading and unwinding of small RNA molecules (Kwak and Tomari 2012), the MID domain which binds to the 5′ end of the small RNA molecule (Boland, Tritschler et al. 2010), the Piwi-Argonaute-Zwille (PAZ) domain which allows binding of the 3' end of the small RNA molecule (Ma, Ye et al. 2004) and the P-element induced wimpy tested (PIWI) domain which provides slicer activity in Argonautes, which cleave the target directly (Song, Smith et al. 2004).

Four Argonaute proteins (AGO1-4) interacting with small RNAs generated by miRNA or RNAi pathways can be found in mammals. Out of the four Argonaute proteins, only AGO2 is endonucleotically active (Liu, Carmell et al. 2004, Meister, Landthaler et al. 2004). The AGO2 protein harbors a catalytic tetrad (DEDH) in the PIWI domain that is necessary for the slicing activity and allows Argonaute proteins to cleave the target (Nakanishi, Weinberg et al. 2012). Unlike AGO1 and AGO4, AGO3 possesses an intact DEDH tetrad in the PIWI domain,

but is unable to mediate cleavage activity (Hauptmann, Dueck et al. 2013, Schurmann, Trabuco et al. 2013). The N-terminal domain of AGO also participates in the cleavage reaction (Hauptmann, Dueck et al. 2013, Schurmann, Trabuco et al. 2013) and thus modifications in the N-terminal domain of AGO3 likely render it catalytically inactive (Park, Phan et al. 2017). The silencing effect caused by cleavage of the target usually requires a perfect Watson-Crick guide-target base pairing. When imperfect pairing is used, the mechanism by which silencing is mediated leads to translational repression, usually followed by target RNA degradation. The latter scenario involves the function of catalytically inactive AGO proteins, which recruit proteins mediating translational repression (reviewed in (Dexheimer and Cochella 2020).

PIWI proteins form a clade of Argonaute proteins that interact with piRNAs and are usually found in animal gonads (Aravin, Gaidatzis et al. 2006, Brennecke, Aravin et al. 2007, Houwing, Berezikov et al. 2008). PIWI proteins are similar to Argonautes but differ in the presence of arginine-rich motifs near their N-terminal part. The methylation of arginines by PRMT5 allows interaction with Tudor family proteins, which in addition to various functions in piRNA biogenesis serve as a scaffold for the piRNA machinery (Vagin, Wohlschlegel et al. 2009, Mathioudakis, Palencia et al. 2012). Four different PIWI proteins (PIWIL1-4) exist in mammals, but only three are present in mice (PIWIL1, PIWIL2, and PIWIL4) likely due to the recombination of the locus carrying *Piwil3* gene (Mouse Genome Sequencing, Waterston et al. 2002, Gutierrez, Platt et al. 2021). PIWI proteins not only serve as effectors mediating silencing, but also as factors participating in piRNA biogenesis (reviewed in (Ozata, Gainetdinov et al. 2019). Murine PIWI proteins will be described in more detail in the piRNA pathway section. In the following sections, I will describe mechanisms and functions of small RNA silencing pathways.

1.2 miRNA pathway

Animals´ miRNAs are small non–coding RNAs with a typical length of 22 nucleotides (nt). They are generated from genome–encoded precursors transcribed by RNA polymerase II (Pol II) as 5´capped and mostly 3´poly(A) tailed transcripts carrying a stem-loop structure (Cai, Hagedorn et al. 2004, Lee, Kim et al. 2004). These so-called pri-miRNAs are then cleaved by the nuclear Microprocessor complex, consisting of Drosha (RNase III enzyme) and double-stranded RNA binding protein DGCR8 (DiGeorge syndrome critical region 8), into hairpins called pre-miRNAs (Lee, Ahn et al. 2003, Denli, Tops et al. 2004). Exportin-5 provides nuclear export of pre-miRNAs to the cytoplasm, where they are further processed by Dicer (Yi, Qin et

al. 2003, Bohnsack, Czaplinski et al. 2004, Lund, Guttinger et al. 2004). Dicer cleaves the hairpin into a 21-23 nt long miRNA duplex, which is loaded onto an Argonaute protein, where one miRNA strand remains loaded while the other is released from AGO. Strand selection is based on the strand‘s thermodynamic properties. In general, a strand with less stable 5′ end is selected (Khvorova, Reynolds et al. 2003, Schwarz, Hutvagner et al. 2003, Kawamata and Tomari 2010).

miRNAs typically bind to 3′ untranslated regions (UTRs) of messenger RNAs (mRNAs). The mechanism of action depends on the level of complementarity with the target. miRNA having extensive complementarity and loaded on the AGO2, the only mammalian AGO protein that possesses endonucleolytic activity, leads to cleavage and subsequent degradation of the target (Liu, Carmell et al. 2004, Meister, Landthaler et al. 2004, Yekta, Shih et al. 2004, Bracken, Szubert et al. 2011). However, the common mechanism of miRNA-mediated repression requires less extensive complementarity. When miRNA recognizes its target with imperfect complementarity, AGO recruits a TNRC6 protein (Jonas and Izaurralde 2015, Elkayam, Faehnle et al. 2017). TNRC6 then recruits additional proteins controlling RNA metabolism, leading either (1) to deadenylation of the target accompanied by de-capping and degradation by 5′-3′ exonuclease activity or (2) to inhibition of translation by blocking the translation elongation complex, which eventually facilitates the exonuclease-mediated transcript degradation (reviewed in (Huntzinger and Izaurralde 2011, Jonas and Izaurralde 2015)).

miRNAs are among the most common small RNAs found in animals and play an important role in many developmental and cellular processes. They also may serve as biomarkers of diseases and it is known that dysregulation of miRNA genes leads to many pathologies (reviewed in (Bartel 2018)). Not only the protein machinery associated with miRNAs, but also many miRNAs are conserved across all bilaterian animals (Prochnik, Rokhsar et al. 2007). miRNA target sites are also highly conserved among related species, which suggests evolutionarily conserved functions of miRNAs in certain biological processes (Xu, Zhang et al. 2013). For example, miRNAs are important for embryonic development of all animals analyzed to date (reviewed in (Dexheimer and Cochella 2020)). In mammals, the function of the miRNA pathway appears to be dispensable in oocytes and during the oocyte-to-zygote transition process due to unfavorable miRNA:mRNA stochiometry (Kataruka, Modrak et al. 2020). However, exceptional miRNAs have been found in porcine and bovine oocytes,

whose expression levels are sufficient to suppress gene expression (Kataruka, Kinterova et al. 2022).

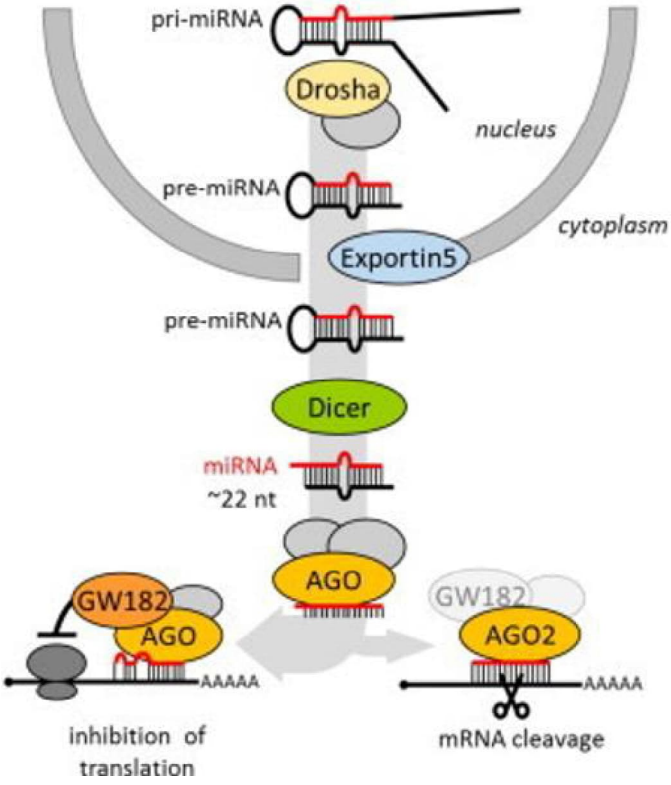

Figure 1: *Molecular mechanism of the miRNA pathway. GW182 (TNRC6). Adapted from (Svoboda 2020).*

1.3 RNAi pathway

The RNAi pathway utilizes 21-23nt long RNA molecules called small–interfering RNAs (siRNAs), which are generated from long double-stranded RNA (dsRNA) substrates (Fire, Xu et al. 1998). dsRNA can be endogenous or form as a result of viral replication in a host cell. RNAi is thus a potential antiviral mechanism; it serves this role in invertebrates and plants (Ding and Voinnet 2007, Obbard, Gordon et al. 2009). In vertebrates, the antiviral role of RNAi has been replaced by an innate immune response sensing dsRNA, where different protein sensor molecules activate the interferon response (reviewed in (Gantier and Williams 2007, Cullen, Cherry et al. 2013)). Endogenous sources of dsRNA can originate from naturally occurring convergent transcription, hairpins generated from inverted repeats, or pairing of sense and antisense RNA transcripts originating *in trans*, such as mRNA and antisense transcribed pseudogenes or retrotransposon transcripts (Tam, Aravin et al. 2008, Watanabe, Totoki et al. 2008).

dsRNA initiating RNAi is processed by Dicer into siRNA duplexes. A siRNA duplex is loaded on an Argonaut protein (AGO2 in mammals), where one strand is selected as the targeting strand, while the other is cleaved by AGO2 activity and degraded (Khvorova, Reynolds et al. 2003, Matranga, Tomari et al. 2005). The strand selection depends on the thermodynamics stability of the ends of the individual strands similarly as for miRNAs (Khvorova, Reynolds et al. 2003). In the case of perfect complementarity, AGO2 cleaves the cognate target in the middle of the base-paired sequence and gene expression is blocked (Song, Smith et al. 2004).

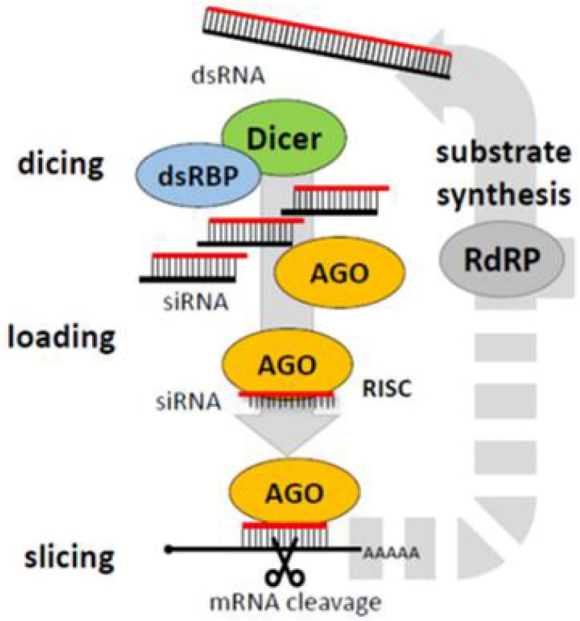

Figure 2: *Molecular mechanism of the RNAi pathway. RdRP, RNA-dependent RNA polymerase used in some species to convert RNA into dsRNA. dsRBP, double-stranded RNA binding protein. Modified from (Svoboda 2020).*

In mammals, RNAi is essentially absent in somatic cells (Nejepinska, Malik et al. 2012, Demeter, Vaskovicova et al. 2019), but interestingly, it is highly active in mouse oocytes, where it controls the expression of protein-coding genes and retrotransposons (Svoboda, Stein et al. 2000, Murchison, Stein et al. 2007, Tam, Aravin et al. 2008, Watanabe, Totoki et al. 2008). High activity of the RNAi pathway stems from an oocyte-specific isoform of Dicer termed Dicer^{O} that emerged during mouse evolution (Fig. 3) along with its substrates (Flemr, Malik et al. 2013). Dicer^{O} is produced from an alternative promoter provided by a Mouse Transcript type C (MTC) retrotransposon, which was inserted into intron 6 of Dicer (Fig. 3) and contains both, the transcription and translation start site (Flemr, Malik et al. 2013). The full–length isoform of Dicer is expressed in somatic cells and contains a tripartite helicase domain (consisting of HEL1

(DExD), HEL2i and HEL2 (HELICc) subdomains), a DUF283 (a domain of the unknown function), a PAZ domain, two RNase III domains, and a dsRNA-binding domain (Bernstein, Caudy et al. 2001, Lau, Guiley et al. 2012). The dsRNA substrate is bound and correctly positioned through the PAZ and dsRNA-binding domains and is cleaved by RNaseIII activity (Ma, Zhou et al. 2012). The helicase domain forms a clamp, the structural base for the substrate, bringing the substrate close to RNase III cleavage sites (Lau, Guiley et al. 2012). The full-length Dicer is efficiently processing pre-miRNAs, but not long dsRNA substrates (Chakravarthy, Sternberg et al. 2010, Ma, Zhou et al. 2012). Dicer^{O} expressed in mouse oocytes lacks the HEL1 (DExD) helicase domain, which leads to the efficient processing of long dsRNA. Interestingly, without compromising miRNA production (Flemr, Malik et al. 2013).

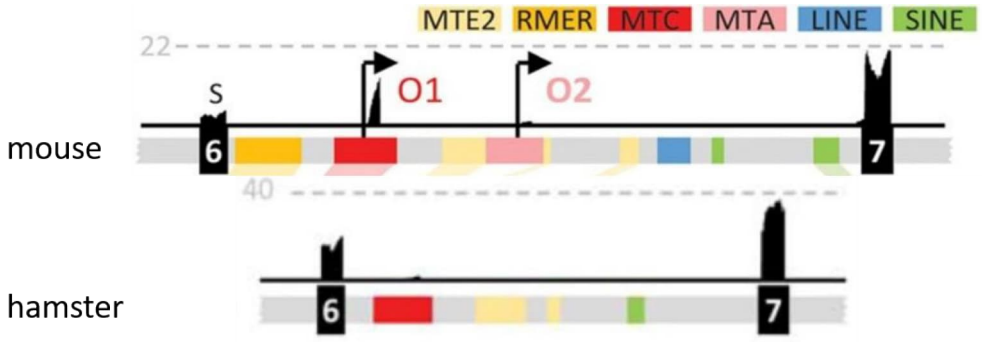

Figure 3: *Dicer^{O} production in mice. Dicer^{O} is generated from promoter provided by MT insertion into intron 6 of the Dicer gene. This insertion occurred in a common ancestor of mouse and hamster, but the MT element adapted its transcriptional activity to the Muridae family. Sequencing reads from Next-generation sequencing of mouse and hamster oocytes are shown above the Dicer gene scheme in each animal. Different retrotransposon insertions are distinguished by colors. Black arrows correspond to transcription start sites in retrotransposons that can generate shorter isoforms of Dicer. Modified from (Franke, Ganesh et al. 2017).*

1.4 piRNA pathway

PIWI-interacting RNAs (piRNAs) are small RNA molecules in the range of 18-35 nt that, as noted above, are produced independently of Dicer and interact with the PIWI clade of Argonautes (Aravin, Gaidatzis et al. 2006, Girard, Sachidanandam et al. 2006, Grivna, Beyret et al. 2006, Vagin, Sigova et al. 2006). The piRNAs have been associated primarily with post-transcriptional and epigenetic control of retrotransposons (Aravin, Hannon et al. 2007, Brennecke, Aravin et al. 2007, Houwing, Kamminga et al. 2007, Aravin, Sachidanandam et al. 2008, Kuramochi-Miyagawa, Watanabe et al. 2008), but have also been linked with the regulation of protein-coding genes (Vourekas, Zheng et al. 2012, Gou, Dai et al. 2014, Wu, Fu

et al. 2020). They were first described in flies as long siRNAs silencing *Stellate*, a gene on the X chromosome of *Drosophila melanogaster*, the expression of which leads to male sterility (Bozzetti, Massari et al. 1995, Aravin, Naumova et al. 2001, Belloni, Tritto et al. 2002).

1.4.1 Sources of piRNAs and PIWI proteins

In mammals, the piRNA pathway has been described in most detail in mouse spermatogenesis. Therefore, my description of the molecular mechanism below is mainly based on this model. Compared to miRNA and RNAi pathways using dsRNA precursors, the piRNA pathway utilizes long single-stranded RNAs, which in mice are transcribed by RNA polymerase II (RNA Pol II) (Vagin, Sigova et al. 2006, Houwing, Kamminga et al. 2007, Li, Roy et al. 2013) from specific loci called piRNA clusters (Aravin, Gaidatzis et al. 2006, Girard, Sachidanandam et al. 2006, Grivna, Beyret et al. 2006). What defines the transcript as a piRNA precursor loaded into the piRNA pathway machinery remains a question in the field. The canonical transcription of piRNA precursors, which is indistinguishable from the transcription of mRNAs, suggests that any RNA Pol II transcript can be processed into piRNAs and thus become a target of the piRNA pathway (Li, Roy et al. 2013). However, the selective processivity of substrates indicates the presence of a currently unknown mechanism for selecting transcripts loaded into the piRNA machinery.

The origin of piRNAs and their regulatory potential changes during mouse spermatogenesis. In the early stages of spermatogenesis, so-called pre–pachytene piRNAs are derived predominantly from transposable elements, but also from the coding and 3′ UTR parts of protein-coding genes (Li, Roy et al. 2013), which indicates that they may play a role in the regulation of protein-coding genes. When spermatogenesis reaches the pachytene stage of the prophase of meiosis I (described in more detail in Chapter 1.6.2 Spermatogenesis), piRNAs are generated from ~ 100 intergenic loci poor in repetitive sequences (Aravin, Gaidatzis et al. 2006, Girard, Sachidanandam et al. 2006). The expression of these loci is driven by the transcription factor A-MYB, which also controls the expression of numerous piRNA pathway components such as PIWIL1 (MIWI in mice) or PIWIL2 (MILI in mice) (Li, Roy et al. 2013). The third PIWI protein expressed in mice, PIWIL4 (MIWI2 in mice), is present in the early stages of germ cell development (Aravin, Sachidanandam et al. 2008). The fourth PIWI (PIWIL3) protein found in mammals is absent in mice, where it was lost during evolution, as noted above (Mouse Genome Sequencing, Waterston et al. 2002, Gutierrez, Platt et al. 2021).

Because the expression pattern of PIWI proteins differs, the modes of regulation mediated by piRNAs in the mouse germline would presumably also differ. MIWI2 is expressed only in prenatal germ cells and the production of MIWI2 bound piRNAs is fully dependent on MILI activity (Aravin, Sachidanandam et al. 2008). MILI is expressed in both prenatal and adult mice, and MIWI expression begins at the pachytene stage of meiosis I (Kuramochi-Miyagawa, Kimura et al. 2001). Therefore, while MILI is functional throughout the whole spermatogenesis, MIWI2 carries pre–pachytene piRNAs and MIWI mediates the function of pachytene piRNAs (Deng and Lin 2002, Grivna, Pyhtila et al. 2006 , Aravin, Sachidanandam et al. 2008).

1.4.2 Molecular mechanism of the piRNA pathway

piRNA precursors are processed in a perinuclear structure called *Nuage*, where they interact with the MOV10L1 helicase, which funnels the long RNA precursor into the piRNA pathway machinery (Aravin, van der Heijden et al. 2009, Zheng, Xiol et al. 2010). The long RNA precursor is cleaved to smaller precursor piRNAs by endonuclease MitoPLD (Watanabe, Chuma et al. 2011, Nishimasu, Ishizu et al. 2012), which appears to define the 5′ ends of piRNAs, resulting in the piRNAs having uracil (U) in the first position (1U-bias) (Aravin, Gaidatzis et al. 2006, Brennecke, Aravin et al. 2007). The 5′ end of the piRNA is then anchored by the MID domain of the PIWI protein. The preference for binding piRNAs harboring U at the first position by the MID domain may be another possible explanation for the observed 1U-bias (Stein, Genzor et al. 2019). When a piRNA is loaded onto a PIWI protein, its 3′ end is defined either by the second MitoPLD cleavage (Watanabe, Chuma et al. 2011) or by trimming to the desired size with 3′-5′ exonuclease PNLDC1 (Ding, Liu et al. 2017). Mature piRNAs are 2–O–methylated at the 3′ end by methyltransferase HENMT1 (Kirino and Mourelatos 2007, Lim, Qu et al. 2015). This 3′ 2-O-methylation is a specific feature of mammalian piRNAs and has been proposed to stabilize small RNAs (Lim, Qu et al. 2015).

PIWI loaded with mature piRNA cleaves the complementary target 10 nucleotides downstream of the 5′ end of the piRNA molecule (Brennecke, Aravin et al. 2007, Aravin, Sachidanandam et al. 2008). In some animals, such as *Drosophila*, the initiator piRNA is inherited maternally (Brennecke, Malone et al. 2008). In mice, however, the initiating process remains unknown. The cleaved target can be recycled and used as a new precursor. Its 5′ end is loaded into the PIWI protein and a secondary piRNA is generated (Brennecke, Aravin et al. 2007, Aravin, Sachidanandam et al. 2008). The first 10 nucleotides of the secondary piRNA

will be complementary to the original primary piRNA and will exhibit a strong bias for adenine (A) at position 10. Adenine bias is likely generated as a consequence of 1U-bias, because the overlap of primary piRNA with its complementary target, from which secondary piRNA is generated, results in the pairing of U at position 1 with A at position 10 (Brennecke, Aravin et al. 2007, Aravin, Sachidanandam et al. 2008). Another study suggests that A at position 10 is the result of PIWI preferential binding to adenine. The model proposes that PIWI (MILI in mice) selects targets irrespective of the 1U-bias of the piRNA guide. Instead, PIWI binds to the target with a preference for A at the first binding position. Cleavage of the target, which occurs 10 nucleotides downstream of the 5′ end of the piRNA molecule, generates a secondary piRNA bearing A at position 10 (Wang, Yoshikawa et al. 2014). This amplification process is called the ping–pong mechanism and serves as an effective weapon in the fight against multiple copies of retrotransposons due to the rapid increase in the number of piRNAs available for retrotransposon silencing (Aravin, Sachidanandam et al. 2007, Brennecke, Aravin et al. 2007, Houwing, Berezikov et al. 2008). The remaining 3′ end of the cleaved target is processed by MitoPLD to produce so-called phased primary piRNAs (Han, Wang et al. 2015). These piRNAs carry new sequences derived from targets and therefore expand the sequence repertoire of the piRNA pool and allow rapid adaptation to target specific sequences (Han, Wang et al. 2015). In general, primary piRNAs interact with MILI, while secondary piRNAs are bound by both, MILI and MIWI2 (Aravin, Sachidanandam et al. 2008). MIWI2 loaded with piRNA can translocate to the nucleus and mediate silencing of nascent transcripts (Aravin, Sachidanandam et al. 2008, Watanabe, Cui et al. 2018). It recognizes nascent transcripts complementary to secondary piRNAs and interacts with TEX15 and SPOCD1 cofactors, which mediate methylation of DNA or H3K9me3 heterochromatin mark, thereby helping to silence retrotransposons (Schopp, Zoch et al. 2020, Zoch, Auchynnikava et al. 2020).

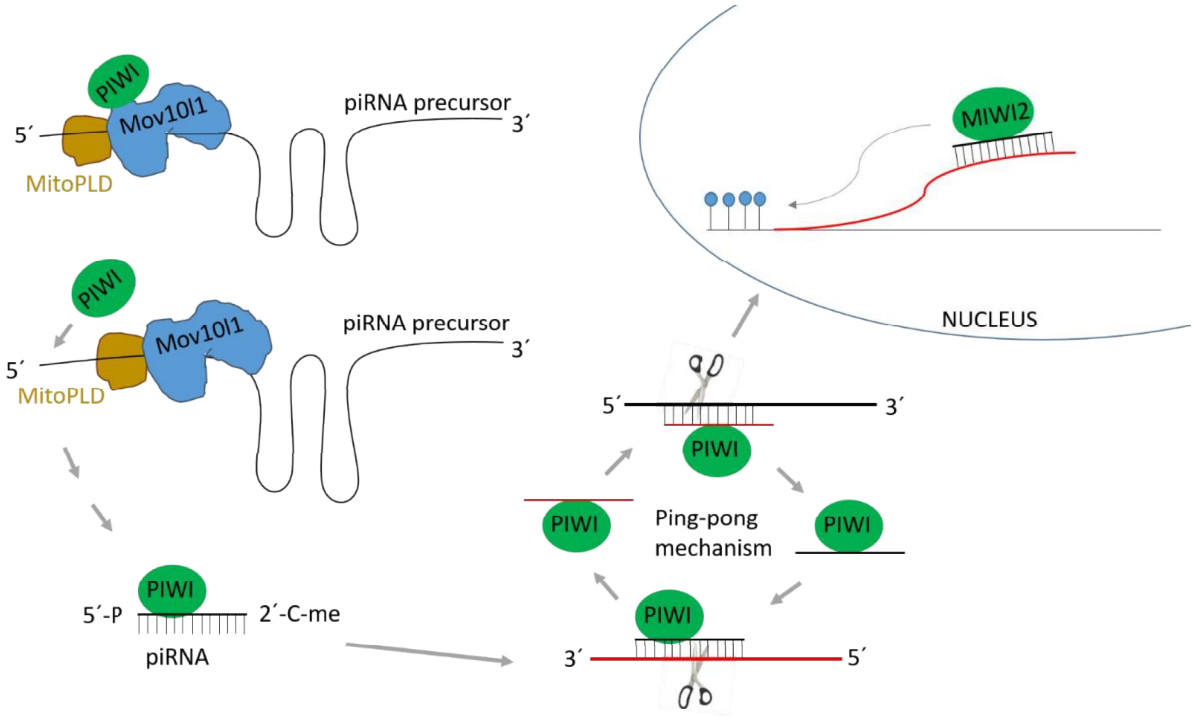

Figure 4: *Molecular mechanism of the piRNA pathway. The piRNA pathway regulates the expression of genes and retrotransposons at transcriptional and post-transcriptional levels.*

1.4.3 Pachytene piRNAs

Pachytene piRNAs show no signs of the ping-pong mechanism and, in addition to the cleavage reaction, have been shown to destabilize targets in a miRNA-like manner (Gou, Dai et al. 2014) or to mediate translational activation when loaded on MIWI (Dai, Wang et al. 2019). Translational activation is mediated by AU-rich elements binding protein HuR and the translation initiation factor EIF3F interacting with the MIWI-piRNA complex (Dai, Wang et al. 2019). Although pachytene piRNAs are very abundant and make up the vast majority of the piRNA population in adult mice, their main function remains unclear. More than 80% of pachytene piRNAs map only to the regions that produce them, suggesting that they have no specific function (Aravin, Gaidatzis et al. 2006, Girard, Sachidanandam et al. 2006, Li, Roy et al. 2013), and so far only a few mRNAs having a role in spermiogenesis have been described as targets of pachytene piRNAs (Gou, Dai et al. 2014, Wu, Fu et al. 2020).

1.4.4 Physiological relevance of piRNAs

Although PIWI proteins are well conserved in animals, piRNA sequences vary among species. It reflects the rapid adaptation to the evolution of individual species and molecular mechanisms producing piRNAs. However, the piRNA pathway appears to have a conserved function in animal germlines, where it controls the activity of transposable elements. The

piRNA pathway offers the evolution of an adaptive response to invading transposable elements. This works as an effective mechanism protecting animal germlines from genomic invaders, which has been described in a variety of animals from invertebrates to mammals (reviewed in (Ozata, Gainetdinov et al. 2019)).

In addition to the ancestral function of silencing of retrotransposons, other functions have emerged during evolution, such as an antiviral role in mosquito somatic cells (Miesen, Girardi et al. 2015) or regulation of embryo patterning in *Drosophila* (Rouget, Papin et al. 2010). In mammals, PIWI and piRNAs were thought to be restricted to the germ cells, where they ensure proper male germline development (Deng and Lin 2002, Kuramochi-Miyagawa, Kimura et al. 2004, Carmell, Girard et al. 2007, Frost, Hamra et al. 2010). Recently, several reports have demonstrated their potential in somatic cells, including control of epithelial–to–mesenchymal neural crest cell transition in chickens through the regulation of a retrotransposon–derived gene (Galton, Fejes-Toth et al. 2021) or their emerging role in human diseases (Riquelme, Perez-Moreno et al. 2021).

Interestingly, it has been shown that piRNA populations can vary from cell to cell and that, in general, only highly abundant piRNAs are present in every cell (Genzor, Konstantinidou et al. 2021). Thus, piRNA function would be conserved for abundant piRNAs, but in the case of rare piRNAs, the function may vary between individual cells. Although abundance appears to determine the function, rare piRNAs provide an opportunity to create functional diversity of the piRNA pathway within cells and organisms (Genzor, Konstantinidou et al. 2021).

1.5 Retrotransposons

Because the main function of the piRNA pathway is silencing of retrotransposons, it is important to understand the basics of their biology, and therefore this chapter discusses retrotransposons in more detail.

Retrotransposons are a major class of transposable elements (reviewed in (Goodier 2016)). Retrotransposons use an RNA intermediate that is reverse transcribed into a double-stranded DNA (dsDNA) molecule, which is then inserted into a new site in the genome. They can be divided based on their structural features into long terminal repeats (LTR) and non-LTR elements (Wicker, Sabot et al. 2007). Retrotransposons occupy a large part of eukaryotic genomes. They contribute to genome expansion and play a role in genetic innovation associated with evolution and speciation (Finnegan 1989, Mouse Genome Sequencing, Waterston et al.

2002, Hughes 2015). On the other hand, their activity can negatively affect genome integrity due to their insertional mutagenesis (Babushok and Kazazian 2007, Payer and Burns 2019).

1.5.1 LTR retrotransposons

The majority of LTR retrotransposons is believed to be derived from retroviruses that have lost their ability to exit the cell in the form of infectious particles (Boeke and Stoye 1997, Kaneko-Ishino and Ishino 2012). They consist of two long terminal repeats at their 5′ and 3′ ends flanking a coding region. The coding region carries the GAG polyprotein, which forms virus-like particles, the POL polyprotein, which is a reverse transcriptase, and some of them have retained the ENV region encoding the viral envelope proteins for viral transmission (Hughes 2015). GAG and POL can be expressed in two different variants depending on the host species. They can either be produced as a single open reading frame (ORF) that is subsequently cleaved, or a frameshift is introduced between the two ORFs leading to the expression of independent ORFs (Gao, Havecker et al. 2003). Transcription is regulated by the host RNA polymerase II from the transcription start site encoded by the 5′ LTR and the host tRNA is used as a primer for reverse transcription (Craig 2002, Hughes 2015, Schorn and Martienssen 2018). The double-stranded cDNA is generated and integrated into the genome (Craig 2002, Hughes 2015). Interestingly, LTR retrotransposon insertions occur as full-length copies or as a solo LTR created by the recombination of the two LTRs of a full–length copy (Mager and Goodchild 1989). As LTRs contain transcription and translation start sites, even a solo LTR can affect neighboring regions, as shown in the example of Dicer^{O} described above (Flemr, Malik et al. 2013, Franke, Ganesh et al. 2017).

Retrotransposons that have retained the competence of retrotransposition in their coding region are called autonomous. Non-autonomous retrotransposons are those that do not have this competence and are thus dependent on the activity of autonomous elements. LTR retrotransposons can be further classified as ERV1, EVRK or ERVL families based on their origin. Currently, the most active elements in the mouse genome belong to the ERVK class (Maksakova, Romanish et al. 2006). The best-described representative is the autonomous Intracisternal A Particle (IAP), specifically in mice the IAPE subfamily of retrotransposons (Ribet, Harper et al. 2008). Moreover, additional families are active in mice such as autonomous MMERVK or nonautonomous Early transposons activated by autonomous MusD family (Mager and Freeman 2000, Baust, Gagnier et al. 2003, McCarthy and McDonald 2004). The most abundant endogenous retroviruses in the mouse genome belong to the ERVL class (Mouse

Genome Sequencing, Waterston et al. 2002), represented by non-autonomous Mammalian apparent LTR Retrotransposons (MaLR), that have contributed to the gene–remodeling events during the mouse oocyte–to–embryo transition due to their ability to become a functional part of genes (Franke, Ganesh et al. 2017). Their expansion was possibly mediated by the autonomous Mouse Endogenous Retrovirus type-L (MuERV-L) element, which does not appear to be retrotransposing anymore, but is still transcriptionally active during early mouse development (Kigami, Minami et al. 2003, Svoboda, Stein et al. 2004). The ERV1 class occupies only a small part of the mouse genome and is represented by the Mouse Leukemia Virus (MuLV). MuLV is a relatively young endogenous retrovirus whose intact copies retained the ability to infect other cells and the number of copies varies among mouse strains (Stocking and Kozak 2008). Other families belonging to the ERV1 class are autonomous RLTR6 (also called MmERV) and non-autonomous VL30 which is most likely derived from the RLTR6 element (French and Norton 1997, Bromham, Clark et al. 2001).

1.5.2 Non-LTR retrotransposons

As their name indicates, non-LTR retrotransposons lack long terminal repeats at their ends. The best representative of this group is the family of long interspersed nuclear elements 1 (LINE1), which is currently the only active autonomous non-LTR family that has been expanding for more than 150 million years of mammalian evolution (Smit, Toth et al. 1995). In mice, a subfamily of independently evolving LINE1 retrotransposons have expanded and is currently active (Goodier, Ostertag et al. 2001). LINE1 elements are more than 6 kb in length and consist of a 5′ UTR providing an internal bidirectional promoter, two open reading frames interacting with LINE1 RNA molecules, and a 3′ UTR with a poly(A) signal. ORF1 encodes an RNA–binding protein that is essential for LINE1 retrotransposition and ORF2 encodes an endonuclease and a reverse transcriptase (Martin and Bushman 2001, Martin, Cruceanu et al. 2005, Kulpa and Moran 2006, Babushok and Kazazian 2007). Retrotransposition is different from that of LTR retrotransposons and is termed target–primed reverse transcription. During this mechanism, the LINE1–encoded endonuclease generates a nick at TTAAAA DNA motif, which anneals to the polyA tail of LINE1 RNA and primes reverse transcription and second-strand DNA synthesis (Jurka 1997, Cost, Feng et al. 2002). This process is prone to truncations of the 5′ UTR, when reverse transcriptase prematurely terminates reverse transcription. This results in an incomplete inactive insertion of LINE1 element (Esnault, Maestre et al. 2000, Szak, Pickeral et al. 2002).

Non-autonomous non-LTR retrotransposons are represented by short interspersed nuclear elements (SINEs), which are dependent on the activity of LINE1 elements (Dewannieux, Esnault et al. 2003). For example, the most successful SINE element in the human genome is the Alu element, which is currently transpositionally active in humans and continuously contributes to genome instability (Deininger and Batzer 1999, Lander, Linton et al. 2001). The most abundant SINE element in the mouse genome is SINE B1. The mouse genome contains three other families, namely B2, ID and B4. Of these families, only families B1 and B2 show signs of ongoing activity in mice (Mouse Genome Sequencing, Waterston et al. 2002, Gibbs, Weinstock et al. 2004).

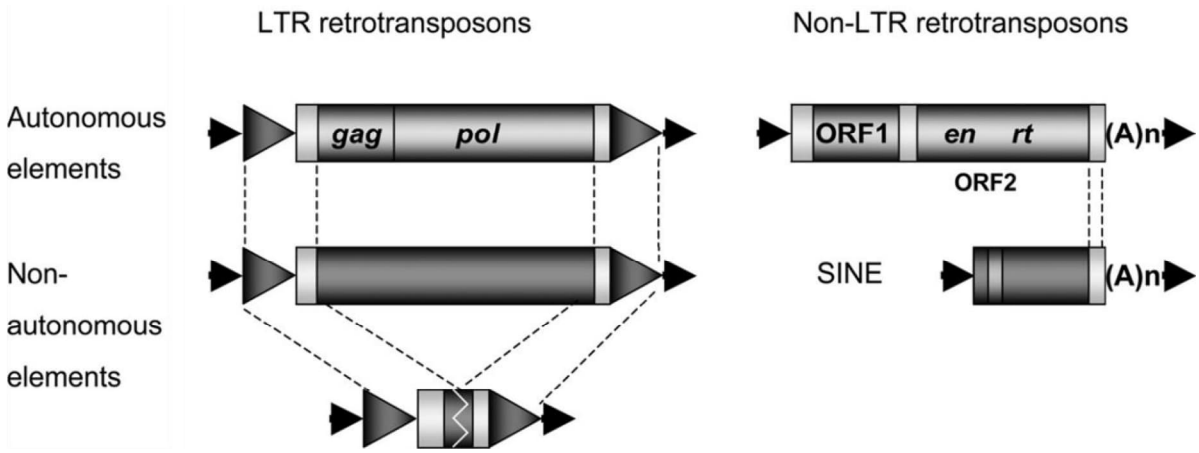

Figure 5: *Structural features of autonomous and non-autonomous LTR and non-LTR retrotransposons. Autonomous retrotransposons encode proteins necessary for independent retrotransposition. Non-autonomous retrotransposons do not encode retrotransposition proteins, but retain the cis sequences necessary for transposition controlled by autonomous elements. Gray arrows represent direct repeats and black arrows correspond to target site duplication, which is the duplication of short genomic sequence at the site of insertion caused by TE integration. Modified from (Wessler 2006).*

1.5.3 Activity of retrotransposons

The vast majority of retrotransposon insertions are not active because they have lost their transposition potential by accumulating mutations. Consequently, older retrotransposons are distinct from each other, because they contain a higher number of substitutions in their sequences compared to younger families with more recent activity. 5′ UTR truncations and accumulations of mutations resulted in less than 3 000 full-length intact (FLI) retrotransposition-competent LINE1 copies out of 20 000 full-length insertions in the mouse genome. At the same time, only around 100 copies capable of retrotransposition are estimated in humans, of which only a small fraction of highly active L1 represents retrotransposition activity (DeBerardinis, Goodier et al. 1998, Goodier, Ostertag et al. 2001, Brouha, Schustak et

al. 2003). A small fraction of retrotransposons that remain active not only play an important role in genome evolution, but as noted above, also pose threat to the integrity of the host genome, leading to DNA damage through insertional mutations (Babushok and Kazazian 2007, Goodier and Kazazian 2008). Retrotransposons not only affect genome stability by insertional mutagenesis, but also serve as a source of homology for non-allelic homologous recombination, which can lead to genetic disorders, as shown in the example of Alu elements (Deininger and Batzer 1999).

To propagate successfully for generations, TEs must be active in cells that will be passed on to the next generation. They are therefore determined to escape repression mechanisms in the germline. On the other hand, their abnormal activity in the germline is associated with host sterility (Rubin, Kidwell et al. 1982, Kuramochi-Miyagawa, Kimura et al. 2004, Carmell, Girard et al. 2007, Houwing, Berezikov et al. 2008, Frost, Hamra et al. 2010, Di Giacomo, Comazzetto et al. 2014) and that is why the host genome has developed various mechanisms to silence retrotransposons in germ cells. Despite these protective mechanisms, the genome is vulnerable to TEs activity during epigenetic reprogramming that occurs during germ cell formation (Molaro, Falciatori et al. 2014) and after genome activation (Kigami, Minami et al. 2003, Svoboda, Stein et al. 2004). The piRNA pathway is one of the major defense mechanisms against retrotransposons in animal germlines. Therefore, the next chapters will focus on germ cell development in mammals and the role of the piRNA pathway in male and female germlines.

1.6 Germ cell development in mammals

Germ cells are unique cell types that undergo meiosis and give rise to highly specified haploid gametes. The mouse primordial germ cells (PGCs) are induced from epiblast around embryonic (E) day 7.25 (Ginsburg, Snow et al. 1990). They start to migrate to the genital ridges around E10.5, where they proliferate (Molyneaux, Stallock et al. 2001). During this period, PGCs become reprogrammed by genome-wide DNA methylation (Monk, Boubelik et al. 1987, Sasaki and Matsui 2008). Underlying these events, associated somatic cells play important roles in germ cell development and differentiation (reviewed in (Rios-Rojas, Bowles et al. 2015)).

1.6.1 Oogenesis and oocyte-to-zygote transition

In mammalian females, gamete formation involves numerous cycles of mitosis before germ cells enter meiosis, where they remain arrested at the prophase stage of the first meiotic division. Female germ cells differentiate during embryonic development to produce mature

gametes (oocytes), which remain at the meiotic arrest until puberty (reviewed in (Edson, Nagaraja et al. 2009)). Together with surrounding ovarian somatic cells, oocytes form follicles. During the growth phase, they increase in volume and accumulate maternal factors for the next events (De Leon, Johnson et al. 1983, Edson, Nagaraja et al. 2009). After puberty, individual or groups of fully-grown oocytes (known as germinal vesicle, GV oocytes) periodically respond to luteinizing hormone, which leads to activation of a metaphase-promoting factor and resumption of meiosis. Oocytes enter the second meiotic division and stop at the metaphase stage (MII) until fertilization. MII oocytes are called mature oocytes as the process between meiosis I and II is called meiotic maturation. Mammalian MII oocytes typically complete the second meiotic division after fertilization, undergo cleavage, and form a zygote (reviewed in (Edson, Nagaraja et al. 2009)).

The transition from oocyte to zygote means that the developmental control is passed from the mother to the zygote. From the moment the oocyte reaches its full-grown stage, it is transcriptionally quiescent until activation of the zygotic genome, which occurs at the 2-cell stage in mice (Bouniol-Baly, Hamraoui et al. 1999, Wang, Piotrowska et al. 2004, Tadros and Lipshitz 2009). As a result, post-transcriptional and translational control of maternal mRNAs during maturation and post-fertilization is fully dependent on proteins and RNAs (including small RNAs) accumulated during oocyte growth. Control includes both stabilization and degradation of maternal mRNAs (De Leon, Johnson et al. 1983, Su, Sugiura et al. 2007, Tadros and Lipshitz 2009, Chen and Shyu 2011). The process of RNA degradation during oocyte maturation and after fertilization is called maternal RNA clearance (De Leon, Johnson et al. 1983, Zeng and Schultz 2005, Su, Sugiura et al. 2007, Abe, Yamamoto et al. 2015).

Other factors required for proper transition of the oocyte to the zygote are small RNAs. Loss of Dicer in mouse oocytes has been shown to lead to transcriptome dysregulation and a meiotic defect leading to sterility (Murchison, Stein et al. 2007, Tang, Kaneda et al. 2007). In contrast, the loss of miRNA processing factor DGCR8 or piRNA processing factor MOV10L1 did not show such defects (Frost, Hamra et al. 2010, Suh, Baehner et al. 2010), indicating the indispensability of only siRNAs in oocyte maturation. The transition from oocyte to zygote also requires changes in chromatin structure, which rely on maternal contribution. Chromatin from two parental cells, oocyte and sperm, must be remodeled into a naive, accessible form. This reprogramming involves changes in DNA methylation and histone marks, but is still not fully understood (Zhou and Dean 2015, Eckersley-Maslin, Alda-Catalinas et al. 2018).

1.6.2 Spermatogenesis

The PGCs forming the male germ cells are called gonocytes. Unlike germ cells in females, gonocytes are mitotically inactive until after birth (reviewed in (McLaren 2003)). Soon after birth, gonocytes resume mitosis, move to the basement membrane of seminiferous tubules and begin to differentiate (reviewed in (Griswold 2016)). They form distinct populations of differentiated and undifferentiated spermatogonia, including a pool of self-renewing spermatogonial stem cells, which serve as precursors of spermatogonia and thus maintain the continuation of spermatogenesis. Spermatogonia further proliferate and differentiate into spermatocytes, cells entering meiosis. Spermatocytes undergo two cycles of meiotic division, resulting in haploid round spermatids, which further differentiate into mature sperms in a process called spermiogenesis. The whole process is dependent on germ cell interactions with somatic cells, including Sertoli, Leydig, and peritubular cells (reviewed in (Phillips, Gassei et al. 2010, Griswold 2016)).

During spermatogenesis, several critical events important for proper germ cell development occur, such as *de novo* DNA methylation ongoing in mitotically quiescent gonocytes or spermiogenesis relying on a genome repacking involving protamin replacement of histones (Kato, Kaneda et al. 2007, Bao and Bedford 2016). Another event, requiring several transcriptional and chromatin changes, is the meiotic process associated with chromosome recombination (Mahadevaiah, Turner et al. 2001, Tachibana, Nozaki et al. 2007). The prophase of meiosis I is the longest stage of meiotic division when the early stages of leptotene and zygotene are transcriptionally inert (Monesi 1964). The main chromatin changes occur at the pachytene stage when the transcription is reactivated and mitotic transcripts are replaced by meiotic factors (reviewed in (Geisinger, Rodriguez-Casuriaga et al. 2021)). These processes require strict transcriptional, translational, and post-transcriptional control. Besides the miRNA pathway regulating numerous transcripts and the piRNA pathway silencing retrotransposons, various RNA-binding proteins, terminal transferases, and mRNA modifications are involved in the regulation of the transcriptome during male germ cell progression (Hayashi, Chuva de Sousa Lopes et al. 2008, Di Giacomo, Comazzetto et al. 2013, Hussain, Tuorto et al. 2013, Wojtas, Pandey et al. 2017, Xu, Yang et al. 2017, Morgan, Kabayama et al. 2019).

1.7 Transposable elements and the piRNA pathway

The function of the piRNA pathway in germ cells appears to be conserved across species. Although certain aspects of piRNA biogenesis vary across species, such as the origin

or transcription of piRNA clusters, the requirement for the piRNA pathway in germ cell development appears to be associated with an ancestral function of silencing retrotransposons (reviewed in (Ozata, Gainetdinov et al. 2019)). This conserved role of piRNAs in germ cell development has been demonstrated in flies, fish, or mice. In this chapter, I will describe how TEs and the defective piRNA pathway affect germ cell development in animal model organisms, with particular attention paid to the mouse model, a mammalian representative in which the impact of the piRNA pathway on germ cell development has been extensively studied.

1.7.1 piRNA pathway in *Drosophila*

In *Drosophila*, disruption of the piRNA pathway leads to male and female sterility. Abnormal germ cell retrotransposon activity has been reported in mutants of the *Drosophila* piRNA pathway (Brennecke, Aravin et al. 2007). Germ cells develop normally at the beginning of gametogenesis in piRNA pathway mutants, but germline stem cell self-renewal and division rate are disrupted, leading to germ cell depletion and final absence of germ cells in adults (Lin and Spradling 1997, Cox, Chao et al. 1998).

Interestingly, transposable elements are active not only in germ cells, but also in somatic cells surrounding germ cells in *Drosophila* ovary (Pelisson, Song et al. 1994, Desset, Buchon et al. 2008). Some of these endogenous retroviruses can infect neighboring germ cells when derepressed in somatic cells (Chalvet, Teysset et al. 1999, Brasset, Taddei et al. 2006). Accordingly, somatic piRNAs can be found in *Drosophila* ovarian cells. Out of the three PIWI proteins that exist in flies, only one PIWI protein is expressed in somatic ovarian cells. Despite this limitation, the piRNA pathway appears to safeguard transposable elements in *Drosophila* ovarian somatic cells, thus protecting the germline from the activity of infectious elements originating in somatic cells. The germline piRNAs are maternally deposited in flies and it has been shown that these piRNAs are involved in the regulation of both, the germline and somatic transposable elements in offsprings (Brennecke, Malone et al. 2008, Akkouche, Grentzinger et al. 2013). It extends the ancestral function of piRNAs observed in germ cells to somatic cells. Furthermore, the function of piRNAs has been reported also during embryogenesis, where they mediate decay of *Nos* mRNA important for embryo patterning. piRNAs are in this case derived from the insertion of TEs in the 3′ UTR of mRNA (Rouget, Papin et al. 2010). It demonstrates an important function of transposable elements in the evolution of genes and their regulatory pathways.

1.7.2 piRNA pathway in zebrafish

Zebrafish genome encodes two PIWI proteins, ZIWI and ZILI, which are important for the fertility of both, males and females (Houwing, Kamminga et al. 2007, Houwing, Berezikov et al. 2008). When ZIWI is lost, germ cells most likely do not enter the germ cell differentiation pathway and are progressively depleted due to apoptosis during larval development (Houwing, Kamminga et al. 2007). All these mutants are phenotypically sterile males likely due to loss of PGCs (Houwing, Kamminga et al. 2007), which leads to the development of male gonads in fish (Slanchev, Stebler et al. 2005). Interestingly, adult animals with reduced ZIWI function maintain germ cells, which, however, show abnormal levels of apoptosis. This results in subfertility of animals (Houwing, Kamminga et al. 2007).

Loss of ZILI leads to derepression of TEs and the inability of germ cells to differentiate, followed by subsequent depletion of germ cells. It indicates that ZILI is important for germ cell maintenance and differentiation (Houwing, Berezikov et al. 2008). Loss of germ cells lacking ZILI, which is zygotically expressed, occurs later than in mutants lacking ZIWI protein, which is provided maternally together with ZIWI-associated piRNAs (Houwing, Kamminga et al. 2007, Houwing, Berezikov et al. 2008). However, consistently with *Ziwi* mutants, all *Zili* mutants are phenotypically sterile males devoid of germ cells. In contrast to *Ziwi* mutants, germ cells in *Zili* mutants do not show signs of apoptosis and are probably depleted by another mechanism (Houwing, Kamminga et al. 2007, Houwing, Berezikov et al. 2008).

Interestingly, the missense mutation introduced into the *Zili* gene allowed normal development of both sexes, but homozygous females were sterile. They produced oocytes that can be fertilized, but exhibit defects in meiosis. However, no elevated levels of transposable elements were detected in these oocytes, implicating that the meiotic function of ZILI is independent of TEs silencing (Houwing, Berezikov et al. 2008).

1.7.3 piRNA pathway in mouse spermatogenesis

In mice, defects in the piRNA pathway lead to male sterility. Unlike in *Drosophila* or zebrafish, where pre-meiotic germ cells are affected, mouse piRNA pathway mutants typically show defects during or after meiosis (Deng and Lin 2002, Kuramochi-Miyagawa, Kimura et al. 2004, Carmell, Girard et al. 2007, Frost, Hamra et al. 2010). Although the cause of defective spermatogenesis may start much earlier than in meiosis, the phenotype is attributed to elevated levels of transposable elements in meiotic spermatocytes. Even when the piRNA pathway factors expressed in pre-meiotic stages of spermatogenesis are lost, the sterile phenotype is not

manifested until the arrest at the pachytene stage of meiosis I (Kuramochi-Miyagawa, Kimura et al. 2004, Carmell, Girard et al. 2007, Frost, Hamra et al. 2010). During the zygotene to pachytene transition of meiosis I, other silencing mechanisms, such as histone marks are erased from retrotransposons, which brings an opportunity for TEs to escape repression (Kuramochi-Miyagawa, Kimura et al. 2004, Frost, Hamra et al. 2010, Di Giacomo, Comazzetto et al. 2013). Therefore, the post-transcriptional regulation by the piRNA pathway is undoubtedly critical at this point. Although germ cell maintenance is not affected in *Mov10l1, Mili* or *Miwi* mutants, as demonstrated by high germ cell turnover in old mutant mice (Deng and Lin 2002, Kuramochi-Miyagawa, Kimura et al. 2004, Frost, Hamra et al. 2010), loss of MIWI2 leads to progressive depletion of pre-meiotic spermatogonia in old mice (Carmell, Girard et al. 2007). It suggests a function of MIWI2 in germ cell maintenance, which appears to be associated with defective reprogramming of spermatogonial transcriptome (Vasiliauskaite, Berrens et al. 2018).

Mutation in MOV10L1, a helicase important for the initial steps of piRNA biogenesis, leads to elevated levels of retrotransposons already in spermatogonia, but spermatogenetic block occurs at the pachytene stage of meiosis I. It is associated with an increased protein level of LINE1 elements and apoptotic germ cell death (Frost, Hamra et al. 2010, Zheng, Xiol et al. 2010). Loss of MILI or MIWI2 leads to similar defects with massive upregulation of LINE1 in meiotic cells (Kuramochi-Miyagawa, Kimura et al. 2004, Carmell, Girard et al. 2007). It is not only related to the post-transcriptional mode of the piRNA pathway, but also to its role in *de novo* DNA methylation in gonocytes, where MILI, MIWI2 and MOV10L1 are expressed (Aravin, Sachidanandam et al. 2008). Defects in DNA methylation of LINE1 and LTR retrotransposons were observed in *Mili* and *Miwi2* knock-out mouse testes with loss of MIWI2 impacting methylation of LINE1 elements more than that of IAP (Kuramochi-Miyagawa, Watanabe et al. 2008).

The mode of repression of the LINE1 and IAP retrotransposons is distinct. Loss of DNA methylation and the piRNA pathway does not affect LINE1 elements until the pachytene stage of meiosis I due to H3K9me2 histone marks deposited by histone methyltransferase G9a (Di Giacomo, Comazzetto et al. 2014). Surprisingly, H3K9me2 alone is not sufficient to suppress IAP elements in spermatogonia. In addition to deregulation of IAP in the *Mili* mutant spermatogonia, the double knockout of *G9a* and *Mili* genes causes derepression of LINE1 elements in spermatogonia, leading to massive loss of all germ cell types in the tubule (Di Giacomo, Comazzetto et al. 2014).

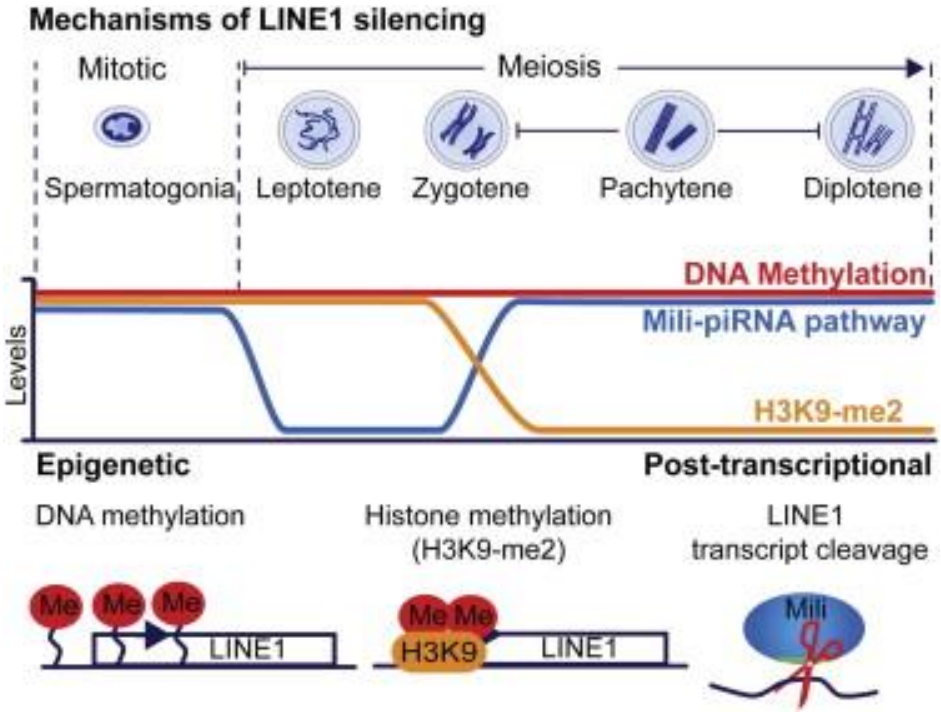

Figure 6: *Scheme of various strategies used to silence LINE1 elements during mouse spermatogenesis. Adapted from (Di Giacomo, Comazzetto et al. 2013).*

Loss of MIWI, whose expression starts in meiotic spermatocytes, results in disruption of spermatogenesis at the stage of round spermatids (Deng and Lin 2002). MIWI plays a role in post-transcriptional silencing of retrotransposons using pachytene piRNAs and has been shown to regulate several mRNA targets important for spermiogenesis (Reuter, Berninger et al. 2011, Gou, Dai et al. 2014). Because MIWI interacts with pachytene piRNAs, the function of MIWI in the piRNA pathway may be limited by the targeting potential of pachytene piRNAs, for most of which the targets are unclear (Vourekas, Zheng et al. 2012).

1.7.4 piRNA pathway in mouse oogenesis

As noted above, the piRNA pathway appears to be important only for spermatogenesis in mice (Kuramochi-Miyagawa, Kimura et al. 2004, Houwing, Berezikov et al. 2008, Frost, Hamra et al. 2010, Ma, Wang et al. 2014, Akkouche, Mugat et al. 2017), suggesting that piRNAs are dispensable for mammalian oogenesis and early development.

However, a piRNA population is readily detectable in mouse oocytes (Watanabe, Totoki et al. 2008, Yang, Li et al. 2019), indicating that piRNA biogenesis is functional. Although mutants of the piRNA pathway did not show any sterile phenotype in females, a decrease in TE-derived piRNA population associated with upregulation of IAP and LINE1 elements was

observed in *Mili* mutant primordial oocytes (Lim, Lorthongpanich et al. 2013). Despite the upregulation of retrotransposons does not lead to sterility, increased LINE1 expression can reduce ovarian follicle reserves and increase the oocyte aneuploidy and embryonic lethality (Malki, van der Heijden et al. 2014)

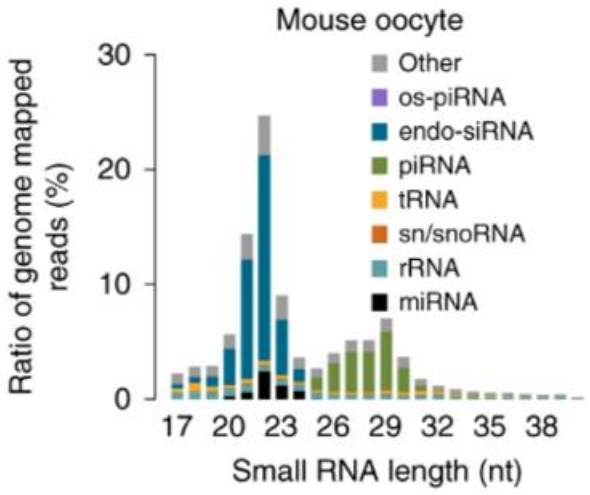

Figure 7: *Next-generation single-cell sequencing of small RNAs from mouse oocytes showing the distribution of different populations of small RNAs. Although piRNAs are present, endo-siRNAs represent the most abundant population of small RNAs in mouse oocytes. Adapted from (Yang, Li et al. 2019).*

Compared to other mammals, mouse oocytes express high levels of siRNAs. The RNAi pathway utilizing siRNA regulates numerous targets, including retrotransposons. The piRNA pathway is partially redundant with the RNAi pathway, for example in silencing of LINE1 retrotransposons (Taborska, Pasulka et al. 2019). The mutant of both pathways showed an increased number of LINE1 transcripts, but no augmented transcriptional or transposable activity was observed, suggesting that another retrotransposon suppression mechanism is present. In any case, these two pathways are partially redundant, because they share common targets in mouse oocytes (Taborska, Pasulka et al. 2019).

An interesting question remains whether highly active RNAi in mouse oocytes can partially serve as a substitute for requirements of piRNA pathway function in the female germline. Also, as noted above, unlike most other mammals encoding four PIWI proteins, the mouse genome lacks *Piwil3* (Mouse Genome Sequencing, Waterston et al. 2002). PIWIL3 is expressed in oocytes of other mammals, such as a golden hamster, cow, or human (Roovers, Rosenkranz et al. 2015, Tan, Tol et al. 2020, Ishino, Hasuwa et al. 2021). Thus, the presence of

RNAi and/or the absence of PIWIL3 in mouse oocytes may be a contributing factor to the insignificance of the piRNA pathway in the female mouse germline.

2 Aim of the study

For more than a decade, there has been a general opinion that piRNA function may be dispensable for mammalian female germline. This view has been supported by numerous mouse piRNA pathway mutants with full fertility in females. piRNAs and retrotransposons have been analyzed in many mammalian species, but all *in vivo* mechanistic studies have been using the mouse model because of its accessibility to genetic manipulations. However, mice have evolved specific adaptations to small RNA pathways. Highly active RNAi in mouse oocytes and the absence of PIWIL3, one of the four PIWI proteins found in mammals, distinguish mice from the majority of other mammals, including humans.

It has to be clarified whether or not the piRNA pathway is essential for mammalian female germline or whether it is a mouse-specific attribute. My thesis aimed to analyze the function of the piRNA pathway in an alternative model organism that would better represent mammalian small RNA pathways. With the presence of PIWIL3 protein and likely lacking highly active RNAi in oocytes, the golden hamster appeared to be a suitable model organism for studying the significance of the piRNA pathway in mammals. The specific objectives of this study were divided into five main parts, which also correspond to the division of section 4 Results:

1. Establishment of golden hamster as a model for the piRNA pathway: Analysis of the piRNA pathway machinery and piRNA populations

2. Analysis of retrotransposons in the golden hamster genome*:* Analysis of young retrotransposon families and full-length intact copies of retrotransposons

3. Generation of golden hamster piRNA pathway mutant: Generation of golden hamster *Mov10l1* mutant, analysis of the mutation and lineage establishment

4. Analysis of the female germline in golden hamster Mov10l1 mutant: Determination of potential defect in female *Mov10l1* hamster mutants and its analysis

5. Analysis of the male germline in golden hamster Mov10l1 mutant: Determination of potential defect in male *Mov10l1* hamster mutants and its analysis

3 Materials and methods

Animals

Golden hamsters were purchased from Japan SLC and Janvier Labs and all animal experiments were approved by the Animal Experimentation Committee at the RIKEN Tsukuba Institute (T2019-J004) and the Institutional Animal Use and Care Committee at the Institute of Molecular Genetics of the Czech Academy of Sciences (approval no. 42/2016 and 70/2018) and were carried out in accordance with the law. Animals were maintained under 12 hours of light and 12 hours of dark periods.

Generation of *Mov10l*-deficient golden hamsters

The sgRNAs targeting intron 19 and 21 (5′-GGGTATCACATGACTTGGGG-3′; 5′-GGTGTTGGGATCATAGTGGGG-3′ and 5′-TCTCCACTCTTCCATGTGGGG-3′; 5′-TACCATTACATTTGTCAGGGG-3′, respectively) were injected together with Cas9 protein into the oviducts of pregnant females, and electrical pulses were immediately applied to the oviducts using a forceps-like electrode (Gurumurthy, Sato et al. 2019, Hirose, Honda et al. 2020).

Establishment of *Mov10l1*-deficient hamster lines

Two heterozygous founders were used for subsequent breeding with WT animals to establish the hamster lines. The heterozygous male did not transmit the mutated allele. The heterozygous female transmitted the allele to 7 of 10 progeny and these were used for subsequent breeding to establish the population.

Animal genotyping

Ear biopsies were lysed in a PCR-friendly buffer with proteinase K (0,6U per sample) (Thermo Fisher Scientific) at 55°C with constant shaking for 2 hours. Samples were then incubated at 90°C for 10 min to deactivate proteinase K. The lysate was used as a template for nested PCR reaction detecting deletion and the presence of exon 20 with the following primers:

1st round	P1 fwd	CTAAGCTACCAGGTGGTTCTCAG
	P2 rev	AGATGATAATCCACACCACTGTCC
2nd round_deletion	P3 fwd	CAGAATACCAGCTGCTGATAGGG
	P2 rev	AGATGATAATCCACACCACTGTCC
2nd round_ex20	P5 fwd	CATGTATTTGTGGACGAGGCAGG
	P6 rev	GACACTCAGAATTGGAGGAGCTG

The PCR product of the deletion region was used for Sanger sequencing to define the exact deletion. The *Mov10l1* mutant allele showed a deletion of 761 bp.

Oocyte and zygote collection

Fully-grown GV oocytes were isolated by puncturing the antral follicles of hamster ovaries and were collected into M2 media containing 0.2 mM 3-isobutyl-1-methyl-xanthine preventing the resumption of meiosis. They were then washed from cumulus cells by repeated pipetting using glass capillaries. Female golden hamsters were superovulated with 15IU to 25IU (based on the bodyweight) pregnant mare´s serum gonadotropin (ProSpec Bio) on the first day of the estrous cycle. They were subsequently injected with 25IU hCG (Sigma-Aldrich) 76h later and eventually mated on the same day with males with proven fertility. MII oocytes were released from the oviductal ampulla of superovulated females 17h after hCG injection without mating. They were incubated in M199TE medium (HEPES, sodium bicarbonate, and Eagle´s salts, Gibco; heat-inactivated (30 min, 56°C) 5% fetal bovine serum, Sigma-Aldrich;5 mM taurine; 25 µM EDTA) containing 0.1% bovine testes hyaluronidase (Sigma-Aldrich) for 1 min at 37°C to wash out the cumulus cells. 2-cell zygotes and 4/8-cell embryos were collected by flushing oviducts 40h and 61h after mating, respectively. Because golden hamster oocytes and zygotes appeared to be sensitive to light and manipulation, isolation was performed as quickly as possible with a red filter on the microscope light source and an equilibrated (5% CO_2, 5% O_2, 90% N_2) M199TE medium kept under paraffin oil.

Western blotting

Tissues were lysed in RIPA buffer containing a 1x protease inhibitor cocktail set (Millipore). 60 µg of protein/lane measured by the Bradford assay and mixed with SDS dye was loaded on 6% polyacrylamide gel and transferred onto a polyvinylidene difluoride membrane (Millipore) using semi-dry blotting. 5% skim milk diluted in TTBS buffer was used to block the membrane and MOV10L1 was detected using an anti-MOV10L1 primary antibody (Zheng, Xiol et al. 2010) (a gift from J. Wang) diluted 1:250 and incubated overnight at 4°C. The protein was then detected using an anti-rabbit-HRP secondary antibody (Thermo Fisher Scientific) diluted 1:50 000 and SuperSignal West Femto Substrate (Thermo Fisher Scientific). Samples for TUBA4A detection were loaded onto 10% polyacrylamide gel and anti-Tubulin (Sigma-Aldrich, T6074) primary antibody diluted 1:10 000 (overnight at 4°C) and anti-mouse-HRP secondary antibody (Thermo Fisher Scientific) diluted 1:50 000 were used.

RT-PCR analysis

Five to ten oocytes or embryos were collected into 3 µl of PBS and snap-frozen in liquid nitrogen. An equal number of oocytes/embryos was used for individual experiments. Samples were lysed by adding 3 µl of lysis buffer (Shatzkes, Teferedegne et al. 2014) and used for reverse transcription using SuperScript III RT (Thermo Fisher Scientific) according to the manufacturer´s instructions. cDNA was amplified using ExTaqHS (TaKaRa) with the following primers:

maActb_RT_F	GTCGTACCACTGGCATTGTGATG
maActb_RT_R	CTTCATGAGGTAGTCTGTCAGGTCC
maHprt_RT_F2 (oocyte/embryo RT)	GGAGACGATCTCTCAACTTTAACTG
maHprt_RT_R	TCCAACACTTCGAGAGGTCC
maMov10l1_RT_F2	GGAGCACTCTTACTGATAAACAAAGG
maMov10l1_RT_R2	AATTGTTGTGCTTTATCCCAGCC
maPiwil1_RT_F1	AGAACCTTGACCATGTCAAAGAGTC
maPiwil1_RT_R1	GGTCTTCATGCTGGAAGAGCAG
mmPiwil2_RT_F1	TATCGCTGTTACCACTGGGAAG
mmPiwil2_RT_R1	TGTTCCTTTTGATCCTTGCTTGAC
maPiwil3_RT_F2	TGTCAGTAAGACTGAAGGTGATGAC
maPiwil3_RT_R2	TGAGTTTTCTGAGACTGGAATCGC
maPiwil4_RT_F2	ACTTTGTCTGACCTAAATCAGCCC
maPiwil4_RT_R2	ATCAGGTGGAAATCCGAGGTTG

PCR products were then run on 1,5% agarose gel and visualized using ethidium bromide.

RNA was isolated from whole testes using the mirPremier microRNA isolation kit (Sigma Aldrich) according to the manufacturer's protocol. RNA was then treated with Turbo DNAse (Invitrogen) for 30 min at 37°C and reverse transcribed using LunaScript RT SuperMix Kit (New England Biolabs) according to the manufacturer´s instructions. qPCR reaction was performed with a 0.5 µl cDNA aliquot, the Maxima SYBR Green qPCR master mix (Thermo Fisher Scientific) and the following primers:

maDmrtb1_F1	CGTCTCCTGTAGCCCCTACCATG
maDmrtb1_R1	CTTTTCACCAGCAAGCTTGCAAC
maDdx4_F1	GTGCTCAAACAGGGTCTGGGAAGA
maDdx4_R1	GACAACAGCTCTTACACAAGTCCC
maKif5c_F1	CCTATGTAAAGGGGTGCACCGAGA
maKif5c_R1	GATACTGTGACTCCTCGAGCTGTG

maIAP3_gag-123F	GTCCATCTGGTGCTGTCAGTCTG
maIAP4_gag-70F	CTGTCAGTCTGGTGCTCGTCAGTC
maIAP3/4_gag+13_R	CTGTAGGGCAGTAACCACTGACTG
maL1_ORF1+1222_F	TCCAGGACCTTCTGGCTTTCAGAG
maL1_ORF1+1069_R	CCTCGCCACATAATAATCAAGACCC
maMySERV_ORF1_F1	ATAGAGGCATGGGTAGGGAAGGCA
maMySERV_ORF1_R1	CTGCATAGACCAGGAGGCTTAGGC
maHPRT_F1	AGACGATCTCTCAACTTTAACTGG
maHPRT_R1	CTTTTCACCAGCAAGCTTGCAAC
maB2MG-F2	GCGACTGATAAATACGCCTGCAGA
maB2MG-R2	CTGATCCAAATGAAGCATCTCCATG

Average Ct values of the technical replicates were normalized to the housekeeping genes maHPRT and maB2MG using the ΔΔCt method (Pfaffl, Horgan et al. 2002).

Fluorescence-activated cell sorting

Testes were isolated from WT animals and *tunica albuginea* was removed. Testes were then incubated in freshly prepared collagenase solution (Hank´s balanced salt solution (HBSS) without calcium or magnesium prepared in the house + 1 mg/ml collagenase + 1:1 000 DNAse I, Fermentas) for 7 min at 35°C with gentle agitation. After 3 min of this period, gentle pipetting with Pasteur pipette was used to assist with tubule dispersion. The tube was then left for 2 min at room temperature to allow tubules to settle to the bottom and supernatant containing somatic cells from the testicular interstitium was removed. 1 ml of freshly prepared collagenase/trypsin solution (Hank´s balanced salt solution without calcium or magnesium prepared in the house + 1 mg/ml collagenase + 1:1 000 DNAse I, Fermentas + 0,05% trypsin) was added to the tube followed by the incubation for 20 min at 35°C with gentle agitation and additional pipetting using Pasteur pipette every 5 min. After 10 min of this period, 8 ul of 2,5% trypsin and 1 µl of DNAse I stock (only if the solution looked overly viscous) were added and the digestion reaction was quenched using 400 µl of fetal bovine serum (FBS) at the end of the incubation period. The cell suspension was then centrifuged for 5 min at 2 000 g, resuspended in 500 µl HBSS with 1% FBS and 20 µl of this suspension was used as a negative control for FACS sorting. The rest was centrifuged for 5 min at 2 000 g and resuspended in 100 µl of 3% FBS in HBSS containing the c-kit-PE-Cyanine7 (dilution 1:100, 25-1171-82, Thermo Fisher) and CD9-FITC (dilution 1:20, MA51686, Thermo Fisher) antibodies. The suspension was incubated with antibodies for 20 min on ice, centrifuged for 5 min at 2 000 g (4°C), washed in 3% FBS in HBSS, centrifuged for 5 min at 2 000 g (4°C), and resuspended in cold HBSS/1%

FBS containing 10 µg/ml Hoechst dye. The suspension was then kept on ice until sorting. Immediately before sorting, cells were passed through a 40 µm membrane and stained with propidium iodide to exclude nonviable cells.

Histology and immunofluorescence staining of histological sections

Tissues used for histology were fixed in Hartmann´s fixative (Sigma Aldrich, H0290) or 4% paraformaldehyde in PBS for 1,5 h or overnight at 4°C, followed by ethanol dehydration and paraffin embedding. Paraffin blocks were then cut into 2,5-6 µm sections and used for hematoxylin and eosin or immunofluorescence staining.

Sections for immunofluorescence staining were deparaffinized and boiled in 10 mM sodium citrate buffer (pH 6) for 18 min to retrieve antigens. Sections were then blocked in PBS with 5% normal donkey serum and 5% bovine serum albumin (BSA) and incubated for 1h at room temperature or overnight at 4°C with following primary antibodies: anti-LINE1 ORF1p (diluted 1:200, provided by D. O'Carroll, University of Edinburgh); anti-SCP3 (diluted 1:200, Abcam, ab976672); anti-ZBTB16 (diluted 1:200, Atlas antibodies, HPA001499); anti-ɣH2AX (diluted 1:200, Millipore, 05-636); anti-MOV10L1 (diluted 1:250, a gift from J. Wang); anti-DDX4 (diluted 1:400, Abcam, ab27591 and ab13840); anti-WT1 (diluted 1:400, Novus Biologicals, NB110-60011); anti-IAP GAG (diluted 1:500, a gift from B. R. Cullen). Samples were then incubated with anti-mouse and anti-rabbit secondary antibodies conjugated with Alexa 488/594 (diluted 1:500, Thermo Fisher Scientific) for 1h at room temperature and stained with DAPI (diluted 1:1000, Sigma, D9542-10MG) for 10 min. Slides were mounted in ProLong Diamond Antifade Mountant (Thermo Fisher Scientific) and images were acquired using the DM6000 or Leica Sp8 confocal microscope.

Immunofluorescence staining of oocytes and zygotes

Samples were (immediately after collection) fixed and permeabilized in 0,2% Triton-X100 in 4% paraformaldehyde for 30 min at room temperature. They were then incubated in a blocking solution (2% BSA in PBS) for 1h or overnight at 4°C. They were then stained with anti-Tubulin (diluted 1:100, Abcam, ab7750), anti-IAP GAG (diluted 1:200, a gift from B. R. Cullen), anti-LINE1 ORF1p (diluted 1:200, provided by D. O'Carroll, University of Edinburgh) or anti- γH2AX (diluted 1:100, Millipore) for 1h at room temperature or with H3K9me3 (diluted 1:1000, Upstate, 07-442) and H3K9Ac (diluted 1:1000, Upstate, 07-352) overnight at 4°C. Samples were incubated with anti-mouse and anti-rabbit secondary antibodies conjugated with Alexa 488/594 (diluted 1:500, Thermo Fisher Scientific) for 1h at room temperature and

stained with DAPI (diluted 1:1000, Sigma, D9542-10MG) for 10 min. Images were collected using an SP8 confocal microscope and processed by LAS AF LITE 3.3 software (Leica). Imaris v.9.6 (Bitplane) was used to analyze the spindle properties of MII oocytes by three-dimensional reconstruction of images from confocal optical sections.

Total RNA sequencing

For RNA sequencing of oocytes, six to twelve fully-grown oocytes were collected into 2 µl drop of 0,2% Polyvinylpyrrolidone in PBS, mixed with 50 µl of extraction buffer provided in Arcturus Picopure RNA isolation kit (Thermo Fisher Scientific), and incubated for 30 min at 42°C. Arcturus Picopure RNA isolation kit was then used according to the manufacturer´s instructions to isolate RNA. Ovation RNA-Seq System V2 (NuGEN) followed by the Ovation Ultralow Library system (DR Multiplex System, NuGEN) were then used according to the manufacturer's protocol to prepare libraries for sequencing. The fragmentation of cDNA was performed using the Bioruptor sonication device (Diagenode) with 18 cycles of the 30s on and 30s off at low intensity. 9 PCR cycles were used to amplify libraries and 100-nucleotide single-end reading using the Illumina NovaSeq6000 platform was used for sequencing.

For RNA sequencing of testes samples, RNA was isolated from hamster testes using the mirPremier microRNA isolation kit (Sigma-Aldrich) according to the manufacturer's protocol. Ribo-Zero rRNA Removal Kit (Human/Mouse/Rat) (Epicentre) and the QIAseq FastSelect–rRNA HMR Kit (Qiagen) were used according to the manufacturer's protocols to remove ribosomal RNA, which was confirmed by 2100 Bioanalyzer (Agilent Technologies) analysis. NEBNext Ultra II Directional RNA Library Prep kit for Illumina (BioLabs, E7765S) was used to prepare libraries for sequencing according to the manufacturer´s protocol. Samples from an adult, 21 dpp and 13 dpp old hamsters were sequenced using 150-nucleotide paired-end reading, while samples from 9 dpp and newborn hamsters were sequenced using the 75-nucleotide single-end reading from the Illumina NextSeq500/550 platform.

Small RNA sequencing

At least five oocytes per sample were collected into 10 µl of water and incubated for 3 min at 70°C to release small RNAs. NextFlex Small-RNA-seq v3 kit (Amplicon) was used according to the manufacturer's protocol to prepare libraries for sequencing. Samples were then separated on 2,5% agarose gel using lithium borate buffer and bands corresponding to the size of 140-170 nt were cut off the gel. MinElute Gel Extraction Kit (Qiagen) was used to extract

DNA from the gel and 75-nucleotide single-end reading was used to sequence libraries with Illumina NextSeq500/550 platform.

For small RNA sequencing of testes, RNA was isolated from hamster testes using the mirPremier microRNA isolation kit (Sigma-Aldrich) according to the manufacturer's protocol. NextFlex Small-RNA-seq v3 kit (Amplicon) was used according to the manufacturer's protocol to prepare libraries for sequencing. NextFlex beads were used for size selection or samples were separated on 2,5% agarose gel using lithium borate buffer and bands corresponding to the size of 140-170 nt were cut off the gel and DNA was extracted using the MinElute Gel Extraction Kit (Qiagen). Libraries were sequenced using the 75-nucleotide single-end reading from the Illumina NextSeq500/550 platform or the 100-nucleotide single-end reading from the NovaSeq6000 platform.

Total RNA and small RNA sequencing depository

Raw data were deposited at the Gene Expression Omnibus (GEO: GSE164658).

Bisulfite sequencing

Ten fully-grown oocytes per sample were directly processed by the EZ DNA Methylation-Direct kit (Zymo Research) for bisulfite conversion. Following modifications were applied to the protocol: samples were digested using proteinase K for 35 min at 50°C and the program for bisulfite conversion was as follows: 98°C for 6 min, 64°C for 30 min, 95°C for 1 min, 64°C for 90 min, 95°C for 1 min and 64°C for 90 min. EpiNext Post-Bisulfite DNA Library Preparation kit was used to prepare libraries according to the manufacturer's protocol, which were sequenced using the 250-nucleotide paired-end sequencing from the Illumina NovaSeq6000 platform.

Bioinformatic analyses

All RNA sequencing data were analyzed by Filip Horvat and Josef Pasulka.

RNA-sequencing data analysis

STAR v.2.7.3a (Dobin, Davis et al. 2013) was used to map raw RNA sequencing data to mouse (mm10), human (hg38), cow (bosTau9), rat (rn6), golden hamster (mesAur1) and the newest golden hamster (PRJDB10770)(Ishino, Hasuwa et al. 2021) genomes with the following parameters optimized for quantification of transposable elements (Teissandier, Servant et al. 2019):

```
STAR --readFilesIn $ {FILE}.fastq.gz --genomeDir $ {GENOME_INDEX} --
runThreadN 12 --genomeLoad LoadAndRemove --limitBAMsortRAM 20000000000 --
readFilesCommand unpigz -c --outFileNamePrefix $ {FILENAME} --outSAMtype BAM
SortedByCoordinate --outReadsUnmapped Fastx --outFilterMultimapNmax 5000 --
winAnchorMultimapNmax 5000 --seedSearchStartLmax 30 --
alignTranscriptsPerReadNmax 30000 --alignWindowsPerReadNmax 30000 --
alignTranscriptsPerWindowNmax 300 --seedPerReadNmax 3000 --seedPerWindowNmax
300 --seedNoneLociPerWindow 1000 --outFilterMultimapScoreRange 0 --
outFilterMismatchNoverLmax 0.05 --sjdbScore 2
```

featureCounts v.2.0.0 (Liao, Smyth et al. 2014) was used for analysis of expression of protein-coding genes mapped to mesAur1 with maximum of 20 multimapping alignments allowed and counted over exon features annotated by Ensembl (release 99):

```
featureCounts -a $ {FILE}.gtf -o $ {FILE}.counts.txt $ {FILE}.bam -T 12 -F
GTF -M -O –fraction
```

-p flag and -s 2 flag were added for the pair-end and stranded libraries, respectively. R (https://www.R-project.org/) using DESeq2 package (Love, Huber et al. 2014) was used for analysis of fold changes in gene expression and statistical significance used adjusted *P* values smaller than 0,01. Principal component analysis used regularized logarithm (rlog) function performed on counts data.

Datasets used for the heatmap showing the expression of individual piRNA pathway components were as follows: bovine oocyte GSE52415 (Graf, Krebs et al. 2014), bovine testis PRJNA471564 (Gao, Li et al. 2019), human oocyte GSE72379 (Hendrickson, Dorais et al. 2017), human testis GSE74896 (Jegou, Sankararaman et al. 2017), mouse oocyte GSE116771 (Horvat, Fulka et al. 2018), mouse testis GSE49417 (Yue, Cheng et al. 2014), rat oocyte GSE137563 (Ganesh, Horvat et al. 2020) and rat testis GSE53960 (Yu, Zhao et al. 2014).

Small RNA sequencing data analysis

bbduk.sh v.38.87 (https://jgi.doe.gov/data-and-tools/bbtools/) was used to trim small RNA sequencing reads. The NextFlext adapter was trimmed as follows:

```
bbduk.sh -Xmx20G threads=6 in=$ {FILE}.fastq.gz out=$ {FILE}.atrim.fastq.gz
literal= TGGAATTCTCGGGTGCCAAGG stats=$ {FILE}.atrim.stats overwrite=t
ktrim=r k=21 rcomp=f mink=10 hdist=1 minoverlap=8
```

Four random nucleotides were then trimmed from both sides of reads, because of the NextFlex kit using randomized adapters.

```
bbduk.sh -Xmx20G threads=6 in=$ {FILE}.atrim.fastq.gz out=$
{FILE}.trimmed.fastq.gz stats=$ {FILE}.ftrim.stats overwrite=t
forcetrimright2=4 forcetrimleft=4 minlength=18
```

In the case of small RNA sequencing from oocytes, libraries were first deduplicated from PCR duplicates and then subjected to random nucleotides trimming. For deduplication, both UMI sequences (four random nucleotides from each side of the read) were added to the read header using custom scripts (available at https://github.com/fhorvat) and then removed from the read sequence with Cutadapt v.2.10 (Martin 2011).

```
cutadapt -u 4 -o ${FILE}.trim_1.fastq -j 6 ${FILE}.umi.fastqcutadapt -m 18 -
u -4 -o ${FILE}.trim_2.fastq -j 6 ${FILE}.trim_1.fastqTrimmed reads were then
mapped to the new golden hamster genome using STAR 2.7.3a:STAR --readFilesIn
$ {FILE}.dedup.fastq.gz --genomeDir $ {GENOME_INDEX} --runThreadN 12 --
genomeLoad LoadAndRemove --limitBAMsortRAM 20000000000 --readFilesCommand
unpigz -c --outFileNamePrefix $ {FILENAME} --outSAMtype BAM
SortedByCoordinate --outReadsUnmapped Fastx --outFilterMismatchNmax 1 --
outFilterMismatchNoverLmax 1 --outFilterMismatchNoverReadLmax 1 --
outFilterMatchNmin 16 --outFilterMatchNminOverLread 0 --
outFilterScoreMinOverLread 0 --outFilterMultimapNmax 5000 --
winAnchorMultimapNmax 5000 --seedSearchStartLmax 30 --
alignTranscriptsPerReadNmax 30000 --alignWindowsPerReadNmax 30000 --
alignTranscriptsPerWindowNmax 300 --seedPerReadNmax 3000 --seedPerWindowNmax
300 --seedNoneLociPerWindow 1000 --outFilterMultimapScoreRange 0 --
alignIntronMax 1 --alignSJDBoverhangMin 999999999999
```

The deduplication of reads was performed on mapped.bam files using UMI tools v.1.1.1 (Smith, Heger et al. 2017).

```
umi_tools dedup --method=directional --multimapping-detection-method=NH -I
${FILE}.trim_1.fastq --output-stats=${FILE}.dedup_stats --
log=${FILE}.dedup_log.txt -S ${FILE}.dedup.bam.
```

And final files were then generated using samtools v.1.10 (Li, Handsaker et al. 2009):

```
samtools fastq -@ 12 ${FILE}.dedup.bam > ${FILE}.dedup.fastq
```

Mapping of reads to genomes was performed as follows:

```
STAR --readFilesIn $ {FILE}.fastq.gz --genomeDir $ {GENOME_INDEX} --
runThreadN 12 --genomeLoad LoadAndRemove --limitBAMsortRAM 20000000000 --
readFilesCommand unpigz -c --outFileNamePrefix $ {FILENAME} --outSAMtype BAM
SortedByCoordinate --outReadsUnmapped Fastx --outFilterMismatchNmax 1 --
outFilterMismatchNoverLmax 1 --outFilterMismatchNoverReadLmax 1 --
outFilterMatchNmin 16 --outFilterMatchNminOverLread 0 --
outFilterScoreMinOverLread 0 --outFilterMultimapNmax 5000 --
winAnchorMultimapNmax 5000 --seedSearchStartLmax 30 --
alignTranscriptsPerReadNmax 30000 --alignWindowsPerReadNmax 30000 --
alignTranscriptsPerWindowNmax 300 --seedPerReadNmax 3000 --seedPerWindowNmax
300 --seedNoneLociPerWindow 1000 --outFilterMultimapScoreRange 0 --
alignIntronMax 1 --alignSJDBoverhangMin 999999999999
```

piRNA cluster analysis

To analyze piRNA clusters, 24-31nt reads were counted with fractional counts and normalized to 19-32nt fraction (RPM). RPMs were then normalized to the length of windows (without counting gaps in assembly) into RPKM values. This was done for each 1 kb window into which the genome was divided and windows with RPKM < 1 were removed. Neighboring

tiles were merged if their log2-transformed fold changes of RPKMs (KO vs WT) were lower than -2. This was done for pre-pachytene clusters in samples from 9 and 13 dpp hamster testes and for pachytene clusters in samples from 21 dpp hamster testes. For pachytene clusters, tiles included in this analysis had to also have log2-transformed fold changes of RPKMs (KO/WT) at 13 dpp higher than −2. Superclusters were generated as a merge of clusters, which were at most 2 kb apart. Only pre-pachytene and pachytene clusters having small RNA densities of more than 10 RPM and 100 RPM per kilobase, respectively, were selected for the piRNA cluster feature analysis.

For oocyte piRNA cluster analysis, the same conditions described above were used, except that the alignments of previously described PIWIL1 and PIWIL3-associating small RNAs (Ishino, Hasuwa et al. 2021) were used for counting. Only clusters having small RNA density (excluding 21-23 nt population including siRNA/miRNA) more than 10 RPMs were selected for further analysis.

Bisulfite sequencing

Bisulfite sequencing reads were first trimmed as follows:

```
bbduk.sh -Xmx20G threads=12 in1=$ {FILE}_1.txt.gz in2=$ {FILE}_2.txt.gz
out1=$ {BASE}_1.trim.txt.gz out2=$ {BASE}_2.trim.txt.gz outs=$
{BASE}_s.trim.txt.gz stats=$ {BASE}.stats literal=AGATCGGAAGAGC overwrite=t
ktrim=r k=12 rcomp=t mink=8 hdist=1 minoverlap=8 minlength=25 minlength=50
tbo
```

and then mapped to the genome using Bismark (Krueger and Andrews 2011):

```
bismark --non_directional --parallel 4 --unmapped --output_dir. --temp_dir.-
-genome_folder $ {BISMARK_INDEX } -1 $ {FILE}_1.trim.txt.gz -2 $
{FILE}_2.trim.txt.gz $ {FILE}_s.trim.txt.gz
```

The deduplicate_bismark script was used to remove duplicated reads generated during PCR amplification and bismark_methylation_extractor was used to analyze methylation in individual cytosines. For analysis of methylation in the consensus sequence of IAP elements, reads were first mapped to the genome and reads mapping to FLI IAP elements were then mapped to the consensus sequence of FLI IAP elements.

Other analysis

The clusterProfiler (Yu, Wang et al. 2012) (R package) was used for gene ontology annotation analysis.

Only primary alignments were used for the sequence logo analysis (Wagih 2017). The reads with aligned first nucleotide were selected and those which were 25-31 nt long and mapped to the piRNA clusters were used.

4 Results

4.1 Golden hamster as a model for the piRNA pathway

The piRNA pathway is a key small RNA pathway silencing retrotransposons in the mammalian germline. Potentially active retrotransposons pose a threat to the genome, so it is important to understand how they are controlled and how they adapt to the host during evolution. piRNAs and retrotransposons were analyzed in several mammals, including mouse, rat, cow or human (Lau, Seto et al. 2006, Aravin, Sachidanandam et al. 2007, Roovers, Rosenkranz et al. 2015, Yang, Li et al. 2019). However, such analysis has been lacking in golden hamsters. Accordingly, the aims of this work included analyzing piRNA populations and retrotransposons in the golden hamster genome.

To determine the properties of the golden hamster piRNA pathway, expression levels of known components of the piRNA pathway in testes and oocytes were first examined. mRNA expression of piRNA pathway factors in golden hamsters germ cells was compared with publicly available datasets from other mammals, including mouse, rat, cow, and human. Expression profiling showed that all analyzed piRNA pathway components were present in testes of adult golden hamsters, including *Piwil4* (Fig. 8a), which was absent in testes of adult mice. PIWIL4 is a PIWI protein involved in *de novo* DNA methylation of retrotransposons in mouse gonocytes (Watanabe, Cui et al. 2018) and its presence implies that PIWIL4 may play a role in adult golden hamster testes. All components of the piRNA pathway were also expressed in golden hamster GV oocytes, except *Spocd1* and *Tdrd6* (Fig. 8a). SPOCD1 is a PIWIL4-associated protein that mediates *de novo* DNA methylation into the promoter region of young TEs in mouse testes (Zoch, Auchynnikava et al. 2020). It also appeared to be missing in oocytes from mammals other than mice (Fig. 8a), suggesting that maternal SPOCD1 expression is a mouse-specific feature. TDRD6 is a protein of the Tudor family of proteins, is required for normal spermiogenesis, and its loss in mice leads to aberrant regulation of miRNAs (Vasileva, Tiedau et al. 2009). *Tdrd6* was expressed in oocytes of all other animals analyzed, except the rat (Fig. 8a), indicating certain similarities between rat and golden hamster oocytes. As expected, *Piwil3* encoding for one of the four PIWI proteins described in mammals was expressed in human and bovine GV oocytes, but was absent in oocytes of mouse and rat (Fig. 8a), documenting a major difference in the piRNA pathway between mouse and rat and other mammals. Overall, the golden hamster genome encodes all described essential components of the piRNA pathway and their expression profile is more similar to that of cow and human than

to mouse and rat, primarily because of the loss of *Piwil3* in mouse and rat genomes. The expression profile of *Mov10l1* and *Piwi* genes in golden hamster testes and ovaries was confirmed by RT-PCR performed with primers specific for each gene (Fig. 8b). Consistent with PIWIL3 being described as an oocyte-specific factor (Roovers, Rosenkranz et al. 2015, Tan, Tol et al. 2020, Ishino, Hasuwa et al. 2021), RT-PCR data showed a lack of *Piwil3* RNA in hamster testes (Fig. 8b). A lack of *Piwil4* gene expression in RT-PCR from ovaries (Fig. 8b) may reflect PIWIL4 expression pattern, which is negligible throughout oocyte development in mice (Kabayama, Toh et al. 2017), and therefore its detection in a sample isolated from hamster adult ovaries may be poor. On the other hand, as noted above, *Piwil4* expression detected in transcriptomic data from hamster oocytes appears to be relatively abundant (Fig. 8a). The expression of *Piwil4*, together with the presence of PIWIL3 in golden hamster oocytes, suggests a different configuration of the piRNA pathway in golden hamsters and mice that separated from a common ancestor more than 20 million years ago (Steppan, Adkins et al. 2004) (Fig. 8c).

Unlike the protein components of the piRNA pathway, piRNA sequences themselves are not conserved among animals, reflecting the rapid response of the piRNA pathway to the evolving genome sequence and retrotransposon load. However, mammalian piRNAs should share common features originating from their biogenesis. Thus, the golden hamster piRNA populations were analyzed and their properties were examined. I decided to analyze piRNAs from hamster testes, because mammalian piRNA studies provide good comparative data for testicular piRNAs. Furthermore, while my thesis project was in progress, hamster ovarian piRNAs were analyzed in Haruhiko Siomi´s lab (Ishino, Hasuwa et al. 2021).

To analyze the properties of golden hamster testicular piRNAs, it was important to examine specific piRNA populations. Two different populations of piRNAs, called pre-pachytene and pachytene piRNAs, have been described in mice. They are distinguished based on the stage at which they are expressed and the genome regions to which they map (Aravin, Gaidatzis et al. 2006, Girard, Sachidanandam et al. 2006, Grivna, Beyret et al. 2006, Aravin, Sachidanandam et al. 2008). In hamsters on day 9 *post-partum* (dpp), gonocytes re-enter mitosis, start moving to the periphery of the seminiferous tubule and differentiate. Spermatogonia are formed by day 13 *post-partum* and on day 21 the germ cells reach the pachytene stage of meiosis I, so that a transition from the zygotene to pachytene stage can be observed (Miething 1998). Therefore, testes from 9 and 13 days old hamsters and testes from 21 days old hamsters were examined for pre-pachytene and pachytene piRNAs, respectively.

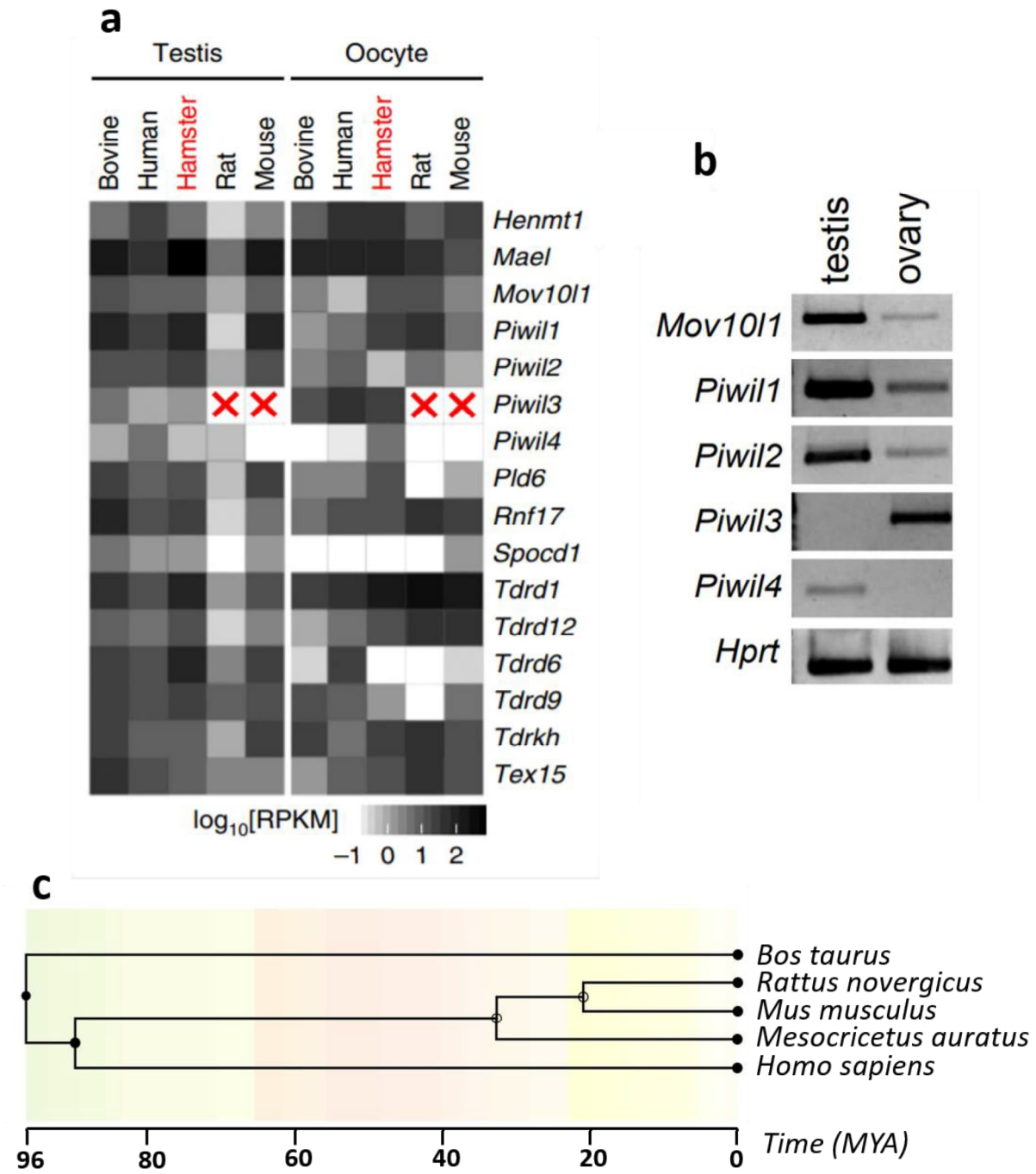

Figure 8: *Analysis of the piRNA pathway components in five different mammals. a) Heatmap generated from transcriptomes of five different species showing expression of piRNA pathway components in their testes and oocytes. RPKM, reads per kilobase per million. b) RT-PCR analysis of piRNA pathway genes in golden hamster testis and ovary. c) A phylogenetic tree showing the divergence of five mammals estimated over a million years of evolution using TimeTree (Kumar, Stecher et al. 2017). It is estimated in the literature that mice and rats diverged about 20 million years ago (Springer, Murphy et al. 2003), mice and hamsters separated 24 million years ago (Steppan, Adkins et al. 2004), rodents and humans separated about 80 million years ago (Springer, Murphy et al. 2003) and humans and cows separated more than 90 million years ago (Liu, Matukumalli et al. 2006). MYA, Million years ago. Modified from (Kumar, Stecher et al. 2017).*

First, I attempted to separate testicular germ cells from somatic cells to obtain cell-specific piRNA populations. Unfortunately, germ cell survival after fluorescence-activated cell sorting (FACS) on hamster testes was unacceptable. Hamster germ cells appeared to be more sensitive to manipulation than mouse germ cells. Hamster germ cells‘ sensitivity to manipulation was also confirmed by Atsuo Ogura (personal communication), an expert on golden hamster germ cell analysis. Another problem with FACS were commercial antibodies, such as c-Kit or CD9, typically used for sorting specific germ cell populations. They apparently did not recognize epitopes on the surface of hamster germ cells, as was indicated by the absence of a positive fluorescent signal during sorting (data not shown).

Thus, I had to overcome this issue by using whole testes from hamsters at different ages. As piRNAs are expected to be expressed specifically in germ cells, I decided to take advantage of the pioneering round of spermatogenesis, where specific populations of germ cells appear gradually at specific age of an animal. Accordingly, I isolated RNA from whole testes of 9, 13 and 21 days old hamsters containing different germ cell populations, as described above, and performed Next-generation sequencing (NGS) of small RNAs. Kits used to prepare small RNA libraries often face the problem of capturing 3′ methylated small RNAs due to the problematic ligation of the 3′ adapter and low efficiency of polyadenylation used for template-switching (Munafo and Robb 2010). This problem was solved using the NextFlex Small RNA-Seq Kit v3 from BIOO Scientific suitable for 3′ methylated small RNAs such as piRNAs, through the use of randomized adapters and polyethylene glycol (PEG), which increase ligation efficiency (Harrison and Zimmerman 1984) and reduce ligation bias (Sorefan, Pais et al. 2012, Zhang, Lee et al. 2013, Song, Liu et al. 2014). The great advantage of adapters using randomized bases is a more accurate composition of small RNA populations and recognition of duplicated reads generated during PCR amplification.

Small RNA sequencing analysis of hamster testes showed that pre-pachytene piRNAs are broadly dispersed along the genome and map to intergenic and genic regions in rather low levels (Fig. 9a, b). Pachytene piRNAs, on the other hand, were extremely abundant and mapped mainly to approximately 100 genomic loci with a coverage of more than 100 reads per million (Fig. 9a, b). The first 50 pachytene piRNA clusters yielded more than 90% of the population of 24-31 nt small RNAs. Many of the piRNA cluster loci were syntenic to mouse, cow and human loci, indicating conservation of mammalian piRNA clusters (Fig. 10). The length of many pre-pachytene and pachytene hamster clusters reached more than 60 kb (Fig. 9c). It is consistent

with mouse data, where most clusters in the mouse genome are within 100 kb, with the largest one reaching a length up to 356 kb (Gan, Lin et al. 2011).

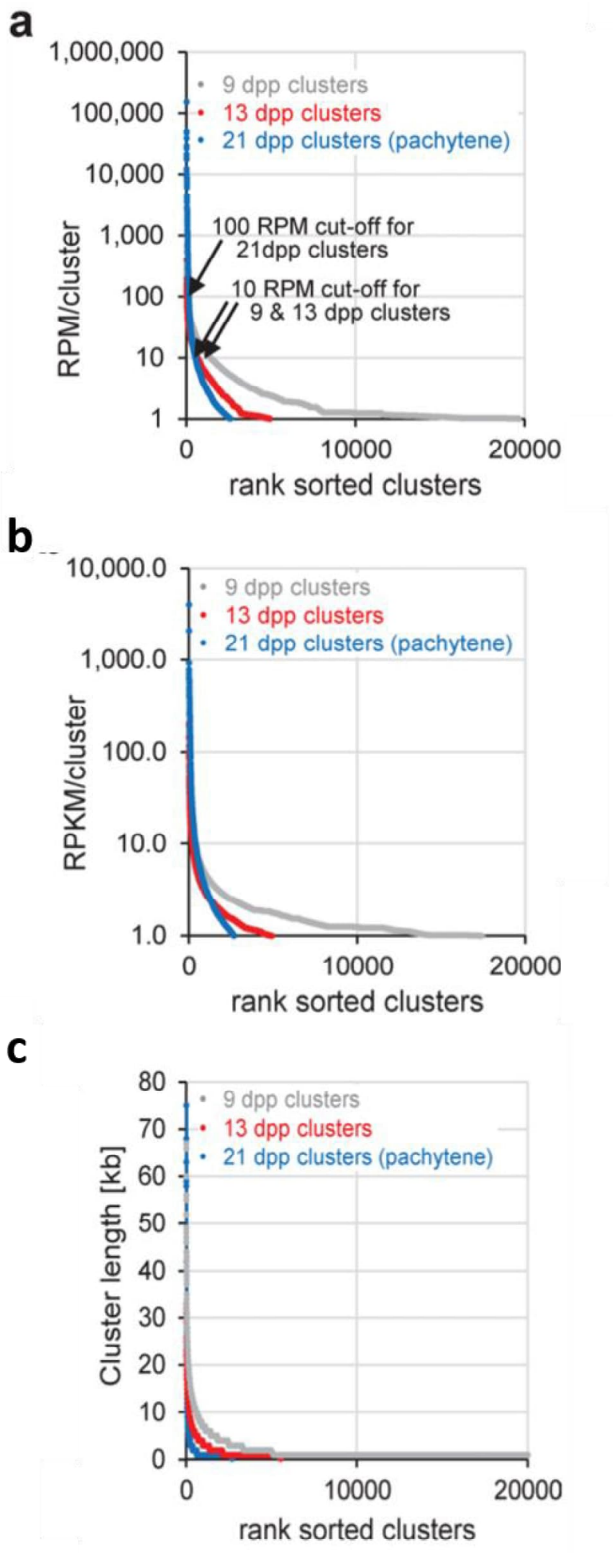

***Fig. 9**: Analysis of golden hamster piRNA clusters. a) Rank-sorted testicular piRNA clusters based on the number of small RNAs (RPM) per cluster, RPM, reads per million. b) Testicular piRNA cluster distribution based on average piRNA density (RPKM). c) Testicular piRNA clusters size. Kb, kilobase.*

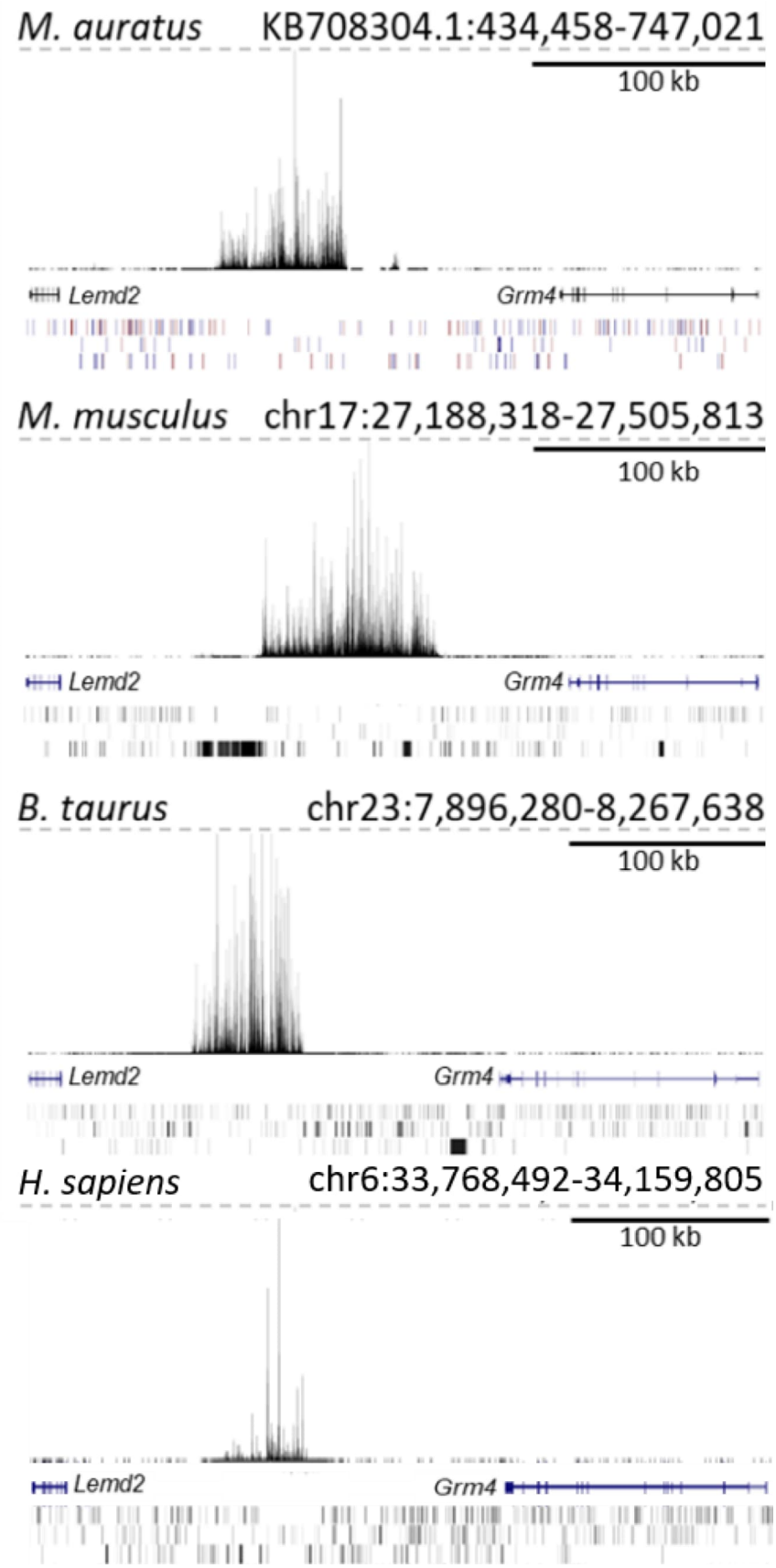

Fig. 10: *Snapshot from the UCSC browser showing an example of a syntenic locus generating pachytene piRNAs in hamster, mouse, cow and human.*

The low abundance of pre-pachytene piRNAs becomes apparent when compared to the expression level of 21-23 nt long miRNAs. The relative amount of pre-pachytene piRNAs decreases between 9 and 13 dpp stages of spermatogenesis, while the relative level of pachytene piRNAs bursts in 21 dpp testes (Fig. 11). Changes in the abundance of piRNAs in various stages of spermatogenesis are consistent with data from mice, where piRNA profiling during spermatogenesis shows analogous changes in the abundance of different piRNA populations (Li, Roy et al. 2013, Sun, Lee et al. 2021). It suggests similar regulation of piRNA levels during spermatogenesis in mice and hamsters. The length of hamster pre-pachytene piRNAs is 27-29 nucleotides, while pachytene piRNAs are 29-31 nt long (Fig. 11). The distinct length of piRNAs has been described as a result of the binding of specific PIWI proteins to RNAs of different lengths (Brennecke, Aravin et al. 2007). In mice, MILI which is expressed throughout the whole spermatogenesis binds piRNAs with an average length of 26 nt, MIWI2 interacts with pre-pachytene piRNAs with an average length of 28 nt, and MIWI associates with pachytene piRNAs whose length peaks at 30 nt (Girard, Sachidanandam et al. 2006, Aravin, Sachidanandam et al. 2007, Aravin, Sachidanandam et al. 2008). Thus, different lengths of hamster piRNA populations suggest that a similar regulation as in mice exists in hamsters. Moreover, pachytene piRNAs were not present in small RNA populations of golden hamster testes on days 9 and 13 (Fig. 12). This suggests that the pachytene-specific transcription factor regulates hamster pachytene piRNA expression similarly to mice, where transcription factor A-MYB drives pachytene piRNA expression in meiotic spermatocytes (Li, Roy et al. 2013).

Sequence analysis of pre-pachytene piRNAs confirmed the presence of 1U bias and a hallmark of the ping-pong mechanism, typical of secondary piRNAs, manifested by the enrichment of adenine at position 10 of the sequence logo (Fig. 13). Pachytene piRNAs also have 1U bias, but unlike pre-pachytene piRNAs, they lack adenine enrichment at position 10, suggesting the absence of the ping-pong mechanism (Fig. 13). This is again consistent with the properties of mouse testicular piRNAs (Aravin, Sachidanandam et al. 2008). Overall, hamster testicular piRNAs share common features with mouse piRNAs, suggesting that the piRNA biogenesis in golden hamsters works in the same way as in other mammals.

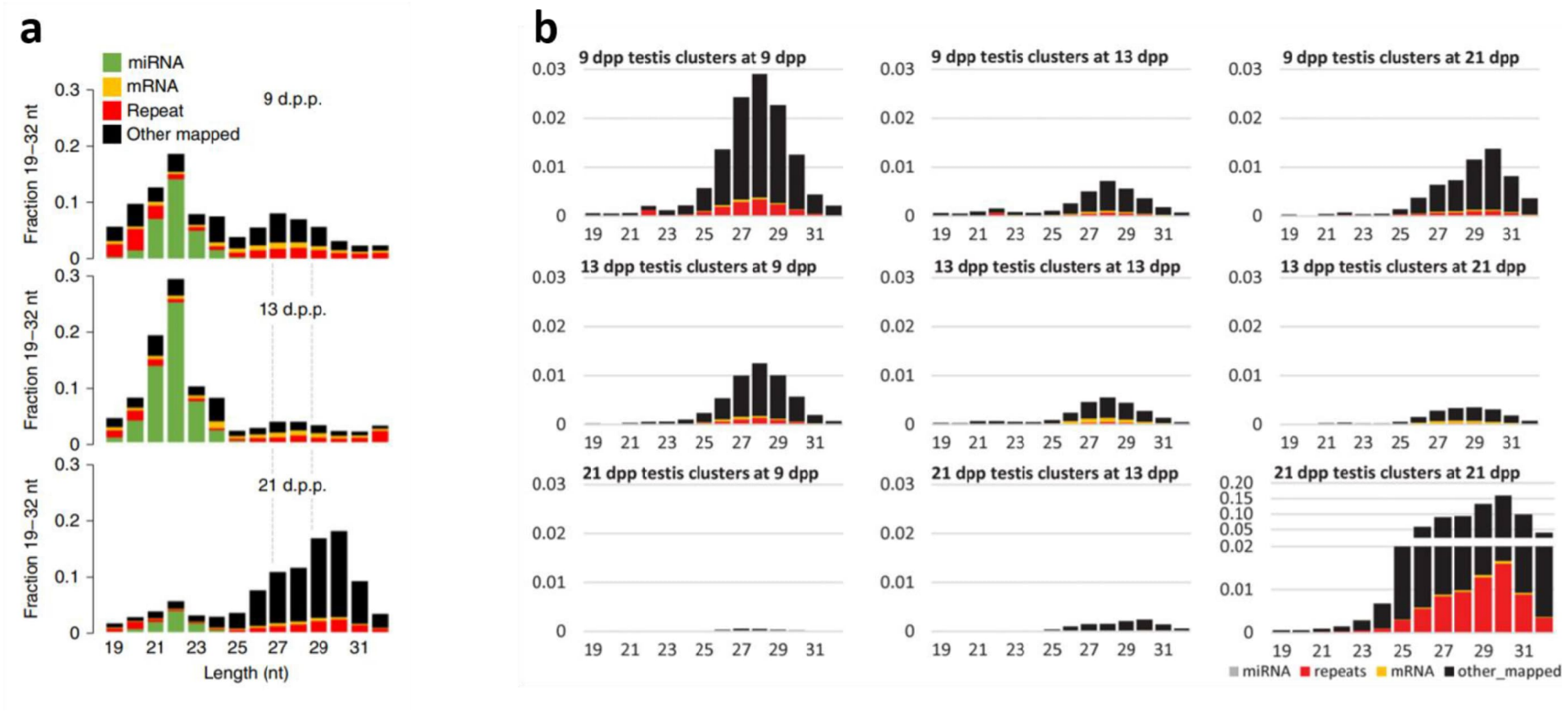

Figure 11: *Small RNA populations in golden hamster testes. a) Distribution of 19-32 nt testicular small RNAs based on length, origin and abundance at three different time-points of spermatogenesis. b) Distribution of 19-32 nt testicular small RNAs mapping to annotated piRNA clusters based on length, origin and abundance at three different time points of spermaotgenesis.*

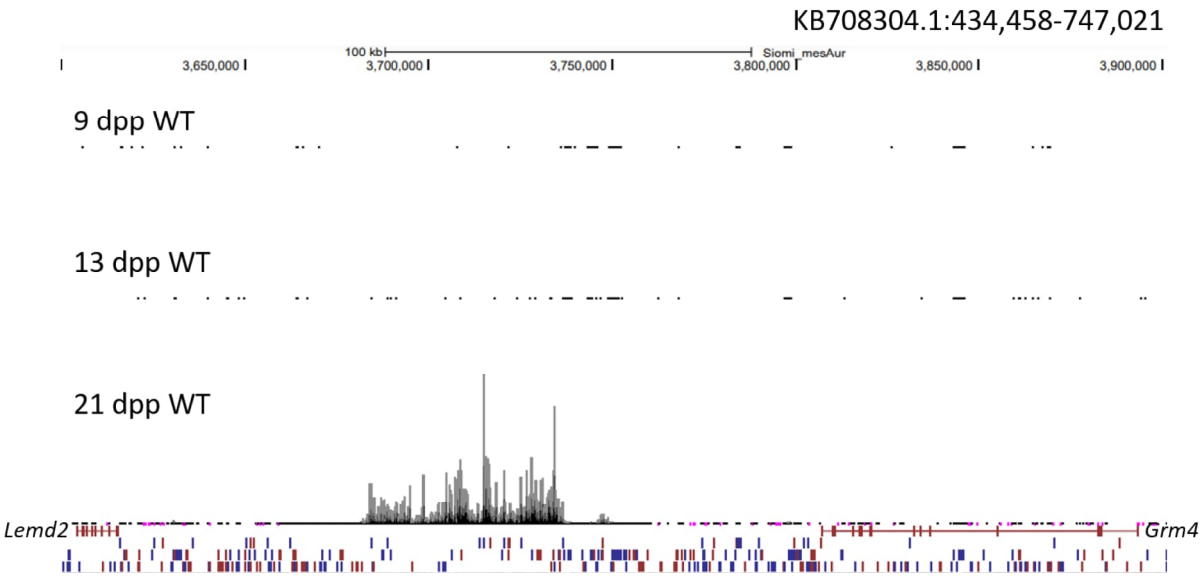

Figure 12: *Stage-specific expression of pachytene piRNAs. Snapshot from the UCSC browser showing the absence of pachytene piRNAs (24-31 nt RNAs normalized to 19-32 nt RNAs) in pre-pachytene stages in 9 dpp (upper) and 13 dpp (middle) golden hamster testes, while expressed in 21 dpp hamster testes (bottom).*

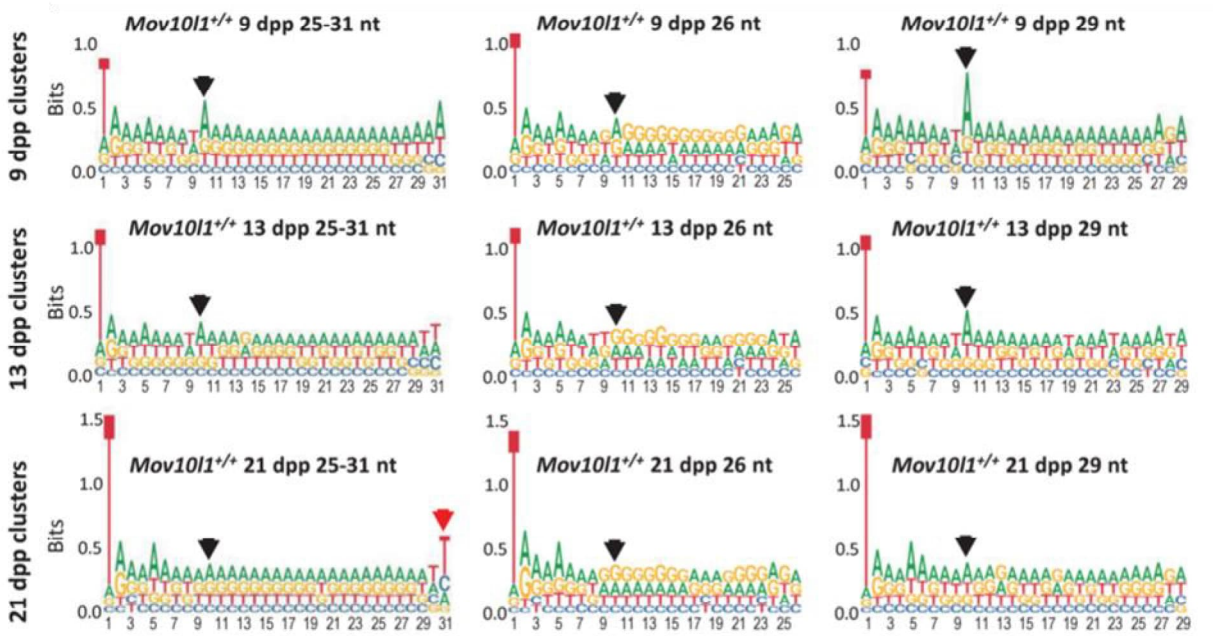

Figure 13: *Sequence analysis of piRNA clusters at three different time-points of spermatogenesis showing 1U-bias, a typical hallmark of piRNAs, and differences in preference for A at position 10, a hallmark of the ping-pong effect.*

4.2 Retrotransposons in the golden hamster genome

The available golden hamster genome assembly was of poor quality (the MesAur 1.0 genome: *https://www.ncbi.nlm.nih.gov/assembly/GCF_000349665.1/*, produced at the Broad Institute) when compared to the mouse model, whose genome sequence is almost complete with only a few unmapped scaffolds and gene annotation includes well-annotated retrotransposons (Mouse Genome Sequencing, Waterston et al. 2002). A high-quality genome assembly is essential for proper retrotransposon analysis, because if the sequence is not complete, then full-length copies of retrotransposons may not be found. Not just the presence of retrotransposon sequences, but specifically potentially active transposable elements should be identified and analyzed, because these are elements that may pose a threat to genome integrity. Mobile elements capable of retrotransposition have full-length intact copies encoding all the necessary proteins for mobility. Despite the low quality of the available golden hamster genome assembly, retrotransposon analysis was performed anyway, as there was no alternative at that moment.

4.2.1 Retrotransposon annotations

Mouse and hamster evolved from a common ancestor and the mouse genome contains ancestral active IAP and LINE1 elements (Mouse Genome Sequencing, Waterston et al. 2002). Therefore, particular attention was paid to these two families of retrotransposons in the hamster genome.

To find all retrotransposon representatives, MesAur 1.0, a publicly available golden hamster genome assembly, was analyzed first. Although short insertions and larger fragments matching internal sequences of LTR retrotransposons could be found, there was not a single full-length intact copy detected corresponding to the published IAP sequence (Ono, Toh et al. 1985). The situation with LINE1 recognition was even worse. However, the analysis was apparently inaccurate, because MesAur 1.0 genome assembly was on the scaffold level due to relatively short sequence reads which it relied on (https://www.ncbi.nlm.nih.gov/assembly/GCF_000349665.1/).

To overcome this problem, the criGriChoV2 genome assembly (https://www.ncbi.nlm.nih.gov/assembly/GCA_900186095.1/) of the Chinese hamster was used for initial analysis, although sequence divergence led to rather unsatisfactory results. However, this analysis showed that the genome of a close relative of the golden hamster contains full-length IAP and LINE1 elements.

While the project was in progress, Ishino and colleagues re-sequenced the golden hamster genome using long reads from the Pacific Biosciences platform and re-assembled the genome into an improved version (Ishino, Hasuwa et al. 2021). This new genome assembly allowed for proper annotation of retrotransposons, which could be used for further analysis. RepetMasker and *de-novo* RepeatModeler were used to identify all retrotransposons from the golden hamster genome. To make a comparison between mouse and hamster elements clear, the RepeatMasker classification used for murine retrotransposons was used for further analysis of hamster transposable elements.

4.2.2 Nucleotide substitution rate analysis of retrotransposons

Recently active retrotransposons accumulated fewer mutations during evolution, and therefore have many copies highly similar to each other. Accordingly, evolutionary older families will have a higher substitution rate among their sequences. To analyze the nucleotide substitution rate of golden hamster retrotransposons, 200 copies of each family and subfamily were randomly selected and analyzed for sequence divergence. If the retrotransposon family or subfamily had less than 200 copies present, all copies available in the genome were used. The mutation rate analysis of LTR elements indicates a recent expansion of the ERV1 and ERVK classes in the hamster genome (Fig. 14a).

The ERV1 class is represented by young, recently expanded LTRIS and MuLV families as shown by the low substitution rate of their insertions (Fig. 14a). The ERVK class appears to be the most recently expanded group of LTR retrotransposons in the hamster genome. The ERVK members with low substitution rates are represented by IAP, MYSERV, MuERV4, MMERVK, or RMERx ERVK families. IAPs exhibited a minimal substitution rate, indicating ongoing retrotransposition in golden hamsters (Fig. 14a). Further analysis of the mutation rate of the IAP family revealed two subfamilies, IAPLTR3 and IAPLTR4, with an outstanding low nucleotide exchange rate (Fig. 14b). Consistent with this, a search for full-length intact elements showed 110 IAP insertions belonging to IAPLTR3/4 subfamilies. Compared to the mouse IAP analysis, where IAPE was described as the only active IAP subgroup (Ribet, Harper et al. 2008), independent evolution of different IAP subfamilies was found in the hamster genome (Fig. 14b). In contrast to the well-described IAP, not much is known about the MYSERV family of retrotransposons. MYSERV existed in a common ancestor of mouse and hamster, but appears to retain its expression and activity in the *Cricetidae* family (Wichman, Potter et al. 1985, Cantrell, Ederer et al. 2005). An internal consensus sequence made from MYSERV insertions

longer than 4 kb extracted from the golden hamster genome was assembled and analyzed (Supplementary Data 1). The MYSERV consensus sequence was first compared with IAPLTR3/4 consensus sequence (Supplementary Data 1). Only 30% of identical sequences were found, suggesting that the two elements are not closely related. The MYSERV consensus sequence was then characterized for its coding potential. Two ORFs were found with the length of 1041 bp and 2 574 bp, translated into 346 and 857 amino acids, respectively (Fig. 15a). When searched in the golden hamster protein sequences, ORF1 and ORF2 were partially recognized as ERVK GAG and POL polyproteins (Fig. 15b) necessary for retrotransposon mobility. The ORF analysis thus indicated that MYSERV could be autonomous and capable of retrotransposition in the golden hamster genome. ERVL class, the most abundant group in the mouse genome (Mouse Genome Sequencing, Waterston et al. 2002) showed no recent expansion in the hamster genome. Consistent with the higher substitution rates of autonomous ERVL families, non-autonomous MaLRs belonging to the ERVL class do not show potential activity either (Fig. 14c).

The substitution rate analysis of LINE1 retrotransposons revealed independent LINE1 expansions in mouse and hamster genomes (Fig. 16). While murine young potentially active LINE1 elements with low mutation rates belong to the L1Md subgroup, relatively high mutation rates can be observed in most L1M families in the hamster genome (Fig. 16). A relatively low substitution rate was observed for the Lx5 subfamily (Fig. 16). Indeed, analysis of full-length intact insertions in the hamster genome showed that 108 of the 110 intact copies belong to the Lx5 subfamily of LINE1 elements. Thus, Lx5 elements represent young and potentially active LINE1 retrotransposons in the golden hamster genome.

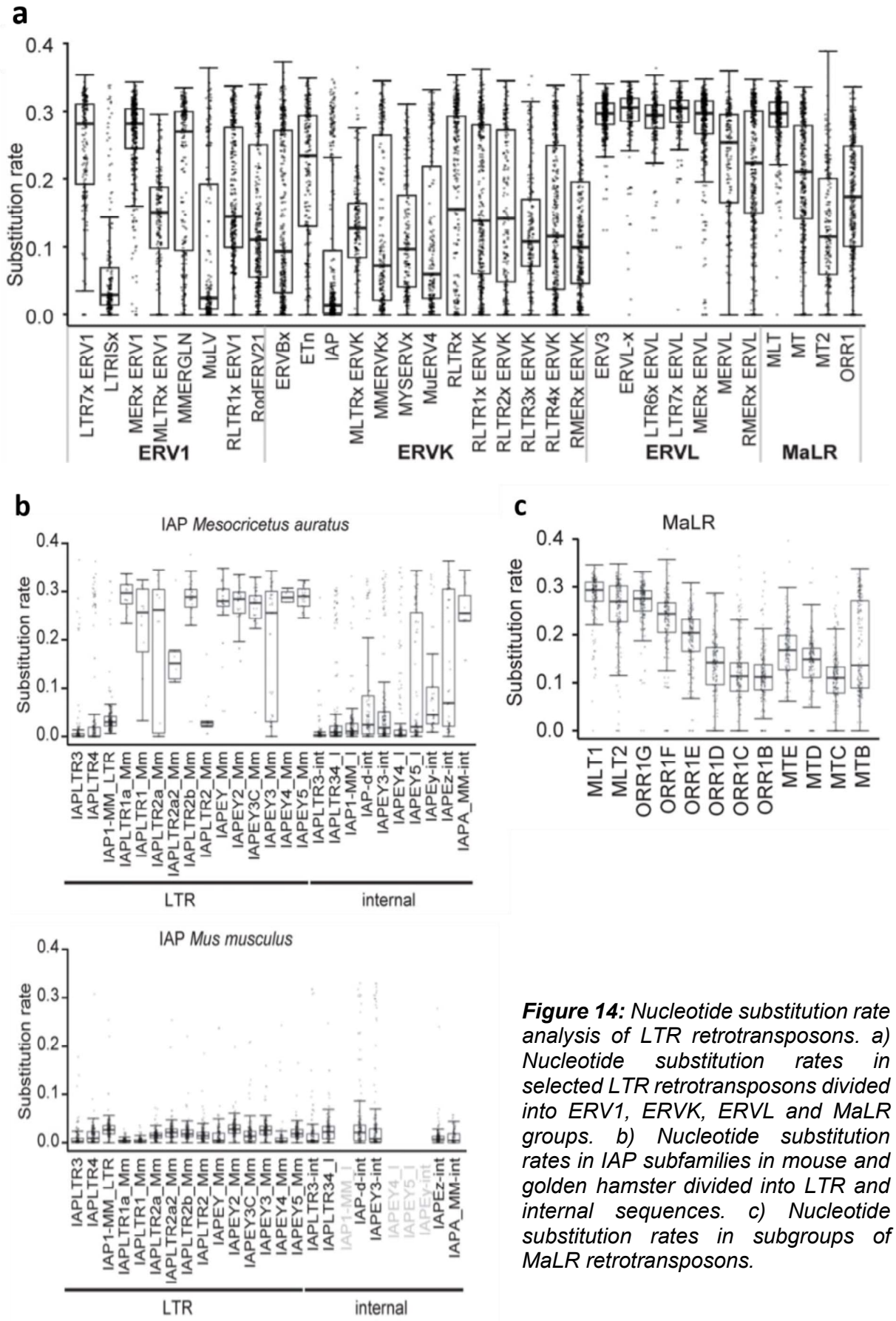

Figure 14: *Nucleotide substitution rate analysis of LTR retrotransposons. a) Nucleotide substitution rates in selected LTR retrotransposons divided into ERV1, ERVK, ERVL and MaLR groups. b) Nucleotide substitution rates in IAP subfamilies in mouse and golden hamster divided into LTR and internal sequences. c) Nucleotide substitution rates in subgroups of MaLR retrotransposons.*

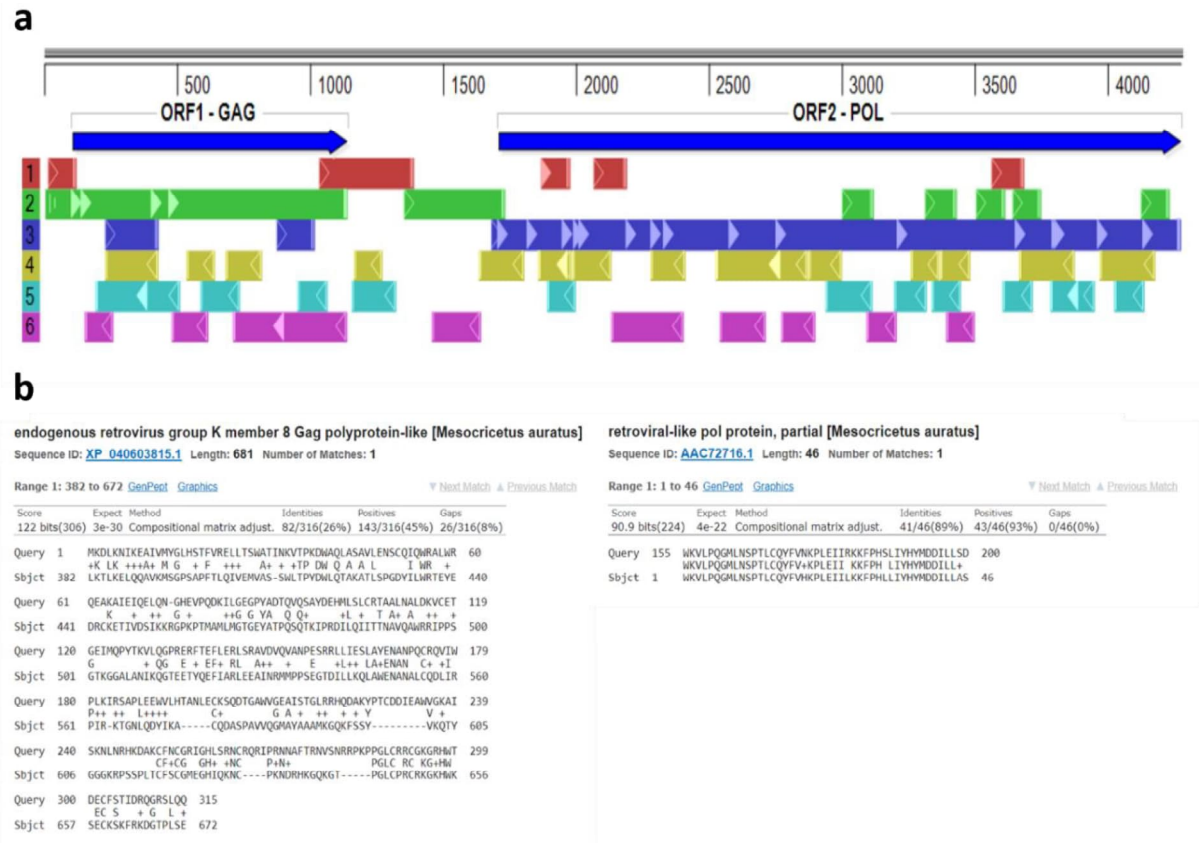

Figure 15: *MYSERV sequence analysis. a) Analysis of open reading frames (ORFs) in the MYSERV consensus sequence generated from insertions longer than 4 kb extracted from the golden hamster genome. b) Analysis of similarities between MYSERV ORFs and golden hamster protein sequences using the BLAST tool (NCBI).*

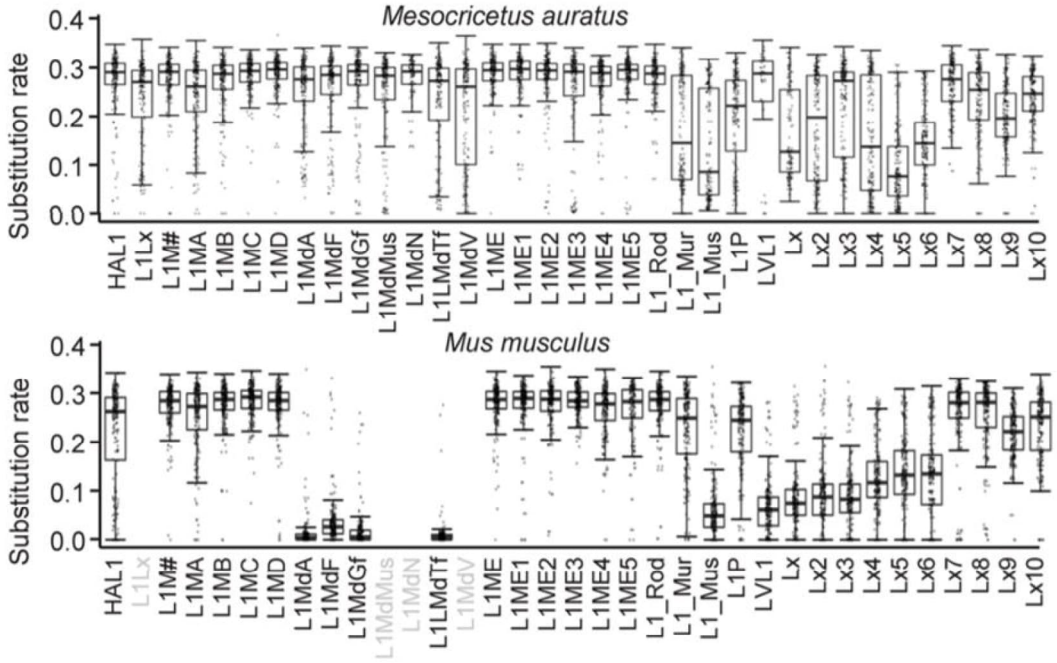

Figure 16: *Nucleotide substitution rates in LINE1 subfamilies in golden hamsters and mice.*

4.2.3 Retrotransposons-derived piRNA analysis

Retrotransposon transcripts serve as substrates of the piRNA pathway for piRNA generation. Basically, retrotransposons are repressed by piRNAs derived from their sequences. Thus, amounts of testicular pre-pachytene and pachytene piRNAs derived from retrotransposons were analyzed to determine whether and at what stage of spermatogenesis retrotransposons are actively regulated by the piRNA pathway. The piRNA populations from days 9, 13 and 21, properties of which are described above, were used.

Analysis of young retrotransposons from the ERV1 class showed that piRNAs carrying LTRIS sequences are hardly detectable, while those derived from MuLV retrotransposons are abundant, especially on day 9 (Fig. 17). This suggests a recent activity of MuLV, which has adapted to the early phase of spermatogenesis, where it is likely regulated by pre-pachytene piRNAs. The activity of the endogenous retrovirus MuLV has also been documented in mice, where it has retained the ability to infect neighboring cells (Stocking and Kozak 2008). In ERVL class, abundant populations of piRNAs carrying IAP, MYSERV and MMERVK sequences were observed, especially on day 9 (Fig. 17), suggesting that the piRNA pathway suppresses these elements in the early stages of spermatogenesis. This implies the potential activity of IAP, MYSERV and MMERVK retrotransposons in the golden hamster genome. The activity of IAP and MMERVK families has been described also in mice (McCarthy and McDonald 2004), suggesting persistent activity originating in a common ancestor of mouse and hamster. Interestingly, an abundant population of piRNAs derived from MaLR elements can be observed on day 21 (Fig. 17). As noted above, MaLR elements did not show a recent expansion in the golden hamster genome based on substitution rate analysis (Fig. 14a, c). However, abundant pachytene piRNA populations suggest that MaLRs are actively regulated by the piRNA pathway during meiosis, which may indicate some ongoing transcriptional activity of these elements in hamster spermatogenesis.

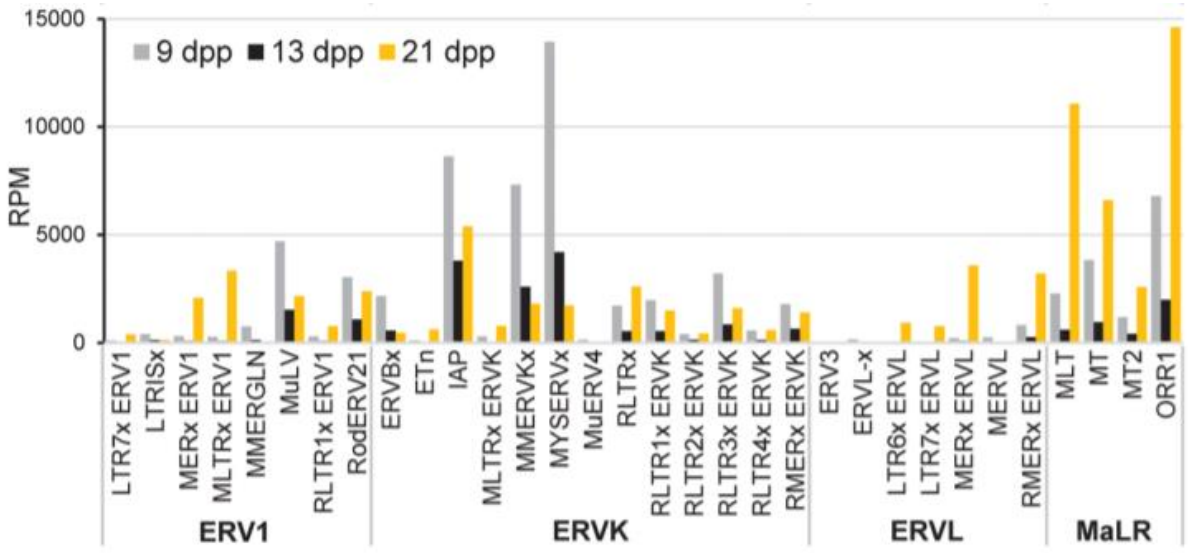

Figure 17: *Abundance of 24-31 nt RNAs derived from selected LTR retrotransposons normalized to 19-32 nt small RNA populations (RPM) analyzed at three different time-points of spermatogenesis.*

4.2.3.1 Full-length intact elements-derived piRNA analysis

To explore the link between FLI IAP and FLI LINE1 insertions and piRNA pathway activity, we examined antisense small RNAs perfectly mapping to FLI intact copies of IAP and LINE1. Antisense small RNAs that perfectly map to FLI elements should be piRNAs derived from these FLI retrotransposons and their presence would indicate active regulation of FLI IAP and LINE1 elements by the piRNA pathway. To check all piRNA populations, small RNA sequencing data from 9, 13 and 21 old hamster testes were used again. Analysis showed that antisense piRNAs derived from FLI IAP were abundant at all three-time points tested, with the highest peak at day 9 (Fig. 18). Interestingly, piRNAs mapping to FLI LINE1 were observed mainly on day 9, followed by reduced levels in later stages (Fig. 18). These data suggest that IAPs are active and thus regulated by piRNAs in all stages of spermatogenesis, at least up to the pachytene stage of meiosis I. On the other hand, LINE1 elements appear to adapt their activity to early stages of spermatogenesis and are therefore regulated mainly by pre-pachytene piRNAs. These results are in contrast to the LINE1 expression pattern in mice, where the piRNA pathway is necessary to suppress LINE1 at the onset of meiosis, when other control mechanisms such as histone modifications are erased (Di Giacomo, Comazzetto et al. 2013, Di Giacomo, Comazzetto et al. 2014).

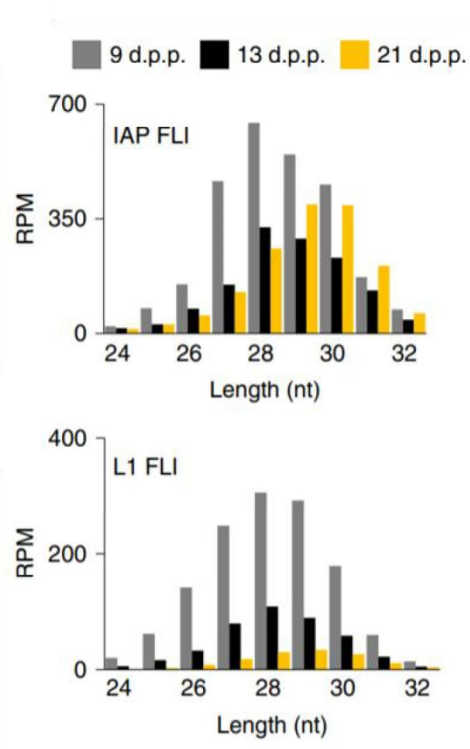

Figure 18: *Abundance of 24-32 nt antisense RNAs perfectly mapping to FLI IAP and FLI LINE1 elements and normalized to 19-32 nt RNA populations (RPM) analyzed at three different time-points of spermatogenesis.*

In conclusion, young retrotransposon families and subfamilies that showed recent expansion in the golden hamster genome are represented by Lx5, MuLV, IAP LTR3/4, MMERVK and MYSERV elements. Ancestral LINE1 and IAP elements evolved independently in mice and hamsters, and full-length intact copies of these elements were found in the golden hamster genome, suggesting that they are capable of retrotransposition. Also, piRNA populations found in golden hamster testes appeared to be predominantly derived from young elements, suggesting that the piRNA pathway regulates their activity during spermatogenesis in golden hamsters.

4.3 Generation of the *Mov10l1* golden hamster mutant

Essentially all *in vivo* mechanistic studies on the mammalian piRNA pathway have been performed in mice. However, the apparent divergence of the mouse model in terms of small RNA pathways in the germline brings the question of whether the documented function of the murine piRNA pathway applies to all mammals or whether it is rather a mouse-specific case. To address this issue, the biological role of the piRNA pathway in golden hamsters was investigated by knocking out the piRNA pathway.

The golden hamster was selected because, like most mammals, including humans, encodes all four PIWI proteins, and likely lacks highly active RNAi in its oocytes. These properties, affordable cost, and biological features shared with mice, such as fast zygotic genome activation or a short reproductive cycle, made the golden hamster a suitable model organism for a genetic approach to study the physiological relevance of the piRNA pathway in mammals. Different factors acting in the piRNA pathway could be deleted to disrupt its function. However, loss of specific *Piwi* genes results in the loss of different piRNA fractions, while we wanted to eliminate piRNAs completely. Therefore, we decided to knock out MOV10L1 helicase, which plays an important role in the initial steps of piRNA biogenesis, as shown in mice (Frost, Hamra et al. 2010, Zheng, Xiol et al. 2010, Vourekas, Zheng et al. 2015).

With the introduction of the CRISPR/Cas9 system (Gasiunas, Barrangou et al. 2012, Jinek, Chylinski et al. 2012), genetic manipulations of various model organisms have become easier and more accessible. However, many species still have limited availability of embryos and handling difficulties of germ cells, so successful use of the CRISPR/Cas9 approach still remains a challenge. Golden hamster oocytes and embryos are extremely vulnerable *in vitro* (Schini and Bavister 1988), which turned out to be a big barrier to the generation of genetically modified hamsters. This issue was solved by Hirose and colleagues in the Atsuo Ogura laboratory (RIKEN, Japan) who employed iGONAD (Hirose, Honda et al. 2020), which is *in vivo* gene-editing system using sgRNAs and Cas9 protein delivery to a pregnant female by ampulla injection and oviduct electroporation using forceps-like electrodes (Gurumurthy, Sato et al. 2019). In collaboration with Helena Fulka and Atsuo Ogura, we used iGONAD to generate the hamster *Mov10l1* knock-out (KO). sgRNAs targeting introns 19 and 21 were used to remove exon 20 encoding the helicase domain (Fig. 19), thus creating an analogous mutation as performed in mice (Frost, Hamra et al. 2010).

As a result, five animals were born. One did not carry the mutation (Fig. 20, number 3) and two were homozygous for the deletion (Fig. 20, numbers 2 and 5). Homozygous animals appeared to be sterile and therefore could not pass the mutation on to the next generation. One male and one female were detected as heterozygotes for the deletion, and these were used to establish the hamster lines upon breeding with wild-type (WT) animals. The heterozygous male was fertile (Fig. 20, number 1), but none of the offspring carried the mutation. The heterozygous female (Fig. 20, number 4) bred with wild-type male transmitted the mutated allele to 7 of 10 progeny. These heterozygotes were used for subsequent breeding with wild-type outbred animals for two generations to minimize possible effects of inbreeding and off-targeting.

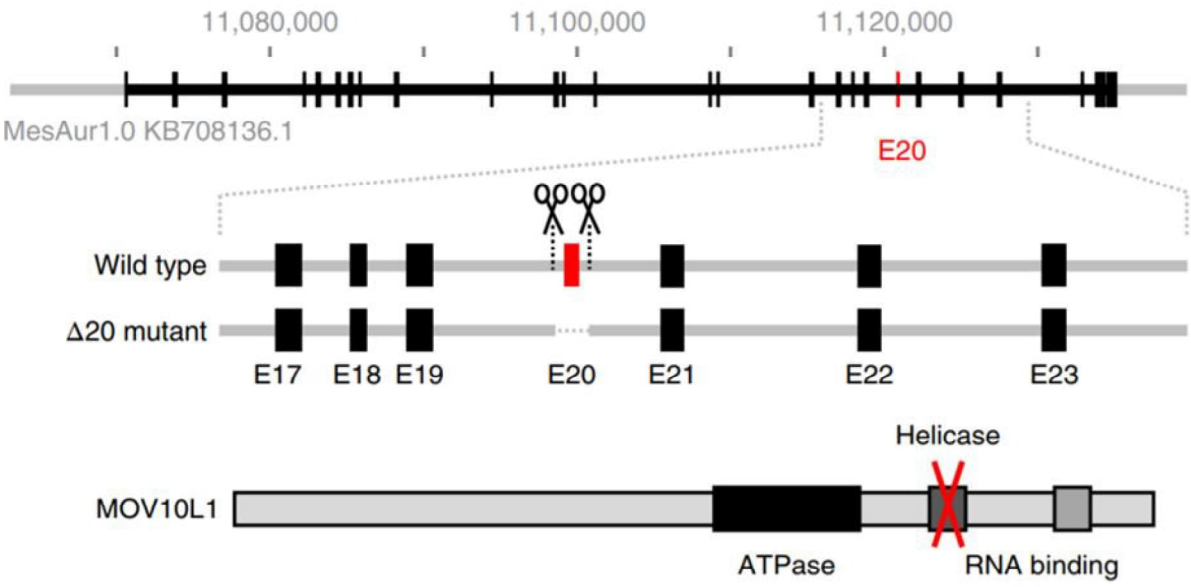

Figure 19: *Targeting strategy for generating golden hamster Mov10l1 mutant*.

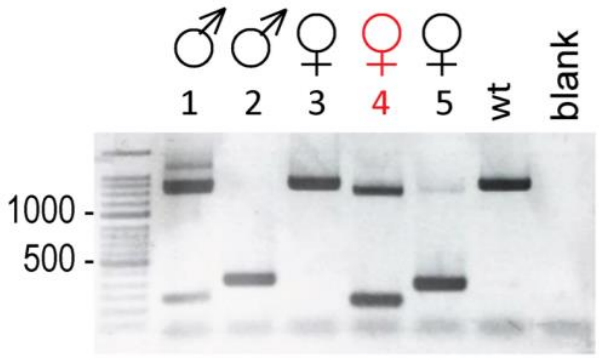

Figure 20: *PCR genotyping of golden hamster founders for the Mov10l1 mutation. The upper band corresponds to the WT allele, the lower band corresponds to the mutated allele.*

Deletion of exon 20 was designed to lead to a frameshift that results in a lack of protein production. Therefore, we analyzed mutant animals to confirm the deletion. The deleted segment was confirmed by Sanger sequencing (Fig. 21) and, as expected, a comparison of RNA sequencing from WT and KO testes showed a lack of reads mapping to exon 20 along with significantly reduced *Mov10l1* RNA levels in mutant testes (Fig. 22).

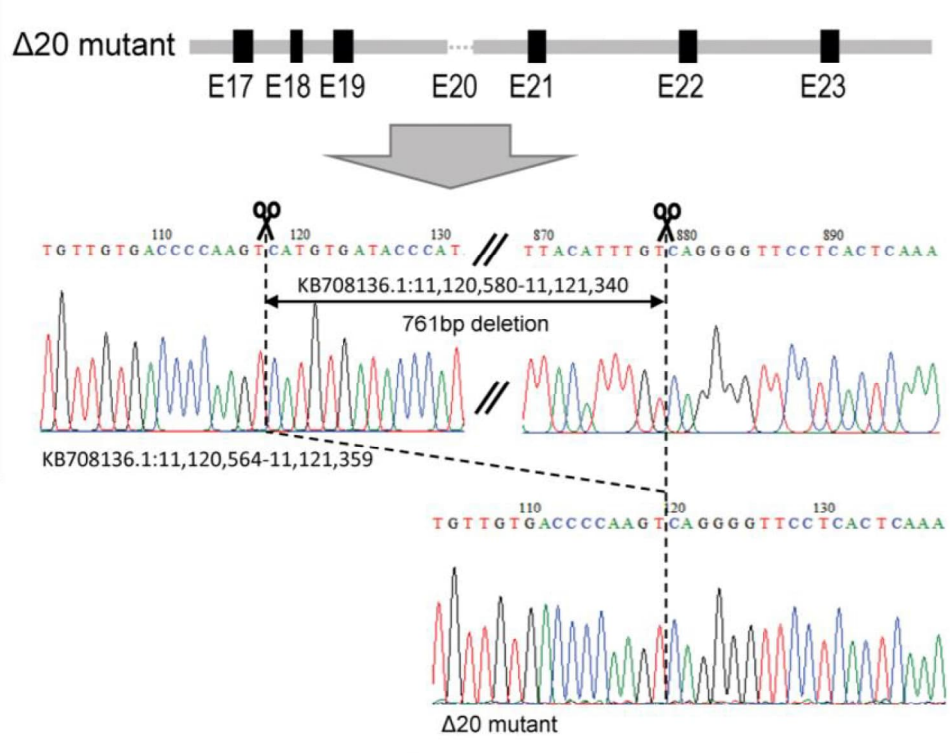

Figure 21: *Validation of the Mov10l1 deletion by Sanger sequencing.*

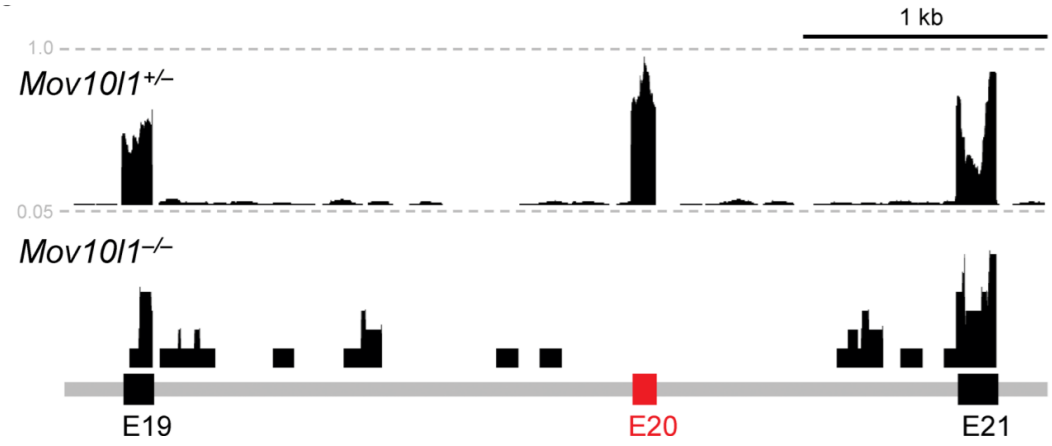

Figure 22: *Snapshot from the UCSC browser showing RNA coverage of the Mov10l1 locus in WT (top) and KO (bottom) 9 dpp golden hamster testes. The absence of reads mapping to the deleted exon 20 is apparent in KO testes. Dashed lines show counts per million normalized to the library size.*

Western blot showed the presence of MOV10L1 in WT hamster testes and loss of the protein in mutant testes (Fig. 23). If, as expected, MOV10L1 is a germ cell-specific protein, then the absence of the protein might reflect massive germ cell loss in adult testes of *Mov10l1* mutant (as described in Chapter 4.5 Sterile phenotype of male *Mov10l1* mutants) and therefore cannot directly prove the absence of protein resulting from exon 20 deletion. I used ovarian

sections to confirm the loss of MOV10L1 protein, but immunofluorescence staining of WT and KO ovaries with MOV10L1 antibody did not show any specific signal, suggesting the protein is either not expressed in adult ovarian cells or the immunofluorescence staining did not work (Fig. 24). However, the minimal level of *Mov10l1* RNA in 9 dpp KO testes (Fig. 22), where germ cells are still present, and loss of the reading frame imply the absence of MOV10L1 protein.

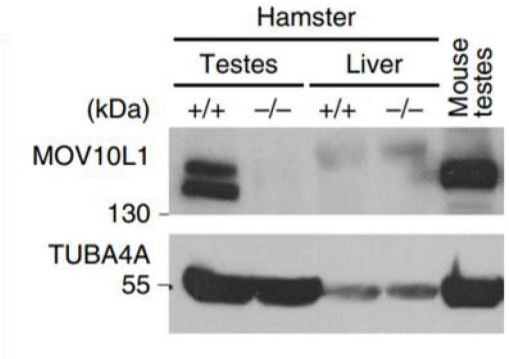

Figure 23: *Western blot analysis of MOV10L1 protein in mouse and golden hamster testes. Liver were used as a negative control for antibody specificity.*

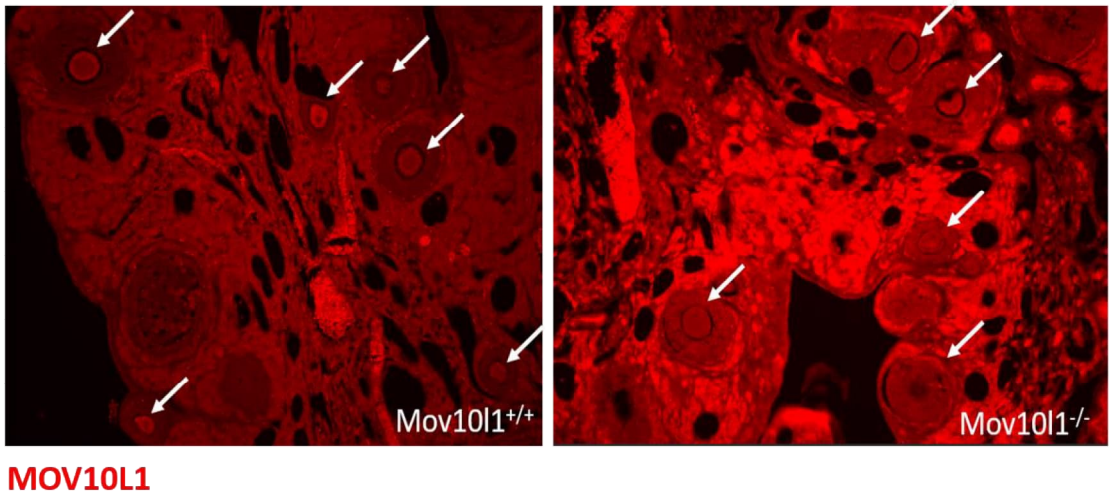

Figure 24: *Immunofluorescence staining of WT and KO adult ovaries using MOV10L1 antibody. White arrows indicate oocytes.*

Interestingly, compared to the mouse protein, hamster MOV10L1 was detected as two bands of different lengths (Fig. 23), indicating the presence of two MOV10L1 isoforms. This result is consistent with the hamster *Mov10l1* sequence having two possible translation start sites, one annotated by Ensembl (Howe, Achuthan et al. 2021) and the other found in the sequence extracted from the golden hamster genome (Fig. 25).

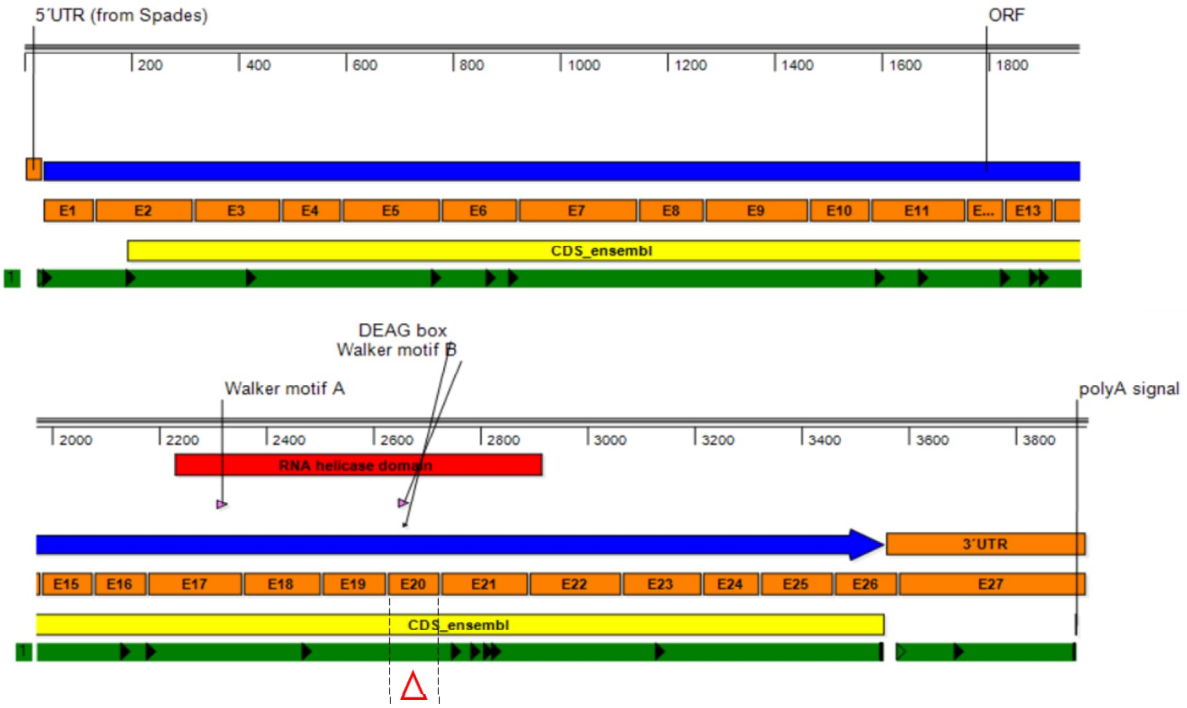

Figure 25: *Annotation of the golden hamster Mov10l1 sequence. The blue arrow indicates the longest ORF, the yellow color corresponds to the coding sequence annotated in Ensembl and the green color corresponds to the coding sequence found in the Mov10l1 sequence extracted from the golden hamster genome. Black triangles in the green rectangle indicate potential translation start sites. The red triangle between dashed lines corresponds to the deleted part of the gene (E20). CDS, Coding DNA sequence; UTR, untranslated region; E, Exon.*

Animals carrying the *Mov10l1* mutation were examined for fertility. Heterozygotes for the *Mov10l1* deletion were fertile and their breeding showed the expected Mendelian ratio of genotypes (Table 1). Homozygotes were viable, but interestingly, both sexes were sterile, as shown by the absence of progeny when 6 mutant males and 10 mutant females were mated with heterozygous animals with proven fertility (Table 1). All matings were monitored to ensure that coitus occurred.

Table 1: *Mating performance*

Male x Female	+/+	+/-	-/-	M	F	coitus	litters	litter size
Mov10l1$^{+/-}$ x *Mov10l1*$^{+/-}$	24	55	17	47	55	21	20	5.8±2.5
Mov10l1$^{+/-}$ x *Mov10l1*$^{+/+}$	5	8	-	10	6	3	3	5.7±3.7
Mov10l1$^{+/+}$ x *Mov10l1*$^{+/-}$	2	12	-	4	10	3	2	7.0±2.0
Mov10l1$^{-/-}$ x *Mov10l1*$^{+/-}$	-	-	-			6	-	-
Mov10l1$^{+/-}$ x *Mov10l1*$^{-/-}$	-	-	-			10	-	-

4.4 Sterile phenotype of female *Mov10l1* mutants

The sterile phenotype of female *Mov10l1* mutant hamsters was interesting, considering that female *Mov10l1* mutant mice do not show any fertility defects (Frost, Hamra et al. 2010). Hence, we inspected ovaries and early development of *Mov10l1* mutants to find the stage at which the defect occurs. Histological sections of *Mov10l1*$^{-/-}$ ovaries did not show any abnormalities. The presence of early antral and antral follicles suggested that oocytes develop into preovulatory oocytes and the presence of corpus luteum indicated normal ovulation of mutant oocytes (Fig. 26).

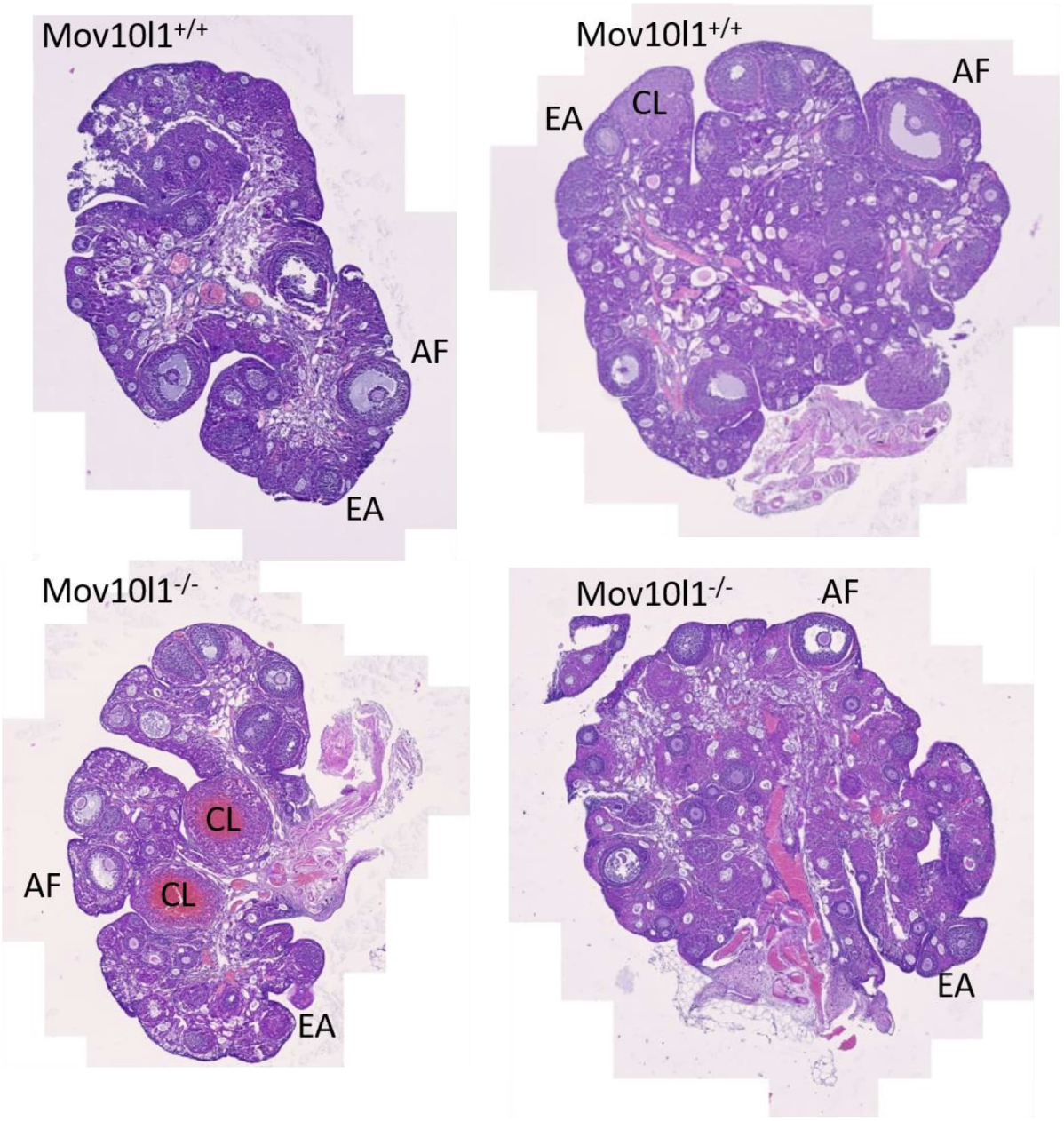

Figure 26: *Hematoxylin and eosin staining of ovaries isolated from adult WT (top) and Mov10l1 mutant (bottom) females. AF, antral follicles; EA, early antral follicles; CL, corpus luteum.*

To investigate whether fully-grown oocytes really can ovulate and mature into metaphase II oocytes, hamster females were superovulated with pregnant mare´s serum gonadotropin (PMSG) and the oocyte maturation was induced by subsequent injection of human chorionic gonadotropin (hCG). Following hCG injection, MII oocytes were collected from ovaries and spindle properties were examined using Tubulin and DNA immunofluorescence staining (Fig. 27). Analysis of the spindle length and volume and the volume of the metaphase plate did not show any significant alterations in *Mov10l*$^{-/-}$ MII oocytes (Fig. 27b). The results showed that mutant GV oocytes retain the meiotic competence and are able to mature into MII oocytes *in vivo*. The high variability in spindle volume measurements (Fig. 27b) can be explained by differences typically caused by the paraformaldehyde fixation or by sensitivity of hamster oocytes to manipulation, light and temperature, which could slightly differ in particular experiments.

The ability of GV mutant oocytes to reach the pre-fertilization MII stage suggested that developmental arrest occurs during early development. Superovulated mutant females were therefore mated with WT or heterozygous males with proven fertility to determine whether *Mov10l1*$^{-/-}$ oocytes can be fertilized and develop further. The mating produced normally looking 1-cell and 2-cell zygotes, showing that *Mov10l1*$^{-/-}$ MII oocytes can be fertilized and undergo cleavage. However, *Mov10l1*$^{-/-}$ zygotes did not develop beyond the 2-cell stage, as shown 61 hours after fertilization, when 4- to 8-cell embryos could be seen in WT, whereas only degenerating 2-cell embryos could be isolated from mutant oviducts (Fig. 28). These results show that developmental arrest occurs at the 2-cell stage, the stage where zygotic genome activation takes place in hamsters (Seshagiri, McKenzie et al. 1992).

Because proper chromatin architecture is essential for normal zygotic genome activation and activity of retrotransposons may affect the chromatin structure, I examined active chromatin and heterochromatin status of *Mov10l1* mutant 2-cell zygotes using H3K9Ac and H3K9me3 immunofluorescence staining (Fig. 29). This analysis could detect only major defects in heterochromatin, however, given the limited amount of material, this was the only insight I could obtain. No difference was observed between WT and *Mov10l1* KO 2-cell zygotes, implying that the formation of zygotic heterochromatin was not severely disrupted at this stage.

Since no apparent defect was found in the chromatin structure of *Mov10l1*$^{-/-}$ 2-cell zygotes, I decided to examine changes in gene expression that could be affected by disruption of the piRNA pathway. Breeding of heterozygotes for *Mov10l1* mutation produced viable

homozygotes in the expected Mendelian ratio, while homozygous females were sterile with development arrested at the 2-cell stage (Table 1). It means that *Mov10l1*-deficient zygotes could develop into a normal individual, while fertilized oocytes produced by *Mov10l1*$^{-/-}$ females could not support development beyond the 2-cell stage (Fig. 28). This implies a maternal defect caused by the loss of MOV10L1.

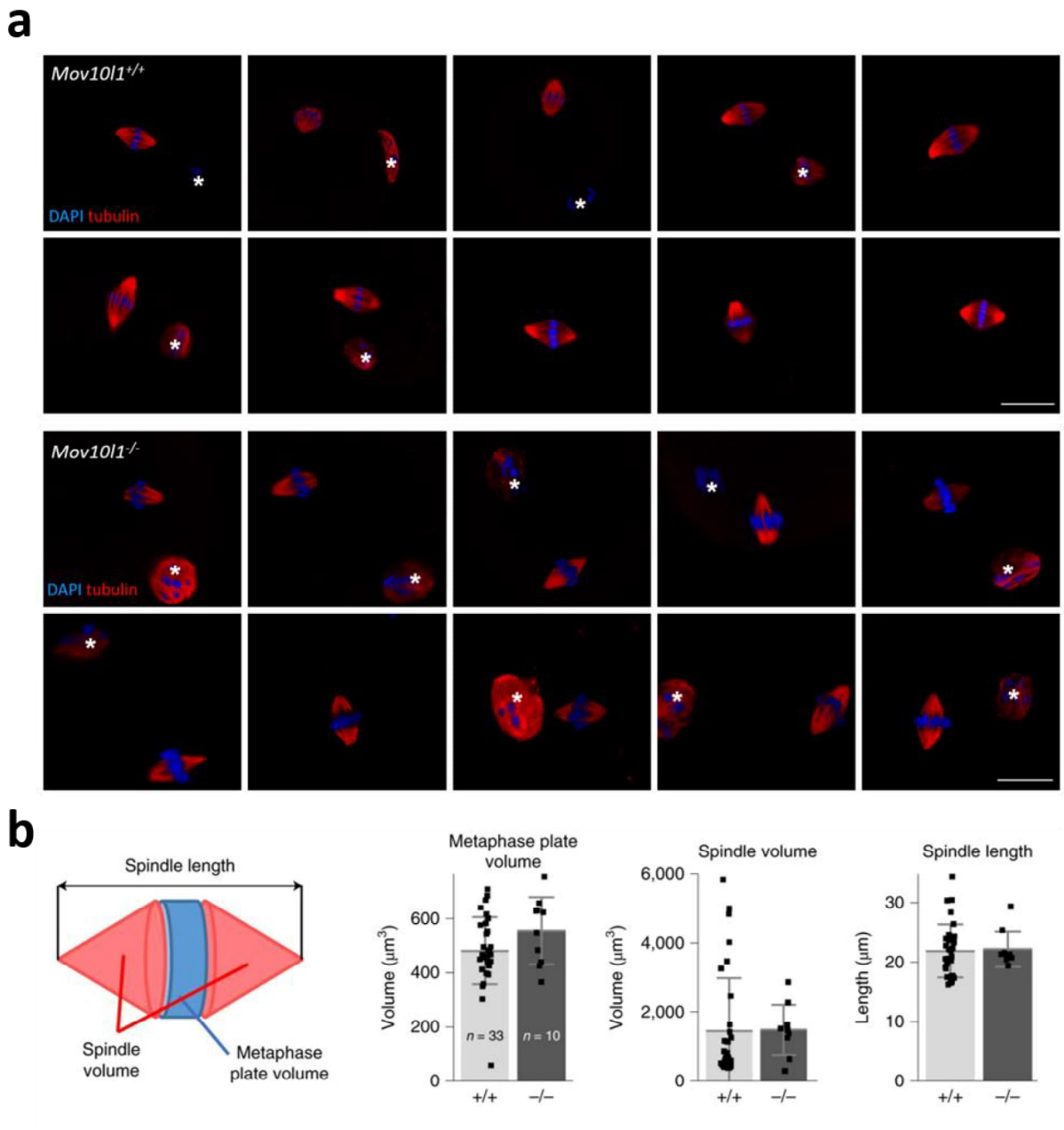

Figure 27: *Spindle analysis in MII oocytes. a) MII oocytes isolated from WT (top) and Mov10l1 mutant (bottom) females 17h after hCG injection and stained with Tubulin (red) and DAPI (blue) antibodies. Asterisks indicate polar bodies. Scale bars, 10 µm. b) Quantitative analysis of MII spindle traits. Tubulin immunofluorescence staining was used to quantify spindle length and volume and DAPI immunofluorescence staining was used to analyze metaphase plate volume using three-dimensional reconstruction of oocytes.*

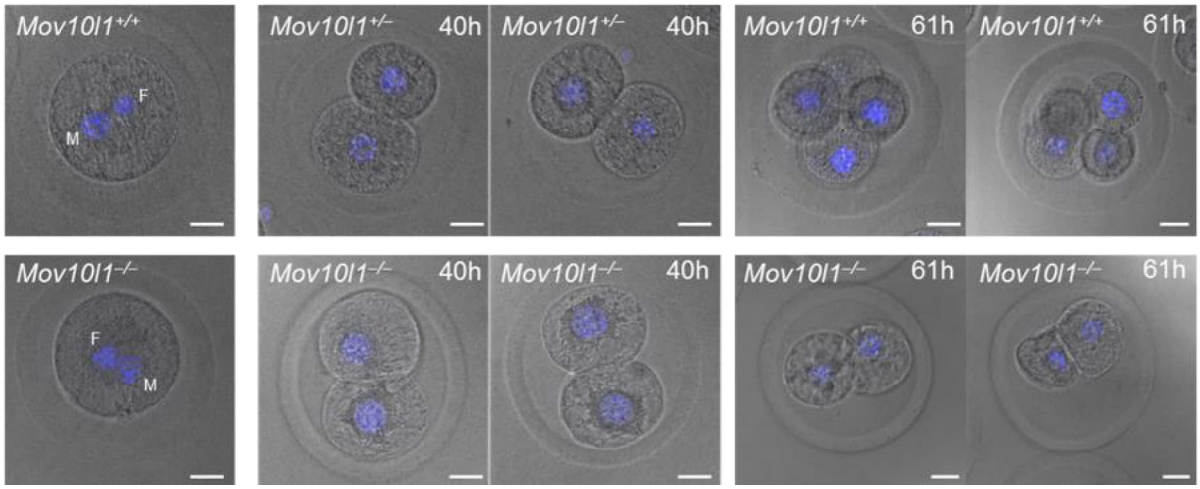

Figure 28: *Analysis of early development in WT and Mov10l1 mutant females. Mutant oocytes can be fertilized, form a 1-cell zygote with male (M) and female (F) pronuclei, undergo cleavage, and form a 2-cell zygote. They cannot support development beyond the 2-cell stage and start to degenerate as shown in 61 hours post-mating. Pictures of zygotes and embryos are shown as an overlap of bright-field and DAPI immunofluorescence staining (blue). Scale bars, 20 µm.*

The maternal function is also consistent with the expression of components of the piRNA pathway, which are expressed maternally as shown by RT-PCR performed on different stages of oogenesis and early development. RT-PCR examined the transcripts of individual piRNA pathway genes in oocytes and embryos of WT animals and used *Actb* and *Hprt* genes as housekeeping genes (Fig. 30). Changes in *Actb* and *Hprt* RNA levels between GV oocytes and 8-cell embryos (Fig. 30) can be explained by clearance of maternal mRNA leading to decreased RNA levels and new transcription originating in the zygotic genome at the 2-cell stage, when RNA levels begin to increase. The *Mov10l1* and *Piwi* genes appear to be well expressed in fully grown and MII oocytes and are absent at other stages tested, except *Piwil1* expression at the 2-cell stage (Fig. 30). Interestingly, *Piwil2* appears to be expressed in fully grown oocytes, but not later (FIg. 30), making the fully grown oocytes the only stage where all PIWI proteins are expressed. It indicates an important function of the piRNA pathway at this stage, suggesting that the loss of developmental competence in *Mov10l1* mutants may have origin in GV oocytes. These data supported the decision to analyze oocytes in their fully-grown stage, where the piRNA pathway is most likely to be functional as shown by the presence of all piRNA pathway components examined and where the very first changes leading to the 2-cell arrest in *Mov10l1* mutants could be found.

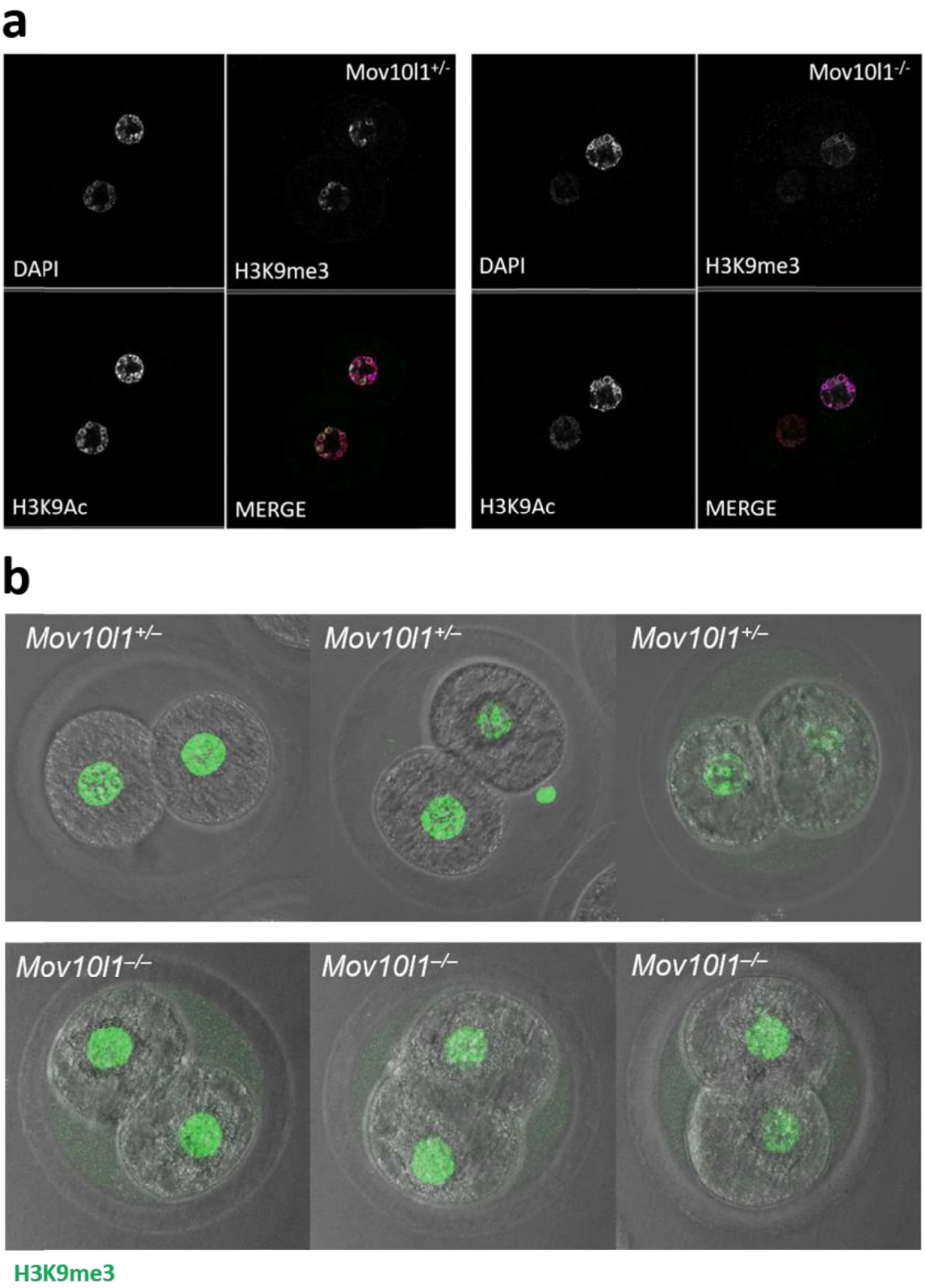

Figure 29: *Analysis of chromatin structure in 2-cell zygotes. a) Immunofluorescence staining of DNA (DAPI, blue in merge), H3K9me3 (green in merge) and H3K9Ac (red in merge) in 2-cell zygotes isolated 40h post-mating from superovulated WT and Mov10l1 mutant females. b) Detailed pictures of 2-cell zygotes isolated 40h post-mating from superovulated WT and Mov10l1 mutant females shown as an overlap of bright-field and H3K9me3 immunofluorescence staining (green).*

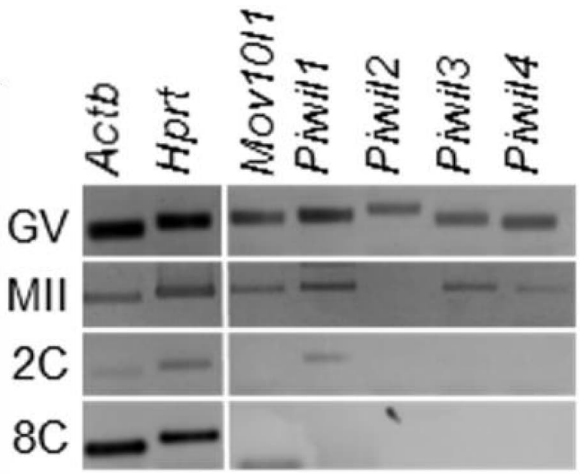

Figure 30: *RT-PCR analysis of piRNA pathway components at different stages of oogenesis and early development. GV, fully grown oocytes; MII, matured oocytes; 2C, 2-cell zygotes; 8C, 8-cell embryos.*

To look for changes in the transcriptome of fully-grown GV oocytes caused by the loss of the *Mov10l1* gene, I performed RNA sequencing of WT and *Mov10l1*$^{-/-}$ fully-grown GV oocytes. 57 differentially expressed genes were identified between WT and *Mov10l1* KO oocytes (Fig. 31a), with only 13 genes upregulated and none downregulated when sequencing from heterozygotes was included in the analysis (Fig. 31b).

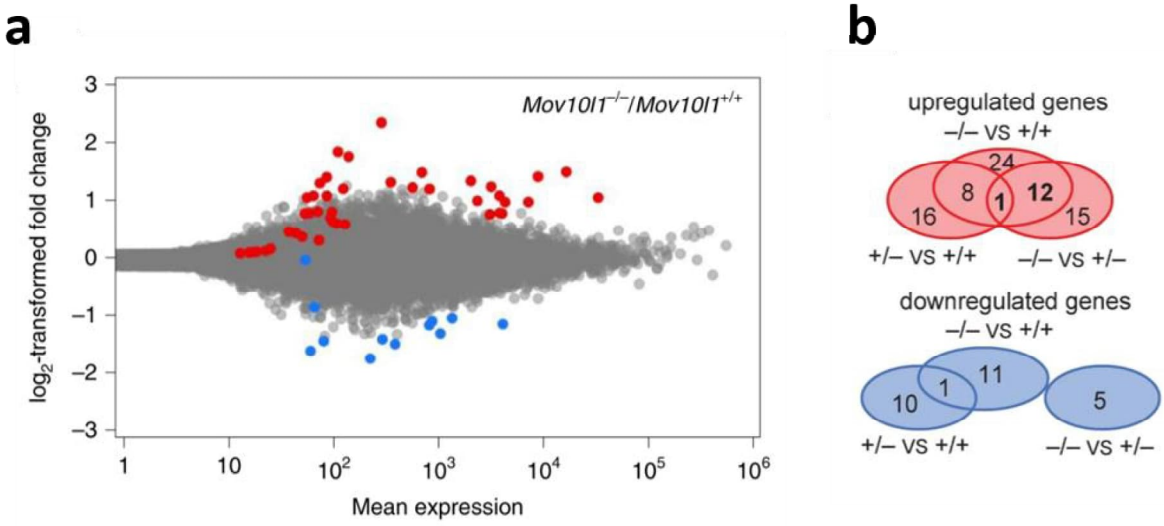

Figure 31: *Analysis of transcriptomes in GV oocytes. a) MA plot of differentially expressed protein-coding genes in GV oocytes isolated from WT and Mov10l1 mutant females. Red dots depict significantly upregulated genes and blue dots depict significantly downregulated genes in Mov10l1-deficient oocytes. b) Venn diagrams showing the overlap between differentially expressed protein-coding genes in GV oocytes isolated from females with different Mov10l1 genotypes.*

At the time this work was being prepared, another group of Dr. Siomi (Keio University School of Medicine, Tokyo, Japan) produced golden hamster *Piwil1* knock-out. This allowed for comparing *Mov10l1* and *Piwil1* sequencing datasets. We hypothesized that the real piRNA pathway targets should be dysregulated in both, *Mov10l1*$^{-/-}$ and *Piwil1*$^{-/-}$ datasets, despite *Mov10l1* sequencing used fully-grown oocytes, while *Piwil1* sequencing was performed on MII oocytes and the loss of each member of the piRNA pathway would affect the piRNA pathway differently. We compared results from the *Mov10l1* differential expression analysis with the *Piwil1* differential expression analysis and found 13 genes that were significantly upregulated in both datasets (Fig. 32a), suggesting that these might be direct targets of the piRNA pathway. Interestingly, no common features were found among these 13 genes that would explain the targeting mechanism, suggesting that piRNA-mediated regulation may work through different paths. However, we found a good example of how regulation by the piRNA pathway may work. *Kif2a*, one of the significantly upregulated genes in both datasets (Fig. 32a), utilizes an insertion of MYSERV-related RLTR31B2 LTR as a promoter and first exon, and its activity appears to be specific for oocytes, as shown by the expression of shorter Kif2a transcript in hamster testes (Fig. 32b). This suggests that control of *Kif2a* gene expression in hamster oocytes may be associated with piRNAs regulating retrotransposon activity.

Although it cannot be ruled out that small transcriptome changes in *Mov10l1* mutant oocytes (Fig. 31a) contributed to the observed phenotype, the known functions of the differentially expressed genes do not clearly explain the developmental incompetence of *Mov10l1* mutants. Therefore, the activity of retrotransposons, which could affect proper development, was investigated next. Maximum 2.4-fold change in reads mapping to different families of LTR retrotransposons in *Mov10l*$^{-/-}$ oocytes was found, with IAP retrotransposons being increased up to 2-fold (Fig. 33a). When specifically focusing on potentially active families in the golden hamster genome, only a slight increase in reads mapping to all LINE and IAP insertions, with a large representation of the Lx5/6 and IAPLTR3/4 subfamilies (Fig. 33b) showing the lowest substitution rates (Fig. 14b, 16), was observed. Next, only reads perfectly mapping to full-length intact LINE and IAP insertions were analyzed and approximately 25% increase in FLI LINE1 and 3.5-fold increase in FLI IAP expression was found (Fig. 33b). These data suggest that LINE1 and IAP elements capable of retrotransposition are derepressed in *Mov10l1*$^{-/-}$ oocytes.

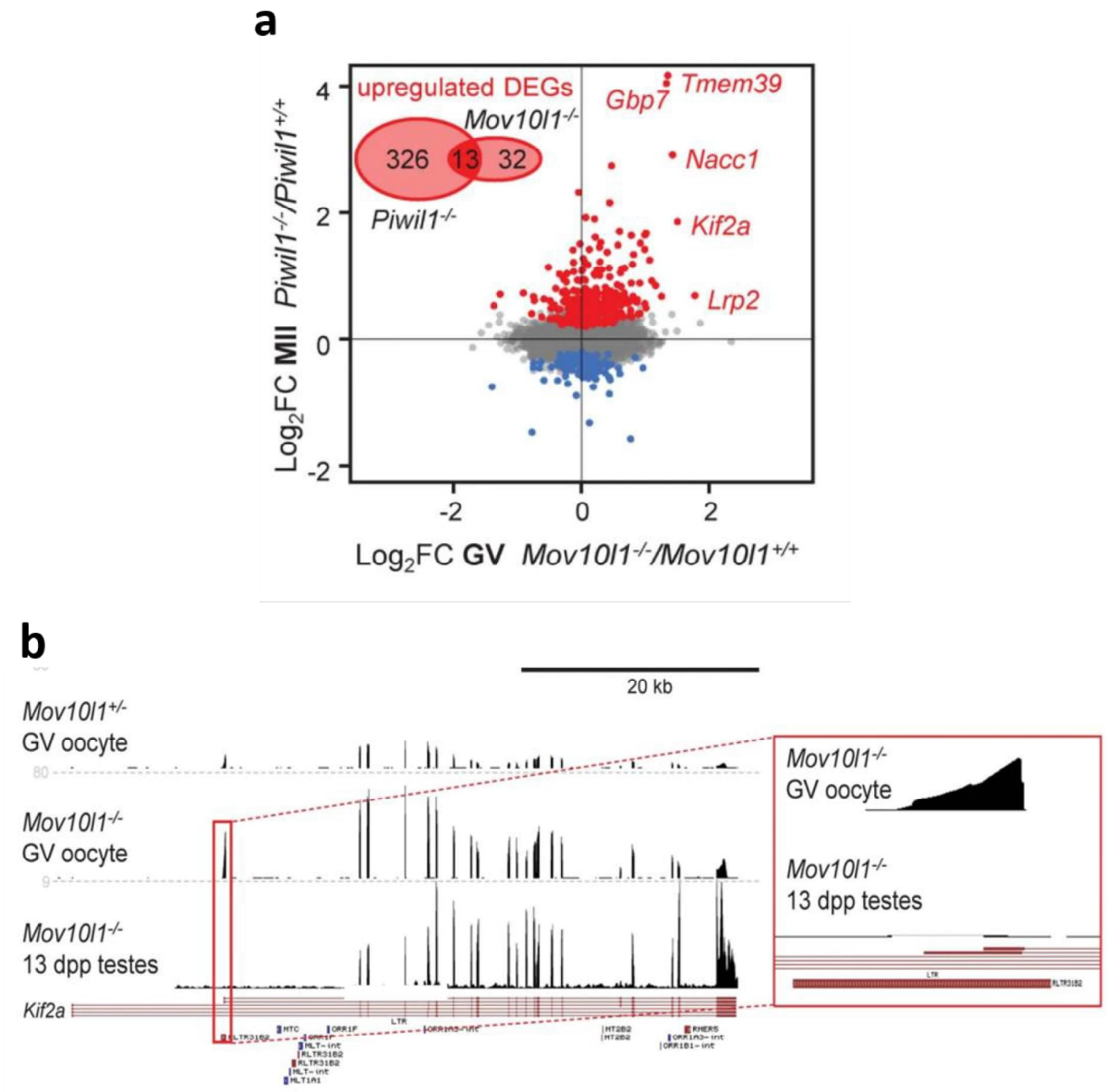

Figure 32: *Analysis of piRNA targets in golden hamster GV oocytes. a) Comparison of Mov10l1 and Piwil1 differential expression analysis showing the overlap in upregulated genes in both datasets. b) Snapshot from the UCSC browser showing Kif2a locus expression in Mov10l1 heterozygous (top) and homozygous (middle) GV oocytes and in 13 dpp Mov10l1 mutant testes. Upregulation of the LTR element providing the first exon is evident in mutant GV oocytes, while its expression is absent in 13 dpp mutant testes, indicating oocyte-specific expression of the LTR element.*

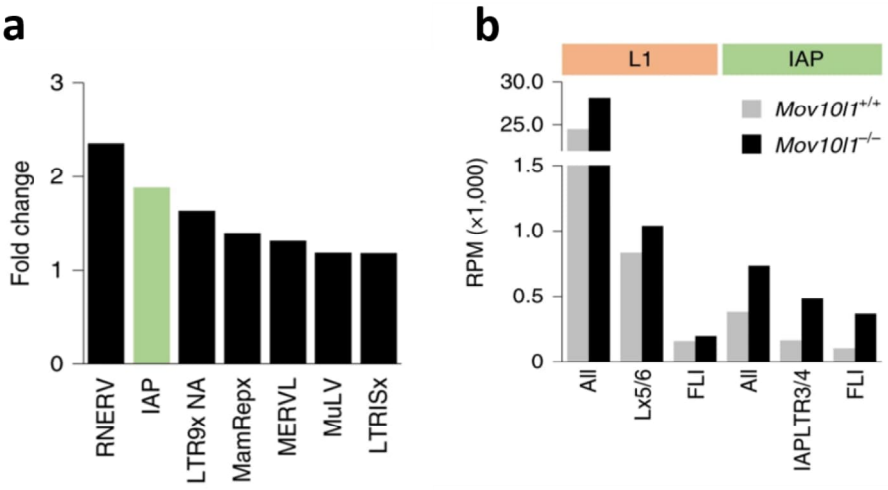

Figure 33: *Analysis of retrotransposon regulation in GV oocytes. a) Graph showing upregulation of LTR retrotransposon transcripts in Mov10l1 mutant oocytes compared to WT oocytes. b) Graph showing mild upregulation of reads mapping to all IAP and LINE1 elements, to young subfamilies of IAP and LINE1 elements selected by nucleotide substitution rate analysis, and to full-length intact copies of IAP and LINE1 elements. FLI, Full-length intact.*

To examine whether the derepression of retrotransposon correlates with piRNA levels, sequencing of small RNAs from fully-grown GV oocytes was performed. Analysis showed a decrease in the expression of all 18-31nt small RNA populations when scaled to the amount of endogenous miRNAs (Fig. 34a, b). The 21-23nt category of small RNAs contains Dicer products, but hamster oocyte piRNAs are present in a wide range of lengths. This includes short 18-20nt piRNAs typically bound to PIWIL3 or piRNAs starting at the length of 20 nt bound to PIWIL1 (Ishino, Hasuwa et al. 2021). When the composition of specific classes of 18-32 nt small RNAs was normalized to miRNA abundance, a massive loss of reads derived from retrotransposons and unannotated regions (referred to as other) was found in *Mov10l1*$^{-/-}$ oocytes (Fig. 34b), suggesting that the derepression of retrotransposons in *Mov10l1* mutant oocytes is indeed associated with piRNA loss. It is consistent with data showing reduced levels of piRNAs derived from different LTR retrotransposons, even though the loss of these small RNAs is not complete (Fig. 34c). This can be explained either by redundancy with another small RNA-producing pathway targeting retrotransposons, or by the presence of MOV10L1-independent piRNAs. Accordingly, when the expression profile of piRNA clusters was examined, specific abundant small RNAs remaining present in these clusters of mutant oocytes were found (Fig. 34d), suggesting the existence of a specific class of MOV10L1-independent piRNAs.

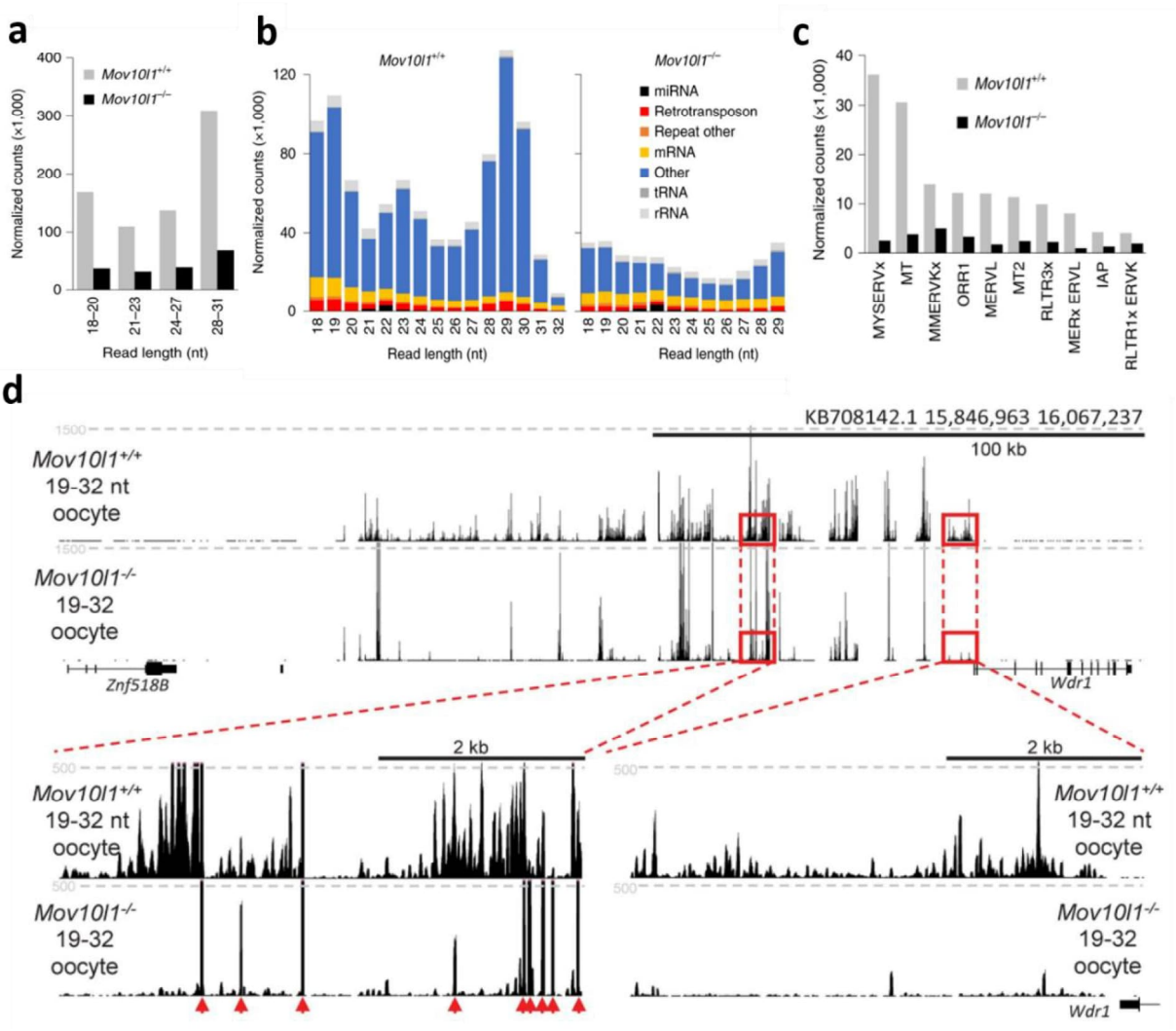

Figure 34: *piRNA analysis in golden hamster GV oocytes. a) Analysis of small RNAs of different lengths mapping to annotated piRNA clusters in WT and Mov10l1 mutant GV oocytes normalized to miRNA abundance. The decline in all Mov10l1 mutant small RNA populations is evident. b) Distribution of 18-32 nt RNAs based on length, origin and abundance normalized to miRNAs in WT and Mov10l1 mutant GV oocytes. c) Abundance of LTR retrotransposon-derived piRNAs in WT and Mov10l1-deficient GV oocytes. d) Snapshot from the UCSC browser showing the expression of 19-32 nt RNAs mapping to an annotated piRNA cluster in WT and Mov10l1 mutant GV oocytes (top). Below is a detail of two different regions showing the presence of specific piRNAs remaining in one of the regions in Mov10l1 mutant oocytes.*

Because the piRNA pathway can regulate gene expression by introducing DNA methylation into the promoter region, I wanted to determine whether impaired repression of FLI retrotransposons may be due to changes in the methylation state. I did not use the traditional bisulfite sequencing with PCR amplification and instead opted for whole-genome bisulfite sequencing of oocytes. Oocytes are of limited availability and using a traditional approach could bring clonal effects and amplification bias in repetitive sequence analysis. Whole-genome bisulfite sequencing allows for eliminating duplicated reads for more accurate analysis. Also,

the whole-genome bisulfite sequencing using multimapping reads mapped to the consensus sequence is equivalent to the traditional bisulfite sequencing, where retrotransposon families would be amplified with primers designed for the consensus sequence.

The very limited amount of material that oocytes provide revealed relatively low (approximately 10%) genome coverage of the converted reads (Fig. 35a). The resolution was not sufficient to estimate the level of methylation at unique loci, but allowed analysis of repetitive sequences. No significant changes in DNA methylation of recently expanded and highly piRNA-targeted retrotransposons were found (Fig. 35b). Next, individual CpG sites in IAP were examined using multimapping reads mapped to the consensus sequence of intact elements, which generated 20-40x coverage of specific regions (Fig. 35d). The IAPLTR3/4 subfamilies did not show a general loss of DNA methylation, although several CpG positions indicated a reduced state of DNA methylation (Fig. 35c). Although small changes in DNA methylation were found, overall these data do not clearly link retrotransposon derepression to defective piRNA-directed methylation.

Because RNA sequencing data imply impaired repression of retrotransposons, especially slightly increased expression of intact full-length copies, the key question remains whether they are actually active. Retrotransposons need to express their proteins for mobility, thus *Mov10l1*$^{-/-}$ GV oocytes were examined for the presence of LINE1 ORF1 and IAP GAG proteins. Immunofluorescence staining of IAP GAG protein did not show any specific signal in mutant oocytes compared to WT oocytes (Fig. 36a). LINE ORF1 staining revealed a slightly increased signal in mutant oocytes compared to WT oocytes (Fig. 36b), indicating that intact copies of LINE1 may be expressed and translated. On the other hand, a positive LINE1 signal also appeared in WT oocytes and the difference between WT and KO oocytes was not very striking (Fig. 36b). Taken together, data from LINE ORF1 immunofluorescence staining of GV oocytes did not provide clear evidence of abnormal LINE1 activity in mutant oocytes.

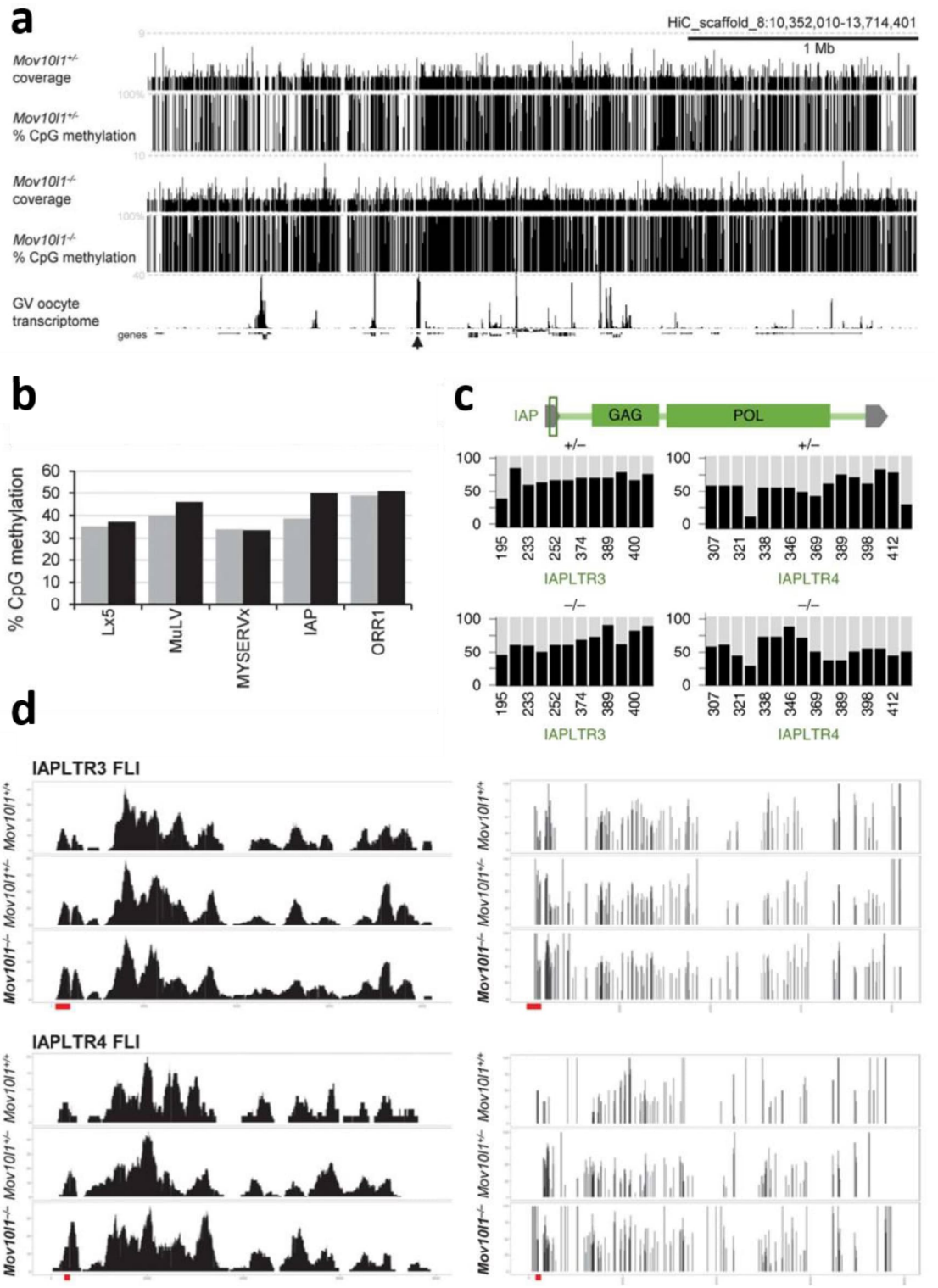

Figure 35: *Bisulfite sequencing of golden hamster GV oocytes. a) Snapshot from the UCSC browser showing coverage of the genome by fragments from bisulfite sequencing and CpG methylation frequency in different Mov10l1 genotypes. b) CpG methylation frequency in selected LTR retrotransposons. c) Methylation frequency at individual CpG sites of 5´ LTR (as indicated in the IAP scheme) of IAP LTR3/4 subfamilies in Mov10l1 heterozygous and homozygous GV oocytes. d) Number of bisulfite sequencing reads mapping to the consensus sequence of FLI IAP LTR3 and FLI IAP LTR4 subfamilies (left) and methylation frequency at individual IAP CpG sites (right) of different Mov10l1 genotypes (right). Red lines correspond to CpG positions analyzed in Fig. 35c.*

Furthermore, there was no difference between WT and KO oocytes, when staining with the DNA damage and repair marker γH2AX (Rogakou, Pilch et al. 1998) was used (Fig. 36), suggesting that the genome does not face a massive attack by mobilizing elements. More to that, I did not observe positive IAP or LINE1 staining, or even an increased signal from γH2AX in 2-cell zygotes isolated from *Mov10l1* mutant females 61 hours after mating (Fig. 37), suggesting that active elements do not accumulate between the GV and 2-cell stage and that the LINE1 signal observed in mutant oocytes was most likely a false-positive result. However, immunofluorescence staining may not be sensitive enough to recognize active elements in *Mov10l1* mutant oocytes and embryos, and impaired repression of retrotransposons indicated by RNA sequencing of mutant GV oocytes may contribute to the developmental incompetence of female *Mov10l1* mutant hamsters.

Taken together, I showed that *Mov10l1*$^{-/-}$ golden hamster females are sterile due to the inability of oocytes to support development beyond the 2-cell stage. The defect is a maternal effect associated with small transcriptome changes and mild derepression of retrotransposons in *Mov10l1*-deficient fully-grown GV oocytes. Analysis of IAP elements in *Mov10l1*$^{-/-}$ fully-grown GV oocytes did not show significant changes in DNA methylation, and interestingly, specific piRNAs remain present in *Mov10l1*-deficient golden hamster oocytes.

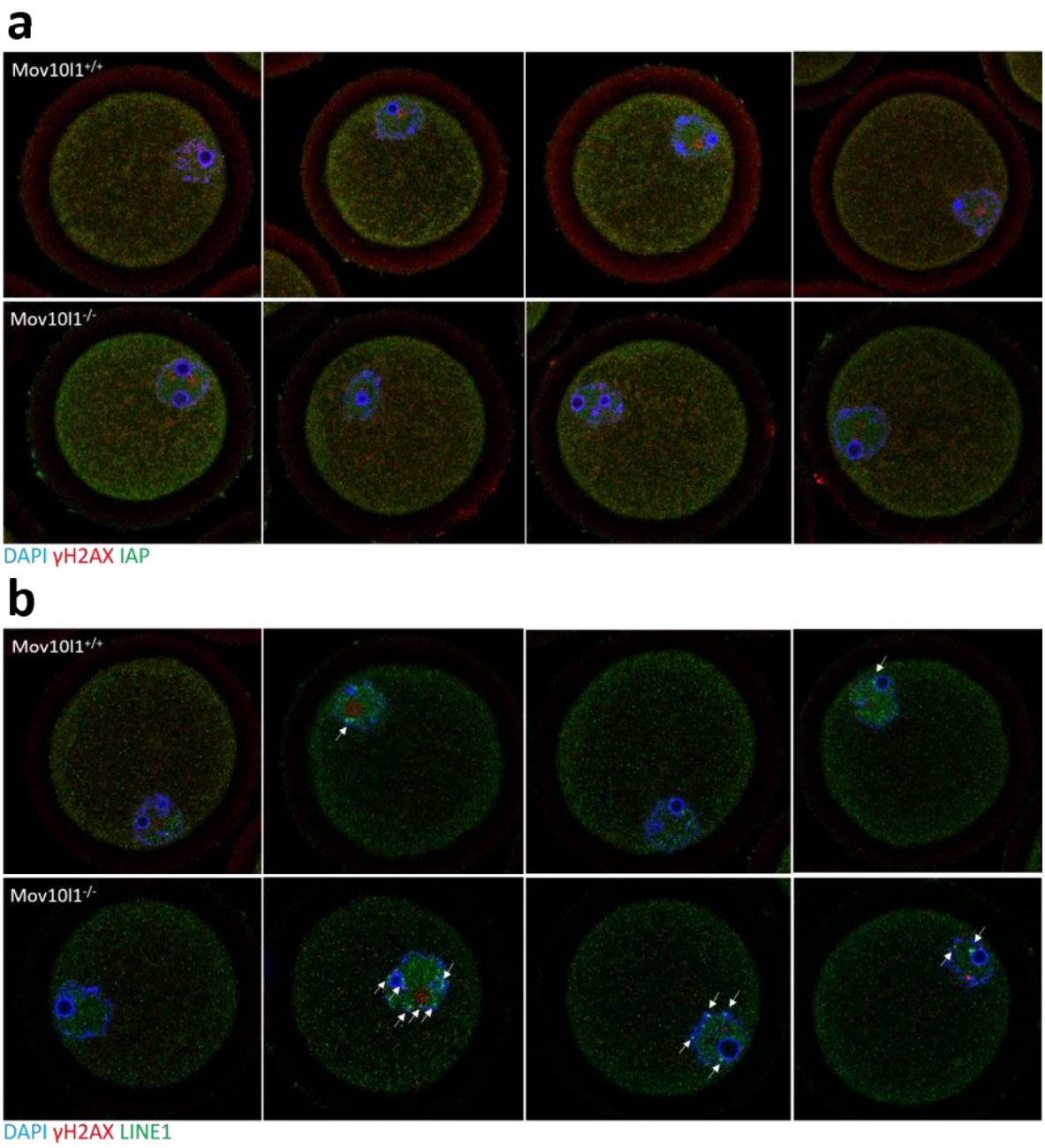

Figure 36: *Analysis of IAP and LINE1 retrotransposon activity in GV oocytes. a) Immunofluorescence staining of WT and Mov10l1 mutant GV oocytes using DAPI (blue), γH2AX (red) and IAP GAG (green) antibodies. b) Immunofluorescence staining of WT and Mov10l1 mutant GV oocytes using DAPI (blue), γH2AX (red) and LINE1 ORF1 (green) antibodies. White arrows depict LINE1 positive staining distinguishable from the background.*

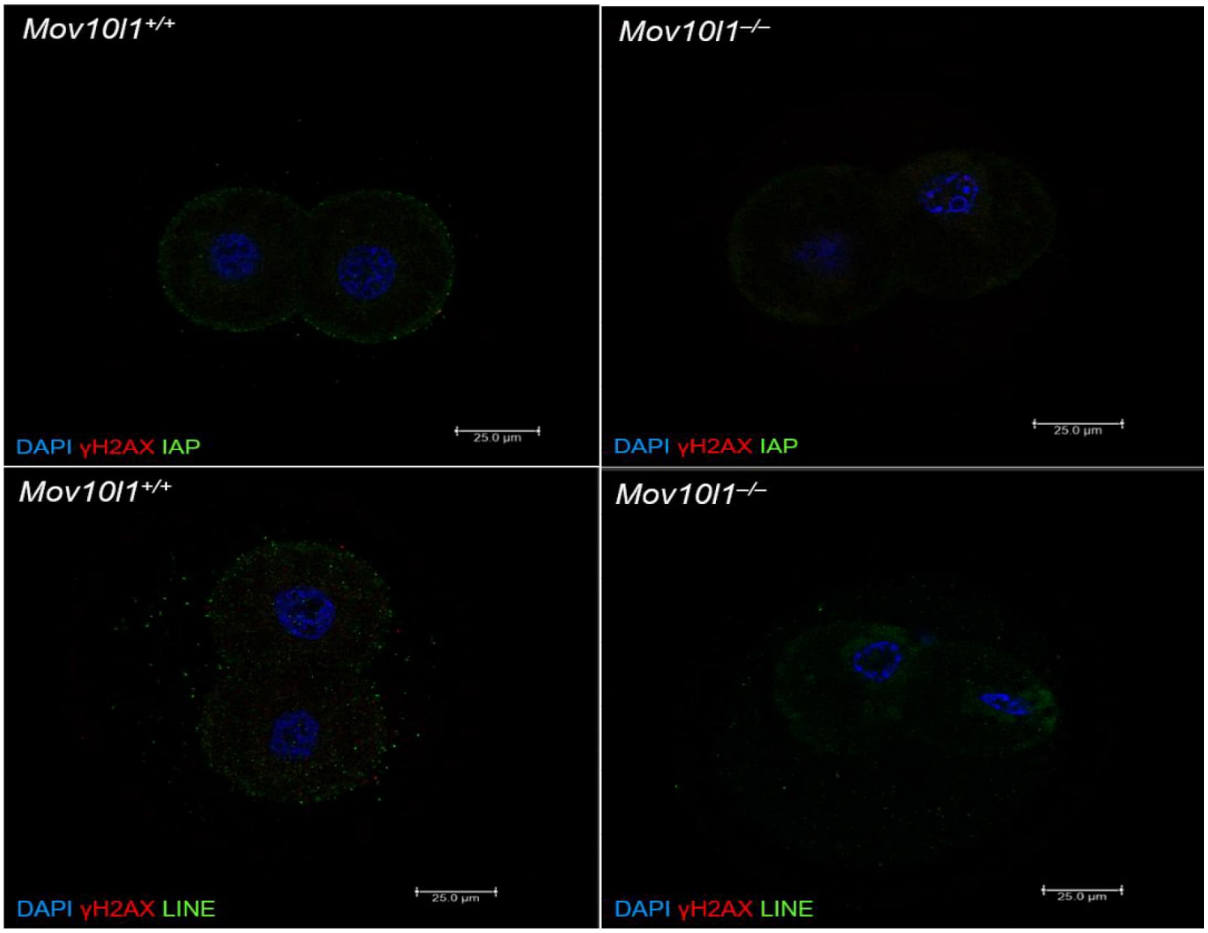

Figure 37: *Immunofluorescence staining of 2-cell zygotes isolated 61h post-mating from WT and Mov10l mutant females using DAPI (blue), γH2AX (red) and IAP GAG (top) or LINE1 ORF1 (bottom) antibodies. Scale bars, 25 µm.*

4.5 Sterile phenotype of male *Mov10l1* mutants

Male *Mov10l* hamster mutants were sterile. It was expected given the sterility observed in *Mov10l1* mouse mutants. Male *Mov10l1*$^{-/-}$ mice were sterile due to arrest at the pachytene stage of meiosis I associated with elevated levels of LINE1 and IAP retrotransposons (Zheng, Xiol et al. 2010). To determine whether the piRNA pathway in golden hamsters operates in the same way as in mice and whether hamster *Mov10l1* mutant males show the same spermatogenic defect as mouse *Mov10l1* mutants, I first examined the histology of adult male hamsters.

Adult *Mov10l1*$^{-/-}$ hamsters had atrophic testes and no sperm present in the epididymis (Fig. 38a, b). The hematoxylin and eosin staining of *Mov10l1*$^{-/-}$ seminiferous tubules showed mainly aspermatogenic tubules containing only somatic Sertoli cells located close to the basement membrane (Fig. 39), as confirmed using immunofluorescence staining of WT1, a marker of Sertoli cells (Fig. 39c) (Gao, Maiti et al. 2006). Interestingly, clusters of surviving

cells were observed in the center of approximately 3% of tubules (Fig. 39a, b). Immunofluorescence staining with germ cell marker DDX4 (Raz 2000) and a meiotic component of the synaptonemal complex SCP3 (Yuan, Liu et al. 2000) showed that cells located in the center of the tubule are germ cells undergoing meiosis (Fig. 39c). To examine the activity of retrotransposons in these rarely surviving germ cells of *Mov10l1*$^{-/-}$ tubules, I performed staining with IAP GAG, LINE1 ORF1 and γH2AX antibodies. A strong signal was observed when IAP GAG and γH2AX staining was used, showing the derepression of IAP retrotransposons associated with increased DNA damage (Fig. 39c). This suggests compromised genome integrity due to the activity of IAP elements. On the other hand, LINE1 ORF1 staining showed no positive signal in *Mov10l1*$^{-/-}$ tubules (Fig. 39c), suggesting that the antibody does not recognize hamster LINE1 protein or that LINE1 elements are not active at this stage. Accordingly, LINE1 inactivity in adults has already been indicated during the analysis of FLI LINE1-derived piRNAs at various stages of spermatogenesis, where abundant piRNA populations appeared on day 9, but were almost absent at later stages (Fig. 18). This is in contrast with the phenotype of *Mov10l1* mutant mice, where LINE1 expression increases dramatically during meiosis (Zheng, Xiol et al. 2010). Overall, the rarely surviving clusters of germ cells in hamster *Mov10l1* mutants exhibit similar manifestation of phenotype as *Mov10l1* mutant mice with germ cells arrested in meiosis.

Besides meiotic cells observed in several *Mov10l1*$^{-/-}$ hamster tubules, it is apparent that germ cell loss occurs in stages preceding entry into meiosis. To find the stage at which the germ cells are lost, the pioneering round of spermatogenesis was investigated. A newborn hamster testis (0 dpp), containing mitotically quiescent gonocytes, showed normal numbers of germ cells without any obvious defect found in KO animals when stained with DDX4 marker (Fig. 40a). It demonstrates that the golden hamster piRNA pathway is not essential for spermatogenesis during embryonic development. The 9 dpp *Mov10l1*$^{-/-}$ testes, where germ cells re-enter mitosis and move to the periphery of the tubule, did not show changes in numbers of cells either, when stained with DDX4 and counted on several histological sections (Fig. 40a, b). However, aberrant nuclear localization of DDX4 marker was observed in several germ cells (Fig. 40c), suggesting that a defect in spermatogenesis appears at this stage. The massive germ cell loss was observed in testes from mutant hamsters on day 13 *post-partum,* when spermatogonia are formed (Fig. 40a). The loss was indicated by tubules filled mainly with Sertoli cells and only a rare occurrence of cells positive for ZBTB16 (Fig. 40a), a marker of undifferentiated spermatogonia (Costoya, Hobbs et al. 2004). This observation was supported

by *Mov10l1*$^{-/-}$ tubules completely devoid of germ cells on day 21 when meiotic germ cells were present in WT tubules (Fig. 40a). It seems that the rarely surviving spermatogonia are compromised and enter meiosis later, given the rare appearance of meiotic cells in adult mutant hamsters (Fig. 39).

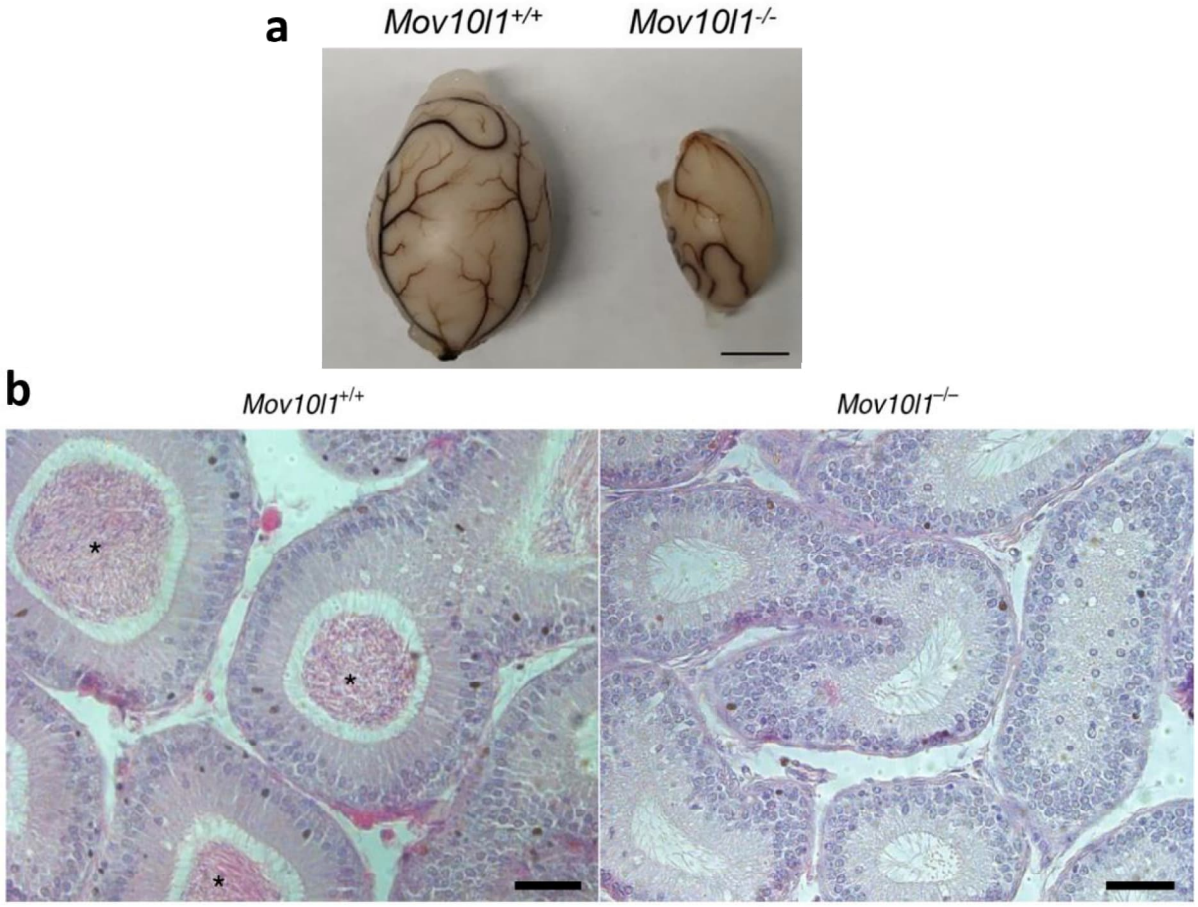

Figure 38: *Sterility of Mov10l1 mutant males. a) Testes isolated from adult WT and Mov10l1 mutant males. Mov10l1 mutants have atrophic testes. Scale bar, 5 mm. b) Hematoxylin and eosin staining of epididymal ducts. The presence of sperm is shown in WT, while the absence of sperm is evident in the Mov10l1 mutant. Black asterisks correspond to epididymal ducts containing sperm. Scale bars, 50 µm.*

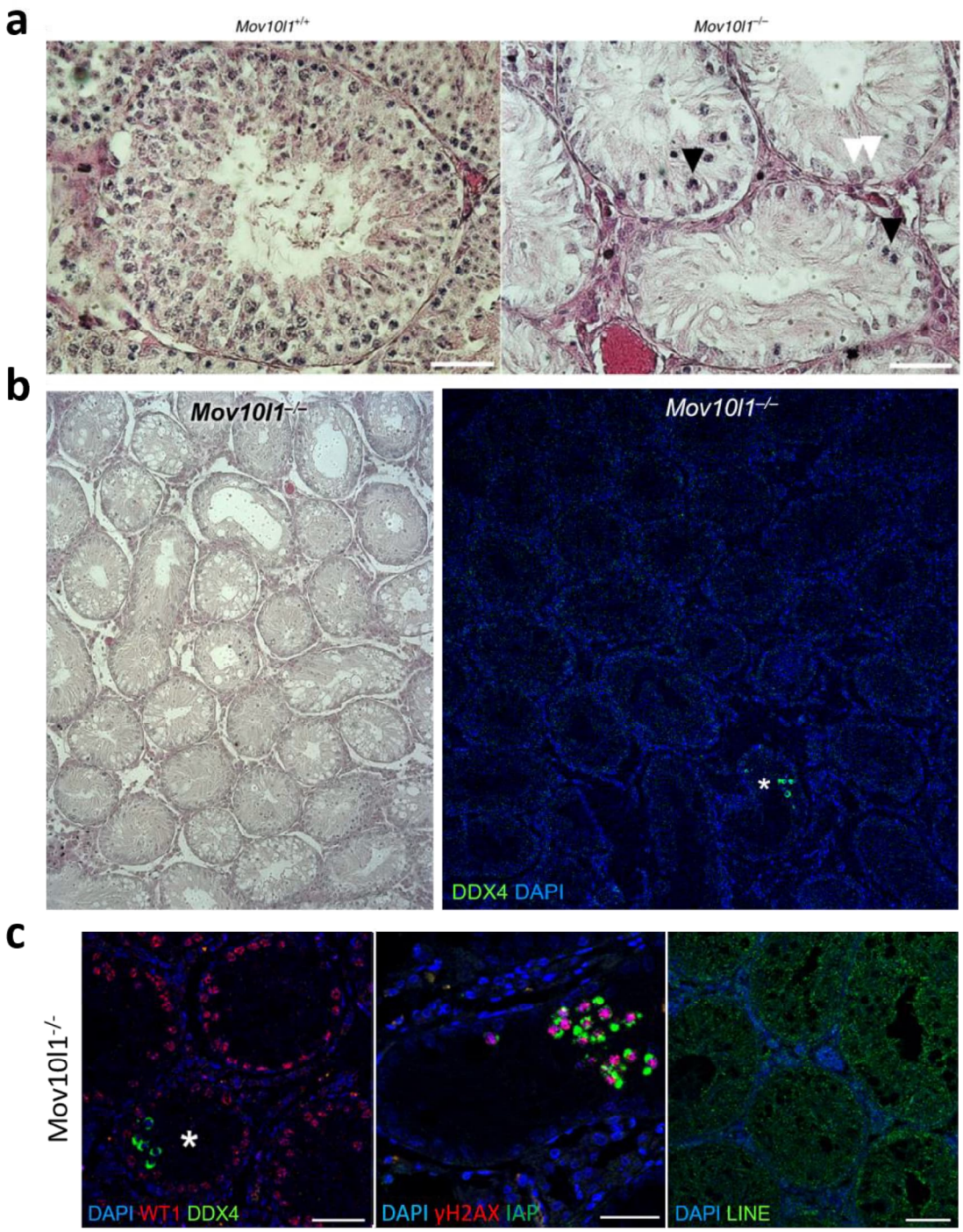

Figure 39: *Analysis of seminiferous tubules in adult Mov10l1 mutants. a) Hematoxylin and eosin staining of seminiferous tubules shows a massive loss of germ cells with a rare appearance of degenerating cells in the center of tubules in Mov10l1 mutants. White arrows depict degenerating cells, black arrows depict somatic Sertoli cells. Scale bars, 50 µm. b) Hematoxylin and eosin staining (left) and immunofluorescence staining using DAPI (blue) and DDX4 (green) show very few germ cells present in the seminiferous tubules of adult Mov10l1 mutants. c) Immunofluorescence staining of Mov10l1 mutant seminiferous tubules analyzing residual cell clusters. Left: Cells near the basement membrane are somatic Sertoli cells (WT1, red), rarely surviving clusters are germ cells (DDX4, green), which, Middle: undergo meiosis (SCP3, red), express IAP elements (green) and show DNA damage (γH2AX, red). Right: LINE1 elements (green) were not detected in seminiferous tubules of adult Mov10l1 mutants. Scale bars, 50 µm.*

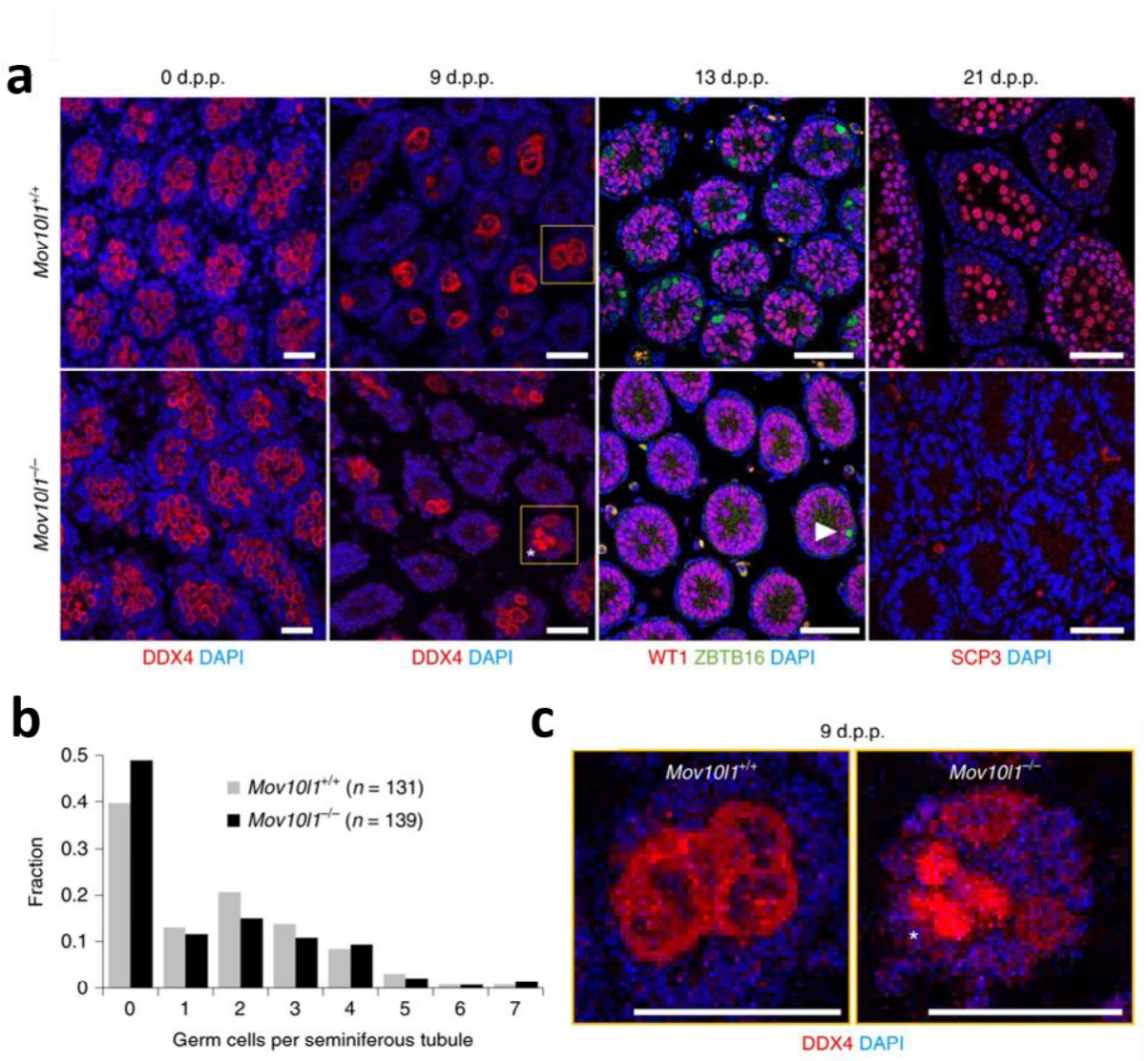

Figure 40: *Analysis of germ cell loss in Mov10l1 mutants. a) Immunofluorescence staining of seminiferous tubules isolated from newborn, 9 dpp, 13 dpp and 21 dpp old hamsters. Somatic Sertoli cells (WT1, red), germ cells (DDX4, red), undifferentiated spermatogonia (ZBTB16, green) and meiotic spermatocytes (SCP3, red) were examined and DNA was stained with DAPI. The analysis shows that massive germ cell loss occurs during spermatogonia formation. The asterisk indicates aberrant DDX4 germ cell localization, the white arrow indicates the only surviving ZBTB16-positive spermatogonium. Scale bars, 50 µm. b) Number of germ cells per seminiferous tubule in WT and Mov10l1 mutant counted in sections made from 9 dpp hamster testes and stained with DDX4. c) Aberrant localization of DDX4 germ cell marker in Mov101l1 mutant shown in detail. Scale bars, 50 µm.*

To find the cause of germ cell loss in *Mov10l1* mutant male hamsters that occurs before spermatogonia are formed, I examined stages preceding the major phenotypic manifestation. Because the piRNA pathway regulates gene expression, I performed an RNA sequencing of whole testes of newborn and 9 dpp old hamsters to examine their transcriptomes. Whole testes

were used for sampling due to difficulties with FACS sorting of the germ cells described in Chapter 4.1 Golden hamster as a model for the piRNA pathway.

The analysis showed approximately 300 genes dysregulated in newborn *Mov10l1*$^{-/-}$ testes and more than 900 genes dysregulated in *Mov10l1*$^{-/-}$ testes isolated from 9 dpp hamsters (Fig. 41a), suggesting a major effect on gene expression, which may contribute to the germ cell loss phenotype. Surprisingly, when the two datasets were compared, only a minimal overlap of differentially expressed genes and no enrichment of any biological function were found (Fig. 41b, c). These data indicate that the loss of MOV10L1 protein affects spermatogenesis already in newborn hamster testes, but the germ cell loss is associated with a different set of differentially expressed genes appearing on day 9.

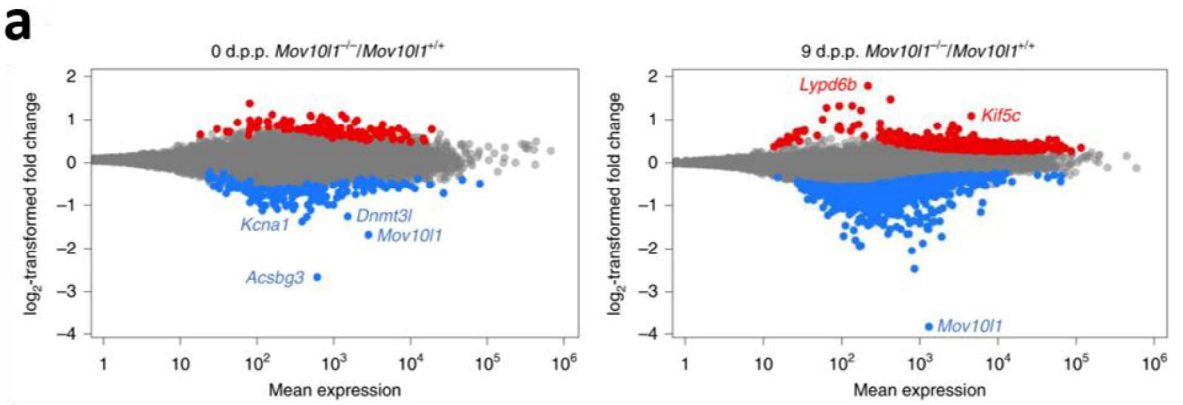

c

biological process – upregulated genes	p-value
chromatin assembly or disassembly	3.43E-09
nucleosome organization	4.24E-09
protein-DNA complex subunit organization	1.60E-07
ATP metabolic process	0.001133
biological process – downregulated genes	**p-value**
cellular process involved in reproduction in multicellular organism	1.69E-10
piRNA metabolic process	1.69E-10
meiotic cell cycle	2.50E-09
DNA methylation involved in gamete generation	1.18E-08
meiotic nuclear division	5.78E-08
transposition	5.92E-08
spermatogenesis	5.99E-08
negative regulation of transposition	1.74E-07
cell-substrate adhesion	4.56E-07
epithelial cell proliferation	6.17E-06

Figure 41: *Analysis of transcriptomes in newborn and 9 dpp hamster testes. a) MA plots of differentially expressed protein-coding genes in newborn and 9 dpp testes isolated from WT and Mov10l1 mutant males. Red dots depict significantly upregulated genes and blue dots depict significantly downregulated genes in Mov10l1-deficient testes. b) Venn diagrams showing the overlap between significantly upregulated or downregulated protein-coding genes selected in Mov10l1 differential expression analysis of newborn and 9 dpp hamster testes. c) Biological function analysis of upregulated and downregulated genes found in newborn and 9 dpp Mov10l1 mutant testes.*

Accordingly, events in 9 dpp testes were examined further. Because the comparative analysis of datasets from day 0 and day 9 did not reveal many candidates to be direct piRNA pathway targets, the targeting potential of piRNAs was examined. Small RNA sequencing of 9 dpp testes showed a massive drop in the population of 25-32nt small RNAs in *Mov10l1* mutants without any effect on the miRNA population (Fig. 42a, b). Interestingly, unlike piRNAs in oocytes, piRNAs in *Mov10l1*$^{-/-}$ testes were completely lost (Fig. 42b), suggesting that all testicular piRNAs are generated in the MOV10L1-dependent process. Because loss of piRNAs derived from non-repetitive sequences, particularly 3´ UTR of protein-coding genes, could lead to the germ cell loss caused by upregulation of genes normally repressed by the piRNA pathway, this scenario was investigated in detail. However, only a small fraction of upregulated genes appeared to be targeted by piRNAs mapping to the same loci (Fig. 42c). On the other hand, this analysis was complicated by the fact, that whole testes RNA sequencing was performed and thus the changes in expression could be under-represented when genes are also expressed in other than germ cells. This is demonstrated by the fraction of germ cell-specific genes that were found when the differential analysis from 13 and 21 dpp WT and mutant testes (lacking germ cells) was compared to the differential analysis of 9 dpp testes (Fig. 43).

The reason behind the spermatogenesis failure could be also derepressed retrotransposons, typical targets of piRNAs. Therefore, I analyzed TE regulation in *Mov10l1* mutants. The analysis revealed different groups of retrotransposons derepressed at various stages of spermatogenesis. In newborn mutant hamster testes, the most upregulated reads map to the MMERVKx family of retrotransposons. In contrast, the reads from 9 dpp mutants suggest that MYSERVx is the most expressed group of elements on day 9 (Fig. 44a, b). When the expression profile of 9 dpp testes was examined, I indeed observed a genome-wide expression activity of MYSERV-related inserts in *Mov10l1* mutants (Fig. 45), suggesting a link between derepressed MYSERV elements and spermatogenesis failure.

The derepression of IAP appeared to be rather low in both stages. The expression analysis of full-length intact LINE1 and IAP elements indicated 56% and 48% increase in 9 dpp mutant testes, respectively (Fig. 46). Results extracted from the RNA sequencing data were confirmed by RT-PCR performed on several genes, supporting the reliability of the data (Fig. 47a). Sanger sequencing of MYSERV RT-PCR products showed that multiple regions are amplified by primers designed for the consensus sequence of FLI insertions (Fig. 47b), indicating derepression of multiple loci.

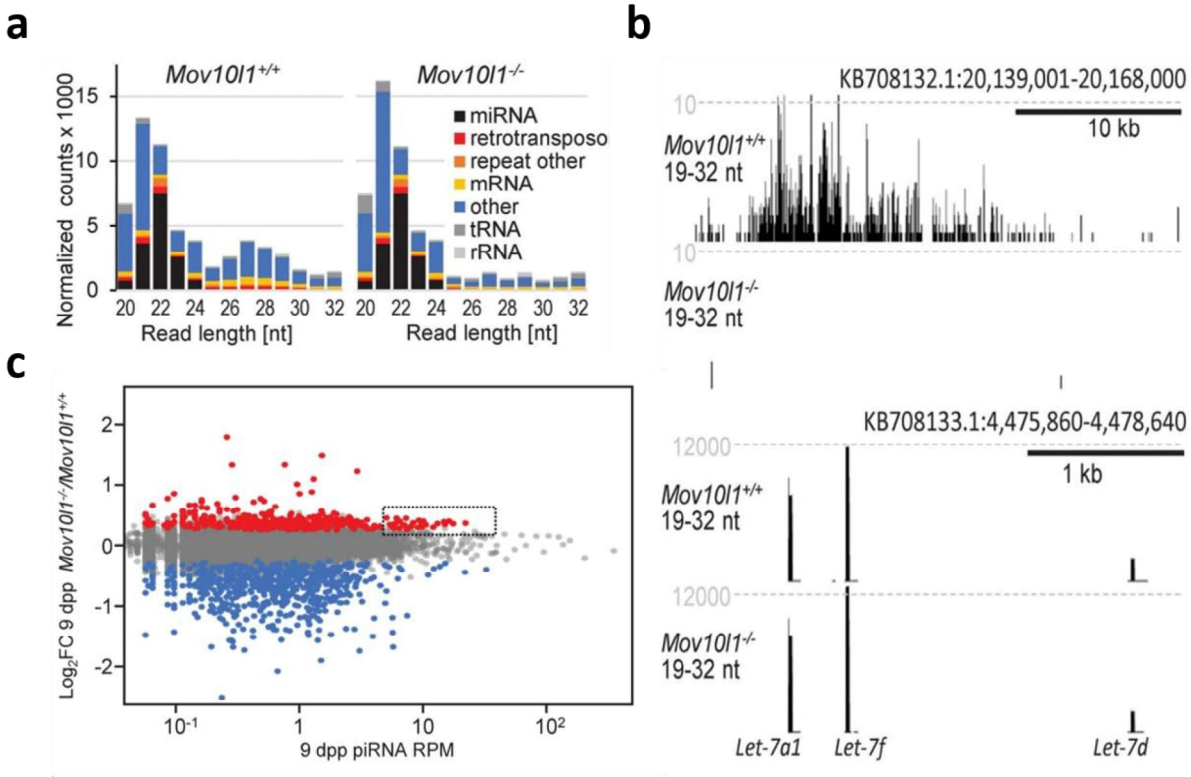

Figure 42: *Analysis of testicular piRNAs in Mov10l1 mutants. a) Distribution of 20-32 nt RNAs based on length, origin and abundance normalized to miRNAs in WT and Mov10l1 mutant 9 dpp testes. b) Snapshot from the UCSC browser showing loss of piRNAs in an annotated piRNA cluster (top) and intact Let-7 miRNA locus (bottom) in Mov10l1 mutant 9 dpp testes. c) MA plot showing the correlation between differentially expressed genes and abundance-scattered 24-31 nt RNAs (RPM) mapping to exons of differentially expressed genes in Mov10l1 mutant 9 dpp testes. The rectangle shows a small fraction of upregulated genes associated with abundant 24-31 nt RNAs (>-5 RPM).*

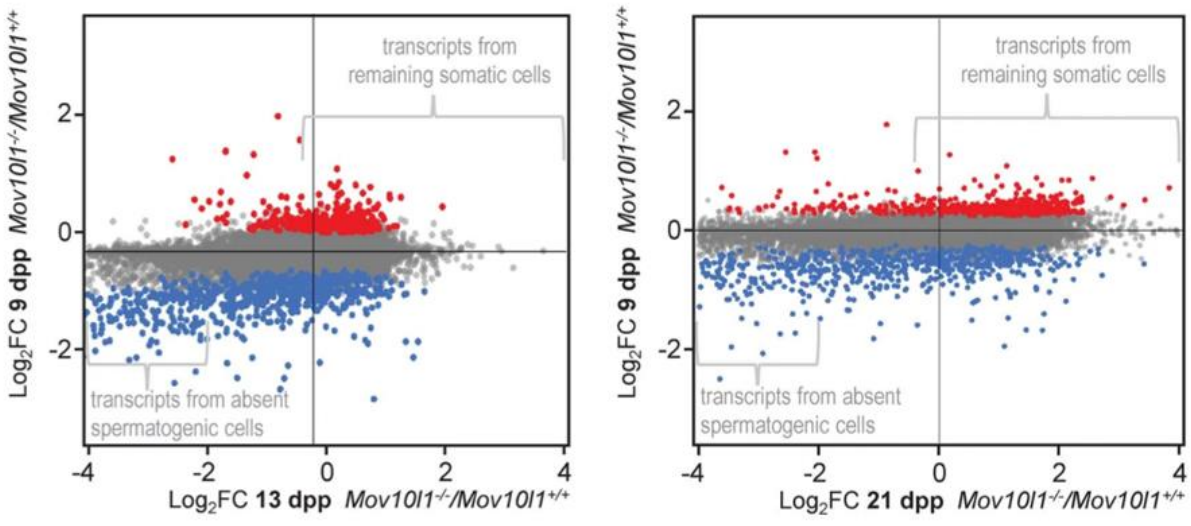

Figure 43: *Analysis of germ cell-specific genes. Differential expression analysis of Mov10l mutant 9 dpp hamster testes was plotted against differential expression analysis of Mov10l mutant testes from 13 dpp (left) and 21 dpp (right) old hamsters devoid of germ cells. Red and blue points depict significantly upregulated and downregulated genes in 9 dpp Mov10l mutant testes.*

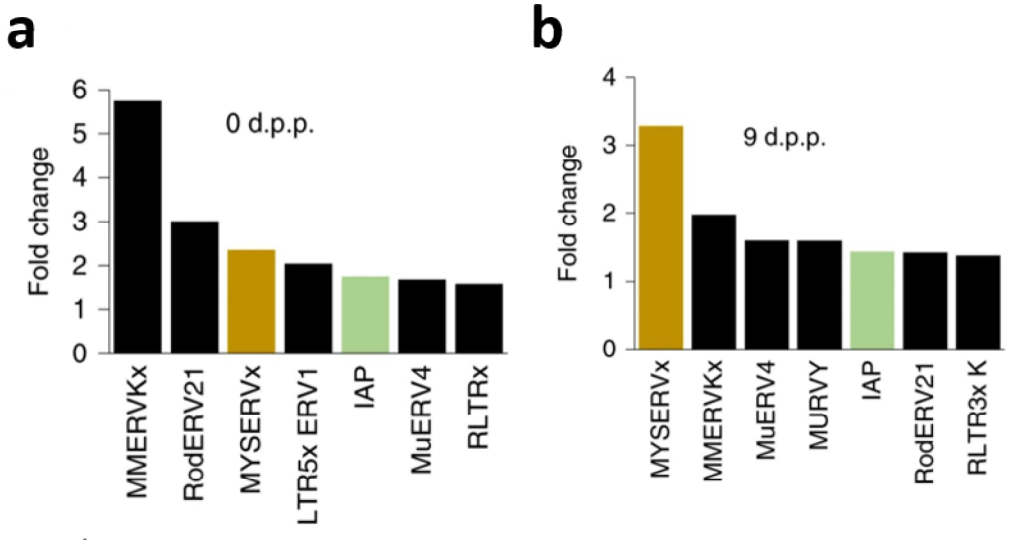

Figure 44: *Analysis of retrotransposon regulation in newborn and 9 dpp testes. a) Upregulation of LTR retrotransposon transcripts in Mov10l1 mutant newborn hamster testes compared to WT. b) Upregulation of LTR retrotransposon transcripts in Mov10l1 mutant 9 dpp hamster testes compared to WT.*

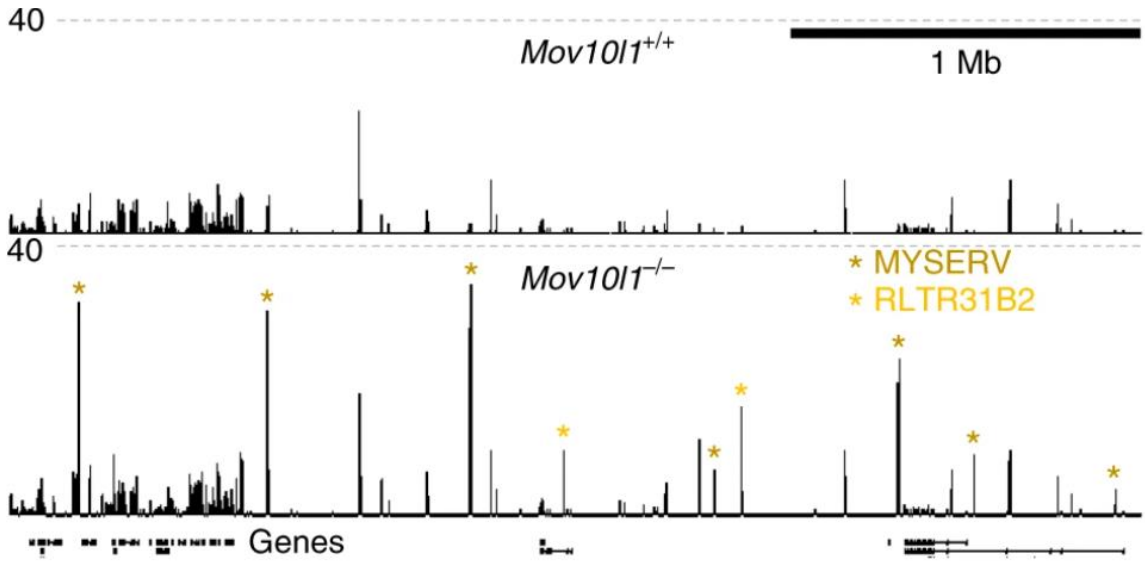

Figure 45: *Snapshot from the UCSC browser showing upregulation of MYSERV and MYSERV-related RLTR31B2 LTR transcripts in Mov10l mutant 9 dpp testes. Asterisks indicate upregulated retrotransposon loci.*

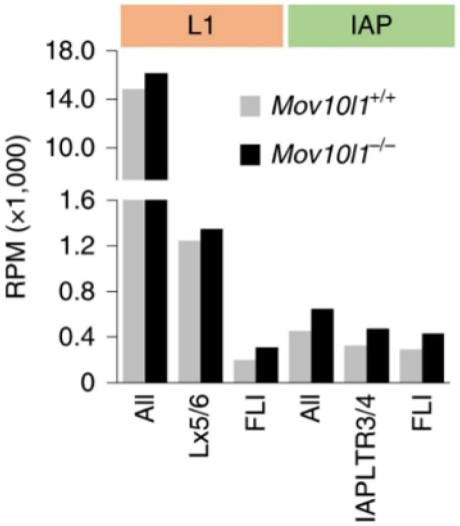

Figure 46: *Graph showing upregulation of reads mapping to all IAP and LINE1 elements, to young subfamilies of IAP and LINE1 elements selected by nucleotide substitution rate analysis, and to full-length intact copies of IAP and LINE1 elements in 9 dpp testes. FLI, Full-length intact.*

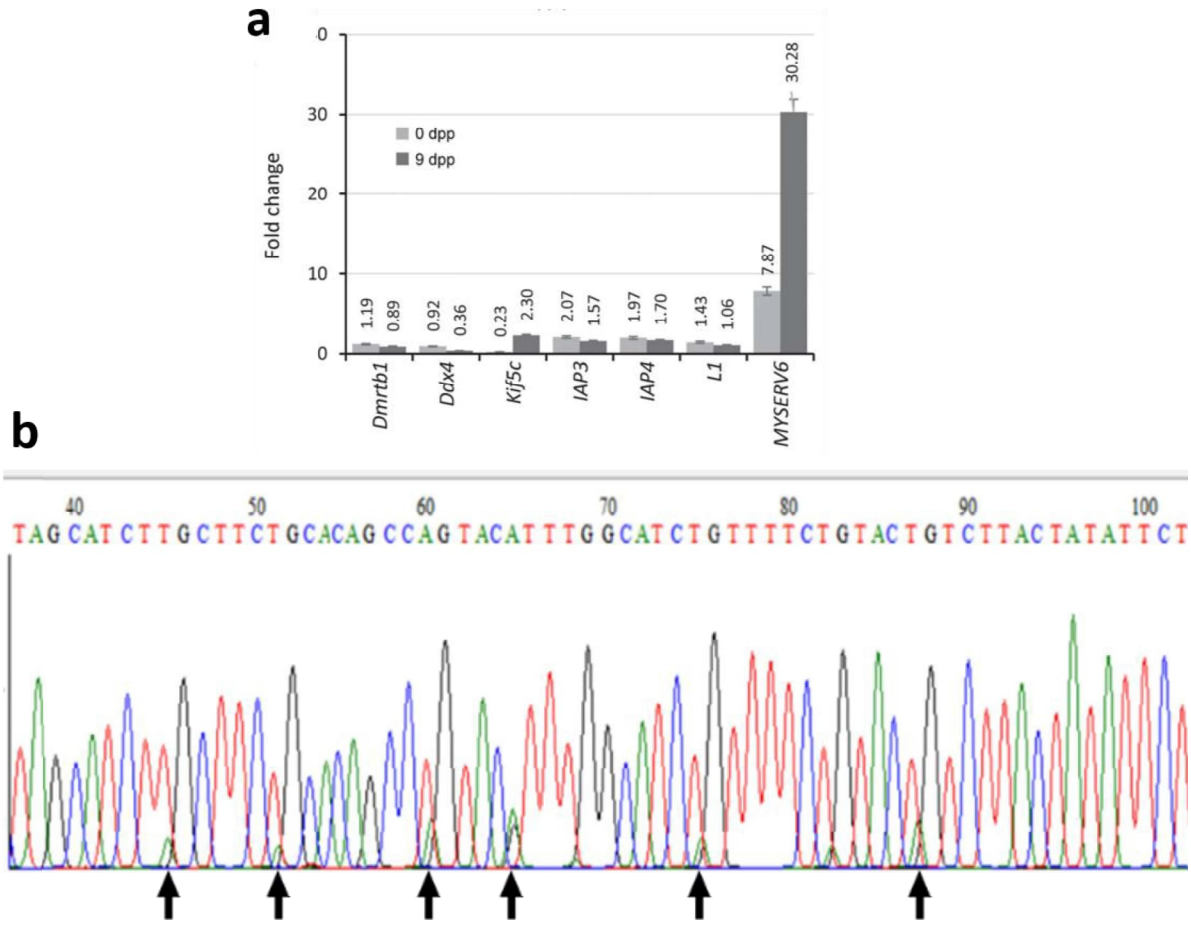

Figure 47: *RT-PCR analysis of selected genes and retrotransposons. a) Quantitative RT-PCR analysis of selected genes and retrotransposons in newborn and 9 dpp hamster testes. Numbers above each bar represent fold change. b) Sanger sequencing of MYSERV RT-PCR product amplified from 9 dpp Mov10l1 mutant testes by primers designed for the MYSERV consensus sequence. Black arrows indicate multiple nucleotides at one position.*

Although a similar increase in IAP expression was observed in both newborn and 9 dpp testes (Fig. 44a, b), the immunofluorescence staining with IAP GAG antibody revealed a specific signal only in 9 dpp mutant testes (Fig. 48). Concurrently, the same observation was made when the LINE1 ORF1 antibody was used. The signal was detected in 9 dpp mutant testes, but not in newborn hamsters testes (Fig. 48), suggesting different post-transcriptional regulation of retrotransposons between the two stages and potential retrotransposable activity of IAP and LINE1 elements emerging on day 9 *post-partum*. Accordingly, increased γH2AX signal was detected in 9 dpp mutant testes (Fig. 48), suggesting compromised genome integrity due to TE mobilization.

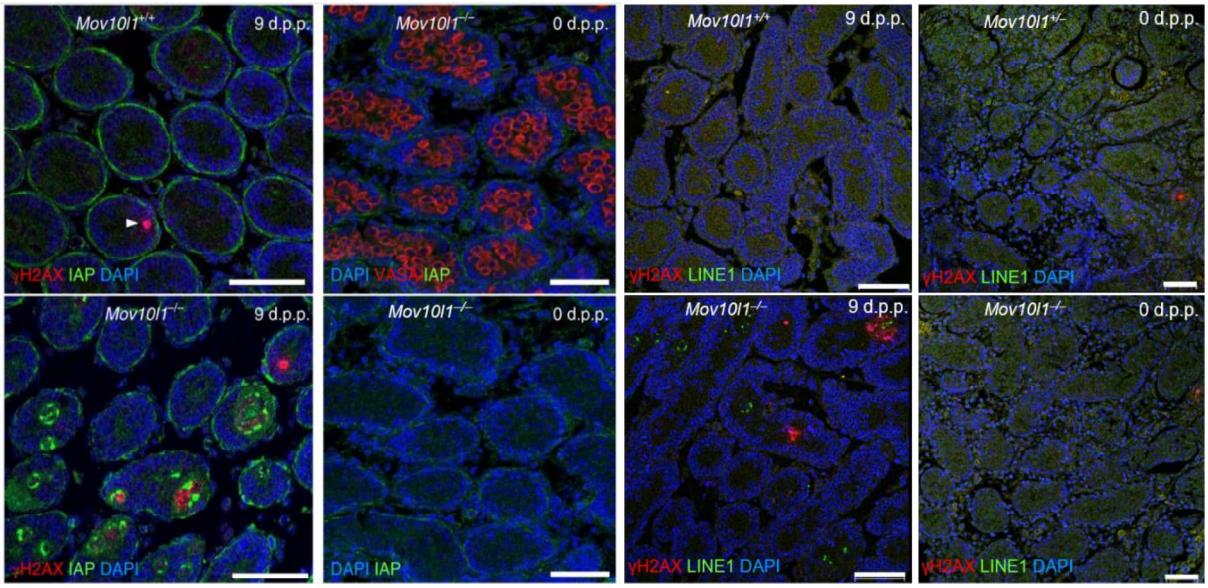

Figure 48: *Analysis of IAP and LINE1 protein expression in newborn and 9 dpp hamster testes. Immunofluorescence staining showed the presence of IAP GAG (green, left) and LINE1 ORF1 (green, right) proteins in 9 dpp Mov10l1 mutant seminiferous tubules, but not in newborn mutants. Elevated expression of IAP and LINE1 elements was associated with increased γH2AX (red) signal. DDX4 (VASA, red) was used to indicate germ cells and DNA was stained with DAPI (blue). Scale bars, 50 μm.*

In conclusion, a more detailed analysis of transcriptome changes in 9 dpp *Mov10l1*$^{-/-}$ testes demonstrated that the regulation of gene and retrotransposon expression by the piRNA pathway may be interrelated. For example, when *Lypd6b* and *Kif5c*, the two of the most upregulated genes in 9 dpp mutant testes were examined, they appeared to be genomic neighbors. This suggests a common regulation of the locus. The expression profile analysis of the transcriptome along with small RNA profiling showed that the regulation may occur via piRNAs derived from the 3′ UTR of the *Kif5c* gene or through the control of a multiple retrotransposon insertion in the *Lypd5* gene (Fig. 49). Therefore, the data do not allow to

distinguish the primary cause of the phenotype and rather refer to the very complex biological system.

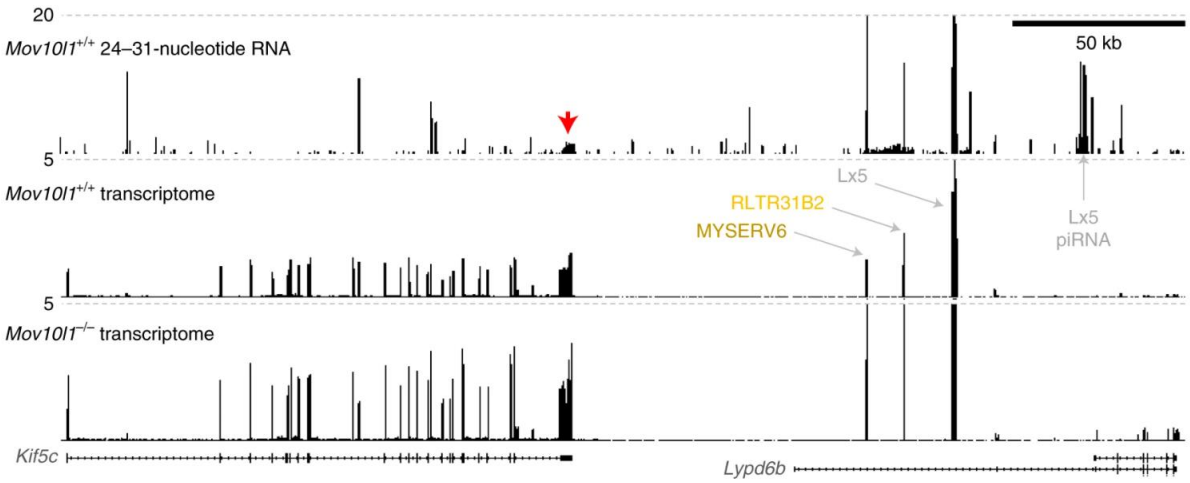

Figure 49: *Snapshot from the UCSC browser showing 24-31 nt RNA profiling in WT 9 dpp testes (top) and long transcripts in WT 9 dpp testes (middle) and Mov10l1 mutant 9 dpp testes (bottom) at the Kif5c-Lypd6 locus. The red arrow indicates piRNAs mapping to 3´ UTR of the Kif5c gene. Multiple insertions of retrotransposons (MYSERV6, RLTR31B2 and Lx5) into intron 1 of the Lypd6b gene and increased density of small RNAs derived from the same region along with piRNAs derived from Lx5 element, which are in close proximity, are also shown.*

Overall, I showed that *Mov10l1*$^{-/-}$ golden hamster males are sterile due to massive germ cell loss during spermatogonia formation. Rarely surviving germ cells show a defect in meiosis, resembling a phenotype in *Mov10l1*$^{-/-}$ mice. Stages preceding the major phenotypic manifestation in hamster *Mov10l1* mutant testes show substantial transcriptome changes, and germ cell loss appears to be associated with elevated levels of MYSERV, a young element identified in golden hamsters, and active full-length intact IAP and LINE1 elements.

5 Discussion

The piRNA pathway is an RNA-silencing mechanism whose ancestral function is to suppress the activity of mobile elements, which can pose a dangerous threat to the genome. The pathway has been extensively studied since the discovery of piRNAs (Aravin, Gaidatzis et al. 2006, Girard, Sachidanandam et al. 2006, Grivna, Beyret et al. 2006). Although our knowledge of the piRNA pathway has expanded in the last few years, many unknowns remain to be explained. The growing interest in the piRNA pathway brought many descriptive analyses of piRNAs and retrotransposons in a wide variety of animals. However, the biological function of the piRNA pathway in mammals has only been experimentally addressed in mice. This study selected the golden hamster as an alternative model organism to analyze the biological significance of the mammalian piRNA pathway beyond the known functions described in mice. Golden hamster is a suitable model for this task, because its small RNA pathways are more similar to other mammals than that of mice.

Golden hamster as a model for the mammalian piRNA pathway

Unlike *Drosophila* or zebrafish, any disruption of the mouse piRNA pathway leads to male sterility with no effect on female fertility (Lin and Spradling 1997, Cox, Chao et al. 1998, Deng and Lin 2002, Kuramochi-Miyagawa, Kimura et al. 2004, Carmell, Girard et al. 2007, Houwing, Kamminga et al. 2007, Houwing, Berezikov et al. 2008, Frost, Hamra et al. 2010). It is remarkable that such an evolutionary conserved pathway like the piRNA pathway would lose its significant function in the mammalian female germline. Notably, mice have evolved specific modifications to small RNA pathways that could mask the biological role of the piRNA pathway in the female germline. The first significant modification to the mouse piRNA pathway is a lack of PIWIL3 protein (Mouse Genome Sequencing, Waterston et al. 2002), one of the four PIWI proteins present in other mammals, like a cow or human (Roovers, Rosenkranz et al. 2015, Tan, Tol et al. 2020). Second, highly active RNAi pathway present in mouse oocytes points towards a unique combination of small RNA pathways in mouse female germline (Flemr, Malik et al. 2013). These specific aspects of small RNA pathways in mice emphasized the need for a new model organism more similar to other mammals, including humans. The presence of PIWIL3 (Ishino, Hasuwa et al. 2021) together with probable lack of highly active RNAi in golden hamster oocytes (Franke, Ganesh et al. 2017) resembles settings of mammalian small RNA pathways much closer than that of mice. Also, given the fast zygotic genome activation, short gestation (Hirose and Ogura 2019) and, above all, the availability of gene editing (Hirose,

Honda et al. 2020), the golden hamster is an optimal model for studying the biological significance of the piRNA pathway in mammals.

Retrotransposons in golden hamsters

Analysis of retrotransposons, the main targets of the piRNA pathway, has revealed several potentially active retrotransposon families in the golden hamster genome. Because mouse and hamster separated from a common ancestor and because ancestral active IAP and LINE1 elements are present in the mouse genome (Mouse Genome Sequencing, Waterston et al. 2002), particular attention was paid to hamster IAP and LINE1 elements. This study found 110 full-length intact copies of IAP and 110 full-length intact copies of LINE1 elements in the hamster genome, which are most likely capable of retrotransposition. It is a low number in comparison to more than 2 800 full-length intact copies of LINE1 elements found in the mouse genome (Mouse Genome Sequencing, Waterston et al. 2002). Also, we showed that different IAP and LINE1 subfamilies expanded in golden hamsters and mice. This offers an insight into retrotransposon divergence during ~24 million years (Steppan, Adkins et al. 2004) of the independent evolution of golden hamsters and mice.

Besides LINE1 and IAP retrotransposon families, the MuLV, MMERVK and MYSERV elements were also selected as young and potentially active elements. The activity of MuLV and MMERVK families has already been described in mice (McCarthy and McDonald 2004, Stocking and Kozak 2008), suggesting that their origin started back in a common ancestor of mouse and hamster. Although MYSERV was also present in the common ancestor of mouse and hamster, its activity has not been reported in mice and its sequence divergence suggests it is dead there. However, MYSERV features observed in this study indicate that MYSERV adapted its expression and acting to the early spermatogenesis in the *Cricetidae* family. MYSERV family is not well characterized and a low degree of homology with IAP elements does not show a close relationship between the two elements. The ORF analysis performed in this study showed that MYSERV can be in fact an autonomous element. A previous study suggested that MYSERV is related to active non-autonomous Mys element (Cantrell, Ederer et al. 2005), which was identified in the *Cricetidae* family (Wichman, Potter et al. 1985). Non-autonomous Mys elements in golden hamsters appear good candidates to be mobilized by MYSERV elements.

A different situation is observed in the case of ERVL elements. MaLR, a non-autonomous group of ERVL elements participating in mouse oocyte-to-zygote transition, which

was possibly driven by the autonomous MuERVL element, exhibits recent expansion in the mouse genome (Mouse Genome Sequencing, Waterston et al. 2002, Franke, Ganesh et al. 2017). However, no recent expansion of MaLR elements was found in the hamster genome based on substitution rate analysis. Accordingly, hamster MuERV-L and other ERVL families did not show recent expansion either, which indicates an absence of recent ERVL activity in the hamster genome. Together, analysis of young potentially active elements in related species offers an insight into the evolutionary divergence of ancestral transposable elements. For example, the above-described differences of ERVK and ERVL families in mouse and hamster genomes reveal dynamics of independent evolution of retrotransposons during the last ~24 million years (Steppan, Adkins et al. 2004).

The golden hamster piRNA pathway

Analysis of the golden hamster piRNA pathway outlined certain differences between male and female germlines. Features of pre-pachytene and pachytene piRNA populations examined at different time points of hamster spermatogenesis showed that hamster testicular piRNAs have the same characteristics as many other mammalian piRNAs, such as 1U-bias or the ping-pong signature (Aravin, Sachidanandam et al. 2008, Yang, Li et al. 2019). This shows that piRNA biogenesis during golden hamster spermatogenesis is essentially as was described in mice (Aravin, Sachidanandam et al. 2008). Surprisingly, we observed specific piRNAs remaining in golden hamster oocytes lacking MOV10L1 helicase. Given that MOV10L1 is an essential helicase for the initial steps of piRNA biogenesis (Zheng, Xiol et al. 2010, Vourekas, Zheng et al. 2015), we hypothesize that yet unknown alternative MOV10L1-independent mechanism of piRNA production may exist in golden hamster oocytes.

The piRNA pathway in golden hamster oocytes was examined through transcriptomic data. The analysis showed that, in addition to the presence of PIWIL3, *Piwil4* is also well expressed in fully grown hamster oocytes. PIWIL4 was not detected in fully grown or growing mouse oocytes (Kabayama, Toh et al. 2017) and is expressed in murine gonocytes and spermatogonia, where it is associated with post-transcriptional silencing of retrotransposons and piRNA-directed methylation of TE promoters (Watanabe, Cui et al. 2018). Thus, not only the presence of PIWIL3, but also the expression of *Piwil4* in hamster oocytes suggests a different mode of operation of the piRNA pathway than in mouse oocytes. Interestingly, transcriptomic data from human oocytes also show *Piwil4* expression in GV oocytes, albeit in low amounts, which suggests other common features in addition to *Piwil3* expression shared by the hamster and human oocytes. It is possible, that the unique physiology of oocytes together

with the expression of specific piRNA pathway components, like PIWIL3, promoted a different strategy of piRNA production compared to testes.

The biological role of the piRNA pathway in female golden hamsters

To investigate the biological significance of the piRNA pathway in golden hamsters, the function of the piRNA pathway had to be disrupted first. There were several possibilities how to do this, e.g. knocking-out one of the PIWI proteins. However, this strategy may be problematic due to possible redundant functions of PIWI proteins. Such redundancy can help the germline to overcome certain defects caused by the loss of one of the PIWI proteins, thus complicating analysis of knock-out phenotypes. As noted above, it was reported earlier that MOV10L1 plays an important role in the initial steps of piRNA biogenesis (Vourekas, Zheng et al. 2015). Given this knowledge, we assumed that loss of MOV10L1 should eliminate piRNA production completely and thus lead to complete loss of the piRNA pathway.

Deletion of MOV10L1 helicase caused impaired fertility in both sexes in golden hamsters, even though not all piRNA populations were lost in *Mov10l1* mutant oocytes, as discussed above. In accordance with our research, two parallel studies of the golden hamster piRNA pathway described a sterile female phenotype of *Piwil1* mutants (Hasuwa, Iwasaki et al. 2021, Zhang, Zhang et al. 2021). Given the consistency in phenotypes of different mutants, we can conclude that female sterility is indeed a result of a non-functional piRNA pathway rather than a result of some hypothetical piRNA-independent function of knocked-out proteins. Our data thus refute the assumption that the piRNA pathway is necessary only for male germline in mammals, as was shown in numerous studies in mice (Deng and Lin 2002, Kuramochi-Miyagawa, Kimura et al. 2004, Carmell, Girard et al. 2007, Frost, Hamra et al. 2010). It also implies that modifications of small RNA pathways present in mice obscured the biological significance of the mammalian piRNA pathway in the female germline.

The sterility of hamster piRNA pathway mutant females comes from a developmental arrest at the 2-cell stage (Hasuwa, Iwasaki et al. 2021, Zhang, Zhang et al. 2021). Activation of the zygotic genome is largely dependent on maternal contribution, and the sterile phenotype is clearly a maternal effect, as shown by viability and normal Mendelian frequency of *Mov10l1*$^{-/-}$ animals derived from heterozygous zygotes. Therefore, our study focused on the fully grown GV stage of oocytes, which is the last stage of ovarian oogenesis. It is also a stage expressing all components of the piRNA pathway, as shown by RT-PCR analysis of hamster oocytes and zygotes, suggesting that the piRNA pathway executes an important function in hamster GV

oocytes. To find out the potential origin of female sterility, we examined changes in gene expression of protein-coding genes in GV oocytes and surprisingly found only 13 genes dysregulated in *Mov10l1* mutants. In contrast, analysis of *Piwil1*-deficient matured oocytes identified 1 612 dysregulated genes (Hasuwa, Iwasaki et al. 2021). Although disruption of the piRNA pathway leads to the same phenotype in both mutants, there may be several differences explaining the transcriptome variability.

First, piRNA populations are affected differentially in the two mutants. Massive, but incomplete loss of piRNAs was observed in *Mov10l1*$^{-/-}$ oocytes. The remaining piRNAs could be effective to mediate the regulatory function required in GV oocytes. In the *Piwil1* mutant, only piRNA populations bound to PIWIL1 would be affected, while those bound by other PIWI proteins would be intact. However, it is possible that the PIWIL1-bound piRNA population is important for regulatory function in GV oocytes and that piRNAs remaining in *Mov10l1* mutants are those that interact with PIWIL1. Second, interaction of other PIWI proteins expressed in *Piwil1* mutant oocytes with piRNAs normally bound by PIWIL1 could have a negative impact on the transcriptome. Third, piRNA-independent role of PIWIL1 (Gou, Kang et al. 2017) could cause additional transcriptome changes to those caused by the loss of piRNAs. However, differences can also be, in part, explained by using oocytes of different stages leading to an escalated differential expression of genes during oocyte maturation.

A direct comparison of the datasets from differential expression analysis of *Mov10l1* and *Piwil1* filtered with the same stringency revealed 13 potential piRNA target genes that were significantly upregulated in both mutants. Yet, no common features were found among these genes, which suggests diverse control of the piRNA pathway. It is also possible that upregulation of these genes is a secondary effect caused by yet unknown primary changes or that the piRNA pathway participates at the posttranscriptional level. Nonetheless, even small changes in the transcriptome of *Mov10l1*$^{-/-}$ hamster oocytes could contribute to developmental incompetence, as exemplified by *Ythdf2* mouse mutants (Ivanova, Much et al. 2017).

Cumulative effect of defective maternal mRNA clearance adversely affecting zygotic genome activation may also be detrimental to ZGA (Rouget, Papin et al. 2010, Halbach, Miesen et al. 2020). Accordingly, Zhang and colleagues (Zhang, Zhang et al. 2021) show accumulation of maternal mRNA transcripts in *Piwil1*-deficient zygotes, suggesting impaired degradation of maternal mRNAs, which could lead to defective ZGA. This suggests a role for piRNAs in the degradation of maternal mRNAs during early development, which could have been omitted in our study, because we focused on earlier stages of development.

Not only changes in protein-coding genes, but also derepression of retrotransposons could lead to a developmental defect in female *Mov10l1* mutant hamsters. Yet, analysis of retrotransposons in hamster GV oocytes showed only a small increase in transcripts of LINE1 and IAP full-length intact elements. This suggests either very mild retrotransposon derepression occurring at only a few loci, or generally limited expression potential of retrotransposons in *Mov10l1* mutant oocytes. It is possible that retrotransposons have not adapted their activity to golden hamster GV oocytes and their expression may peak at later developmental stages or piRNAs remaining in *Mov10l1* mutant oocytes may be effective to suppress these elements. Moreover, the whole-genome bisulfite sequencing of *Mov10l1*-deficient GV oocytes did not reveal significant changes in DNA methylation status of IAP retrotransposons. This suggests that the repression of retrotransposons in *Mov10l1*-deficient oocytes is still present. Again, it is possible that piRNAs remaining in *Mov10l1*$^{-/-}$ oocytes may still sufficiently contribute to maintaining DNA methylation in *Mov10l1* mutants and the above-mentioned presence of PIWIL4 in hamster oocytes may help control the DNA methylation status. However, the possibility that retrotransposon repression is not associated with piRNA-directed methylation should also be considered.

Although we did not observe major derepression of retrotransposons in *Mov10l1*-deficient GV oocytes, their activity could start later and/or they could accumulate between GV oocytes and 2-cell zygotes. The 2-cell stage is the stage at which the zygotic genome activation starts in golden hamsters (Seshagiri, McKenzie et al. 1992) and is therefore very sensitive to any transcriptional and chromatin changes. When we examined *Mov10l1*$^{-/-}$ 2-cell zygotes by immunofluorescence staining with H3K9Ac and H3K9me3 antibodies, we did not find any unexpected major change in active chromatin or heterochromatin marks. The unaltered configuration of chromatin indicates normal heterochromatin formation in zygotes prior to zygotic genome activation. We also did not find any positive staining of LINE1 ORF1 and IAP GAG proteins in 2-cell zygotes lacking *Mov10l1*. In contrast, a parallel publication reported a significant increase of TE transcripts from *Piwil1*-deficient GV oocytes to 1-cell embryos (Zhang, Zhang et al. 2021), which suggests a cumulation of derepressed retrotransposons in the piRNA pathway-defective zygotes. However, the loss of *Mov10l1* and *Piwil1* could affect retrotransposons differentially. Our RT-PCR analysis of piRNA pathway transcripts at various time points of development showed persistence of only the *Piwil1* transcript up to the 2-cell stage. This would imply that PIWIL1 is the only PIWI protein translated and mediating piRNA-related function during early embryonic development. However, it is necessary to consider also

protein stability of other PIWI proteins. Accordingly, incomplete loss of piRNAs in *Mov10l1*$^{-/-}$ oocytes could lead to milder retrotransposon derepression effects than the loss of PIWIL1. In any case, activity of mobile elements requires retrotransposon-encoded proteins that were not detected in *Mov10l1*-deficient zygotes by immunofluorescence staining. This approach is either not sensitive enough to detect active elements in embryos, or retrotransposons are not active at the protein level. Possibly, as Zhang et al. (Zhang, Zhang et al. 2021) analyzed TEs at the RNA level, another post-transcriptional mechanism could prevent protein translation, or detected RNA signal may not represent full-length intact elements.

The biological role of the piRNA pathway in male golden hamsters

Our work shows that *Mov10l1*-deficient hamster males are sterile. The phenotype is manifested by massive germ cell loss during spermatogonia formation. This is different from mice where male *Mov10l1* mutants show arrest in meiotic spermatocytes (Frost, Hamra et al. 2010). In hamsters, only rarely surviving germ cells develop into meiotic cells. The surviving hamster meiotic cells show activity of IAP elements associated with impaired genome integrity. This observation suggests a secondary effect of the loss of the piRNA pathway in hamster meiotic cells, which is reminiscent of the *Mov10l*$^{-/-}$ mouse phenotype (Frost, Hamra et al. 2010). Thus, it appears that besides the common meiotic function of the MOV10L1 protein, a specific function evolved in golden hamster pre-meiotic cells. Interestingly, analysis of MOV10L1 protein in testes of mice and hamsters showed that, in contrast to mice, golden hamsters express two MOV10L1 isoforms. Whether this difference may reflect an additional function of MOV10L1 protein remains unknown and would require further investigation.

Germ cell loss in the early stages of spermatogenesis appears to be associated with massive transcriptomic changes in newborn and 9 dpp testes, stages preceding the phenotype. It is possible that loss of the piRNA pathway led to upregulation of protein-coding genes normally regulated by piRNAs, which resulted in defective germ cell development. Differential expression analysis showed around 300 and more than 900 genes dysregulated in newborn and 9 dpp mutant testes, respectively. We expected that real targets of the piRNA pathway should be present in both datasets. However, this was not the case, because different sets of genes were dysregulated in newborn and 9 dpp testes. This minimal overlap of differentially expressed genes indicates that cumulative trend of differentially expressed genes is not the reason behind the male germ cell loss. Notably, only a minimum of upregulated genes appeared to be directly targeted by piRNAs. Although real changes could be masked by bulk sequencing of all testicular cell populations, which makes detecting changes in smaller populations difficult.

Also, exact requirements for piRNA-target pairing have not yet been fully clarified and it appears that targeting flexibility is provided beyond the seed and is tolerant of mismatches (Anzelon, Chowdhury et al. 2021).

The rare occurrence of germ cells, which has led to the formation of meiotic cells in adult mutant hamsters, suggests a stochastic element in the mechanism leading to germ cell death, which allows for fortuitous survival of specific cells. This could be explained by the activity of retrotransposons, which may compromise the genome control rather stochastically. Indeed, a genome-wide derepression of MYSERV loci was found in 9 dpp testes, a stage preceding the germ cell loss. It suggests that MYSERV derepression is involved in the failure of spermatogenesis. Also, positive staining of IAP and LINE1 proteins found in *Mov10l1* mutant 9 dpp testes indicates that these full-length intact elements are capable of retrotransposition at this stage. This is surprising, because sequencing reads perfectly mapping to full-length intact copies of IAP and LINE1 elements were only slightly increased in mutants at day 9. This could be a situation where full-length intact retrotransposons escaped repression at only a few loci. High activity of these several copies may be detrimental for the host cell, while there would be a low increase at the RNA level.

Interestingly, MYSERV derepression in newborn mutant testes did not appear as massive as in 9 dpp mutant testes. Also, no signal was detected when IAP and LINE1 proteins were stained in newborn mutant testes, even though IAP RNA analysis showed similar results as in 9 dpp mutant testes. It suggests a different post-transcriptional regulation of retrotransposons in newborn and 9 dpp testes and emerging activity of IAP and LINE1 retrotransposons in testes of 9 days old hamsters. Moreover, the MMERVK family of retrotransposons appears to be massively upregulated in newborn mutant testes, whereas its expression decreases on day 9. These results suggest that different retrotransposon families have adapted their activity to different stages of germ cell development. Consequently, different sets of differentially expressed genes in newborn and 9 dpp mutant testes may be the result of activity of different retrotransposon groups affecting transcriptome in various ways. Thus, the massive loss of germ cells would be associated with detrimental activity of retrotransposons, which have adapted their expression to the stage preceding the phenotype.

The example of MMERVK elements upregulated in newborn *Mov10l1* mutant hamster testes shows that not all transposable elements have a destructive effect when derepressed. We cannot say whether these elements were translated into protein and therefore capable of retrotransposition. However, a somewhat similar observation was made in mice. The

derepressed IAP activity in mouse spermatogonia does not cause a defect in spermatogenesis until LINE1 elements are massively upregulated during meiosis in mouse piRNA pathway mutants (Kuramochi-Miyagawa, Kimura et al. 2004, Carmell, Girard et al. 2007). When LINE1 elements are elevated in spermatogonia in *Mili* and *G9a* double mutants, massive loss of pre-meiotic cells occurs in early stages of spermatogenesis (Di Giacomo, Comazzetto et al. 2014). This raises an interesting question of whether the mutual activity of IAP and LINE1 retrotransposons or LINE1 activity itself causes fatal cell damage in mice. Likewise, it remains to be determined whether the combined activity of TEs or a specific family of retrotransposons causes germ cell death in hamster spermatogenesis. Possibly, MYSERV activity alone, which peaks on day 9, may damage cells during spermatogonia formation. On the other hand, the absence of IAP and LINE1 proteins in newborn mutant testes suggests that TEs become transpositionally active later, and therefore cells may die at day 9 and later due to the mutual activity of different TE families capable of retrotransposition. Not only mobile activity, but also transcriptional activity of derepressed retrotransposons can affect neighboring genes and lead to transcriptomic changes resulting in germ cell loss. Finally, we cannot exclude the possibility that TEs are only "bystanders" of more general transcriptional changes underlying the observed phenotype. Therefore, finding the primary cause of germ cell loss in *Mov10l1* mutant golden hamsters still needs further investigation.

Adaptability of retrotransposons

Our study reports an important regulatory role of the piRNA pathway in pre-meiotic, meiotic and post-meiotic stages of germline development. Interestingly, while the phenotype manifests in pre-meiotic and meiotic stages of spermatogenesis, females exhibit post-meiotic and post-zygotic arrest at the 2-cell stage. Golden hamster testicular and oocytic piRNAs have been shown to differ and rarely overlap (Ishino, Hasuwa et al. 2021), which suggests that different targets and thus different biological functions may exist in the two cell types. Accordingly, we did not observe derepression of MYSERV elements in *Mov10l1* mutant oocytes, whereas it was massively upregulated in spermatogenic cells. MYSERV thus seems to have adapted its expression exclusively to the male germline of the *Cricetidae* family and perhaps stages of female germline development we did not analyze. Also, piRNAs remaining in *Mov10l1*$^{-/-}$ oocytes could protect the genome from MYSERV derepression. However, because the evolutionarily conserved role of the piRNA pathway is retrotransposon silencing, we can assume that the biological role of the piRNA pathway is the same in both sexes. In this case, differences in phenotypes of males and females can be explained by adaptation of the

pathway to the stage where active retrotransposons have adjusted their expression. Adaptation of retrotransposon expression to specific cell types is likely random and depends on selective pressure and recruitment of host cell transcription factors. The stage to which active retrotransposons have adapted their expression is most likely to be the same where loss of the piRNA pathway causes a defect, as suggested by MYSERV, LINE1 and IAP expression in 9 dpp hamster testes.

In this respect, the group of golden hamster MaLR elements appears to be an interesting case. Since no recent expansion of the MaLR group of elements was found in the golden hamster genome, it is surprising that abundant piRNA populations targeting MaLR elements exist in golden hamster testes. MaLR-derived piRNAs appear mainly on day 21 *post-partum*, suggesting that these elements may be transcriptionally active during meiosis. Although they appear to be transpositionally inactive, as indicated by nucleotide substitution rate analysis, their expression could negatively affect germ cell development. Unfortunately, the absence of meiotic cells in male *Mov10l1* mutants precludes examining the transcriptional potential of these elements in golden hamsters. Anyway, combined analysis of piRNAs and potentially active retrotransposons appears to have considerable predictive value for the biological function of the piRNA pathway in a given animal species.

Different adaptation of retrotransposons to host germ cell development can be exemplified by mouse and golden hamster spermatogenesis. Hamster IAP and LINE1 elements apparently adapted their expression during spermatogenesis differently than in mice. Whereas the LINE1 family can be observed throughout the whole spermatogenesis in mice (Di Giacomo, Comazzetto et al. 2013, Di Giacomo, Comazzetto et al. 2014), it adjusted its activity to the early stages of hamster spermatogenesis. This is demonstrated by the abundant population of LINE1-targeting piRNAs found mainly in 9 dpp testes. It also corresponds with positive staining of LINE1 ORF1 protein observed in juvenile, but not adult *Mov10l1* mutants. In contrast, IAP protein was observed in juvenile germ cells, as well as in meiotic spermatocytes in adult *Mov10l1* mutant hamster testes, corresponding to the presence of piRNAs targeting IAP elements at all stages tested. This suggests that IAP is active during a large part of hamster spermatogenesis. Adaptation of retrotransposon activity to a particular developmental stage appears to correspond to the subsequent biological function of the piRNA pathway, as shown by the loss of hamster germ cells associated with MYSERV, IAP, and LINE1 activity in 9 dpp mutant testes and the loss of mouse pre-meiotic/meiotic germ cells associated with elevated activity of LINE1. These data show that adaptation of TE activity to different stages of germ

cell development in animals is stochastic and may vary between species. Accordingly, these data provide an evolutionary perspective of the endless fight between the piRNA pathway and parasitic transposable elements, demonstrating the adaptive nature of the pathway, which allows for an active response to emerging threats to the genome.

Evolutionary aspects of the piRNA pathway

The piRNA pathway is well conserved from invertebrates to mammals, but many differences can be found, such as sources and targets of piRNAs or specific adaptations of piRNA biogenesis (reviewed in (Ozata, Gainetdinov et al. 2019)). For example, piRNA-generating loci in flies lack hallmarks of typical transcription, such as active promoter histone marks or splicing signals (Moshkovich and Lei 2010, Ozata, Gainetdinov et al. 2019), while they are indistinguishable from canonical transcription in mammals. Also, while *Drosophila* and zebrafish piRNA pathway mutants show defects in pre-meiotic cells during germ cell establishment (Lin and Spradling 1997, Cox, Chao et al. 1998, Houwing, Kamminga et al. 2007, Houwing, Berezikov et al. 2008), defects in mouse male piRNA pathway mutants manifest in specified meiotic and post-meiotic cells (Deng and Lin 2002, Kuramochi-Miyagawa, Kimura et al. 2004, Carmell, Girard et al. 2007, Frost, Hamra et al. 2010). This implies differences in the regulation of germ cell development between *Drosophila*, zebrafish and mice. Also, as noted at the beginning, disruption of the piRNA pathway leads to male and female sterility in *Drosophila* or zebrafish (reviewed in (Ketting 2011)), while the piRNA pathway is only essential for male fertility in mice (Deng and Lin 2002, Kuramochi-Miyagawa, Kimura et al. 2004, Carmell, Girard et al. 2007, Frost, Hamra et al. 2010). Despite unimpaired female fertility in mouse piRNA pathway mutants, the importance of the piRNA pathway in female germline of non-*Muridae* mammals has been anticipated (Roovers, Rosenkranz et al. 2015).

Accordingly, my thesis research showed that the piRNA pathway is essential for fertility of both sexes in golden hamsters, reminiscent of phenotype of piRNA pathway mutants in *Drosophila* and zebrafish (Lin and Spradling 1997, Cox, Chao et al. 1998, Houwing, Kamminga et al. 2007, Houwing, Berezikov et al. 2008). For example, the piRNA pathway is necessary for germ stem cell maintenance in *Drosophila* (Lin and Spradling 1997, Cox, Chao et al. 1998) and we did not observe other than rarely surviving meiotic cells in adult *Mov10l1*$^{-/-}$ golden hamster males. This suggests that, similarly to *Drosophila*, the piRNA pathway is important for germ stem cell maintenance in golden hamsters. Zebrafish is a special case, where all piRNA pathway mutants are phenotypically sterile males due to the loss of PGCs necessary for development of female gonads (Houwing, Kamminga et al. 2007, Houwing, Berezikov et al.

2008). However, a specific missense mutation in *Zili* allowed the development of females, which were sterile (Houwing, Berezikov et al. 2008). Similar to golden hamster mutant females, missense *Zili* zebrafish mutant females formed oocytes, which could be fertilized, but showed defects in meiosis (Houwing, Berezikov et al. 2008). This is in contrast with our observation, that golden hamster oocytes lacking *Mov10l1* do not have any apparent defects in meiosis. Also, complete loss of ZILI showed that, unlike golden hamster piRNA pathway mutants, *Zili* mutants in zebrafish do not form oocytes due to the inability of germ cells to differentiate (Houwing, Berezikov et al. 2008).

To characterize differences and similarities between *Drosophila*, zebrafish and golden hamster piRNA pathway mutants, we must consider that the biology of germ cell development differs profoundly among these species. Despite such differences, the common requirement for the piRNA pathway in germ cell development of different species is remarkable, given almost 800 million years of independent evolution of *Drosophila* and golden hamsters (Kumar, Stecher et al. 2017) and evolutionary modifications in the piRNA pathway, such as the presence of only two PIWI proteins in zebrafish (Houwing, Kamminga et al. 2007), while four are encoded in the golden hamster genome (Ishino, Hasuwa et al. 2021). This shows that the biological role of the piRNA pathway is evolutionary conserved and that sexual dimorphism of mouse piRNA pathway mutants is presumably caused by specific modifications in small RNA pathways that differentiate mice from other mammals.

One of the specific aspects in mouse oocytes is highly active RNAi, which is driven by an oocyte-specific shorter isoform of Dicer ($Dicer^{O}$) (Flemr, Malik et al. 2013). $Dicer^{O}$ is generated from an alternative promoter provided by retrotransposon LTR which was inserted in the common ancestor of mouse, rat, and hamster, but preferentially adapted its promoter activity to the *Muridae* family (Flemr, Malik et al. 2013, Franke, Ganesh et al. 2017). Although the promoter in rat oocytes is not as active as in mouse oocytes, rat oocytes express more $Dicer^{O}$ isoform transcript than the full-length Dicer mRNA (Franke, Ganesh et al. 2017). Thus, it would be interesting to see whether RNAi is also active in rat oocytes. In hamster oocytes, the full-length Dicer expression dominates while $Dicer^{O}$ expression is negligible (Franke, Ganesh et al. 2017).

Another modification to small RNA pathways in mice is loss of *Piwil3,* which is present in other mammals, including hamster, cow and human (Roovers, Rosenkranz et al. 2015, Tan, Tol et al. 2020, Ishino, Hasuwa et al. 2021). *Piwil3* was lost due to recombination of the locus carrying the gene in the common ancestor of mice and rats. Loss of oocyte-specific PIWIL3 in

golden hamster females leads to a milder phenotype than the loss of MOV10L1 or PIWIL1. *Piwil3*-deficient oocytes can support development, although *Piwil3*$^{-/-}$ females are subfertile. It is associated with altered methylation which was observed in *Piwil3* mutant oocytes (Hasuwa, Iwasaki et al. 2021). In contrast, whole-genome bisulfite sequencing of *Mov10l1*-deficient oocytes did not report such changes, which could have several reasons: (1) our analysis of *Mov10l1* mutants may have omitted these changes due to low genome coverage, (2) remaining piRNAs in *Mov10l1*$^{-/-}$ oocytes could prevent these changes or (3) PIWIL3 has a piRNA-independent role in DNA methylation. Accordingly, *Piwil3*-deficient oocytes did not show significant TE derepression like *Mov10l1* or *Piwil1* mutants (Hasuwa, Iwasaki et al. 2021, Zhang, Zhang et al. 2021). This would again point towards an alternative piRNA-independent role of PIWIL3 in hamster oocytes.

This also suggests that lack of *Piwil3* in the mouse genome is not a major reason for nonessential function of the piRNA pathway in mouse oocytes. While we cannot rule out that insignificance of the piRNA pathway in mouse oocytes may be based on changing requirements for the piRNA pathway during evolution, highly active RNAi should be considered as the key difference between biology of small RNA pathways in mice and other mammals. Notably, a study showing the redundant function of piRNA and RNAi pathways in suppression of retrotransposons (Taborska, Pasulka et al. 2019) suggests evolution of redundant targeting of specific transcripts. Recent work also shows an interesting cross-talk between these two pathways in *Drosophila*, where maternally inherited siRNAs initiate the formation of piRNA clusters (Luo, He et al. 2022). We can thus speculate to what extent siRNAs in mouse oocytes take over the function of piRNAs. Unfortunately, the meiotic defect in mouse oocytes lacking RNAi (Murchison, Stein et al. 2007) prevents a study of overlapping and independent roles of the two pathways after fertilization.

Therefore, it would be very interesting to see how would loss of the piRNA pathway affect rats, given the presence of Dicer^{O} and lack of PIWIL3 in their oocytes. In this case, the RNAi pathway in rat oocytes does control different genes than in mice (unpublished data) and it is unclear whether it is important at all. Thus, the piRNA pathway might be presumably important for rat female germline. At the same time, rat RNAi and piRNA pathways could eventually evolve targeting redundancy, which could lead to the same situation as observed in mice. In any case, rat appears to be an interesting model for further study of RNAi and piRNA pathways.

Taken together, our study along with those of Zhang et al. and Hasuwa et al. (Hasuwa, Iwasaki et al. 2021, Zhang, Zhang et al. 2021) demonstrate that, unlike the mouse model suggested, PIWI proteins together with piRNAs are not dispensable in mammalian oocytes and are important for female fertility. Although the exact molecular mechanism has not been uncovered, these studies show requirements for the piRNA pathway at various stages of mammalian development. Although we have pushed the boundaries of our knowledge little further, many questions remain to be answered. For example, how does the system recognize which transcript is to be processed by the piRNA pathway, or how is the biogenesis of piRNAs initiated in mammals? Is there an initiator piRNA or is the process initiated *de novo*? What is the function of abundant pachytene piRNAs, and do somatic piRNAs exist in mammals? Furthermore, the pioneering studies of the piRNA pathway in golden hamsters bring other questions to the field of small RNA pathways. For example, how are *Mov10l1*-independent piRNAs remaining in oocytes of female *Mov10l1*$^{-/-}$ mutant hamsters produced, and what is their function? What is the primary cause of sterility in hamster piRNA pathway mutants? What would be the phenotype in other mammals where the piRNA pathway would be disrupted? It would be very interesting to determine conserved and derived features of the piRNA pathway among golden hamsters and other mammals. With the invention of the CRISPR/Cas9 technique, we may not have to wait long to see functional genomic piRNA studies in other mammalian models. To all this, our study together with those of Hasuwa et al. (Hasuwa, Iwasaki et al. 2021) and Zhang et al. (Zhang, Zhang et al. 2021) provide valuable insight into the evolution of transposable elements in rodents and open a new window of opportunity to study properties of retrotransposons along with adaptations to the host genome. The demonstrated requirement of the piRNA pathway for germ cell development in golden hamsters may also bring a valuable contribution to fertility-related studies in the future.

6 Conclusions

My PhD project brings a new perspective on the physiological relevance of the piRNA pathway in mammals and addresses the evolution and adaptation of retrotransposons in golden hamsters. The main conclusions are:

- The piRNA pathway is essential for male and female fertility in golden hamsters.
- *Mov10l1*-deficient golden hamster oocytes lack developmental competence and do not support development beyond the 2-cell stage.
- *Mov10l1*-deficient golden hamster oocytes show small transcriptome changes and mild retrotransposon derepression. IAP elements do not show changes in DNA methylation in *Mov10l1*$^{-/-}$ golden hamster oocytes.
- Specific population of piRNAs remains present in *Mov10l1*$^{-/-}$ golden hamster oocytes.
- Male *Mov10l1* mutant golden hamsters are sterile due to massive germ cell loss during spermatogonia formation.
- Secondary phenotype of male *Mov10l1* mutant golden hamsters shows the meiotic failure of rarely surviving germ cells.
- The golden hamster genome encodes full-length intact IAP and LINE1 elements capable of retrotransposition.
- Loss of germ cells in *Mov10l* mutant golden hamster males is associated with elevated levels of MYSERV element and derepressed full-length intact IAP and LINE1 elements.
- Young families of retrotransposons in golden hamsters are represented by Lx5 (LINE1), MuLV, IAP LTR3/4, MERVK and MYSERV elements.
- Independent evolution of ancestral LINE1 and IAP occurred in mice and hamsters. MYSERV expression adapted to the *Cricetidae* family.

7 References

Abe, K., R. Yamamoto, V. Franke, M. Cao, Y. Suzuki, M. G. Suzuki, K. Vlahovicek, P. Svoboda, R. M. Schultz and F. Aoki (2015). "The first murine zygotic transcription is promiscuous and uncoupled from splicing and 3' processing." EMBO J **34**(11): 1523-1537.

Akkouche, A., T. Grentzinger, M. Fablet, C. Armenise, N. Burlet, V. Braman, S. Chambeyron and C. Vieira (2013). "Maternally deposited germline piRNAs silence the tirant retrotransposon in somatic cells." EMBO Rep **14**(5): 458-464.

Akkouche, A., B. Mugat, B. Barckmann, C. Varela-Chavez, B. Li, R. Raffel, A. Pelisson and S. Chambeyron (2017). "Piwi Is Required during Drosophila Embryogenesis to License Dual-Strand piRNA Clusters for Transposon Repression in Adult Ovaries." Mol Cell **66**(3): 411-419 e414.

Anzelon, T. A., S. Chowdhury, S. M. Hughes, Y. Xiao, G. C. Lander and I. J. MacRae (2021). "Structural basis for piRNA targeting." Nature **597**(7875): 285-289.

Aravin, A., D. Gaidatzis, S. Pfeffer, M. Lagos-Quintana, P. Landgraf, N. Iovino, P. Morris, M. J. Brownstein, S. Kuramochi-Miyagawa, T. Nakano, M. Chien, J. J. Russo, J. Ju, R. Sheridan, C. Sander, M. Zavolan and T. Tuschl (2006). "A novel class of small RNAs bind to MILI protein in mouse testes." Nature **442**(7099): 203-207.

Aravin, A. A., G. J. Hannon and J. Brennecke (2007). "The Piwi-piRNA pathway provides an adaptive defense in the transposon arms race." Science **318**(5851): 761-764.

Aravin, A. A., N. M. Naumova, A. V. Tulin, V. V. Vagin, Y. M. Rozovsky and V. A. Gvozdev (2001). "Double-stranded RNA-mediated silencing of genomic tandem repeats and transposable elements in the D. melanogaster germline." Curr Biol **11**(13): 1017-1027.

Aravin, A. A., R. Sachidanandam, D. Bourc'his, C. Schaefer, D. Pezic, K. F. Toth, T. Bestor and G. J. Hannon (2008). "A piRNA pathway primed by individual transposons is linked to de novo DNA methylation in mice." Mol Cell **31**(6): 785-799.

Aravin, A. A., R. Sachidanandam, A. Girard, K. Fejes-Toth and G. J. Hannon (2007). "Developmentally regulated piRNA clusters implicate MILI in transposon control." Science **316**(5825): 744-747.

Aravin, A. A., G. W. van der Heijden, J. Castaneda, V. V. Vagin, G. J. Hannon and A. Bortvin (2009). "Cytoplasmic compartmentalization of the fetal piRNA pathway in mice." PLoS Genet **5**(12): e1000764.

Babushok, D. V. and H. H. Kazazian, Jr. (2007). "Progress in understanding the biology of the human mutagen LINE-1." Hum Mutat **28**(6): 527-539.

Bao, J. and M. T. Bedford (2016). "Epigenetic regulation of the histone-to-protamine transition during spermiogenesis." Reproduction **151**(5): R55-70.

Bartel, D. P. (2018). "Metazoan MicroRNAs." Cell **173**(1): 20-51.

Baust, C., L. Gagnier, G. J. Baillie, M. J. Harris, D. M. Juriloff and D. L. Mager (2003). "Structure and expression of mobile ETnII retroelements and their coding-competent MusD relatives in the mouse." J Virol **77**(21): 11448-11458.

Belloni, M., P. Tritto, M. P. Bozzetti, G. Palumbo and L. G. Robbins (2002). "Does Stellate cause meiotic drive in Drosophila melanogaster?" Genetics **161**(4): 1551-1559.

Bernstein, E., A. A. Caudy, S. M. Hammond and G. J. Hannon (2001). "Role for a bidentate ribonuclease in the initiation step of RNA interference." Nature **409**(6818): 363-366.

Boeke, J. D. and J. P. Stoye (1997). Retrotransposons, Endogenous Retroviruses, and the Evolution of Retroelements. Retroviruses. J. M. Coffin, S. H. Hughes and H. E. Varmus. Cold Spring Harbor (NY).

Bohnsack, M. T., K. Czaplinski and D. Gorlich (2004). "Exportin 5 is a RanGTP-dependent dsRNA-binding protein that mediates nuclear export of pre-miRNAs." RNA **10**(2): 185-191.

Boland, A., F. Tritschler, S. Heimstadt, E. Izaurralde and O. Weichenrieder (2010). "Crystal structure and ligand binding of the MID domain of a eukaryotic Argonaute protein." EMBO Rep **11**(7): 522-527.

Bouniol-Baly, C., L. Hamraoui, J. Guibert, N. Beaujean, M. S. Szollosi and P. Debey (1999). "Differential transcriptional activity associated with chromatin configuration in fully grown mouse germinal vesicle oocytes." Biol Reprod **60**(3): 580-587.

Bozzetti, M. P., S. Massari, P. Finelli, F. Meggio, L. A. Pinna, B. Boldyreff, O. G. Issinger, G. Palumbo, C. Ciriaco, S. Bonaccorsi and et al. (1995). "The Ste locus, a component of the parasitic cry-Ste system of Drosophila melanogaster, encodes a protein that forms crystals in primary spermatocytes and mimics properties of the beta subunit of casein kinase 2." Proc Natl Acad Sci U S A **92**(13): 6067-6071.

Bracken, C. P., J. M. Szubert, T. R. Mercer, M. E. Dinger, D. W. Thomson, J. S. Mattick, M. Z. Michael and G. J. Goodall (2011). "Global analysis of the mammalian RNA degradome reveals widespread miRNA-dependent and miRNA-independent endonucleolytic cleavage." Nucleic Acids Res **39**(13): 5658-5668.

Brasset, E., A. R. Taddei, F. Arnaud, B. Faye, A. M. Fausto, M. Mazzini, F. Giorgi and C. Vaury (2006). "Viral particles of the endogenous retrovirus ZAM from Drosophila melanogaster use a pre-existing endosome/exosome pathway for transfer to the oocyte." Retrovirology **3**: 25.

Brennecke, J., A. A. Aravin, A. Stark, M. Dus, M. Kellis, R. Sachidanandam and G. J. Hannon (2007). "Discrete small RNA-generating loci as master regulators of transposon activity in Drosophila." Cell **128**(6): 1089-1103.

Brennecke, J., C. D. Malone, A. A. Aravin, R. Sachidanandam, A. Stark and G. J. Hannon (2008). "An epigenetic role for maternally inherited piRNAs in transposon silencing." Science **322**(5906): 1387-1392.

Bromham, L., F. Clark and J. J. McKee (2001). "Discovery of a novel murine type C retrovirus by data mining." J Virol **75**(6): 3053-3057.

Brouha, B., J. Schustak, R. M. Badge, S. Lutz-Prigge, A. H. Farley, J. V. Moran and H. H. Kazazian, Jr. (2003). "Hot L1s account for the bulk of retrotransposition in the human population." Proc Natl Acad Sci U S A **100**(9): 5280-5285.

Burgos, M., A. Hurtado, R. Jimenez and F. J. Barrionuevo (2021). "Non-Coding RNAs: lncRNAs, miRNAs, and piRNAs in Sexual Development." Sex Dev **15**(5-6): 335-350.

Cai, X., C. H. Hagedorn and B. R. Cullen (2004). "Human microRNAs are processed from capped, polyadenylated transcripts that can also function as mRNAs." RNA **10**(12): 1957-1966.

Cantrell, M. A., M. M. Ederer, I. K. Erickson, V. J. Swier, R. J. Baker and H. A. Wichman (2005). "MysTR: an endogenous retrovirus family in mammals that is undergoing recent amplifications to unprecedented copy numbers." J Virol **79**(23): 14698-14707.

Carmell, M. A., A. Girard, H. J. van de Kant, D. Bourc'his, T. H. Bestor, D. G. de Rooij and G. J. Hannon (2007). "MIWI2 is essential for spermatogenesis and repression of transposons in the mouse male germline." Dev Cell **12**(4): 503-514.

Cost, G. J., Q. Feng, A. Jacquier and J. D. Boeke (2002). "Human L1 element target-primed reverse transcription in vitro." EMBO J **21**(21): 5899-5910.

Costoya, J. A., R. M. Hobbs, M. Barna, G. Cattoretti, K. Manova, M. Sukhwani, K. E. Orwig, D. J. Wolgemuth and P. P. Pandolfi (2004). "Essential role of Plzf in maintenance of spermatogonial stem cells." Nat Genet **36**(6): 653-659.

Cox, D. N., A. Chao, J. Baker, L. Chang, D. Qiao and H. Lin (1998). "A novel class of evolutionarily conserved genes defined by piwi are essential for stem cell self-renewal." Genes Dev **12**(23): 3715-3727.

Craig, N. L. (2002). Mobile DNA II. Washington, D.C., ASM Press.

Cullen, B. R., S. Cherry and B. R. tenOever (2013). "Is RNA interference a physiologically relevant innate antiviral immune response in mammals?" Cell Host Microbe **14**(4): 374-378.

Dai, P., X. Wang, L. T. Gou, Z. T. Li, Z. Wen, Z. G. Chen, M. M. Hua, A. Zhong, L. Wang, H. Su, H. Wan, K. Qian, L. Liao, J. Li, B. Tian, D. Li, X. D. Fu, H. J. Shi, Y. Zhou and M. F. Liu (2019). "A Translation-Activating Function of MIWI/piRNA during Mouse Spermiogenesis." Cell **179**(7): 1566-1581 e1516.

De Leon, V., A. Johnson and R. Bachvarova (1983). "Half-lives and relative amounts of stored and polysomal ribosomes and poly(A) + RNA in mouse oocytes." Dev Biol **98**(2): 400-408.

DeBerardinis, R. J., J. L. Goodier, E. M. Ostertag and H. H. Kazazian, Jr. (1998). "Rapid amplification of a retrotransposon subfamily is evolving the mouse genome." Nat Genet **20**(3): 288-290.

Deininger, P. L. and M. A. Batzer (1999). "Alu repeats and human disease." Mol Genet Metab **67**(3): 183-193.

Demeter, T., M. Vaskovicova, R. Malik, F. Horvat, J. Pasulka, E. Svobodova, M. Flemr and P. Svoboda (2019). "Main constraints for RNAi induced by expressed long dsRNA in mouse cells." Life Sci Alliance **2**(1).

Deng, W. and H. Lin (2002). "miwi, a murine homolog of piwi, encodes a cytoplasmic protein essential for spermatogenesis." Dev Cell **2**(6): 819-830.

Denli, A. M., B. B. Tops, R. H. Plasterk, R. F. Ketting and G. J. Hannon (2004). "Processing of primary microRNAs by the Microprocessor complex." Nature **432**(7014): 231-235.

Desset, S., N. Buchon, C. Meignin, M. Coiffet and C. Vaury (2008). "In Drosophila melanogaster the COM locus directs the somatic silencing of two retrotransposons through both Piwi-dependent and -independent pathways." PLoS One **3**(2): e1526.

Dewannieux, M., C. Esnault and T. Heidmann (2003). "LINE-mediated retrotransposition of marked Alu sequences." Nat Genet **35**(1): 41-48.

Dexheimer, P. J. and L. Cochella (2020). "MicroRNAs: From Mechanism to Organism." Front Cell Dev Biol **8**: 409.

Di Giacomo, M., S. Comazzetto, H. Saini, S. De Fazio, C. Carrieri, M. Morgan, L. Vasiliauskaite, V. Benes, A. J. Enright and D. O'Carroll (2013). "Multiple epigenetic mechanisms and the piRNA pathway enforce LINE1 silencing during adult spermatogenesis." Mol Cell **50**(4): 601-608.

Di Giacomo, M., S. Comazzetto, S. C. Sampath, S. C. Sampath and D. O'Carroll (2014). "G9a co-suppresses LINE1 elements in spermatogonia." Epigenetics Chromatin **7**: 24.

Ding, D., J. Liu, K. Dong, U. Midic, R. A. Hess, H. Xie, E. Y. Demireva and C. Chen (2017). "PNLDC1 is essential for piRNA 3' end trimming and transposon silencing during spermatogenesis in mice." Nat Commun **8**(1): 819.

Ding, S. W. and O. Voinnet (2007). "Antiviral immunity directed by small RNAs." Cell **130**(3): 413-426.

Dobin, A., C. A. Davis, F. Schlesinger, J. Drenkow, C. Zaleski, S. Jha, P. Batut, M. Chaisson and T. R. Gingeras (2013). "STAR: ultrafast universal RNA-seq aligner." Bioinformatics **29**(1): 15-21.

Eckersley-Maslin, M. A., C. Alda-Catalinas and W. Reik (2018). "Dynamics of the epigenetic landscape during the maternal-to-zygotic transition." Nat Rev Mol Cell Biol **19**(7): 436-450.

Edson, M. A., A. K. Nagaraja and M. M. Matzuk (2009). "The mammalian ovary from genesis to revelation." Endocr Rev **30**(6): 624-712.

Elkayam, E., C. R. Faehnle, M. Morales, J. Sun, H. Li and L. Joshua-Tor (2017). "Multivalent Recruitment of Human Argonaute by GW182." Mol Cell **67**(4): 646-658 e643.

Ender, C. and G. Meister (2010). "Argonaute proteins at a glance." J Cell Sci **123**(Pt 11): 1819-1823.

Esnault, C., J. Maestre and T. Heidmann (2000). "Human LINE retrotransposons generate processed pseudogenes." Nat Genet **24**(4): 363-367.

Finnegan, D. J. (1989). "Eukaryotic transposable elements and genome evolution." Trends Genet **5**(4): 103-107.

Fire, A., S. Xu, M. K. Montgomery, S. A. Kostas, S. E. Driver and C. C. Mello (1998). "Potent and specific genetic interference by double-stranded RNA in Caenorhabditis elegans." Nature **391**(6669): 806-811.

Flemr, M., R. Malik, V. Franke, J. Nejepinska, R. Sedlacek, K. Vlahovicek and P. Svoboda (2013). "A retrotransposon-driven dicer isoform directs endogenous small interfering RNA production in mouse oocytes." Cell **155**(4): 807-816.

Franke, V., S. Ganesh, R. Karlic, R. Malik, J. Pasulka, F. Horvat, M. Kuzman, H. Fulka, M. Cernohorska, J. Urbanova, E. Svobodova, J. Ma, Y. Suzuki, F. Aoki, R. M. Schultz, K. Vlahovicek and P. Svoboda (2017). "Long terminal repeats power evolution of genes and gene expression programs in mammalian oocytes and zygotes." Genome Res **27**(8): 1384-1394.

French, N. S. and J. D. Norton (1997). "Structure and functional properties of mouse VL30 retrotransposons." Biochim Biophys Acta **1352**(1): 33-47.

Frost, R. J., F. K. Hamra, J. A. Richardson, X. Qi, R. Bassel-Duby and E. N. Olson (2010). "MOV10L1 is necessary for protection of spermatocytes against retrotransposons by Piwi-interacting RNAs." Proc Natl Acad Sci U S A **107**(26): 11847-11852.

Galton, R., K. Fejes-Toth and M. E. Bronner (2021). "A somatic piRNA pathway regulates epithelial-to-mesenchymal transition of chick neural crest cells." bioRxiv: 2021.2004.2030.442165.

Gan, H., X. Lin, Z. Zhang, W. Zhang, S. Liao, L. Wang and C. Han (2011). "piRNA profiling during specific stages of mouse spermatogenesis." RNA **17**(7): 1191-1203.

Ganesh, S., F. Horvat, D. Drutovic, M. Efenberkova, D. Pinkas, A. Jindrova, J. Pasulka, R. Iyyappan, R. Malik, A. Susor, K. Vlahovicek, P. Solc and P. Svoboda (2020). "The most abundant maternal lncRNA Sirena1 acts post-transcriptionally and impacts mitochondrial distribution." Nucleic Acids Res **48**(6): 3211-3227.

Gantier, M. P. and B. R. Williams (2007). "The response of mammalian cells to double-stranded RNA." Cytokine Growth Factor Rev **18**(5-6): 363-371.

Gao, F., S. Maiti, N. Alam, Z. Zhang, J. M. Deng, R. R. Behringer, C. Lecureuil, F. Guillou and V. Huff (2006). "The Wilms tumor gene, Wt1, is required for Sox9 expression and maintenance of tubular architecture in the developing testis." Proc Natl Acad Sci U S A **103**(32): 11987-11992.

Gao, X., E. R. Havecker, P. V. Baranov, J. F. Atkins and D. F. Voytas (2003). "Translational recoding signals between gag and pol in diverse LTR retrotransposons." RNA **9**(12): 1422-1430.

Gao, Y., S. Li, Z. Lai, Z. Zhou, F. Wu, Y. Huang, X. Lan, C. Lei, H. Chen and R. Dang (2019). "Analysis of Long Non-Coding RNA and mRNA Expression Profiling in Immature and Mature Bovine (Bos taurus) Testes." Front Genet **10**: 646.

Gasiunas, G., R. Barrangou, P. Horvath and V. Siksnys (2012). "Cas9-crRNA ribonucleoprotein complex mediates specific DNA cleavage for adaptive immunity in bacteria." Proc Natl Acad Sci U S A **109**(39): E2579-2586.

Geisinger, A., R. Rodriguez-Casuriaga and R. Benavente (2021). "Transcriptomics of Meiosis in the Male Mouse." Front Cell Dev Biol **9**: 626020.

Genzor, P., P. Konstantinidou, D. Stoyko, A. Manzourolajdad, C. Marlin Andrews, A. R. Elchert, C. Stathopoulos and A. D. Haase (2021). "Cellular abundance shapes function in piRNA-guided genome defense." Genome Res **31**(11): 2058-2068.

Gibbs, R. A., G. M. Weinstock, M. L. Metzker, D. M. Muzny, E. J. Sodergren, S. Scherer, G. Scott, D. Steffen, K. C. Worley, P. E. Burch, G. Okwuonu, S. Hines, L. Lewis, C. DeRamo, O. Delgado, S. Dugan-Rocha, G. Miner, M. Morgan, A. Hawes, R. Gill, Celera, R. A. Holt, M. D. Adams, P. G. Amanatides, H. Baden-Tillson, M. Barnstead, S. Chin, C. A. Evans, S. Ferriera, C. Fosler, A. Glodek, Z. Gu, D. Jennings, C. L. Kraft, T. Nguyen, C. M. Pfannkoch, C. Sitter, G. G. Sutton, J. C. Venter, T. Woodage, D. Smith, H. M. Lee, E. Gustafson, P. Cahill, A. Kana, L. Doucette-Stamm, K. Weinstock, K. Fechtel, R. B. Weiss, D. M. Dunn, E. D. Green, R. W. Blakesley, G. G. Bouffard, P. J. De Jong, K. Osoegawa, B. Zhu, M. Marra, J. Schein, I. Bosdet, C. Fjell, S. Jones, M. Krzywinski, C. Mathewson, A. Siddiqui, N. Wye, J. McPherson, S. Zhao, C. M. Fraser, J. Shetty, S. Shatsman, K. Geer, Y. Chen, S. Abramzon, W. C. Nierman, P. H. Havlak, R. Chen, K. J. Durbin, A. Egan, Y. Ren, X. Z. Song, B. Li, Y. Liu, X. Qin, S. Cawley, K. C. Worley, A. J. Cooney, L. M. D'Souza, K. Martin, J. Q. Wu, M. L. Gonzalez-Garay, A. R. Jackson, K. J. Kalafus, M. P. McLeod, A. Milosavljevic, D. Virk, A. Volkov, D. A. Wheeler, Z. Zhang, J. A. Bailey, E. E. Eichler, E. Tuzun, E. Birney, E. Mongin, A. Ureta-Vidal, C. Woodwark, E. Zdobnov, P. Bork, M. Suyama, D. Torrents, M. Alexandersson, B. J. Trask, J. M. Young, H. Huang, H. Wang, H. Xing, S. Daniels, D. Gietzen, J. Schmidt, K. Stevens, U. Vitt, J. Wingrove, F. Camara, M. Mar Alba, J. F. Abril, R. Guigo, A. Smit, I. Dubchak, E. M. Rubin, O. Couronne, A. Poliakov, N. Hubner, D. Ganten, C. Goesele, O. Hummel, T. Kreitler, Y. A. Lee, J. Monti, H. Schulz, H. Zimdahl, H. Himmelbauer, H. Lehrach, H. J. Jacob, S. Bromberg, J. Gullings-Handley, M. I. Jensen-Seaman, A. E. Kwitek, J. Lazar, D. Pasko, P. J. Tonellato, S. Twigger, C. P. Ponting, J. M. Duarte, S. Rice, L. Goodstadt, S. A. Beatson, R. D. Emes, E. E. Winter, C. Webber, P. Brandt, G. Nyakatura, M. Adetobi, F. Chiaromonte, L. Elnitski, P. Eswara, R. C. Hardison, M. Hou, D. Kolbe, K. Makova, W. Miller, A. Nekrutenko, C. Riemer, S. Schwartz, J. Taylor, S. Yang, Y. Zhang, K. Lindpaintner, T. D. Andrews, M. Caccamo, M. Clamp, L. Clarke, V. Curwen, R. Durbin, E. Eyras, S. M. Searle, G. M. Cooper, S. Batzoglou, M. Brudno, A. Sidow, E. A. Stone, J. C. Venter, B. A. Payseur, G. Bourque, C. Lopez-Otin, X. S. Puente, K. Chakrabarti, S. Chatterji, C. Dewey, L. Pachter, N. Bray, V. B. Yap, A. Caspi, G. Tesler, P. A. Pevzner, D. Haussler, K. M. Roskin, R. Baertsch, H. Clawson, T. S. Furey, A. S. Hinrichs, D. Karolchik, W. J. Kent, K. R. Rosenbloom, H. Trumbower, M. Weirauch, D. N. Cooper, P. D. Stenson, B. Ma, M. Brent, M. Arumugam, D. Shteynberg, R. R. Copley, M. S. Taylor, H. Riethman, U. Mudunuri, J. Peterson, M. Guyer, A. Felsenfeld, S. Old, S. Mockrin, F. Collins and C. Rat Genome Sequencing Project (2004). "Genome sequence of the Brown Norway rat yields insights into mammalian evolution." Nature **428**(6982): 493-521.

Ginsburg, M., M. H. Snow and A. McLaren (1990). "Primordial germ cells in the mouse embryo during gastrulation." Development **110**(2): 521-528.

Girard, A., R. Sachidanandam, G. J. Hannon and M. A. Carmell (2006). "A germline-specific class of small RNAs binds mammalian Piwi proteins." Nature **442**(7099): 199-202.

Goodier, J. L. (2016). "Restricting retrotransposons: a review." Mob DNA **7**: 16.

Goodier, J. L. and H. H. Kazazian, Jr. (2008). "Retrotransposons revisited: the restraint and rehabilitation of parasites." Cell **135**(1): 23-35.

Goodier, J. L., E. M. Ostertag, K. Du and H. H. Kazazian, Jr. (2001). "A novel active L1 retrotransposon subfamily in the mouse." Genome Res **11**(10): 1677-1685.

Gou, L. T., P. Dai, J. H. Yang, Y. Xue, Y. P. Hu, Y. Zhou, J. Y. Kang, X. Wang, H. Li, M. M. Hua, S. Zhao, S. D. Hu, L. G. Wu, H. J. Shi, Y. Li, X. D. Fu, L. H. Qu, E. D. Wang and M. F. Liu (2014). "Pachytene piRNAs instruct massive mRNA elimination during late spermiogenesis." Cell Res **24**(6): 680-700.

Gou, L. T., J. Y. Kang, P. Dai, X. Wang, F. Li, S. Zhao, M. Zhang, M. M. Hua, Y. Lu, Y. Zhu, Z. Li, H. Chen, L. G. Wu, D. Li, X. D. Fu, J. Li, H. J. Shi and M. F. Liu (2017). "Ubiquitination-Deficient Mutations in Human Piwi Cause Male Infertility by Impairing Histone-to-Protamine Exchange during Spermiogenesis." Cell **169**(6): 1090-1104 e1013.

Graf, A., S. Krebs, V. Zakhartchenko, B. Schwalb, H. Blum and E. Wolf (2014). "Fine mapping of genome activation in bovine embryos by RNA sequencing." Proc Natl Acad Sci U S A **111**(11): 4139-4144.

Gregory, R. I., T. P. Chendrimada, N. Cooch and R. Shiekhattar (2005). "Human RISC couples microRNA biogenesis and posttranscriptional gene silencing." Cell **123**(4): 631-640.

Griswold, M. D. (2016). "Spermatogenesis: The Commitment to Meiosis." Physiol Rev **96**(1): 1-17.

Grivna, S. T., E. Beyret, Z. Wang and H. Lin (2006). "A novel class of small RNAs in mouse spermatogenic cells." Genes Dev **20**(13): 1709-1714.

Grivna, S. T., B. Pyhtila and H. Lin (2006). "MIWI associates with translational machinery and PIWI-interacting RNAs (piRNAs) in regulating spermatogenesis." Proc Natl Acad Sci U S A **103**(36): 13415-13420.

Gurumurthy, C. B., M. Sato, A. Nakamura, M. Inui, N. Kawano, M. A. Islam, S. Ogiwara, S. Takabayashi, M. Matsuyama, S. Nakagawa, H. Miura and M. Ohtsuka (2019). "Creation of CRISPR-based germline-genome-engineered mice without ex vivo handling of zygotes by i-GONAD." Nat Protoc **14**(8): 2452-2482.

Gutierrez, J., R. Platt, J. C. Opazo, D. A. Ray, F. Hoffmann and M. Vandewege (2021). "Evolutionary history of the vertebrate Piwi gene family." PeerJ **9**: e12451.

Halbach, R., P. Miesen, J. Joosten, E. Taskopru, I. Rondeel, B. Pennings, C. B. F. Vogels, S. H. Merkling, C. J. Koenraadt, L. Lambrechts and R. P. van Rij (2020). "A satellite repeat-derived piRNA controls embryonic development of Aedes." Nature **580**(7802): 274-277.

Han, B. W., W. Wang, C. Li, Z. Weng and P. D. Zamore (2015). "Noncoding RNA. piRNA-guided transposon cleavage initiates Zucchini-dependent, phased piRNA production." Science **348**(6236): 817-821.

Harrison, B. and S. B. Zimmerman (1984). "Polymer-stimulated ligation: enhanced ligation of oligo- and polynucleotides by T4 RNA ligase in polymer solutions." Nucleic Acids Res **12**(21): 8235-8251.

Hasuwa, H., Y. W. Iwasaki, W. K. Au Yeung, K. Ishino, H. Masuda, H. Sasaki and H. Siomi (2021). "Production of functional oocytes requires maternally expressed PIWI genes and piRNAs in golden hamsters." Nat Cell Biol **23**(9): 1002-1012.

Hauptmann, J., A. Dueck, S. Harlander, J. Pfaff, R. Merkl and G. Meister (2013). "Turning catalytically inactive human Argonaute proteins into active slicer enzymes." Nat Struct Mol Biol **20**(7): 814-817.

Hayashi, K., S. M. Chuva de Sousa Lopes, M. Kaneda, F. Tang, P. Hajkova, K. Lao, D. O'Carroll, P. P. Das, A. Tarakhovsky, E. A. Miska and M. A. Surani (2008). "MicroRNA biogenesis is required for mouse primordial germ cell development and spermatogenesis." PLoS One **3**(3): e1738.

Hendrickson, P. G., J. A. Dorais, E. J. Grow, J. L. Whiddon, J. W. Lim, C. L. Wike, B. D. Weaver, C. Pflueger, B. R. Emery, A. L. Wilcox, D. A. Nix, C. M. Peterson, S. J. Tapscott, D. T. Carrell and B. R. Cairns (2017). "Conserved roles of mouse DUX and human DUX4 in activating cleavage-stage genes and MERVL/HERVL retrotransposons." Nat Genet **49**(6): 925-934.

Hirose, M., A. Honda, H. Fulka, M. Tamura-Nakano, S. Matoba, T. Tomishima, K. Mochida, A. Hasegawa, K. Nagashima, K. Inoue, M. Ohtsuka, T. Baba, R. Yanagimachi and A. Ogura (2020). "Acrosin is essential for sperm penetration through the zona pellucida in hamsters." Proc Natl Acad Sci U S A **117**(5): 2513-2518.

Hirose, M. and A. Ogura (2019). "The golden (Syrian) hamster as a model for the study of reproductive biology: Past, present, and future." Reprod Med Biol **18**(1): 34-39.

Hock, J. and G. Meister (2008). "The Argonaute protein family." Genome Biol **9**(2): 210.

Horvat, F., H. Fulka, R. Jankele, R. Malik, M. Jun, K. Solcova, R. Sedlacek, K. Vlahovicek, R. M. Schultz and P. Svoboda (2018). "Role of Cnot6l in maternal mRNA turnover." Life Sci Alliance **1**(4): e201800084.

Houwing, S., E. Berezikov and R. F. Ketting (2008). "Zili is required for germ cell differentiation and meiosis in zebrafish." EMBO J **27**(20): 2702-2711.

Houwing, S., L. M. Kamminga, E. Berezikov, D. Cronembold, A. Girard, H. van den Elst, D. V. Filippov, H. Blaser, E. Raz, C. B. Moens, R. H. Plasterk, G. J. Hannon, B. W. Draper and R. F. Ketting (2007). "A role for Piwi and piRNAs in germ cell maintenance and transposon silencing in Zebrafish." Cell **129**(1): 69-82.

Howe, K. L., P. Achuthan, J. Allen, J. Allen, J. Alvarez-Jarreta, M. R. Amode, I. M. Armean, A. G. Azov, R. Bennett, J. Bhai, K. Billis, S. Boddu, M. Charkhchi, C. Cummins, L. Da Rin Fioretto, C. Davidson, K. Dodiya, B. El Houdaigui, R. Fatima, A. Gall, C. Garcia Giron, T. Grego, C. Guijarro-Clarke, L. Haggerty, A. Hemrom, T. Hourlier, O. G. Izuogu, T. Juettemann, V. Kaikala, M. Kay, I. Lavidas, T. Le, D. Lemos, J. Gonzalez Martinez, J. C. Marugan, T. Maurel, A. C. McMahon, S. Mohanan, B. Moore, M. Muffato, D. N. Oheh, D. Paraschas, A. Parker, A. Parton, I. Prosovetskaia, M. P. Sakthivel, A. I. A. Salam, B. M. Schmitt, H. Schuilenburg, D. Sheppard, E. Steed, M. Szpak, M. Szuba, K. Taylor, A. Thormann, G. Threadgold, B. Walts, A. Winterbottom, M. Chakiachvili, A. Chaubal, N. De Silva, B. Flint, A. Frankish, S. E. Hunt, I. I. GR, N. Langridge, J. E. Loveland, F. J. Martin, J. M. Mudge, J. Morales, E. Perry, M. Ruffier, J. Tate, D. Thybert, S. J. Trevanion, F. Cunningham, A. D. Yates, D. R. Zerbino and P. Flicek (2021). "Ensembl 2021." Nucleic Acids Res **49**(D1): D884-D891.

Hughes, S. H. (2015). "Reverse Transcription of Retroviruses and LTR Retrotransposons." Microbiol Spectr **3**(2): MDNA3-0027-2014.

Huntzinger, E. and E. Izaurralde (2011). "Gene silencing by microRNAs: contributions of translational repression and mRNA decay." Nat Rev Genet **12**(2): 99-110.

Hussain, S., F. Tuorto, S. Menon, S. Blanco, C. Cox, J. V. Flores, S. Watt, N. R. Kudo, F. Lyko and M. Frye (2013). "The mouse cytosine-5 RNA methyltransferase NSun2 is a component of the chromatoid body and required for testis differentiation." Mol Cell Biol **33**(8): 1561-1570.

Chakravarthy, S., S. H. Sternberg, C. A. Kellenberger and J. A. Doudna (2010). "Substrate-specific kinetics of Dicer-catalyzed RNA processing." J Mol Biol **404**(3): 392-402.

Chalvet, F., L. Teysset, C. Terzian, N. Prud'homme, P. Santamaria, A. Bucheton and A. Pelisson (1999). "Proviral amplification of the Gypsy endogenous retrovirus of Drosophila melanogaster involves env-independent invasion of the female germline." EMBO J **18**(9): 2659-2669.

Chen, C. Y. and A. B. Shyu (2011). "Mechanisms of deadenylation-dependent decay." Wiley Interdiscip Rev RNA **2**(2): 167-183.

Cheng, E. C., D. Kang, Z. Wang and H. Lin (2014). "PIWI proteins are dispensable for mouse somatic development and reprogramming of fibroblasts into pluripotent stem cells." PLoS One **9**(9): e97821.

Ishino, K., H. Hasuwa, J. Yoshimura, Y. W. Iwasaki, H. Nishihara, N. M. Seki, T. Hirano, M. Tsuchiya, H. Ishizaki, H. Masuda, T. Kuramoto, K. Saito, Y. Sakakibara, A. Toyoda, T. Itoh, M. C. Siomi, S. Morishita and H. Siomi (2021). "Hamster PIWI proteins bind to piRNAs with stage-specific size variations during oocyte maturation." Nucleic Acids Res **49**(5): 2700-2720.

Ivanova, I., C. Much, M. Di Giacomo, C. Azzi, M. Morgan, P. N. Moreira, J. Monahan, C. Carrieri, A. J. Enright and D. O'Carroll (2017). "The RNA m(6)A Reader YTHDF2 Is Essential for the Post-transcriptional Regulation of the Maternal Transcriptome and Oocyte Competence." Mol Cell **67**(6): 1059-1067 e1054.

Jegou, B., S. Sankararaman, A. D. Rolland, D. Reich and F. Chalmel (2017). "Meiotic Genes Are Enriched in Regions of Reduced Archaic Ancestry." Mol Biol Evol **34**(8): 1974-1980.

Jinek, M., K. Chylinski, I. Fonfara, M. Hauer, J. A. Doudna and E. Charpentier (2012). "A programmable dual-RNA-guided DNA endonuclease in adaptive bacterial immunity." Science **337**(6096): 816-821.

Jonas, S. and E. Izaurralde (2015). "Towards a molecular understanding of microRNA-mediated gene silencing." Nat Rev Genet **16**(7): 421-433.

Jurka, J. (1997). "Sequence patterns indicate an enzymatic involvement in integration of mammalian retroposons." Proc Natl Acad Sci U S A **94**(5): 1872-1877.

Kabayama, Y., H. Toh, A. Katanaya, T. Sakurai, S. Chuma, S. Kuramochi-Miyagawa, Y. Saga, T. Nakano and H. Sasaki (2017). "Roles of MIWI, MILI and PLD6 in small RNA regulation in mouse growing oocytes." Nucleic Acids Res **45**(9): 5387-5398.

Kaneko-Ishino, T. and F. Ishino (2012). "The role of genes domesticated from LTR retrotransposons and retroviruses in mammals." Front Microbiol **3**: 262.

Kataruka, S., V. Kinterova, F. Horvat, M. I. R. Kulmann, J. Kanka and P. Svoboda (2022). "Physiologically relevant miRNAs in mammalian oocytes are rare and highly abundant." EMBO Rep **23**(2): e53514.

Kataruka, S., M. Modrak, V. Kinterova, R. Malik, D. M. Zeitler, F. Horvat, J. Kanka, G. Meister and P. Svoboda (2020). "MicroRNA dilution during oocyte growth disables the microRNA pathway in mammalian oocytes." Nucleic Acids Res **48**(14): 8050-8062.

Kato, Y., M. Kaneda, K. Hata, K. Kumaki, M. Hisano, Y. Kohara, M. Okano, E. Li, M. Nozaki and H. Sasaki (2007). "Role of the Dnmt3 family in de novo methylation of imprinted and repetitive sequences during male germ cell development in the mouse." Hum Mol Genet **16**(19): 2272-2280.

Kawamata, T. and Y. Tomari (2010). "Making RISC." Trends Biochem Sci **35**(7): 368-376.

Ketting, R. F. (2011). "The many faces of RNAi." Dev Cell **20**(2): 148-161.

Khvorova, A., A. Reynolds and S. D. Jayasena (2003). "Functional siRNAs and miRNAs exhibit strand bias." Cell **115**(2): 209-216.

Kigami, D., N. Minami, H. Takayama and H. Imai (2003). "MuERV-L is one of the earliest transcribed genes in mouse one-cell embryos." Biol Reprod **68**(2): 651-654.

Kirino, Y. and Z. Mourelatos (2007). "The mouse homolog of HEN1 is a potential methylase for Piwi-interacting RNAs." RNA **13**(9): 1397-1401.

Krueger, F. and S. R. Andrews (2011). "Bismark: a flexible aligner and methylation caller for Bisulfite-Seq applications." Bioinformatics **27**(11): 1571-1572.

Kulpa, D. A. and J. V. Moran (2006). "Cis-preferential LINE-1 reverse transcriptase activity in ribonucleoprotein particles." Nat Struct Mol Biol **13**(7): 655-660.

Kumar, S., G. Stecher, M. Suleski and S. B. Hedges (2017). "TimeTree: A Resource for Timelines, Timetrees, and Divergence Times." Mol Biol Evol **34**(7): 1812-1819.

Kuramochi-Miyagawa, S., T. Kimura, T. W. Ijiri, T. Isobe, N. Asada, Y. Fujita, M. Ikawa, N. Iwai, M. Okabe, W. Deng, H. Lin, Y. Matsuda and T. Nakano (2004). "Mili, a mammalian member of piwi family gene, is essential for spermatogenesis." Development **131**(4): 839-849.

Kuramochi-Miyagawa, S., T. Kimura, K. Yomogida, A. Kuroiwa, Y. Tadokoro, Y. Fujita, M. Sato, Y. Matsuda and T. Nakano (2001). "Two mouse piwi-related genes: miwi and mili." Mech Dev **108**(1-2): 121-133.

Kuramochi-Miyagawa, S., T. Watanabe, K. Gotoh, Y. Totoki, A. Toyoda, M. Ikawa, N. Asada, K. Kojima, Y. Yamaguchi, T. W. Ijiri, K. Hata, E. Li, Y. Matsuda, T. Kimura, M. Okabe, Y. Sakaki, H. Sasaki and T.

Nakano (2008). "DNA methylation of retrotransposon genes is regulated by Piwi family members MILI and MIWI2 in murine fetal testes." Genes Dev **22**(7): 908-917.

Kwak, P. B. and Y. Tomari (2012). "The N domain of Argonaute drives duplex unwinding during RISC assembly." Nat Struct Mol Biol **19**(2): 145-151.

Lander, E. S., L. M. Linton, B. Birren, C. Nusbaum, M. C. Zody, J. Baldwin, K. Devon, K. Dewar, M. Doyle, W. FitzHugh, R. Funke, D. Gage, K. Harris, A. Heaford, J. Howland, L. Kann, J. Lehoczky, R. LeVine, P. McEwan, K. McKernan, J. Meldrim, J. P. Mesirov, C. Miranda, W. Morris, J. Naylor, C. Raymond, M. Rosetti, R. Santos, A. Sheridan, C. Sougnez, Y. Stange-Thomann, N. Stojanovic, A. Subramanian, D. Wyman, J. Rogers, J. Sulston, R. Ainscough, S. Beck, D. Bentley, J. Burton, C. Clee, N. Carter, A. Coulson, R. Deadman, P. Deloukas, A. Dunham, I. Dunham, R. Durbin, L. French, D. Grafham, S. Gregory, T. Hubbard, S. Humphray, A. Hunt, M. Jones, C. Lloyd, A. McMurray, L. Matthews, S. Mercer, S. Milne, J. C. Mullikin, A. Mungall, R. Plumb, M. Ross, R. Shownkeen, S. Sims, R. H. Waterston, R. K. Wilson, L. W. Hillier, J. D. McPherson, M. A. Marra, E. R. Mardis, L. A. Fulton, A. T. Chinwalla, K. H. Pepin, W. R. Gish, S. L. Chissoe, M. C. Wendl, K. D. Delehaunty, T. L. Miner, A. Delehaunty, J. B. Kramer, L. L. Cook, R. S. Fulton, D. L. Johnson, P. J. Minx, S. W. Clifton, T. Hawkins, E. Branscomb, P. Predki, P. Richardson, S. Wenning, T. Slezak, N. Doggett, J. F. Cheng, A. Olsen, S. Lucas, C. Elkin, E. Uberbacher, M. Frazier, R. A. Gibbs, D. M. Muzny, S. E. Scherer, J. B. Bouck, E. J. Sodergren, K. C. Worley, C. M. Rives, J. H. Gorrell, M. L. Metzker, S. L. Naylor, R. S. Kucherlapati, D. L. Nelson, G. M. Weinstock, Y. Sakaki, A. Fujiyama, M. Hattori, T. Yada, A. Toyoda, T. Itoh, C. Kawagoe, H. Watanabe, Y. Totoki, T. Taylor, J. Weissenbach, R. Heilig, W. Saurin, F. Artiguenave, P. Brottier, T. Bruls, E. Pelletier, C. Robert, P. Wincker, D. R. Smith, L. Doucette-Stamm, M. Rubenfield, K. Weinstock, H. M. Lee, J. Dubois, A. Rosenthal, M. Platzer, G. Nyakatura, S. Taudien, A. Rump, H. Yang, J. Yu, J. Wang, G. Huang, J. Gu, L. Hood, L. Rowen, A. Madan, S. Qin, R. W. Davis, N. A. Federspiel, A. P. Abola, M. J. Proctor, R. M. Myers, J. Schmutz, M. Dickson, J. Grimwood, D. R. Cox, M. V. Olson, R. Kaul, C. Raymond, N. Shimizu, K. Kawasaki, S. Minoshima, G. A. Evans, M. Athanasiou, R. Schultz, B. A. Roe, F. Chen, H. Pan, J. Ramser, H. Lehrach, R. Reinhardt, W. R. McCombie, M. de la Bastide, N. Dedhia, H. Blocker, K. Hornischer, G. Nordsiek, R. Agarwala, L. Aravind, J. A. Bailey, A. Bateman, S. Batzoglou, E. Birney, P. Bork, D. G. Brown, C. B. Burge, L. Cerutti, H. C. Chen, D. Church, M. Clamp, R. R. Copley, T. Doerks, S. R. Eddy, E. E. Eichler, T. S. Furey, J. Galagan, J. G. Gilbert, C. Harmon, Y. Hayashizaki, D. Haussler, H. Hermjakob, K. Hokamp, W. Jang, L. S. Johnson, T. A. Jones, S. Kasif, A. Kaspryzk, S. Kennedy, W. J. Kent, P. Kitts, E. V. Koonin, I. Korf, D. Kulp, D. Lancet, T. M. Lowe, A. McLysaght, T. Mikkelsen, J. V. Moran, N. Mulder, V. J. Pollara, C. P. Ponting, G. Schuler, J. Schultz, G. Slater, A. F. Smit, E. Stupka, J. Szustakowki, D. Thierry-Mieg, J. Thierry-Mieg, L. Wagner, J. Wallis, R. Wheeler, A. Williams, Y. I. Wolf, K. H. Wolfe, S. P. Yang, R. F. Yeh, F. Collins, M. S. Guyer, J. Peterson, A. Felsenfeld, K. A. Wetterstrand, A. Patrinos, M. J. Morgan, P. de Jong, J. J. Catanese, K. Osoegawa, H. Shizuya, S. Choi, Y. J. Chen, J. Szustakowki and C. International Human Genome Sequencing (2001). "Initial sequencing and analysis of the human genome." Nature **409**(6822): 860-921.

Lau, N. C., A. G. Seto, J. Kim, S. Kuramochi-Miyagawa, T. Nakano, D. P. Bartel and R. E. Kingston (2006). "Characterization of the piRNA complex from rat testes." Science **313**(5785): 363-367.

Lau, P. W., K. Z. Guiley, N. De, C. S. Potter, B. Carragher and I. J. MacRae (2012). "The molecular architecture of human Dicer." Nat Struct Mol Biol **19**(4): 436-440.

Lee, Y., C. Ahn, J. Han, H. Choi, J. Kim, J. Yim, J. Lee, P. Provost, O. Radmark, S. Kim and V. N. Kim (2003). "The nuclear RNase III Drosha initiates microRNA processing." Nature **425**(6956): 415-419.

Lee, Y., M. Kim, J. Han, K. H. Yeom, S. Lee, S. H. Baek and V. N. Kim (2004). "MicroRNA genes are transcribed by RNA polymerase II." EMBO J **23**(20): 4051-4060.

Li, H., B. Handsaker, A. Wysoker, T. Fennell, J. Ruan, N. Homer, G. Marth, G. Abecasis, R. Durbin and S. Genome Project Data Processing (2009). "The Sequence Alignment/Map format and SAMtools." Bioinformatics **25**(16): 2078-2079.

Li, X. Z., C. K. Roy, X. Dong, E. Bolcun-Filas, J. Wang, B. W. Han, J. Xu, M. J. Moore, J. C. Schimenti, Z. Weng and P. D. Zamore (2013). "An ancient transcription factor initiates the burst of piRNA production during early meiosis in mouse testes." Mol Cell **50**(1): 67-81.

Liao, Y., G. K. Smyth and W. Shi (2014). "featureCounts: an efficient general purpose program for assigning sequence reads to genomic features." Bioinformatics **30**(7): 923-930.

Lim, A. K., C. Lorthongpanich, T. G. Chew, C. W. Tan, Y. T. Shue, S. Balu, N. Gounko, S. Kuramochi-Miyagawa, M. M. Matzuk, S. Chuma, D. M. Messerschmidt, D. Solter and B. B. Knowles (2013). "The nuage mediates retrotransposon silencing in mouse primordial ovarian follicles." Development **140**(18): 3819-3825.

Lim, S. L., Z. P. Qu, R. D. Kortschak, D. M. Lawrence, J. Geoghegan, A. L. Hempfling, M. Bergmann, C. C. Goodnow, C. J. Ormandy, L. Wong, J. Mann, H. S. Scott, D. Jamsai, D. L. Adelson and M. K. O'Bryan (2015). "HENMT1 and piRNA Stability Are Required for Adult Male Germ Cell Transposon Repression and to Define the Spermatogenic Program in the Mouse." PLoS Genet **11**(10): e1005620.

Lin, H. and A. C. Spradling (1997). "A novel group of pumilio mutations affects the asymmetric division of germline stem cells in the Drosophila ovary." Development **124**(12): 2463-2476.

Liu, G. E., L. K. Matukumalli, T. S. Sonstegard, L. L. Shade and C. P. Van Tassell (2006). "Genomic divergences among cattle, dog and human estimated from large-scale alignments of genomic sequences." BMC Genomics **7**: 140.

Liu, J., M. A. Carmell, F. V. Rivas, C. G. Marsden, J. M. Thomson, J. J. Song, S. M. Hammond, L. Joshua-Tor and G. J. Hannon (2004). "Argonaute2 is the catalytic engine of mammalian RNAi." Science **305**(5689): 1437-1441.

Love, M. I., W. Huber and S. Anders (2014). "Moderated estimation of fold change and dispersion for RNA-seq data with DESeq2." Genome Biol **15**(12): 550.

Lund, E., S. Guttinger, A. Calado, J. E. Dahlberg and U. Kutay (2004). "Nuclear export of microRNA precursors." Science **303**(5654): 95-98.

Luo, Y., P. He, N. Kanrar, K. F. Toth and A. A. Aravin (2022). "Maternally inherited siRNAs initiate piRNA cluster formation." bioRxiv: 2022.2002.2008.479612.

Ma, E., K. Zhou, M. A. Kidwell and J. A. Doudna (2012). "Coordinated activities of human dicer domains in regulatory RNA processing." J Mol Biol **422**(4): 466-476.

Ma, J., M. Flemr, P. Stein, P. Berninger, R. Malik, M. Zavolan, P. Svoboda and R. M. Schultz (2010). "MicroRNA activity is suppressed in mouse oocytes." Curr Biol **20**(3): 265-270.

Ma, J. B., K. Ye and D. J. Patel (2004). "Structural basis for overhang-specific small interfering RNA recognition by the PAZ domain." Nature **429**(6989): 318-322.

Ma, X., S. Wang, T. Do, X. Song, M. Inaba, Y. Nishimoto, L. P. Liu, Y. Gao, Y. Mao, H. Li, W. McDowell, J. Park, K. Malanowski, A. Peak, A. Perera, H. Li, K. Gaudenz, J. Haug, Y. Yamashita, H. Lin, J. Q. Ni and T. Xie (2014). "Piwi is required in multiple cell types to control germline stem cell lineage development in the Drosophila ovary." PLoS One **9**(3): e90267.

Mager, D. L. and J. D. Freeman (2000). "Novel mouse type D endogenous proviruses and ETn elements share long terminal repeat and internal sequences." J Virol **74**(16): 7221-7229.

Mager, D. L. and N. L. Goodchild (1989). "Homologous recombination between the LTRs of a human retrovirus-like element causes a 5-kb deletion in two siblings." Am J Hum Genet **45**(6): 848-854.

Mahadevaiah, S. K., J. M. Turner, F. Baudat, E. P. Rogakou, P. de Boer, J. Blanco-Rodriguez, M. Jasin, S. Keeney, W. M. Bonner and P. S. Burgoyne (2001). "Recombinational DNA double-strand breaks in mice precede synapsis." Nat Genet **27**(3): 271-276.

Maksakova, I. A., M. T. Romanish, L. Gagnier, C. A. Dunn, L. N. van de Lagemaat and D. L. Mager (2006). "Retroviral elements and their hosts: insertional mutagenesis in the mouse germ line." PLoS Genet **2**(1): e2.

Malki, S., G. W. van der Heijden, K. A. O'Donnell, S. L. Martin and A. Bortvin (2014). "A role for retrotransposon LINE-1 in fetal oocyte attrition in mice." Dev Cell **29**(5): 521-533.

Martin, M. (2011). "Cutadapt removes adapter sequences from high-throughput sequencing reads." EMBnet.journal **[S.l.], v. 17, n. 1, p. pp. 10-12,** (ISSN 2226-6089).

Martin, S. L. and F. D. Bushman (2001). "Nucleic acid chaperone activity of the ORF1 protein from the mouse LINE-1 retrotransposon." Mol Cell Biol **21**(2): 467-475.

Martin, S. L., M. Cruceanu, D. Branciforte, P. Wai-Lun Li, S. C. Kwok, R. S. Hodges and M. C. Williams (2005). "LINE-1 retrotransposition requires the nucleic acid chaperone activity of the ORF1 protein." J Mol Biol **348**(3): 549-561.

Mathioudakis, N., A. Palencia, J. Kadlec, A. Round, K. Tripsianes, M. Sattler, R. S. Pillai and S. Cusack (2012). "The multiple Tudor domain-containing protein TDRD1 is a molecular scaffold for mouse Piwi proteins and piRNA biogenesis factors." RNA **18**(11): 2056-2072.

Matranga, C., Y. Tomari, C. Shin, D. P. Bartel and P. D. Zamore (2005). "Passenger-strand cleavage facilitates assembly of siRNA into Ago2-containing RNAi enzyme complexes." Cell **123**(4): 607-620.

McCarthy, E. M. and J. F. McDonald (2004). "Long terminal repeat retrotransposons of Mus musculus." Genome Biol **5**(3): R14.

McLaren, A. (2003). "Primordial germ cells in the mouse." Dev Biol **262**(1): 1-15.

Meister, G. (2013). "Argonaute proteins: functional insights and emerging roles." Nat Rev Genet **14**(7): 447-459.

Meister, G., M. Landthaler, A. Patkaniowska, Y. Dorsett, G. Teng and T. Tuschl (2004). "Human Argonaute2 mediates RNA cleavage targeted by miRNAs and siRNAs." Mol Cell **15**(2): 185-197.

Miesen, P., E. Girardi and R. P. van Rij (2015). "Distinct sets of PIWI proteins produce arbovirus and transposon-derived piRNAs in Aedes aegypti mosquito cells." Nucleic Acids Res **43**(13): 6545-6556.

Miething, A. (1998). "The establishment of spermatogenesis in the seminiferous epithelium of the pubertal golden hamster (Mesocricetus auratus)." Adv Anat Embryol Cell Biol **140**: 1-92.

Molaro, A., I. Falciatori, E. Hodges, A. A. Aravin, K. Marran, S. Rafii, W. R. McCombie, A. D. Smith and G. J. Hannon (2014). "Two waves of de novo methylation during mouse germ cell development." Genes Dev **28**(14): 1544-1549.

Molyneaux, K. A., J. Stallock, K. Schaible and C. Wylie (2001). "Time-lapse analysis of living mouse germ cell migration." Dev Biol **240**(2): 488-498.

Monesi, V. (1964). "Ribonucleic Acid Synthesis during Mitosis and Meiosis in the Mouse Testis." J Cell Biol **22**: 521-532.

Monk, M., M. Boubelik and S. Lehnert (1987). "Temporal and regional changes in DNA methylation in the embryonic, extraembryonic and germ cell lineages during mouse embryo development." Development **99**(3): 371-382.

Morgan, M., Y. Kabayama, C. Much, I. Ivanova, M. Di Giacomo, T. Auchynnikava, J. M. Monahan, D. M. Vitsios, L. Vasiliauskaite, S. Comazzetto, J. Rappsilber, R. C. Allshire, B. T. Porse, A. J. Enright and D. O'Carroll (2019). "A programmed wave of uridylation-primed mRNA degradation is essential for meiotic progression and mammalian spermatogenesis." Cell Res **29**(3): 221-232.

Moshkovich, N. and E. P. Lei (2010). "HP1 recruitment in the absence of argonaute proteins in Drosophila." PLoS Genet **6**(3): e1000880.

Mouse Genome Sequencing, C., R. H. Waterston, K. Lindblad-Toh, E. Birney, J. Rogers, J. F. Abril, P. Agarwal, R. Agarwala, R. Ainscough, M. Alexandersson, P. An, S. E. Antonarakis, J. Attwood, R. Baertsch, J. Bailey, K. Barlow, S. Beck, E. Berry, B. Birren, T. Bloom, P. Bork, M. Botcherby, N. Bray, M. R. Brent, D. G. Brown, S. D. Brown, C. Bult, J. Burton, J. Butler, R. D. Campbell, P. Carninci, S. Cawley, F. Chiaromonte, A. T. Chinwalla, D. M. Church, M. Clamp, C. Clee, F. S. Collins, L. L. Cook, R. R. Copley, A. Coulson, O. Couronne, J. Cuff, V. Curwen, T. Cutts, M. Daly, R. David, J. Davies, K. D. Delehaunty, J. Deri, E. T. Dermitzakis, C. Dewey, N. J. Dickens, M. Diekhans, S. Dodge, I. Dubchak, D. M. Dunn, S. R. Eddy, L. Elnitski, R. D. Emes, P. Eswara, E. Eyras, A. Felsenfeld, G. A. Fewell, P. Flicek, K. Foley, W. N. Frankel, L. A. Fulton, R. S. Fulton, T. S. Furey, D. Gage, R. A. Gibbs, G. Glusman, S. Gnerre, N. Goldman, L. Goodstadt, D. Grafham, T. A. Graves, E. D. Green, S. Gregory, R. Guigo, M. Guyer, R. C. Hardison, D. Haussler, Y. Hayashizaki, L. W. Hillier, A. Hinrichs, W. Hlavina, T. Holzer, F. Hsu, A. Hua, T. Hubbard, A. Hunt, I. Jackson, D. B. Jaffe, L. S. Johnson, M. Jones, T. A. Jones, A. Joy, M. Kamal, E. K. Karlsson, D. Karolchik, A. Kasprzyk, J. Kawai, E. Keibler, C. Kells, W. J. Kent, A. Kirby, D. L. Kolbe, I. Korf, R. S. Kucherlapati, E. J. Kulbokas, D. Kulp, T. Landers, J. P. Leger, S. Leonard, I. Letunic, R. Levine, J. Li, M. Li, C. Lloyd, S. Lucas, B. Ma, D. R. Maglott, E. R. Mardis, L. Matthews, E. Mauceli, J. H. Mayer, M. McCarthy, W. R. McCombie, S. McLaren, K. McLay, J. D. McPherson, J. Meldrim, B. Meredith, J. P. Mesirov, W. Miller, T. L. Miner, E. Mongin, K. T. Montgomery, M. Morgan, R. Mott, J. C. Mullikin, D. M. Muzny, W. E. Nash, J. O. Nelson, M. N. Nhan, R. Nicol, Z. Ning, C. Nusbaum, M. J. O'Connor, Y. Okazaki, K. Oliver, E. Overton-Larty, L. Pachter, G. Parra, K. H. Pepin, J. Peterson, P. Pevzner, R. Plumb, C. S. Pohl, A. Poliakov, T. C. Ponce, C. P. Ponting, S. Potter, M. Quail, A. Reymond, B. A. Roe, K. M. Roskin, E. M. Rubin, A. G. Rust, R. Santos, V. Sapojnikov, B. Schultz, J. Schultz, M. S. Schwartz, S. Schwartz, C. Scott, S. Seaman, S. Searle, T. Sharpe, A. Sheridan, R. Shownkeen, S. Sims, J. B. Singer, G. Slater, A. Smit, D. R. Smith, B. Spencer, A. Stabenau, N. Stange-Thomann, C. Sugnet, M. Suyama, G. Tesler, J. Thompson, D. Torrents, E. Trevaskis, J. Tromp, C. Ucla, A. Ureta-Vidal, J. P. Vinson, A. C. Von Niederhausern, C. M. Wade, M. Wall, R. J. Weber, R. B. Weiss, M. C. Wendl, A. P. West, K. Wetterstrand, R. Wheeler, S. Whelan, J. Wierzbowski, D. Willey, S. Williams, R. K. Wilson, E. Winter, K. C. Worley, D. Wyman, S. Yang, S. P. Yang, E. M. Zdobnov, M. C. Zody and E. S. Lander (2002). "Initial sequencing and comparative analysis of the mouse genome." Nature **420**(6915): 520-562.

Muller, M., F. Fazi and C. Ciaudo (2019). "Argonaute Proteins: From Structure to Function in Development and Pathological Cell Fate Determination." Front Cell Dev Biol **7**: 360.

Munafo, D. B. and G. B. Robb (2010). "Optimization of enzymatic reaction conditions for generating representative pools of cDNA from small RNA." RNA **16**(12): 2537-2552.

Murchison, E. P., P. Stein, Z. Xuan, H. Pan, M. Q. Zhang, R. M. Schultz and G. J. Hannon (2007). "Critical roles for Dicer in the female germline." Genes Dev **21**(6): 682-693.

Nakanishi, K., D. E. Weinberg, D. P. Bartel and D. J. Patel (2012). "Structure of yeast Argonaute with guide RNA." Nature **486**(7403): 368-374.

Nejepinska, J., R. Malik, J. Filkowski, M. Flemr, W. Filipowicz and P. Svoboda (2012). "dsRNA expression in the mouse elicits RNAi in oocytes and low adenosine deamination in somatic cells." Nucleic Acids Res **40**(1): 399-413.

Nishimasu, H., H. Ishizu, K. Saito, S. Fukuhara, M. K. Kamatani, L. Bonnefond, N. Matsumoto, T. Nishizawa, K. Nakanaga, J. Aoki, R. Ishitani, H. Siomi, M. C. Siomi and O. Nureki (2012). "Structure and function of Zucchini endoribonuclease in piRNA biogenesis." Nature **491**(7423): 284-287.

Obbard, D. J., K. H. Gordon, A. H. Buck and F. M. Jiggins (2009). "The evolution of RNAi as a defence against viruses and transposable elements." Philos Trans R Soc Lond B Biol Sci **364**(1513): 99-115.

Ono, M., H. Toh, T. Miyata and T. Awaya (1985). "Nucleotide sequence of the Syrian hamster intracisternal A-particle gene: close evolutionary relationship of type A particle gene to types B and D oncovirus genes." J Virol **55**(2): 387-394.

Ozata, D. M., I. Gainetdinov, A. Zoch, D. O'Carroll and P. D. Zamore (2019). "PIWI-interacting RNAs: small RNAs with big functions." Nat Rev Genet **20**(2): 89-108.

Park, M. S., H. D. Phan, F. Busch, S. H. Hinckley, J. A. Brackbill, V. H. Wysocki and K. Nakanishi (2017). "Human Argonaute3 has slicer activity." Nucleic Acids Res **45**(20): 11867-11877.

Payer, L. M. and K. H. Burns (2019). "Transposable elements in human genetic disease." Nat Rev Genet **20**(12): 760-772.

Pelisson, A., S. U. Song, N. Prud'homme, P. A. Smith, A. Bucheton and V. G. Corces (1994). "Gypsy transposition correlates with the production of a retroviral envelope-like protein under the tissue-specific control of the Drosophila flamenco gene." EMBO J **13**(18): 4401-4411.

Pfaffl, M. W., G. W. Horgan and L. Dempfle (2002). "Relative expression software tool (REST) for group-wise comparison and statistical analysis of relative expression results in real-time PCR." Nucleic Acids Res **30**(9): e36.

Phillips, B. T., K. Gassei and K. E. Orwig (2010). "Spermatogonial stem cell regulation and spermatogenesis." Philos Trans R Soc Lond B Biol Sci **365**(1546): 1663-1678.

Prochnik, S. E., D. S. Rokhsar and A. A. Aboobaker (2007). "Evidence for a microRNA expansion in the bilaterian ancestor." Dev Genes Evol **217**(1): 73-77.

Raz, E. (2000). "The function and regulation of vasa-like genes in germ-cell development." Genome Biol **1**(3): REVIEWS1017.

Reuter, M., P. Berninger, S. Chuma, H. Shah, M. Hosokawa, C. Funaya, C. Antony, R. Sachidanandam and R. S. Pillai (2011). "Miwi catalysis is required for piRNA amplification-independent LINE1 transposon silencing." Nature **480**(7376): 264-267.

Ribet, D., F. Harper, A. Dupressoir, M. Dewannieux, G. Pierron and T. Heidmann (2008). "An infectious progenitor for the murine IAP retrotransposon: emergence of an intracellular genetic parasite from an ancient retrovirus." Genome Res **18**(4): 597-609.

Rios-Rojas, C., J. Bowles and P. Koopman (2015). "On the role of germ cells in mammalian gonad development: quiet passengers or back-seat drivers?" Reproduction **149**(4): R181-191.

Riquelme, I., P. Perez-Moreno, P. Letelier, P. Brebi and J. C. Roa (2021). "The Emerging Role of PIWI-Interacting RNAs (piRNAs) in Gastrointestinal Cancers: An Updated Perspective." Cancers (Basel) **14**(1).

Rogakou, E. P., D. R. Pilch, A. H. Orr, V. S. Ivanova and W. M. Bonner (1998). "DNA double-stranded breaks induce histone H2AX phosphorylation on serine 139." J Biol Chem **273**(10): 5858-5868.

Roovers, E. F., D. Rosenkranz, M. Mahdipour, C. T. Han, N. He, S. M. Chuva de Sousa Lopes, L. A. van der Westerlaken, H. Zischler, F. Butter, B. A. Roelen and R. F. Ketting (2015). "Piwi proteins and piRNAs in mammalian oocytes and early embryos." Cell Rep **10**(12): 2069-2082.

Rouget, C., C. Papin, A. Boureux, A. C. Meunier, B. Franco, N. Robine, E. C. Lai, A. Pelisson and M. Simonelig (2010). "Maternal mRNA deadenylation and decay by the piRNA pathway in the early Drosophila embryo." Nature **467**(7319): 1128-1132.

Rubin, G. M., M. G. Kidwell and P. M. Bingham (1982). "The molecular basis of P-M hybrid dysgenesis: the nature of induced mutations." Cell **29**(3): 987-994.

Sasaki, H. and Y. Matsui (2008). "Epigenetic events in mammalian germ-cell development: reprogramming and beyond." Nat Rev Genet **9**(2): 129-140.

Seshagiri, P. B., D. I. McKenzie, B. D. Bavister, J. L. Williamson and J. M. Aiken (1992). "Golden hamster embryonic genome activation occurs at the two-cell stage: correlation with major developmental changes." Mol Reprod Dev **32**(3): 229-235.

Shatzkes, K., B. Teferedegne and H. Murata (2014). "A simple, inexpensive method for preparing cell lysates suitable for downstream reverse transcription quantitative PCR." Sci Rep **4**: 4659.

Schini, S. A. and B. D. Bavister (1988). "Two-cell block to development of cultured hamster embryos is caused by phosphate and glucose." Biol Reprod **39**(5): 1183-1192.

Schopp, T., A. Zoch, R. V. Berrens, T. Auchynnikava, Y. Kabayama, L. Vasiliauskaite, J. Rappsilber, R. C. Allshire and D. O'Carroll (2020). "TEX15 is an essential executor of MIWI2-directed transposon DNA methylation and silencing." Nat Commun **11**(1): 3739.

Schorn, A. J. and R. Martienssen (2018). "Tie-Break: Host and Retrotransposons Play tRNA." Trends Cell Biol **28**(10): 793-806.

Schurmann, N., L. G. Trabuco, C. Bender, R. B. Russell and D. Grimm (2013). "Molecular dissection of human Argonaute proteins by DNA shuffling." Nat Struct Mol Biol **20**(7): 818-826.

Schwarz, D. S., G. Hutvagner, T. Du, Z. Xu, N. Aronin and P. D. Zamore (2003). "Asymmetry in the assembly of the RNAi enzyme complex." Cell **115**(2): 199-208.

Slanchev, K., J. Stebler, G. de la Cueva-Mendez and E. Raz (2005). "Development without germ cells: the role of the germ line in zebrafish sex differentiation." Proc Natl Acad Sci U S A **102**(11): 4074-4079.

Smit, A. F., G. Toth, A. D. Riggs and J. Jurka (1995). "Ancestral, mammalian-wide subfamilies of LINE-1 repetitive sequences." J Mol Biol **246**(3): 401-417.

Smith, T., A. Heger and I. Sudbery (2017). "UMI-tools: modeling sequencing errors in Unique Molecular Identifiers to improve quantification accuracy." Genome Res **27**(3): 491-499.

Song, J. J., S. K. Smith, G. J. Hannon and L. Joshua-Tor (2004). "Crystal structure of Argonaute and its implications for RISC slicer activity." Science **305**(5689): 1434-1437.

Song, Y., K. J. Liu and T. H. Wang (2014). "Elimination of ligation dependent artifacts in T4 RNA ligase to achieve high efficiency and low bias microRNA capture." PLoS One **9**(4): e94619.

Sorefan, K., H. Pais, A. E. Hall, A. Kozomara, S. Griffiths-Jones, V. Moulton and T. Dalmay (2012). "Reducing ligation bias of small RNAs in libraries for next generation sequencing." Silence **3**(1): 4.

Springer, M. S., W. J. Murphy, E. Eizirik and S. J. O'Brien (2003). "Placental mammal diversification and the Cretaceous-Tertiary boundary." Proc Natl Acad Sci U S A **100**(3): 1056-1061.

Stein, C. B., P. Genzor, S. Mitra, A. R. Elchert, J. J. Ipsaro, L. Benner, S. Sobti, Y. Su, M. Hammell, L. Joshua-Tor and A. D. Haase (2019). "Decoding the 5' nucleotide bias of PIWI-interacting RNAs." Nat Commun **10**(1): 828.

Steppan, S., R. Adkins and J. Anderson (2004). "Phylogeny and divergence-date estimates of rapid radiations in muroid rodents based on multiple nuclear genes." Syst Biol **53**(4): 533-553.

Stocking, C. and C. A. Kozak (2008). "Murine endogenous retroviruses." Cell Mol Life Sci **65**(21): 3383-3398.

Su, Y. Q., K. Sugiura, Y. Woo, K. Wigglesworth, S. Kamdar, J. Affourtit and J. J. Eppig (2007). "Selective degradation of transcripts during meiotic maturation of mouse oocytes." Dev Biol **302**(1): 104-117.

Suh, N., L. Baehner, F. Moltzahn, C. Melton, A. Shenoy, J. Chen and R. Blelloch (2010). "MicroRNA function is globally suppressed in mouse oocytes and early embryos." Curr Biol **20**(3): 271-277.

Sun, Y. H., B. Lee and X. Z. Li (2021). "The birth of piRNAs: how mammalian piRNAs are produced, originated, and evolved." Mamm Genome.

Svoboda, P. (2020). "Introduction to RNAi and miRNA pathways." Nakladatelstv Karolinum.

Svoboda, P., P. Stein, M. Anger, E. Bernstein, G. J. Hannon and R. M. Schultz (2004). "RNAi and expression of retrotransposons MuERV-L and IAP in preimplantation mouse embryos." Dev Biol **269**(1): 276-285.

Svoboda, P., P. Stein, H. Hayashi and R. M. Schultz (2000). "Selective reduction of dormant maternal mRNAs in mouse oocytes by RNA interference." Development **127**(19): 4147-4156.

Szak, S. T., O. K. Pickeral, W. Makalowski, M. S. Boguski, D. Landsman and J. D. Boeke (2002). "Molecular archeology of L1 insertions in the human genome." Genome Biol **3**(10): research0052.

Taborska, E., J. Pasulka, R. Malik, F. Horvat, I. Jenickova, Z. Jelic Matosevic and P. Svoboda (2019). "Restricted and non-essential redundancy of RNAi and piRNA pathways in mouse oocytes." PLoS Genet **15**(12): e1008261.

Tadros, W. and H. D. Lipshitz (2009). "The maternal-to-zygotic transition: a play in two acts." Development **136**(18): 3033-3042.

Tachibana, M., M. Nozaki, N. Takeda and Y. Shinkai (2007). "Functional dynamics of H3K9 methylation during meiotic prophase progression." EMBO J **26**(14): 3346-3359.

Tam, O. H., A. A. Aravin, P. Stein, A. Girard, E. P. Murchison, S. Cheloufi, E. Hodges, M. Anger, R. Sachidanandam, R. M. Schultz and G. J. Hannon (2008). "Pseudogene-derived small interfering RNAs regulate gene expression in mouse oocytes." Nature **453**(7194): 534-538.

Tan, M., H. Tol, D. Rosenkranz, E. F. Roovers, M. J. Damen, T. A. E. Stout, W. Wu and B. A. J. Roelen (2020). "PIWIL3 Forms a Complex with TDRKH in Mammalian Oocytes." Cells **9**(6).

Tang, F., M. Kaneda, D. O'Carroll, P. Hajkova, S. C. Barton, Y. A. Sun, C. Lee, A. Tarakhovsky, K. Lao and M. A. Surani (2007). "Maternal microRNAs are essential for mouse zygotic development." Genes Dev **21**(6): 644-648.

Teissandier, A., N. Servant, E. Barillot and D. Bourc'his (2019). "Tools and best practices for retrotransposon analysis using high-throughput sequencing data." Mob DNA **10**: 52.

Vagin, V. V., A. Sigova, C. Li, H. Seitz, V. Gvozdev and P. D. Zamore (2006). "A distinct small RNA pathway silences selfish genetic elements in the germline." Science **313**(5785): 320-324.

Vagin, V. V., J. Wohlschlegel, J. Qu, Z. Jonsson, X. Huang, S. Chuma, A. Girard, R. Sachidanandam, G. J. Hannon and A. A. Aravin (2009). "Proteomic analysis of murine Piwi proteins reveals a role for arginine methylation in specifying interaction with Tudor family members." Genes Dev **23**(15): 1749-1762.

Vasileva, A., D. Tiedau, A. Firooznia, T. Muller-Reichert and R. Jessberger (2009). "Tdrd6 is required for spermiogenesis, chromatoid body architecture, and regulation of miRNA expression." Curr Biol **19**(8): 630-639.

Vasiliauskaite, L., R. V. Berrens, I. Ivanova, C. Carrieri, W. Reik, A. J. Enright and D. O'Carroll (2018). "Defective germline reprogramming rewires the spermatogonial transcriptome." Nat Struct Mol Biol **25**(5): 394-404.

Vourekas, A., K. Zheng, Q. Fu, M. Maragkakis, P. Alexiou, J. Ma, R. S. Pillai, Z. Mourelatos and P. J. Wang (2015). "The RNA helicase MOV10L1 binds piRNA precursors to initiate piRNA processing." Genes Dev **29**(6): 617-629.

Vourekas, A., Q. Zheng, P. Alexiou, M. Maragkakis, Y. Kirino, B. D. Gregory and Z. Mourelatos (2012). "Mili and Miwi target RNA repertoire reveals piRNA biogenesis and function of Miwi in spermiogenesis." Nat Struct Mol Biol **19**(8): 773-781.

Wagih, O. (2017). "ggseqlogo: a versatile R package for drawing sequence logos." Bioinformatics **33**(22): 3645-3647.

Wang, Q. T., K. Piotrowska, M. A. Ciemerych, L. Milenkovic, M. P. Scott, R. W. Davis and M. Zernicka-Goetz (2004). "A genome-wide study of gene activity reveals developmental signaling pathways in the preimplantation mouse embryo." Dev Cell **6**(1): 133-144.

Wang, W., M. Yoshikawa, B. W. Han, N. Izumi, Y. Tomari, Z. Weng and P. D. Zamore (2014). "The initial uridine of primary piRNAs does not create the tenth adenine that Is the hallmark of secondary piRNAs." Mol Cell **56**(5): 708-716.

Watanabe, T., X. Cui, Z. Yuan, H. Qi and H. Lin (2018). "MIWI2 targets RNAs transcribed from piRNA-dependent regions to drive DNA methylation in mouse prospermatogonia." EMBO J **37**(18).

Watanabe, T., S. Chuma, Y. Yamamoto, S. Kuramochi-Miyagawa, Y. Totoki, A. Toyoda, Y. Hoki, A. Fujiyama, T. Shibata, T. Sado, T. Noce, T. Nakano, N. Nakatsuji, H. Lin and H. Sasaki (2011). "MITOPLD is a mitochondrial protein essential for nuage formation and piRNA biogenesis in the mouse germline." Dev Cell **20**(3): 364-375.

Watanabe, T., Y. Totoki, A. Toyoda, M. Kaneda, S. Kuramochi-Miyagawa, Y. Obata, H. Chiba, Y. Kohara, T. Kono, T. Nakano, M. A. Surani, Y. Sakaki and H. Sasaki (2008). "Endogenous siRNAs from naturally formed dsRNAs regulate transcripts in mouse oocytes." Nature **453**(7194): 539-543.

Wessler, S. R. (2006). "Transposable elements and the evolution of eukaryotic genomes." Proc Natl Acad Sci U S A **103**(47): 17600-17601.

Wicker, T., F. Sabot, A. Hua-Van, J. L. Bennetzen, P. Capy, B. Chalhoub, A. Flavell, P. Leroy, M. Morgante, O. Panaud, E. Paux, P. SanMiguel and A. H. Schulman (2007). "A unified classification system for eukaryotic transposable elements." Nat Rev Genet **8**(12): 973-982.

Wichman, H. A., S. S. Potter and D. S. Pine (1985). "Mys, a family of mammalian transposable elements isolated by phylogenetic screening." Nature **317**(6032): 77-81.

Wojtas, M. N., R. R. Pandey, M. Mendel, D. Homolka, R. Sachidanandam and R. S. Pillai (2017). "Regulation of m(6)A Transcripts by the 3'-->5' RNA Helicase YTHDC2 Is Essential for a Successful Meiotic Program in the Mammalian Germline." Mol Cell **68**(2): 374-387 e312.

Wu, P. H., Y. Fu, K. Cecchini, D. M. Ozata, A. Arif, T. Yu, C. Colpan, I. Gainetdinov, Z. Weng and P. D. Zamore (2020). "The evolutionarily conserved piRNA-producing locus pi6 is required for male mouse fertility." Nat Genet **52**(7): 728-739.

Xu, J., R. Zhang, Y. Shen, G. Liu, X. Lu and C. I. Wu (2013). "The evolution of evolvability in microRNA target sites in vertebrates." Genome Res **23**(11): 1810-1816.

Xu, K., Y. Yang, G. H. Feng, B. F. Sun, J. Q. Chen, Y. F. Li, Y. S. Chen, X. X. Zhang, C. X. Wang, L. Y. Jiang, C. Liu, Z. Y. Zhang, X. J. Wang, Q. Zhou, Y. G. Yang and W. Li (2017). "Mettl3-mediated m(6)A regulates spermatogonial differentiation and meiosis initiation." Cell Res **27**(9): 1100-1114.

Yang, Q., R. Li, Q. Lyu, L. Hou, Z. Liu, Q. Sun, M. Liu, H. Shi, B. Xu, M. Yin, Z. Yan, Y. Huang, M. Liu, Y. Li and L. Wu (2019). "Single-cell CAS-seq reveals a class of short PIWI-interacting RNAs in human oocytes." Nat Commun **10**(1): 3389.

Yekta, S., I. H. Shih and D. P. Bartel (2004). "MicroRNA-directed cleavage of HOXB8 mRNA." Science **304**(5670): 594-596.

Yi, R., Y. Qin, I. G. Macara and B. R. Cullen (2003). "Exportin-5 mediates the nuclear export of pre-microRNAs and short hairpin RNAs." Genes Dev **17**(24): 3011-3016.

Yu, G., L. G. Wang, Y. Han and Q. Y. He (2012). "clusterProfiler: an R package for comparing biological themes among gene clusters." OMICS **16**(5): 284-287.

Yu, Y., C. Zhao, Z. Su, C. Wang, J. C. Fuscoe, W. Tong and L. Shi (2014). "Comprehensive RNA-Seq transcriptomic profiling across 11 organs, 4 ages, and 2 sexes of Fischer 344 rats." Sci Data **1**: 140013.

Yuan, L., J. G. Liu, J. Zhao, E. Brundell, B. Daneholt and C. Hoog (2000). "The murine SCP3 gene is required for synaptonemal complex assembly, chromosome synapsis, and male fertility." Mol Cell **5**(1): 73-83.

Yue, F., Y. Cheng, A. Breschi, J. Vierstra, W. Wu, T. Ryba, R. Sandstrom, Z. Ma, C. Davis, B. D. Pope, Y. Shen, D. D. Pervouchine, S. Djebali, R. E. Thurman, R. Kaul, E. Rynes, A. Kirilusha, G. K. Marinov, B. A. Williams, D. Trout, H. Amrhein, K. Fisher-Aylor, I. Antoshechkin, G. DeSalvo, L. H. See, M. Fastuca, J. Drenkow, C. Zaleski, A. Dobin, P. Prieto, J. Lagarde, G. Bussotti, A. Tanzer, O. Denas, K. Li, M. A. Bender, M. Zhang, R. Byron, M. T. Groudine, D. McCleary, L. Pham, Z. Ye, S. Kuan, L. Edsall, Y. C. Wu, M. D. Rasmussen, M. S. Bansal, M. Kellis, C. A. Keller, C. S. Morrissey, T. Mishra, D. Jain, N. Dogan, R. S. Harris, P. Cayting, T. Kawli, A. P. Boyle, G. Euskirchen, A. Kundaje, S. Lin, Y. Lin, C. Jansen, V. S. Malladi, M. S. Cline, D. T. Erickson, V. M. Kirkup, K. Learned, C. A. Sloan, K. R. Rosenbloom, B. Lacerda de Sousa, K. Beal, M. Pignatelli, P. Flicek, J. Lian, T. Kahveci, D. Lee, W. J. Kent, M. Ramalho Santos, J. Herrero, C. Notredame, A. Johnson, S. Vong, K. Lee, D. Bates, F. Neri, M. Diegel, T. Canfield, P. J. Sabo, M. S. Wilken, T. A. Reh, E. Giste, A. Shafer, T. Kutyavin, E. Haugen, D. Dunn, A. P. Reynolds, S. Neph, R. Humbert, R. S. Hansen, M. De Bruijn, L. Selleri, A. Rudensky, S. Josefowicz, R. Samstein, E. E. Eichler, S. H. Orkin, D. Levasseur, T. Papayannopoulou, K. H. Chang, A. Skoultchi, S. Gosh, C. Disteche, P. Treuting, Y. Wang, M. J. Weiss, G. A. Blobel, X. Cao, S. Zhong, T. Wang, P. J. Good, R. F. Lowdon, L. B. Adams, X. Q. Zhou, M. J. Pazin, E. A. Feingold, B. Wold, J. Taylor, A. Mortazavi, S. M. Weissman, J. A. Stamatoyannopoulos, M. P. Snyder, R. Guigo, T. R. Gingeras, D. M. Gilbert, R. C. Hardison, M. A. Beer, B. Ren and E. C. Mouse (2014). "A comparative encyclopedia of DNA elements in the mouse genome." Nature **515**(7527): 355-364.

Zeng, F. and R. M. Schultz (2005). "RNA transcript profiling during zygotic gene activation in the preimplantation mouse embryo." Dev Biol **283**(1): 40-57.

Zhang, C. (2009). "Novel functions for small RNA molecules." Curr Opin Mol Ther **11**(6): 641-651.

Zhang, H., F. Zhang, Q. Chen, M. Li, X. Lv, Y. Xiao, Z. Zhang, L. Hou, Y. Lai, Y. Zhang, A. Zhang, S. Gao, H. Fu, W. Xiao, J. Zhou, F. Diao, A. Shi, Y. Q. Su, W. Zeng, L. Wu and J. Li (2021). "The piRNA pathway is essential for generating functional oocytes in golden hamsters." Nat Cell Biol **23**(9): 1013-1022.

Zhang, Z., J. E. Lee, K. Riemondy, E. M. Anderson and R. Yi (2013). "High-efficiency RNA cloning enables accurate quantification of miRNA expression by deep sequencing." Genome Biol **14**(10): R109.

Zheng, K., J. Xiol, M. Reuter, S. Eckardt, N. A. Leu, K. J. McLaughlin, A. Stark, R. Sachidanandam, R. S. Pillai and P. J. Wang (2010). "Mouse MOV10L1 associates with Piwi proteins and is an essential component of the Piwi-interacting RNA (piRNA) pathway." Proc Natl Acad Sci U S A **107**(26): 11841-11846.

Zhou, L. Q. and J. Dean (2015). "Reprogramming the genome to totipotency in mouse embryos." Trends Cell Biol **25**(2): 82-91.

Zoch, A., T. Auchynnikava, R. V. Berrens, Y. Kabayama, T. Schopp, M. Heep, L. Vasiliauskaite, Y. A. Perez-Rico, A. G. Cook, A. Shkumatava, J. Rappsilber, R. C. Allshire and D. O'Carroll (2020). "SPOCD1 is an essential executor of piRNA-directed de novo DNA methylation." Nature **584**(7822): 635-639.

Supplementary files

Supplementary Data 1: Golden hamster MYSERV and IAP consensus sequences

>MYSERV6-int.consensus

TAGACATCCTAAGGTGGTTTTTCCAGTATCTGTATCAGAAAAACCAGCAACAAAAAAACAACCAAATGGTCCCAT
TGCTTATCACTGGGAGCCTATACAGATGAAGGATCTAAAAAATATTAAGGAGGCCATTGTCATGTATGGTCTTCA
TTCTACCTTTGTCAGAGAGCTCCTAACCTCATGGGCTACTATAAATAAAGTAACCCCAAAAGACTGGGCCCAATT
AGCCTCTGCAGTGCTCGAAAATTCTTGCCAAATTCAATGGAGAGCTTTGTGGAGGCAAGAAGCAAAAGCAATTGA
AATTCAGGAATTGCAGAACGGTCATGAAGTACCCCAAGACAAGATTCTTGGGGAGGGTCCTTATGCTGACACGCA
GGTTCAATCTGCATATGATGAGCACATGTTGTCTTTGTGCCGTACAGCTGCTTTAAATGCCTTGGATAAGGTTTG
TGAAACAGGAGAGATAATGCAACCCTACACCAAGGTATTACAGGGCCCAAGGGAAAGGTTCACTGAATTTTTAGA
GAGATTATCCAGAGCAGTAGATGTACAGGTAGCGAACCCAGAATCCAGGCGTCTTCTTATAGAATCTTTGGCGTA
TGAGAACGCGAATCCTCAATGCAGGCAGGTAATTTGGCCATTAAAAATAAGATCAGCACCATTGGAGGAATGGGT
CCTACATACAGCGAACCTGGAATGTAAAAGTCAGGATACAGGAGCTTGGGTAGGTGAAGCTATTTCTACAGGATT
GAGGAGGCACCAGGATGCCAAATACCCTACCTGTGATGATATAGAGGCATGGGTAGGGAAGGCAATCTCAAAGAA
TTTAAATAGGCATAAAGATGCAAAATGCTTTAACTGTGGTAGAATAGGACATCTTAGTAGGAACTGTAGACAACG
CATTCCTAGAAATAATGCTTTTACCAGGAATGTATCAAACAGAAGGCCTAAGCCTCCTGGTCTATGCAGGAGGTG
TGGGAAGGGGCGCCATTGGACTGATGAATGCTTTTCCACAATAGACAGACAAGGTAGATCTTTACAGCAGGGAAA
CGGGCTTCCGGGGCTCAATGGAGCCCCAAAAAGAAAGATTATCCGGTCATTCCCAGTGACAATGGAGGACAGCCT
CTCCCAGGACAATTAGAAAAGGAAGATTATCCGGTCATTCCCAGTGACAGTGGAGGACAGCCTCTCCCAGGACAA
TTAGAAGATCCACTGCCCATTGTAAATAATACGGCACTGGATAATACATTAGCTCCAGAGGATGAATCAATTACA
TCAGGAGGAGATACAAAACATATATTTTGGCAAACTTCTATACAATATCATAGACCCAAACTTCCAGTTAAGGTA
AATAATAAGGGTGATTTACGGATTACTGGACACCGGAAGTGACGTCACTATCCTTAATCAGCAGTCCTGGCCACA
AAACTGGGCTTTAAAAGAGGTTAATGTTCAATTCTTAGGGATCGGAACCCTATCTGAAGTTAAACAGAGCGTTAG
ATGGATTGACTTTATTGGGCCAGAAGGACAGAGAGGAAGGTTAAAGCCATACGTTGCAGATATTGCTATAAACCT
CTGGGGTCGTGATCTACTCCAGCAATGGAATACGCAGATTAAAATTCCTCCTGTATCAGCTAGGAATTATAGACA
AGCTCTTAGTGGTAGTAAGAATATAGTAAGACAGTACAGAAAACAGATGCCAAATGTACAGGCTGTACAGAAAGC
AAGATGCTAGTGCCAAACCTACAGAGCAACCAAAAGCTCTACCATTAAAATGGCTGACAGATGAACCCGTCTGGG
TGGGTCAATGGCCTATGACATCTGAGAAGTTAGAGGCTTTGGAGAAGTTAGTTCAGGAACAGCTAGATGCTGGAC
ATATTGAGGAATCAACTAGTGCATGGAATTCGCCTGTTTTTGTTGTCAAGAAGAAGTCTGGTAAGTGGAGAATGG
TTACTGATCTTAGAGCCATCAACAAGGTAATTCAGCCTATGGGGTCTCTACAACCTGGGATGCCGTTACCTTCTC
TAATTCCTAAGGATTGGCCAATTATAGTTATAGACTTAAAAGATTGTTTCTTCACCATACCGTTACAAGAAAACG
ACAGAGAAAAGTTCGCCTTCACAGTACCTACCTATAATAATTCCCGTCCGGTACAGAGATTCCAGTGGAAGGTAC
TACCTCAAGGTATGTTAAACAGTCCAACTTTGTGTCAATATTTTGTGAATAAACCTCTAGAAATAATTCGTAAAA
AATTTCCACATTCGTTAATATATCATTATATGGATGACATATTATTGTCTGATTCAAATAAGGATACTTTGGAAA
AGATGTTTGAGGCAGTAAAGGAAATTTTGCCTCGCTGGGGATTACAAATTGCCCCAGAAAAAATACAAAGAGGAG
ATTCTATTAACTATTTAGGTTATAAAATAGATGCTCAGAAAATTAGACCACAGAAAGTACAGATCAGAAGAGATC
GTTACCGGACTCTTAATGATCTTCAAAAACTATTAGGAGAAATCTCTCAATTACAGACGATTATTGGTGTAGAAG
GGCATGATTTAAAACACCTGAAAATGGCTTTAAAAGGAGATAAAGACCTAAACAGCCCACGAGTACTATCAGCTG
AGGCTGAAAAAGAATTAGAATGGGTAGAAAAGAGAATATTAGAAGCACATGTGGACCGTGTGGATCCAAATCTGG
ACTGTATTCTGGTTATTTTACCATCTAGAGAATACCCCTCAGGAATATTAATGCAGAGGGAAGACATCATTCTAG
AATGGGTATTTCTGCCACATAAACAGAATAAAAAATTGAAAACATATATAGAAAAGATCTCTGATTTGATATTAA
AAGGTAAATTAAGGCTTCGTCAACTGACTGGGAAAGACCCAGCTGAAATTATTGTACCTTTAACGAATGAGGAAA
TTTCCTCCTTATGGAAGGATAATGAGTATTGGCAAATAGCTTGCAGTGACTTTTTGGGAAGTATTAGTAATAACT
ATCCCAAAACAGAGAGAATCAAATTCATAAAGAAAACAATTTGGATTCTTCCACGTATCGTGAGGCAAACACCTA
TTTCTGGAGTTCTTACCTTCTACACGGATGCAAACAAATCAGGTAAAGCAGGGTATAAATCAGGAAATATAAGTA
AAGTAGTTCAAAGCCCTTACAACTCCGTACAAAAGGCAGAGTTATATGCCATTCTCATGGTACTTAAAGACTTTA
CAGAGCCTCTCAATATAGTCACGGATTCTCAGTATGCAGAAAGAGTTGTCCTGCACATTGAGACTGCAGAATTTG
TTCCTGATAATACAGAATTAACCTCATTGTTTTTACAATTGCAGGAAATCATCAGAAACAGGACTCATCCTATAT
ATATAACACACATCAGATCCCATACAGGTCTGCCAGGTCCTCTGGCACAAGGCAATGATGAAATTGATCGTTTAT
TAGTAGGTAATGTGTTGGAAGCTTCAGAATTTCATAAGAAACACCATGTTAACAGCAAAGGTTTAAAGAAGGATT
TTTCTATCACCTGGCAACAAGCCAAAGAAATAGTAAGAAATTGTCCCAGTTGCTCATTGTACAATCAAACTCCAT
TACCAGCAGGTTGTAATCCTAAAGGTGTTCACAGAAATGAACTTTTGCAAATGGATGTATTTCACTTCCCAGAAT
TTGGCAGTTTGAAATATGTACACCATACTATAGACACGTTCTCAGGCTTCCAATGGGCTACTGCCCTCAGCTCTG
AAAAAGCTGACTCTGTTATTACACACCTCTTAGAGGTAATGGCTGTTATGGGTATACCTAAAACAATAAAAACTG
ACAATGGTCCAGCATATGTCTCCAGTAAATTGGAACAATTCTTCAAATATTATAATATAAAACATGTAACTGGTA
TACCTTACAATCCCACAGGACAAGCAATAATTGAAAGGTCTAACCGAACCTTAAAAGAGATGCTTCATAAACAGC
CAGGGAAAACAAAGACACCTAAACACAGGTTACACAATGCTTTACTAACGTTGAATTTTCTTAATGCTGATGAAA

AAGGACAAACTGCAGCAGAAAGACACTGGACTACAGAGAAGACTTCTGAACTGAACCAACCGGTGTATTTTAAGG
ATGTTATGACCTCAGTCTGGAAACCAGGATATGTGTTACGTTGGGGAAGGGGTTATGCTTTTGTTTCCACAGGAG
AAGAAAAGATTTGGGTTCCATCAAAATTAATTAAAATTCGATCAGAACAGAAAACATCTCAGGAGGAGGAAGGAT
GACAGCTCATC

>IAPLTR3/4.consensus

GAAAGCGTTGTGAGGAGCCGCCCTCGCTATCGCTATTGCCGTTAGAAGATGGCGCTGACATCCACTGTCAGTTGG
AGTTAACTGTCGCTGTCAGTTGGAGTTAACTGTTGCTGTCAGTTGGAGTTAACTGTCGTTAGAAGATGGCGCTGA
CATCTGCTGTCAGTTGGAGTTAACCGTTTAAGCTGTGCCTCTCCCGTGGCGTCATCTGGGGTGATGTGCAAACCA
CCAATCCCGGCTCTACACGTCTCACTCGGAGCTCCTAGGCTTATATATAAGGGGCTGGGTTTCTTAGCTTGGGGT
CTCCCTCTAAGAAGCTGATCATCTATCTCTCAAGATGCATTAAAGCTTTACTGCAGAAGGATCCGAGTGTTCCTG
CGTCGTTCTTGCTGGCGAGACGGTAGCGCGGGACATCTAGTGCCGAGGTGCCGAAACCCGGGAACTCTTCAACAT
CGCCGGCGCCGCCGCGGGAGACCCCTCGGAAGACGGGGCGGATTCAGAACTGCAGGGACGTAAGTTCAGAGAGGT
ATGCTTTATCCTGAACACCCCTTTTTCTCGACTTTGGCCTTAGTTTGTCATCACCGTGGGACGGGTCAGTGGAGG
CTTTGGTGCTAGTCCTGTTTGTCCTTCTCCTTCATCGTGGCTGGTGCTGTAACAGAACGGTGCTGTCAGTCTGGT
GCTGTCAGTCTGGCGCTGTCCGTCTGGCGCTGTCCGTCTGGCGCTGTCCGTCTGGCGCTGTCCGTCTGGCGCTGT
CCATCTGGCGCTGTCCATCTGGCGCTGTCCATCTGGTGCTGTCAGTCTGGCGCTGTCAGTCTGGTGCTGTCAGTC
TGGTGCTGTCAGTCTGGTGCTCGTCAGTCTGGTAACGGAGTTGAGCGCCTGTTTTTTAGATAAGCCGCCTAGCGC
GATGGGGTTGTCACAGTCAGTGGTTACTGCCCTACAGACTGTGCTAAAACAAAGAGATCTTAAAATTGCACCACG
AACACTTCAAAATTTTGTGAAGGAGGTAGATAGAGTGGCACCATGGTATGCTTGTTCCGGGTCCCTCACTGTGGC
CTCATGGAACAAGCTAGGTAAAGAACTAGACAGGAAGCATGCAGAAGGAGATCTCCACTTAGGTACCAAGCATGC
AGAAGGAGATCTCCACTTAGGTACCAAAGCCATTTGGAAGCTAGTTAAAAACTGCTTGGAGGATGAGGCCTGTCA
CCCTGCTATAATAGAAAGTCAGGGAACCTTAGAGGAAGTTCAGGATAGCATGTCAGAAACTGAACGGAGTGAGAG
AATGGGAGCTCGCAAAAGGAAAGACATGTCTAAGAAAAAAGGCCCTCCCCAAGAAGTTAAGAAAGGGGGAGAGAA
AGAAGGGAGTGATCATTCACCCCCTAACAAATCTAAGAAAAAGAAAAAGCCAGAATCTAGTCTATACCCTACAGT
AGAGCTAGAAGCCTTGGAGCTAGATAATTCTGATTCTGACACTCTGGATTCTAGCGAAGAAGGTGGTCTAGAGGA
GGAGGTGGCACGGTATGAGGAAGAAAGATATCACCCTGATAGACACCGGCCACTGAAAACAAAAATGAATGTGAG
GCCACCGCCTATAAATCCGGCGGGCTCACGCCCCTCAGCGCCTCCGCAGTATGAGCTTCGGCTGAATACTGGTAC
TGACTCCTTTTTACCTTTAGAGGAACTGGAGAAAAATACAAATGGCTTTTCCAGTATTCGAGAATGTGGAAGGCG
GAAGAGTACATACCCCCGTAGATTACAATCAAATCAAAGAATTGGCCGAATCCGTTCGTAATTATGGGGTCAATG
CTAACTTTACCACATTACAGGTGGAAAGGCTTGCTAATTTTGCCATGACTCCCACTGACTGGCAGACGACAGTGA
AAGCAGTGCTTCCCAACATGGGACAATACATGGAATGGAAGGCTCTCTGGTATGATGCAGCCCAGGCACAAGCTA
GAGTTAATGCCACGGCTGAAGATGAGAATCAGAGGCAGTGGACATTTGAAATGCTGACAGGTCAGGGTCAACATG
CCCTTAATCAAACCAACTACATCTGGGGCGTCTATGGTCAGGTGTCGGCCGCCGCTATTAAAGCATGGAAGGCCC
TCACAAAAAGGGGAGAGTCCAGTGGACACCTTACAAAGATTGTCCAAGGACCCCAAGAGCCATTTTCAGACTTTG
TGGCCAGAATGACAGAGGCCGCCAGTCGCATCTTTGGTGATTCAGAACAAGCTATGCCCCTGATTGAGCAACTTG
TCTATGAACAAGCAACCCAGGAATGTCGAGCGGCTATCGCCCCTCGCAAAAGCAAAGGTTTACAAGATTGGCTCA
GAGTGTGCAGGGAGCTGGGGGGACCCCTAACCAATGCAGGACTAGCTGCCGCCATTTTACAAACGCACAGGTATA
GAGATTTATCTAAGTCGAAAAGCTTGTTTTAATTGTGGGAGAATGGGGACACCTTAAGAAAGATTGTCAAGCCCC
TGAAAGAACAAGAGAATCGAAGCTTTGCCATCGTTGTGGTAAAGGTTATCATAGGGCTAGCGAATGCAGGTCAGT
CCTGGGATGTAAAAGGGAGGCTTCTGCCCCCTATTGAAGAACCCAAGGTACCCCAATCAAAAAACGGGTCACGGG
GCCCAGTGGTCCCAGGGCCCTCAGAAATATGGGAACCAATTTCAGAAAAGCAATCAAGAGGAAGTAGAGGTTTCC
GAGGAACCCCCGGAATGGACTTTGCGTGCCGCCTCCGACTTCTTACTCATGCCCCAAATGAATGTTCAACCGGTC
CCAGTCCATTCCCCTGGACCTTTGCCCCCTGCCACCATTGGGCTTATTCTGGGCCGTGGCTCCTTAACTTTACAG
GGACTCATTATATATCCTGGGATTGTTGACCCGTATCATAAAGAGGAGATTCAAGTTCTCTGTTCTAGCCCTCGG
GGTGTATTTTCTATAAAGCAGGGAGATAGAATTGCACAACTGGTGTTGCTGCCCTCCCTCGGGGATGGAGAAACC
TACACTTTACAAAAAAAGGGCTATGGGATCTTCTGGAAGTGATTCAGCCTATCTGGCTATACCCCTAAATGAGAG
ACCTACAATAAAATTGTTAATTAATGGAAAAGAATTTGAAGGGATAATGGATACGGGAGCAGACAAAAGCATTAT
TTCACTCCATTGGTGGCCGAAGTCTTGGCCCACTGTTGTTTCATCTCATTCTCTACAAGGTCTTGGATACCAGTC
CTCTCCTGCCATCAGTGCCTCAGCCTTAACCTGGCGGAATGCTGAGGGCAAACAGGGATGTTTTACCCCCTATGT
GTTGCCACTCCCTGTAAATTTATGGGGACGGGATGTGTTACAAGCCATGGGCATGACCCTAACTAATGAATACTC
CCCCCCAGGCATCAGCCATTATGGCAAAGATGGGGTATACAAAGGGTAGAGGCTTGGGTAGGCAAGAACAAGGCA
GAATAAAACCCATTACACAACACGGAAATCGGGGTAGAAAAGGACTGGGTTTTATTTAGGGGCCGTTGAGGCTTC
ACGACCCATACCATGGAAAACAGAGGAGCCGTTATGGGTCTCTCAATGGCCTCTATCCTCTGAAAAATTAGAGGC
TGTCACAAGATTAGTGCAAGAAGAACAGGAACGGCTGGGGCATCTAGAGCCTTCTACCTCCCCATGGAATACACC
AATTTTTGTTATTAAGAAGAAATCTGGGAAGTGGAGATTACTCCATGACCTGCGGGCCATTAACAATCAGATGCA
TCTTTTTGGCCCTGTTCAAAGAGGCCTTCCTTTGCTTTCTGCACTTCCTCAAGATTGGAAGCTTATTATTATAGA
TATTAAGGATTGTTTCTTCTCTATTCCACTTTACCCACGGGATAGACCAATGGTTTGCCTTCACTATCCCTTCTC
TTAATCATATGGAACCAGACAAGAGATTTCAGTGGAAGGTACTGCCGCAAGGCATGGCCAATAGCCCAACAATAT
GTCAGCTGTATGTGCAGGAGGCTTTGGAGCCAATTAGGAAGCAATTTACATCTTTAATCGTTATCCATTATATGG
ACGATATTCTTATTTGTCACAAAGAGTTAGATGTTTTACAAAAGGCTTTTCCCATGCTGGTGGCTGAATTAAAAC

AAGTGGGGATTAGAGATTGCCTCAGAAAAGGTTCAAATTGCAGATACAGGCCTCTTTTTGGGCTCAATGATTACT
CCCAAAAATATAGTTCCTCAGAAAATAGAAATTCGCAAAGACCACTTACAAACATTAAATGATTTTCAGAAACTT
CTGGGAGATATAAATTGGTTGAGGCCCTTTTTAAAAATTCCATCTGCTGATCTAAAACCCCTCTTCGATCTCCTG
GAGGGTGAGCCTCATATCTCCTCACCCAGAAAATTTACCCCTGCCGCCCACCGAGCCTTACAGATGGTGGAAGAG
GCCTTACAGGAAGCACAATTACAACGTATTGAGGAGTCACTACCTTTTAATCTGTGTGTTTTTAAGACAGCTCAA
TTGCCAACTGCAGTCCTGTGGCAACATGGACCATTACTTTGGATTCATCCAAATGCTTCCCCTGCTAAGATTATT
GACTGGTACCCTGATGCTGTTGCACAGCTCGCGCTTCGCGGAATAAAAGCAGCTGTTACACATTTTGGCAGGGAT
CCTGATTCCTTGATTGTGCCTTATACTGCTGCACAAGTTCAGACCTTGGCAGCCACATCTAGTGATTGGGCAGTT
TTAGTTACTTCCTTTTCAGGACAAATTGATAATCATTTTCCAAAGCATCCAATTTTACAGTTTGCCCTAAACCAG
GCTATAGTGTTTCCACAAGTGACAGCTAAAGACCCACTCCCAGATGGGACTGTGGTGTACACTGATGGATCAAAA
ACTGGTATGGGAGCTTATGTGGTCAAGGATAGGGTTATATCTAAACAATATAATGAAACTTCACCTCAAGTTGTA
GAATGTCTGATAGTACTGGAGGTTCTTGAGGCTTTTCCAGGACCCCTCAATATTGTATCAGATTCCTCTTATGTG
GTTAATGCAGTTAATCTCCTTGAGATAGCTGGAATAATAAGATCCTCCAGCAGAGTTGCTAACATCTTTCAGAAG
ATACAAGCTGCCTTGTTAAATAGGAGATTTCCTGTTTTCATTACCCATGTCCGAGCACATTCTGGACTCCCAGGT
CCCATGTCCTTAGGGAATGACTTAGCGGACAAGGCTACAAAGCTGGTGGCCGCTGCCTTGTCTACCCATGCACAA
GCAGCAAAAGAATTCCATAAGCGCTTTCATGTGACGGCTGAGACCTTGCGCCAGTCGTTTTGCTCTATCCAGGAA
AGAGGCTAGGGAAATTGTTACTCAATGCCAGAATTGCTGCGAATTCTTACCTACTCCCCACATGGGAATAAACCC
ACGTGGCATTAGACCATTGCAGATGTGGCAGATGGATGTTACTCATATTCCCTCTTTTGGAAGGCTTCAATATGT
TCATGTTTCTGTTGACACCTGTTCTGGCGTAATGTTTGCCACACCCCTAACAGGGGAAAAGGCCTCATATGTGAT
TCAACATTGCCTTGAGGCCTGGAGTGCTTGGGGAAAACCCAGAATTTTAAAAACAGACAATGGACCAGCATATAC
CTCTCAAAAATTCCGACAGTTTTGTCGGCAAATGGATGTTACCCATCTAACTGGCCTACCTTATAACCCTCAAGG
ACAGGGCATTGTGGAACGTGCCCATCGTACACTCAAATCATATCTGATTAAACAAAAGGGGAGTATTGAGATTGA
GGATGTTCTACCCTCGGTACCAAGAGTTGCTGTATCCATGGCACTTTTTACCCTTAATTTCTTGAACTCTGATGC
CCAAGGCCACACTGCGGCCGATCGCCACAGTTTAGAGCCTGATAGGCCAAAAGAAATGGTAAAATGGAAAGATGT
CTTGACTGATCTCTGGAAAGGCCCGGATCCTATTCTTATAAGATCCAGGGGAGCTGTGTGTGTGTTTTTCCACAG
GAGGAAGAAAACCCCCTGTGGATCCCTGAAAGACTCACTCGAAGAGCTCCTTCACAACTCCAGAATAAGAAGGAT
GGAGGCCAAGTGGGTGATGAAGACTCTCCTCAACTCGGGATGATGGTTCCTAGTATGATGGGAGAGTTACGGTGG
GCCATCATGTCTACCTTTCCCCCTACCGATGCCAGTGATGCAGAATGCCCAGGTGTTCCCTAGATTTTTCACAAC
TAATAGAGAGTTGGGGACTTGCCTTTTTGCCTTTAGATCCTCAGATACAGAGTTTTCAGGATGAGAGAACCTTGT
CATTAGTAGGAAGCTTGTGCTTTACTGTGATTTCTTCATTAAAGGATAATTTTATTCATATGGATCCAGAAAGAT
CTAATGCTAATCCTTTTGAATTAATGGAAGCTGTACTGATCTTTCTCCTATGGCAATGATTGCTGGAGGATATAG
TGAGAAGGGACAGATTACTTTTGATTGGAAAGGGGCATTAGGCAACAGTCTGAGTGAGGGACAGAGCTCTGGATC
ATCTGATTGGTCCTCCTCCAATGTTAAGTATACCCCTTTTAAGAGAACTAATTATTCAGCTGCTCCAATTTGTGT
TTGGCTGCCCTTTATTTGGGTTGTGAGTAATGATACCTTAGGTAAGAATCAGAAAGAAATAAATTGCTCTGCTTA
GAATTGTTTTTATGCATTATGCTGGGATGCTATTAAGCACCCTTTTGCTTTGGTAATGCGCATGCCTCGATTTGT
TCCAGTTCCTGTTGAGGCGCCAAGTAATTTGAGTTTGTTTAGGGAAAAGCGAGATTTTTGGGATCTCTGCTATTA
TTGTGGGCCTGATAGCCACCGCCAGCGGTTACTGCTTCGGTTACCGCCTCGGCCCTTGCACTTTCCTGCCACTGT
GCAGACAACTCAAACCATTAATGAACTATAGGCCACTGTGACCATGGTCCTAGGATAAACAGGCCACTGCCAATT
CTCAGATACAAGGAGGCCTGATGTTGGTAAACCAACAGATTAATTTGGTTCAGGAACAATTGGATATATTGTGGC
AGATGGCCCAATTGGGATGTGAACAAAAGTTGCCTGGCCTTTGTGTTCACTTCAGTACAATATGAGAATTTTACA
AGAGCAGCTAACCTGTCAAAAGCTCTGTCTCAACATTTATTACAGAATTGGACTTTTGAGTTTGAGCAGACACTC
CGTGAGTTGAGAATGGCGATCCTGCAAGTGAATTCGACGCATCTGGATCTTTCTCTGATGGAAGGCCTCTCCTCC
TGGATTTCATCTGCATTTTCTTATTTTAAGGAATGGGTGGGGGTAGGATCATTTAGCCTAGTTCTCTGCTGTGGA
ATAGTGTTGATGCTTTGGATGGTGTGTAAGCTACAGAGCCCAAACAAAAGAGACGAAAGTGGTGGTGGCACAAGC
ACCTTGCTGCCTTAGAACACGGAGCCTCCCCTGACATTTGGTTAACCATGTTAAAGCAATAGGTCGCTGGCCTCC
CAGCTCTTGCACCCCACGAGGCTAGTCTCATTGCACGGGATAGAGTGGGTAGGCTTCAGCAGCCCAAGGAGTTGC
AAGGCTAAGCACTGCACAGGAGAGGTCTGCGGTAATAACGACTTTCTCCTGGGAGATAAGTCATCTTGCATGAAG
GTTCTATGTCATGATCTCCTTCCCCCAGAAAAAACGACATCGGGACTGGTCAGGGCTCCCTCTGGGGATAAAGAC
CCTGGAGAGGAGCTTTGTACATGTTCCGAATTTGCACATGGGGATTTGACCTCTATCTCCACTCCAAAGTTGTGG
GTGTCCTATTGCTTCAAAAATAAATGAATAGGGGGAGATAGTGAGGAGCCGCCCTCGCTATCGCTATTGCCGTTA
GAAGATGGCAGCTGACATCTGCTGTCAGTTGGAGTTAACTGTCGTTAGAAGATGGCGCTGACATCTGCTGTCAGT
TGGAGTTAACTGTCGCTGTCAGTTAGAGTTAACTGTCGCTGTCAGTTGGAGTTAACCGTTTAAGCTGTGCCTCTC
CCGTGGCGTCATCTGGGGTGATGTGGCAAACCACCAATCCCGGCTCTACACGTCTCACTCGGAGCTCCTAGGCTT
ATATATAAGGGGCTGGGTTTCTTAGCTTGGGGGTCTCCCTCTAAGAAGCTGATCATCTATCTCTCAAGATGCATT
AAAGCTTTACTGCAGAAGGATCCGAGTGTTCTGCGTCGTTCTTGCTGGCGAGACGGGACGTTAGCGCGGGACA

Publication

ARTICLES
https://doi.org/10.1038/s41556-021-00746-2

nature cell biology

Check for updates

OPEN

Formation of spermatogonia and fertile oocytes in golden hamsters requires piRNAs

Zuzana Loubalova[1,6], Helena Fulka[1,5,6], Filip Horvat[1,2], Josef Pasulka[1], Radek Malik[1], Michiko Hirose[3], Atsuo Ogura[3,4]✉ and Petr Svoboda[1]✉

PIWI-interacting RNAs (piRNAs) support the germline by suppressing retrotransposons. Studies of the pathway in mice have strongly shaped the view that mammalian piRNAs are essential for male but not for female fertility. Here, we report that the role of the piRNA pathway substantially differs in golden hamsters (*Mesocricetus auratus*), the piRNA pathway setup of which more closely resembles that of other mammals, including humans. The loss of the *Mov10l1* RNA helicase—an essential piRNA biogenesis factor—leads to striking phenotypes in both sexes. In contrast to mice, female *Mov10l1*$^{-/-}$ hamsters are sterile because their oocytes do not sustain zygotic development. Furthermore, *Mov10l1*$^{-/-}$ male hamsters have impaired establishment of spermatogonia accompanied by transcriptome dysregulation and an expression surge of a young retrotransposon subfamily. Our results show that the mammalian piRNA pathway has essential roles in both sexes and its adaptive nature allows it to manage emerging genomic threats and acquire new critical roles in the germline.

The piRNA pathway is a key germline-specific silencing mechanism that is crucial for defending the integrity of the genome against transposable elements (reviewed previously[1,2]). Mammalian primary piRNAs originate from specific loci (piRNA clusters) as long precursor transcripts that interact with the essential and conserved helicase MOV10L1, which feeds precursor transcripts into the piRNA biogenesis mechanism[3–5]. Mammalian piRNAs fall into the following four categories: (1) 26–28-nucleotide retrotransposon-derived piRNAs produced mainly in fetal testes; (2) 26–27-nucleotide postnatal piRNAs from non-repetitive sequences including the 3′ ends of mRNAs; (3) 29–30-nucleotide mostly non-repetitive highly abundant pachytene piRNAs produced from ~100 loci in spermatocytes and spermatids; and (4) oocyte-specific 19–20-nucleotide piRNAs that are enriched in antisense sequences of recently evolved transposable elements[6–11]. Mature piRNAs associate with the PIWI subfamily of Argonaute proteins[12]. Mice (*Mus musculus*), the leading mammalian model for the piRNA pathway, use three PIWI proteins—PIWIL1, PIWIL2 and PIWIL4 (also known as MIWI, MILI and MIWI2, respectively). Loss of MOV10L1 or PIWI proteins in mice revealed specific essential roles of piRNAs in spermatogenesis but not in oogenesis[3,4,13–16]. However, it is unclear whether the dispensability of piRNAs in females is common among mammals. piRNAs target retrotransposons during mouse oogenesis[17,18], but the maternal piRNA pathway is partially redundant with RNA interference (RNAi)[19]. High endogenous RNAi activity specifically evolved in mouse oocytes[20] and seems to be absent in bovine and human oocytes[10,21]. Furthermore, mice lack PIWIL3, which binds to 19–20-nucleotide piRNAs in human and golden hamster oocytes and exists in many mammals, suggesting that there is a major difference between oocyte piRNA biology in mice versus other mammals[10,11,21]. However, it is unclear whether differences in the piRNA pathway set-up are associated with biologically important roles.

To delineate the conserved and derived aspects of the mammalian piRNA pathway, we selected the golden hamster (*Mesocricetus auratus*) as an optimal experimentally tractable comparative model that is amenable to genetic manipulations[22]. Despite ~24 million years of independent evolution[23], hamsters share many anatomical and physiological features with mice, including fast zygotic genome activation, short gestation and a large litter size[24,25]. At the same time, the hamster outclassed the mouse model for specific aspects of human biology[25,26]. Crucially, in contrast to mice and similar to humans, golden hamster retained four PIWI paralogues expressed in the germline and its oocytes probably lack highly active RNAi[27].

Results

Hamster piRNAs and retrotransposons. To develop the golden hamster into a model for the piRNA pathway, we first mapped the expression of the piRNA pathway components and the properties of golden hamster piRNAs (Fig. 1a–e). We focused on testicular piRNAs as there was plenty of comparative data from other mammals, particularly from extensively studied mice. Ovarian hamster piRNAs have recently been investigated[11].

We examined testicular piRNAs at 9 days postpartum (d.p.p.) when spermatogonia form; at 13 d.p.p. when testes contain spermatogonia but not meiotic spermatocytes; and at 21 d.p.p. when meiosis in primary spermatocytes reaches the pachytene stage[28] (Extended Data Fig. 1a–c and Supplementary Tables 1–3). Pre-pachytene piRNAs were broadly dispersed at a relatively low density in intergenic and genic regions, while most pachytene piRNAs mapped to ~100 loci, many of which were syntenic with mouse, cow and human testicular piRNA loci. Unique and repetitive 27–29-nucleotide pre-pachytene piRNAs and highly abundant non-repetitive 29–30-nucleotide pachytene piRNAs had typical mammalian piRNA features, including the presence of uridine at the 5′ end (Fig. 1b and Extended Data Fig. 1d,e). Notably, sequence

[1]Institute of Molecular Genetics of the Czech Academy of Sciences, Prague, Czech Republic. [2]Bioinformatics Group, Division of Molecular Biology, Department of Biology, Faculty of Science, University of Zagreb, Zagreb, Croatia. [3]Bioresource Engineering Division, RIKEN BioResource Research Center, Ibaraki, Japan. [4]Bioresource Engineering Laboratory, RIKEN Cluster for Pioneering Research, Saitama, Japan. [5]Present address: Institute of Experimental Medicine of the Czech Academy of Sciences, Prague, Czech Republic. [6]These authors contributed equally: Zuzana Loubalova, Helena Fulka.
✉e-mail: ogura@rtc.riken.go.jp; svobodap@img.cas.cz

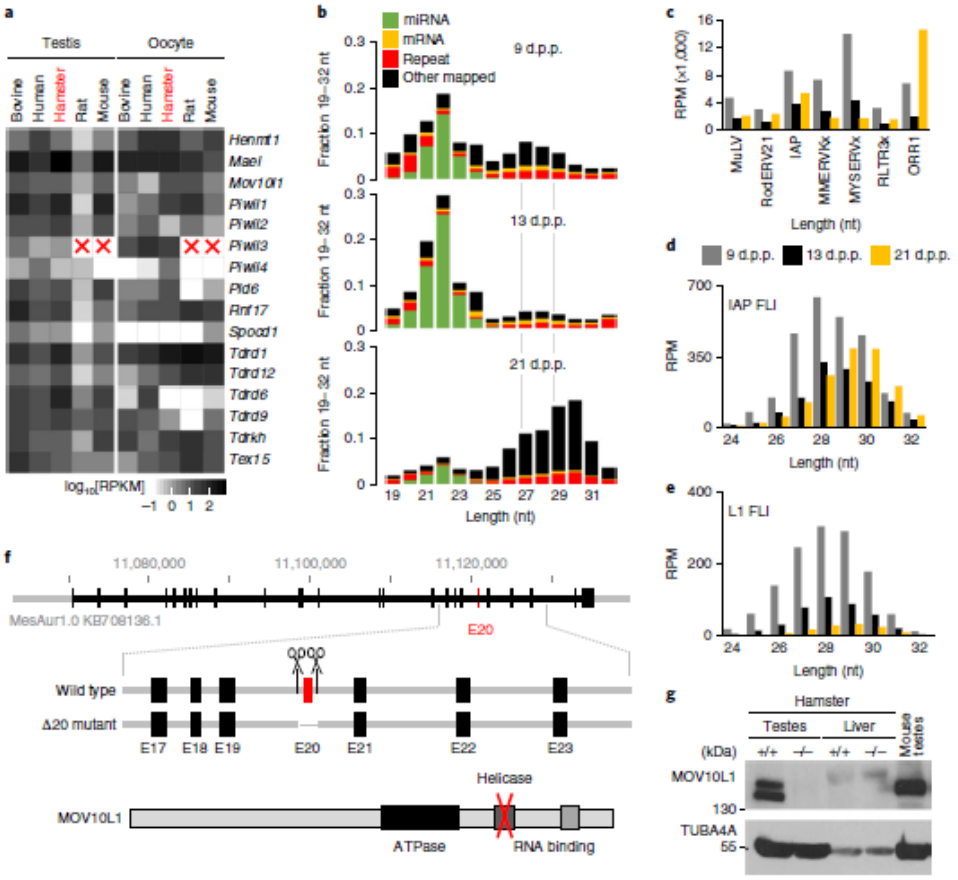

Fig. 1 | Golden hamster piRNA pathway and the *Mov10l1* knockout. a, The expression of piRNA pathway factors in the testes and oocytes of five mammals. Mouse and rat lack *Piwil3*. RPKM, reads per kilobase of transcript per million mapped reads. **b**, The distribution of 19–32-nucleotide-long RNAs from testes at 9, 13 and 21 d.p.p. nt, nucleotide. **c**, Testicular 24–32-nucleotide small RNAs mapping to LTR retrotransposon groups selected for low nucleotide exchange rate and high abundance of putative piRNAs (Extended Data Fig. 2a). The *y* axis displays reads per million (RPM) of 19–32-nucleotide RNAs. **d**,**e**, The distribution of 24–32-nucleotide antisense RNAs from testes at 9, 13 and 21 d.p.p. that perfectly map to FLI IAP (**d**) or L1 (**e**) insertions, respectively. The *y* axis displays the RPM of 19–32-nucleotide sequence reads. For **b**–**e**, values were calculated as the mean values of two biological replicates of wild-type testis samples (Supplementary Table 10). **f**, MOV10L1 protein organization and the knockout strategy. The CRISPR–Cas9 cleavage positions (scissors) flanking exon 20 (red rectangle; E20) are shown. **g**, Western blot analysis showing the absence of MOV10L1 in mutant adult testes. Liver and mouse testes were used as negative and positive controls, respectively, for antibody specificity. This experiment was performed once; the impact of the mutation on *Mov10l1* expression in the testes was confirmed using RNA-seq analysis (Extended Data Fig. 3c).

analysis of 29-nucleotide pre-pachytene piRNAs revealed an increased frequency of adenosine at nucleotide 10 (Extended Data Fig. 1e), which is a signature of the 'ping pong' mechanism that generates secondary piRNAs[2]. Together, hamster postnatal testicular piRNAs shared features with those of other mammals.

As piRNAs provide an adaptive defence against transposable elements, we investigated which golden hamster retrotransposons are the main targets of the piRNA pathway. Using an improved golden hamster genome assembly[11], we determined the entire complement of hamster retrotransposons, identified potentially active retrotransposon subfamilies and estimated the abundances of retrotransposon-derived piRNAs. An analysis of mutation rates of long terminal repeat (LTR) retrotransposons in hamster and mouse genomes revealed divergent evolutionary paths of specific subfamilies (Supplementary Text, Extended Data Fig. 2 and Supplementary Data 1–3). We observed that the ERVK class, exemplified by rodent-specific intracisternal A particle (IAP) and MYSERV retrotransposons, expanded during the evolution of the hamster (Supplementary Data 1 and Extended Data Fig. 2a). Notably, MYSERV and IAP-derived piRNAs were also the most abundant piRNAs targeting autonomous transposable elements (Fig. 1c and Extended Data Fig. 2a). In contrast to MYSERV retrotransposons, IAPs are well characterized transposable elements that evolved from a retrovirus in the common ancestor of hamsters and mice[29,30]. Thousands IAP insertions can be identified in mouse and hamster genomes, but only a small fraction are full-length intact (FLI, hereafter denoted as intact) insertions, possibly supporting retrotransposition. In the golden hamster genome, we identified 110 intact IAP insertions, classified as the IAPLTR3/4 subgroup (Supplementary Data 4), whereas a different subgroup (IAPE) is

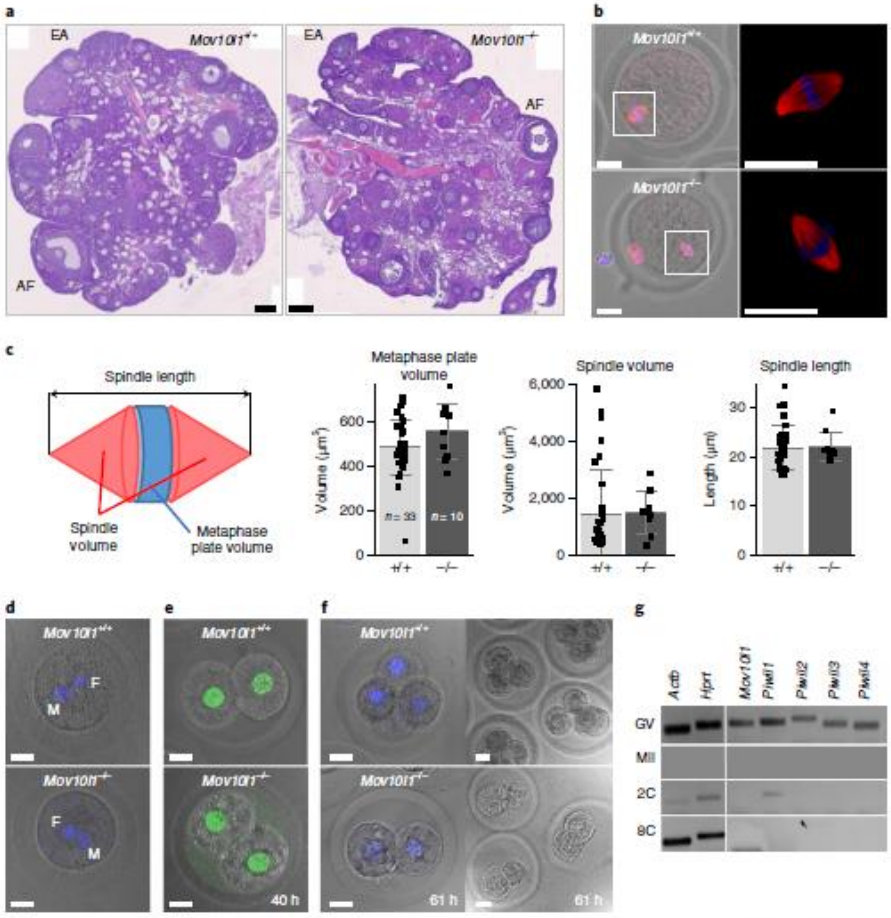

Fig. 2 | Female *Mov10l1*$^{-/-}$ phenotype. a, Haematoxylin and eosin (H&E) staining of ovarian sections. Antral follicles (AF) and early antral follicles (EA) indicate normal follicular development. The ovaries of four *Mov10l1*$^{-/-}$ and two *Mov10l1*$^{+/+}$ female hamsters were analysed and representative images are shown. Scale bars, 200 µm. **b**,**c**, Mutant oocytes mature to the MII stage with a normal spindle 17 h after injection of human chorionic gonadotropin (hCG) (red, tubulin; blue, DNA (4,6-diamidino-2-phenylindole (DAPI))). Images of spindles are shown (**b**) and quantitatively analysed (**c**). **c**, Quantitative analysis of MII spindle traits. The spindle length, spindle volume (tubulin staining signal) and metaphase plate volume (DAPI signal) of MII eggs (isolated 17 h after hCG injection) were quantified using three-dimensional spindle reconstruction from confocal optical sections. Data are mean ± s.d. from 33 *Mov10l1*$^{+/+}$ and 10 *Mov10l1*$^{-/-}$ eggs. **d**, *Mov10l1*$^{-/-}$ eggs can be fertilized and form one-cell zygotes. Bright-field confocal images are overlaid with DNA staining by DAPI. Larger male (M) and a smaller female (F) pronuclei are shown. **e**, *Mov10l1*$^{-/-}$ eggs give rise to two-cell zygotes 40 h after mating. Bright-field confocal images are overlaid with H3K9me3 staining (green) showing that two-cell zygotes from *Mov10l1*$^{-/-}$ eggs have no major heterochromatin defect. **f**, Fertilized *Mov10l1*$^{-/-}$ eggs do not develop beyond two-cell zygotes. Zygotes were isolated 61 h after mating. Representative bright-field confocal images overlaid with DNA staining by DAPI are shown. Mating and zygote isolation at 40 h or 61 h after mating was performed twice with the same results. For **b** and **d**–**f**, scale bars, 20 µm. **g**, RT–PCR analysis of transcripts of piRNA pathway genes in oocytes and zygotes. This analysis was replicated four times for germinal vesicle-intact (GV) oocytes, twice for MII and three times for two-cell (2C) stages. Analysis of the eight-cell stage was performed once.

mobile in mice[31] (Extended Data Fig. 2c). Interestingly, piRNAs antisense to intact IAPs were abundant at all three of the tested time points (Fig. 1d). In contrast to the ERVK class, there was no notable recent expansion among hamster's autonomous elements from the ERVL class (Supplementary Data 2 and Extended Data Fig. 2a); this class underwent substantial expansion in mice with a major impact on gene expression in oocytes and zygotes[27].

The most relevant non-LTR retrotransposon is the long interspersed nuclear element L1, the most successful autonomous transposable element invading mammalian genomes[32]. L1 analysis revealed 110 intact L1 elements from the Lx5/6 subfamily (Supplementary Data 5), which is comparable to the 146 intact L1 elements in the human genome but much smaller than the 2,811 intact L1 elements in the mouse genome[33], which come from a different L1 subfamily (Extended Data Fig. 2d). Analysis of piRNA sequences suggested that hamster intact L1s are most targeted by pre-pachytene antisense piRNAs (Fig. 1e).

Sterile phenotype of *Mov10l1*$^{-/-}$ females. To examine how the biological significance of the hamster piRNA pathway compares with that of the mouse, we knocked-out *Mov10l1* by deleting exon 20, which encodes the helicase domain (Fig. 1f and Extended Data Fig. 3),

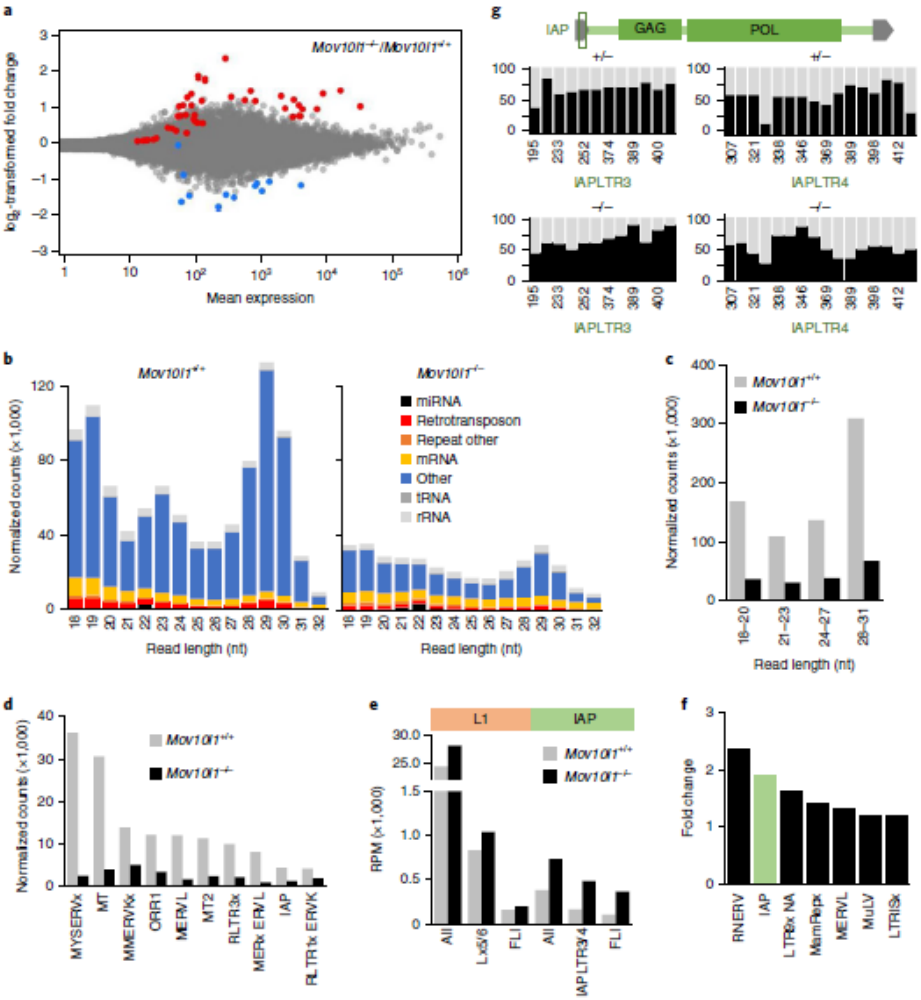

Fig. 3 | Transcriptome changes in *Mov10l1*$^{-/-}$ oocytes. a, MA plot of differentially expressed protein-coding genes (DESeq2, $P < 0.01$). The red and blue points depict genes of which the transcripts were present at significantly higher or lower levels in fully-grown *Mov10l1*$^{-/-}$ oocytes, respectively. The full DEG list is provided in Supplementary Table 5. **b**, Composition of an 18–32-nucleotide segment of RNA-seq libraries from fully grown *Mov10l1*$^{+/+}$ and *Mov10l1*$^{-/-}$ oocytes. The abundance of small RNAs in the wild-type control corresponds to the RPM of 18–32-nucleotide reads (average value from two libraries). The *Mov10l1*$^{-/-}$ library was normalized to the amount of maternal miRNAs. **c**, Reduced levels of different classes of piRNAs in *Mov10l1*$^{-/-}$ oocytes. The abundance of reads of different sizes mapping to annotated oocyte piRNA clusters (Supplementary Table 6) is shown. *Mov10l1*$^{-/-}$ values were scaled by miRNA abundance. Read sizes were divided into categories to separate putative PIWIL3-bound piRNAs (18–20 nucleotides), Dicer products (21–23 nucleotides), and smaller and longer piRNAs (24–27 nucleotides and 28–31 nucleotides). **d**, Reduction of LTR retrotransposon-derived piRNAs in *Mov10l1*$^{-/-}$ oocytes. **e**, Changes in RNAs from L1 and IAP families and subfamilies. The RPMs of RNAs mapping to L1 or IAP elements (all), active subfamilies and FLI only are shown. Data are the mean values of two (*Mov10l1*$^{+/+}$) and three (*Mov10l1*$^{-/-}$) biological replicates. **f**, LTR retrotransposon groups ranked by the highest transcript upregulation in *Mov10l1*$^{-/-}$ oocytes. Data are the mean values from two (*Mov10l1*$^{+/+}$) and three (*Mov10l1*$^{-/-}$) replicates. **g**, DNA methylation of intact IAPs. The vertical bars represent methylation (black portion) observed for the indicated 5′ CpG dinucleotides covered by at least ten sequence reads; the analysed region corresponds to the central and 3′ part of the 5′ LTR, as indicated in the IAP scheme and by CpG position. Data are from a single genome-wide bisulfite sequencing experiment.

generating a deletion analogous to one studied in mice[3]. Western blot analysis showed the lack of MOV10L1 in *Mov10l1*$^{-/-}$ testes (Fig. 1g). Heterozygotes were fertile and segregation of genotypes did not deviate significantly from the Mendelian ratio but homozygotes of both sexes were sterile (Supplementary Table 4). Male *Mov10l1*$^{-/-}$ sterility could be expected, but female *Mov10l1*$^{-/-}$ sterility was surprising given the normal fertility of female *Mov10l1*$^{-/-}$ mice[3,4].

We first determined the basis of *Mov10l1*$^{-/-}$ female sterility. *Mov10l1*$^{-/-}$ ovaries appeared to be histologically normal, suggesting that mutant oocytes enter the first meiotic block and develop to

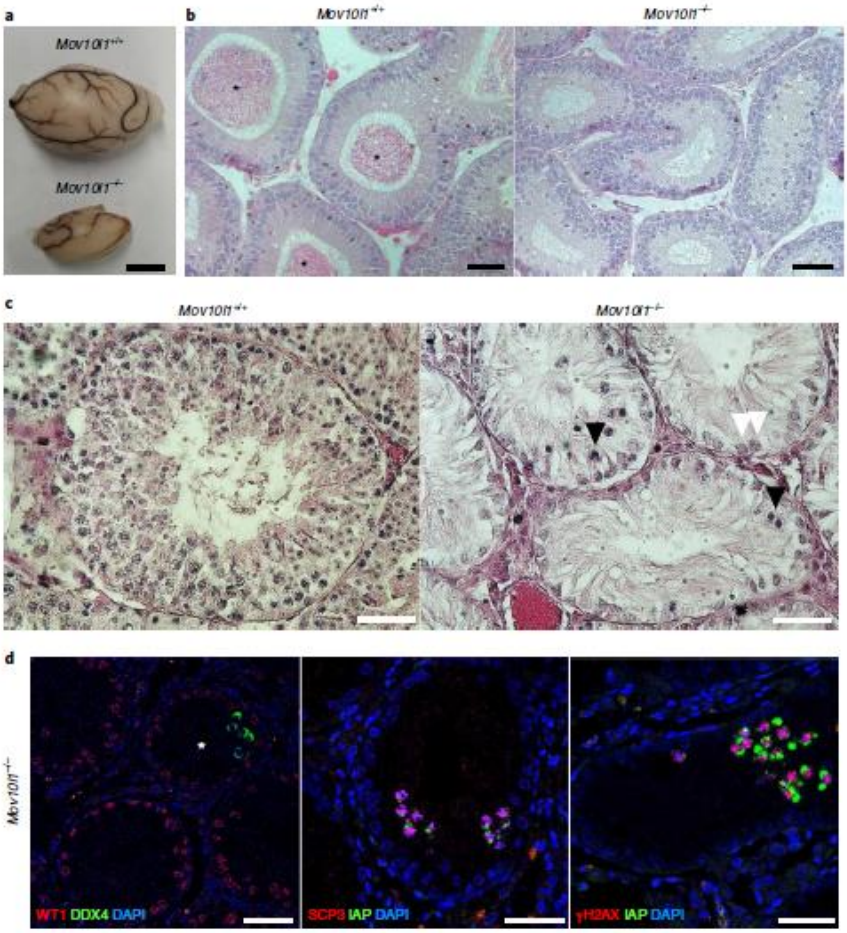

Fig. 4 | Male *Mov10l1*$^{-/-}$ phenotype. a, *Mov10l1*$^{-/-}$ males have atrophic testes. Scale bar, 5 mm. **b**, H&E staining of epididymal ducts shows a lack of sperm production in adult *Mov10l1*$^{-/-}$ testes. Sperms in *Mov10l1*$^{+/+}$ epididymal ducts are indicated (asterisks). Scale bars, 50 µm. **c**, H&E staining of testes from *Mov10l1*$^{+/+}$ (aged 102 weeks) and *Mov10l1*$^{-/-}$ (aged 63 weeks) male hamsters. The white arrowheads indicate Sertoli cells and the black arrowheads indicate degenerated cells (a large field of view is provided in Extended Data Fig. 6). Scale bars, 50 µm. **d**, Analysis of residual clusters of spermatogenic cells in seminiferous tubules in *Mov10l1*$^{-/-}$ adult testes (asterisk). Left, somatic Sertoli cells (WT1, red) and a cluster of germ cells (DDX4, green)[37–39]. Middle, SCP3^{+} clusters exhibit IAP expression (green). Right, cells expressing IAP (green) have DNA damage (γH2AX, red). Two animals with each genotype were used for histological analyses, three sections from each animal were stained and representative images are shown. Scale bars, 50 µm.

preovulatory oocytes in the antral follicles (Fig. 2a). *Mov10l1*$^{-/-}$ oocytes ovulated and matured in vivo into apparently normal metaphase II (MII) oocytes (Fig. 2b,c). However, zygotes from *Mov10l1*$^{-/-}$ females did not develop beyond the two-cell stage (Fig. 2d–f), a stage during which the major zygotic activation occurs[38]. As the breeding of heterozygotes yielded a Mendelian frequency of *Mov10l1*$^{-/-}$ progeny (Supplementary Table 4), this implied a maternal effect phenotype whereby *Mov10l1*$^{-/-}$ oocytes retain meiotic competence but lack the ability to support development irrespective of the genotype of the zygote.

As *Mov10l1* and *Piwil* genes are expressed maternally (Fig. 2g), we hypothesized that transcriptomes of fully grown oocytes, the final stage of ovarian oogenesis, might exhibit early signs of the loss of developmental competence. We identified 57 differentially expressed genes (DEGs) in *Mov10l1*$^{-/-}$ oocytes (Fig. 3a, Extended Data Fig. 4a,b and Supplementary Table 5). By contrast, 1,612 DEGs were reported in *Piwil1*$^{-/-}$ ovulated MII hamster oocytes, which also fail to support zygotic development[34]. However, maternal transcriptome remodelling may differ because piRNA populations in *Mov10l1*$^{-/-}$ and *Piwil1*$^{-/-}$ oocytes are affected differently. *Mov10l1*$^{-/-}$ oocytes have a massive but incomplete loss of piRNAs (Fig. 3b–d) whereby the production of specific abundant maternal piRNAs remains even in the absence of MOV10L1 (Extended Data Fig. 4c). Furthermore, we analysed pre-ovulatory oocytes while *Piwil1*$^{-/-}$ analysis concerned a later MII stage[35] at which meiotic transcriptome remodelling[36] could enhance transcriptome changes that are considered to be statistically not significant in fully grown oocytes. A direct comparison of *Mov10l1*$^{-/-}$ and *Piwil1*$^{-/-}$ data filtered with the same stringency implies a common trend for upregulated genes (Extended Data Fig. 4d). DEGs that are commonly upregulated in *Mov10l1*$^{-/-}$ and *Piwil1*$^{-/-}$ oocytes did not exhibit common features, suggesting diverse control by

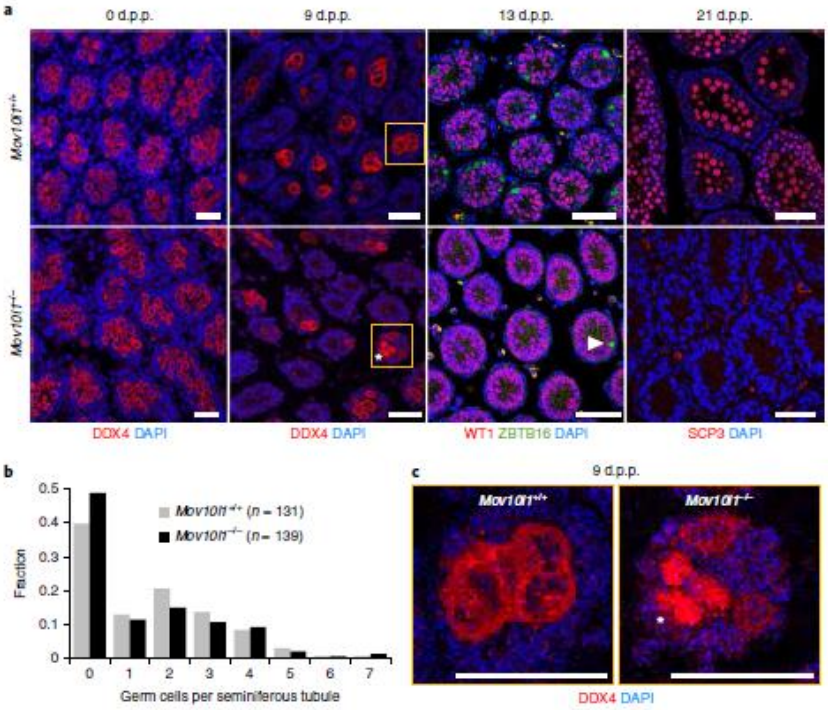

Fig. 5 | Analysis of the timing of the spermatogenesis defect in *Mov10l1*$^{-/-}$ males. a, Immunofluorescence staining of *Mov10l1*$^{+/+}$ and *Mov10l1*$^{-/-}$ testes at 0 d.p.p., 9 d.p.p., 13 d.p.p. and 21 d.p.p. to examine the presence of germ cells (marked by DDX4), undifferentiated spermatogonia (marked by ZBTB16)[39] and spermatocytes (marked by SCP3)[38]. DNA was stained with DAPI. Several histological sections from two different animals were analysed at all stages. Aberrant DDX4 staining observed at 9 d.p.p. is indicated (asterisk) (a magnified image is shown in **c**). The arrowhead indicates a single ZBTB16^{+} spermatogonium in a *Mov10l1*$^{-/-}$ 13 d.p.p. sample. Scale bars, 50 µm. **b**, Quantitative analysis of germ cell distribution in sections of 9 d.p.p. seminiferous tubules. For each genotype, the indicated number of seminiferous tubules on several sections was examined for the presence of DDX4^{+} germ cells. There was no statistically significant association between genotype and tubules being empty or non-empty (χ^2 test, $P = 0.138$). **c**, Higher magnification of the seminiferous tubule cross-sections shown in **a**. *Mov10l1*$^{-/-}$ germ cells are indicated (asterisk), which show deviation from the normal DDX4 staining pattern in which strong cytoplasmic staining would surround a nucleus with a minimal signal. Scale bars, 50 µm.

piRNAs. For example, *Kif2a* was unique in employing an LTR-derived promoter to control its expression in oocytes (Extended Data Fig. 4e), suggesting that *Kif2a* expression control could occur through retrotransposon-targeting piRNAs.

Developmental competence could also be affected by derepression of TEs. A small increase (~25%) in reads mapping to intact L1 transcripts was observed in *Mov10l1*$^{-/-}$ oocytes (Fig. 3e). RNA-sequencing (RNA-seq) analysis also revealed a limited increase in LTR retrotransposon transcripts in *Mov10l1*$^{-/-}$ oocytes—a 2-fold increase for all IAP sequence reads (Fig. 3f) and a 3.5-fold increase for reads perfectly matching intact elements (Fig. 3e). This suggests impaired repression of intact IAPs in *Mov10l1*$^{-/-}$ oocytes, without global IAP derepression. This notion was supported by whole-genome bisulfite sequencing (Fig. 3g). The limited amount of material yielded information about ~10% of the hamster genome (Extended Data Fig. 5). While the loss of DNA methylation at unique loci would have escaped detection (including those identified in *Ptwtl3*$^{-/-}$ hamster oocytes[34]), bisulfite sequencing of *Mov10l1*$^{-/-}$ oocytes yielded enough unique sequencing reads to examine global methylation levels of retrotransposon subfamilies (Extended Data Fig. 5d). Overall DNA methylation of intact IAP elements was preserved, although several CpG positions in LTRs could have reduced methylation frequency (Fig. 3g and Extended Data Fig. 5e). Furthermore, retrotransposon subfamilies that recently expanded in the hamster genome and were associated with high amounts of piRNAs in hamster testes (Extended Data Fig. 2a) did not show reduced DNA methylation either (Extended Data Fig. 5d).

Sterile phenotype of *Mov10l1*$^{-/-}$ males. Adult *Mov10l1*$^{-/-}$ males were sterile and had atrophic testes (Fig. 4a) as well as epididymal ducts devoid of sperm (Fig. 4b). Although the sterility of *Mov10l1*$^{-/-}$ male hamsters was consistent with the mouse *Mov10l1*$^{-/-}$ model phenotype[3–5], we sought to determine whether there is the same spermatogenesis defect. Histological analysis of old *Mov10l1*$^{-/-}$ males (>50 weeks) revealed aspermatogenic seminiferous tubules (Fig. 4c and Extended Data Fig. 6a). Approximately 3% of adult seminiferous tubules contained small clusters of cells positive for the germ cell marker DDX4 (VASA)[37] and the marker of meiotic cells synaptonemal complex protein 3 (SCP3)[38] (Fig. 4d and Extended Data Fig. 6b). These clusters were also positive for the IAP GAG protein and γH2AX, a common marker of DNA damage suggesting compromised genome integrity (Fig. 4d). Derepression of L1 retrotransposons was absent or the anti-ORF1 antibody did not cross-react with the hamster protein. The clusters of rare survivors of germ cell 'atresia' therefore seem to develop a secondary phenotype that is

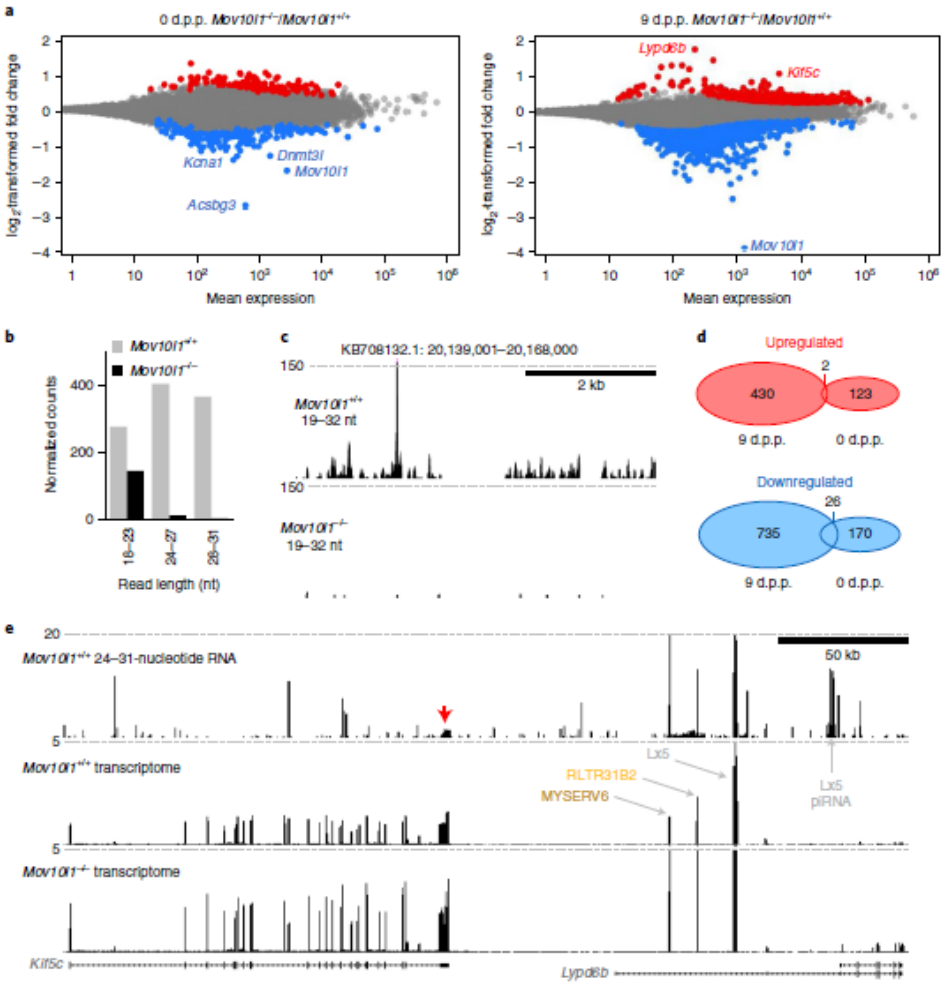

Fig. 6 | Spermatogenesis defects in *Mov10l1*$^{-/-}$ testes. a, MA plots showing differentially expressed protein-coding genes at 0 d.p.p. and 9 d.p.p. (two sequencing libraries per genotype and per time point; DESeq2, $P < 0.01$). The red and blue points depict genes of which the transcripts were present at significantly higher or lower levels, respectively, in *Mov10l1*$^{-/-}$ testes (DEG lists are provided in Supplementary Tables 7 and 8). **b**, Loss of piRNAs in *Mov10l1*$^{-/-}$ 9 d.p.p. testes. The abundance of reads of different sizes mapping to annotated 9 d.p.p. piRNA clusters (Supplementary Table 1) is shown. Data are the mean values of three (*Mov10l1*$^{+/+}$) and two (*Mov10l1*$^{-/-}$) RNA-seq libraries. **c**, A snapshot from the UCSC genome browser revealing a loss of piRNAs in the top 9 d.p.p. cluster. **d**, The number of DEGs and a minimal overlap between significantly upregulated (red Venn diagram) and downregulated (blue Venn diagram) DEGs in *Mov10l1*$^{-/-}$ 0 d.p.p. and 9 d.p.p. testes. **e**, A UCSC browser snapshot showing small RNAs and longer transcripts in *Mov10l1*$^{+/+}$ and *Mov10l1*$^{-/-}$ testes at the *Klf5c-Lypd6b* locus. The red arrow indicates a cluster of unique piRNAs derived from the *Klf5c* 3′ UTR. Three retrotransposon insertions in intron 1 of *Lypd6b* with increased density of mapped reads are also shown. Only perfectly mapping RNA-seq reads were used to construct the image.

similar to the main phenotype of *Mov10l1*$^{-/-}$ mice, whereby spermatogenesis fails after entry into meiosis[3–5]. By contrast, the primary spermatogenesis defect in *Mov10l1*$^{-/-}$ hamsters appears before the entry into meiosis.

To understand the loss of germ cells in *Mov10l1*$^{-/-}$ hamster testes, we examined new-born (0 d.p.p.), 9 d.p.p., 13 d.p.p. and 21 d.p.p. animals (Fig. 5a). Previous research has shown that new-born testes contain mitotically quiescent gonocytes that reinitiate mitosis and move to the seminiferous tubule periphery by 9 d.p.p. and give rise to spermatogonia by 13 d.p.p. (ref. [28]). In 21 d.p.p. testes, spermatogenesis proceeds as far as the pachytene stage of meiosis I (ref. [28]). We detected DDX4^{+} cells in new-born and 9 d.p.p. *Mov10l1*$^{-/-}$ testes (Fig. 5a). Although 9 d.p.p. *Mov10l1*$^{-/-}$ testes appeared normal (Fig. 5b), some seminiferous tubules exhibited aberrant localization of DDX4 (Fig. 5c), suggesting that the main spermatogenesis defect precedes the formation of spermatogonia. Accordingly, 13 d.p.p. seminiferous tubules were almost devoid of ZBTB16^{+} cells, the marker of undifferentiated spermatogonia[39] (Fig. 5a). At 21 d.p.p., we observed smaller testes, altered seminiferous tubule architecture and a complete absence of SCP3^{+} meiotic

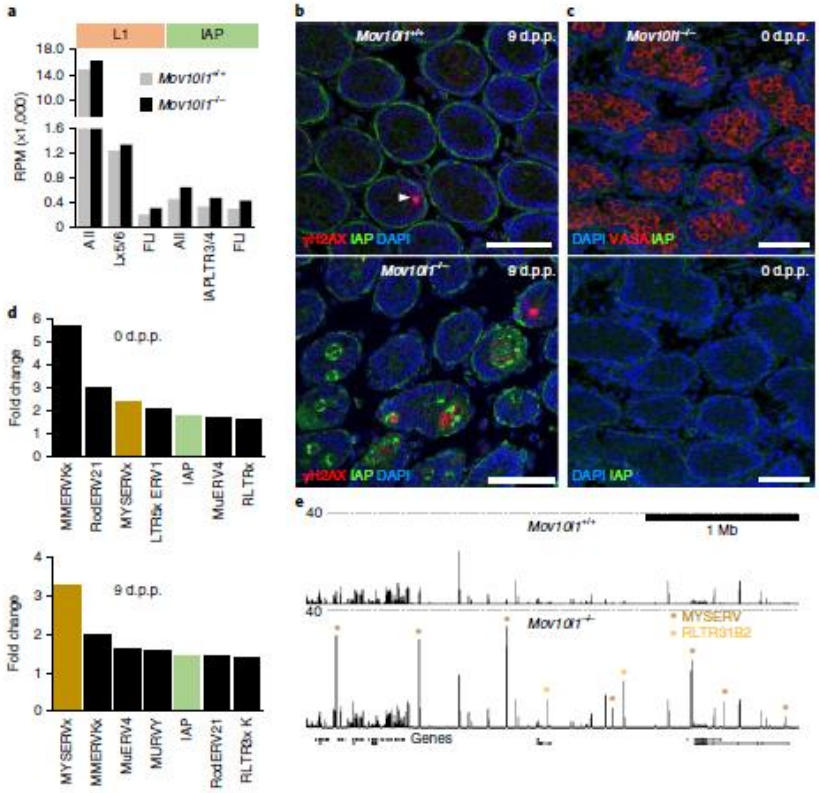

Fig. 7 | Retrotransposon mobilization in *Mov10l1*$^{-/-}$ testes at 9 d.p.p. a, Changes in RNAs from L1 and IAP families and subfamilies. RPM values of RNAs mapping to L1 or IAP elements (all), active subfamilies and FLI elements only are shown. Data are the mean values of two biological replicates. **b**, Immunofluorescence staining of IAP GAG (green) and γH2AX (red) in *Mov10l1*$^{+/+}$ and *Mov10l1*$^{-/-}$ testes at 9 d.p.p. suggests IAP expression and DNA damage in germ cells in seminiferous tubules. Scale bars, 50 µm. **c**, 0 d.p.p. *Mov10l1*$^{-/-}$ testes show a normal presence of the germ cell marker DDX4 (VASA) and no mobilization of IAP expression. Four (**b**) and three (**c**) sections from one testis with a given genotype were individually stained. Representative images are shown. **d**, Changes in retrotransposon expression. The graphs rank the most upregulated LTR retrotransposon groups in *Mov10l1*$^{-/-}$ testes at 0 d.p.p. and 9 d.p.p. Values were calculated as RPM mean values from two RNA-seq libraries (Supplementary Table 10) from each time point and genotype. **e**, MYSERV and related RLTR31B2 LTR-derived transcripts are upregulated in *Mov10l1*$^{-/-}$ testes at 9 d.p.p. A UCSC browser snapshot shows a 3 Mb genomic region with upregulated retrotransposon loci (asterisks). Only perfectly mapping RNA-seq reads were used to construct the image.

cells (Fig. 5a). This implied that the surviving *Mov10l1*$^{-/-}$ spermatogonia were probably compromised as they did not enter the first wave of meiosis on time.

The cause of the germ cell loss was further investigated by transcriptome profiling of 9 d.p.p. testes, which identified a complete loss of piRNAs and >900 DEGs (Fig. 6, Extended Data Fig. 7 and Supplementary Table 7). Many downregulated genes were factors expressed in spermatogenic cells (Extended Data Fig. 7d,e), including germline factors *Sohlh1* (ref. [40]) *Ddx25* (ref. [41]), *Ddx4* (ref. [37]), *Dazl* (ref. [42]) and many piRNA pathway components (Supplementary Table 7). By contrast, new-born *Mov10l1*$^{-/-}$ testes exhibited ~300 DEGs (Supplementary Table 8 and Fig. 6a) but there was minimal overlap with 9 d.p.p. testes (Fig. 6d) and no significant enrichment of any biological process according to a Gene Ontology analysis. This shows that the loss of piRNAs affects gene expression already in new-born testes, but germ cell development fails later and the failure involves a different set of DEGs. Thus, the prespermatogonial germline failure may have two causes.

First, the loss of 26–27-nucleotide postnatal piRNAs originating from non-repetitive sequences, including mRNA 3′ untranslated regions (UTRs)[8], may increase gene expression that is otherwise restricted by the piRNA pathway. However, we observed that only a small fraction of upregulated genes was associated with higher amounts of non-repetitive piRNAs from the same loci (Extended Data Fig. 7f). Most of the observed increases in gene expression appeared small (Fig. 6a), but expression changes could be under-represented when genes are also expressed in cells other than spermatogenic cells (Extended Data Fig. 7d). Notably, *Lypd6b* and *Klf5c*, two of the three most upregulated genes are genomic neighbours, suggesting a common regulation of the locus, which might involve *Klf5c* 3′-UTR-derived piRNAs and/or derepression of retrotransposons in the first *Lypd6b* intron (Fig. 6e).

Second, formation of spermatogonia in 9 d.p.p. *Mov10l1*$^{-/-}$ testes could also be perturbed by derepression of specific retrotransposons. An analysis of intact L1 and IAP transcripts suggested respective approximate increases of 56% and 48% in their abundance (Fig. 7a). This mild increase contrasted with IAP and γH2AX

signals in *Mov10l1*$^{-/-}$ seminiferous tubules that were detected at 9 d.p.p. but not at 0 d.p.p. (Fig. 7b,c). However, a similar situation concerning IAP transcript levels and immunofluorescent staining occurred when comparing mouse *G9a*$^{-/-}$ and *Mili*$^{-/-}$ (Piwil2) spermatogonia[43]. Notably, IAP and γH2AX patterns differed among 9 d.p.p. seminiferous tubules. Some contained mostly IAP signal, some massive γH2AX, and some both, probably capturing the demise of germ cells at 9 d.p.p. (Fig. 7b and Extended Data Fig. 8).

An analysis of MYSERV LTR retrotransposons provides even stronger support that the mobilization of retrotransposons may explain the loss of control over spermatogenesis. MYSERV elements give rise to highly abundant 9 d.p.p. piRNAs (Fig. 1c and Extended Data Fig. 2a). In 9 d.p.p. *Mov10l1*$^{-/-}$ testes, MYSERV-derived reads were 3.3-fold more abundant (Fig. 7d), but MYSERV6 subfamily insertions across the genome exhibited a ~20-fold increase (Fig. 7e), which is consistent with quantitative PCR (qPCR) data (Extended Data Fig. 7g). Derepression of MYSERV retrotransposons, which was already apparent at day 0 (Fig. 7d), implies that there was genome-wide failure to silence MYSERV insertion loci, which could subsequently contribute to the failure of germ cells to form spermatogonia.

Discussion

Our analysis of *Mov10l1*$^{-/-}$ golden hamsters, complemented by analysis of additional piRNA pathway mutants by Hasuwa et al[34]. and Zhang et al.[44], reports critical pre-meiotic, meiotic and post-meiotic functions of the mammalian piRNA pathway. Our results substantially expand the known roles of the pathway in control of the mammalian germline cycle. Furthermore, we provide an evolutionary perspective for the piRNA pathway roles while refuting the notion that the mammalian piRNA pathway is important only for the male germline.

The post-meiotic and post-zygotic sterility observed in female *Mov10l1*$^{-/-}$ hamsters adds to the repertoire of critical roles of the mammalian piRNA pathway contribution to formation of developmentally competent oocytes, which can support early development. This contrasts with mice, in which the females remain fertile even in the absence of the piRNA pathway[3,4,13–16].

One of the notable differences between mice and golden hamsters is that mice lost *Piwil3* while golden hamsters have four different PIWI effector proteins like most mammals, including humans. *Piwil3* seems to represent an oocyte-specific aspect of the mammalian piRNA pathway[10,11,21,34,44]. However, female subfertility of *Piwil3*$^{-/-}$ golden hamsters is a weaker phenotype[34] than female sterility observed in mutants in other components of the pathway in golden hamsters, which include *Mov10l1* reported here and in ref. [44], *Piwil1* (refs. [34,44]) and *Pld6* (ref. [44]). This suggests that, although the *Piwil3* is an important factor, the piRNA pathway has additional important non-overlapping functions. What these functions are remains to be clarified. Although we observed changes in *Mov10l1*$^{-/-}$ oocytes, which possibly contribute to the sterile phenotype, the mechanism of the loss of developmental competence of *Mov10l1*$^{-/-}$ oocytes remains to be further delineated.

Changing requirements for the piRNA pathway during evolution could lead to the apparent insignificance of the piRNA pathway in mouse oocytes. However, our results provoke the question of whether the piRNA pathway in mouse oocytes could have a similar role in formation of developmental competence, which would be masked in piRNA-pathway mutants by overlapping functions of the murine RNAi pathway[19]. Unfortunately, massive transcriptome changes and meiotic defects in oocytes lacking RNAi[45,46] preclude the examination of the functional significance of the piRNA pathway in mouse zygotes in the absence of RNAi.

An analysis of *Mov10l1*$^{-/-}$ male hamsters showed that MOV10L1 is required for the postnatal formation of pre-meiotic spermatogonia. The massive loss of germ cells before the spermatogonia form differs from the phenotypes in mice with mutations in the piRNA pathway, which occur after the spermatogonia form. Although *Miwi2*$^{-/-}$ mice revealed that piRNAs regulate DNA methylation in prospermatogonia, this role is not important for the establishment of spermatogonia, which form in *Miwi2*$^{-/-}$ mice but are then lost progressively until the testes become aspermatogenic by 9 months[15,47–49].

The failure of male *Mov10l1*$^{-/-}$ hamsters to produce spermatogonia appears to be associated with the derepression of the MYSERV, hamster-specific retrotransposon subfamily expressed in juvenile testes. First, the absence of the piRNA pathway in the male germline yielded a failure at a stage at which MYSERV expression peaks. Second, an outstanding abundance of MYSERV-targeting piRNAs in juvenile testes implies that the element is a major target of the piRNA pathway at that stage. While most retrotransposons in mouse and hamster genomes probably descended from the common ancestor, recently expanded subfamilies represent independently evolved retrotransposon pools, which would provoke an independent adaptive response of the piRNA pathway. Hamster-specific retrotransposon derepression could therefore explain why spermatogonia form in mice lacking *Mov10l1* (refs. [3–5]). The model of retrotransposon-induced failure of spermatogenesis is also consistent with a rapid demise of mouse spermatogonia whereby retrotransposon derepression was enhanced by mutating *G9a* in addition to *Mili*[50].

Taken together, our work does not just demonstrate that the mammalian piRNA pathway is important beyond spermatogenesis. Equally important is that the divergent hamster and mouse *Mov10l1*$^{-/-}$ phenotypes illuminate the adaptive nature of the piRNA pathway, which leads to new gene regulations and flexibly protects the germline cycle against retrotransposons whenever they would pose a new threat.

Online content

Any methods, additional references, Nature Research reporting summaries, source data, extended data, supplementary information, acknowledgements, peer review information; details of author contributions and competing interests; and statements of data and code availability are available at https://doi.org/10.1038/s41556-021-00746-2.

Received: 18 February 2021; Accepted: 27 July 2021;
Published online: 6 September 2021

References

1. Aravin, A. A., Hannon, G. J. & Brennecke, J. The Piwi-piRNA pathway provides an adaptive defense in the transposon arms race. *Science* **318**, 761–764 (2007).
2. Ozata, D. M., Gainetdinov, I., Zoch, A., O'Carroll, D. & Zamore, P. D. PIWI-interacting RNAs: small RNAs with big functions. *Nat. Rev. Genet.* **20**, 89–108 (2019).
3. Frost, R. J. et al. MOV10L1 is necessary for protection of spermatocytes against retrotransposons by Piwi-interacting RNAs. *Proc. Natl Acad. Sci. USA* **107**, 11847–11852 (2010).
4. Zheng, K. et al. Mouse MOV10L1 associates with Piwi proteins and is an essential component of the Piwi-interacting RNA (piRNA) pathway. *Proc. Natl Acad. Sci. USA* **107**, 11841–11846 (2010).
5. Vourekas, A. et al. The RNA helicase MOV10L1 binds piRNA precursors to initiate piRNA processing. *Genes Dev.* **29**, 617–629 (2015).
6. Aravin, A. A., Sachidanandam, R., Girard, A., Fejes-Toth, K. & Hannon, G. J. Developmentally regulated piRNA clusters implicate MILI in transposon control. *Science* **316**, 744–747 (2007).
7. Kuramochi-Miyagawa, S. et al. DNA methylation of retrotransposon genes is regulated by Piwi family members MILI and MIWI2 in murine fetal testes. *Genes Dev.* **22**, 908–917 (2008).
8. Robine, N. et al. A broadly conserved pathway generates 3′UTR-directed primary piRNAs. *Curr. Biol.* **19**, 2066–2076 (2009).
9. Chirn, G. W. et al. Conserved piRNA expression from a distinct Set of piRNA cluster loci in eutherian mammals. *PLoS Genet.* **11**, e1005652 (2015).

10. Yang, Q. et al. Single-cell CAS-seq reveals a class of short PIWI-interacting RNAs in human oocytes. *Nat. Commun.* **10**, 3389 (2019).
11. Ishino, K. et al. Hamster PIWI proteins bind to piRNAs with stage-specific size variations during oocyte maturation. *Nucleic Acids Res.* **49**, 2700–2720 (2021).
12. Meister, G. Argonaute proteins: functional insights and emerging roles. *Nat. Rev. Genet.* **14**, 447–459 (2013).
13. Kuramochi-Miyagawa, S. et al. *Mili*, a mammalian member of *piwi* family gene, is essential for spermatogenesis. *Development* **131**, 839–849 (2004).
14. Deng, W. & Lin, H. F. *miwi*, a murine homolog of *piwi*, encodes a cytoplasmic protein essential for spermatogenesis. *Dev. Cell* **2**, 819–830 (2002).
15. Carmell, M. A. et al. MIWI2 is essential for spermatogenesis and repression of transposons in the mouse male germline. *Dev. Cell* **12**, 503–514 (2007).
16. Cheng, E. C., Kang, D., Wang, Z. & Lin, H. PIWI proteins are dispensable for mouse somatic development and reprogramming of fibroblasts into pluripotent stem cells. *PLoS ONE* **9**, e97821 (2014).
17. Lim, A. K. et al. The nuage mediates retrotransposon silencing in mouse primordial ovarian follicles. *Development* **140**, 3819–3825 (2013).
18. Kabayama, Y. et al. Roles of MIWI, MILI and PLD6 in small RNA regulation in mouse growing oocytes. *Nucleic Acids Res.* **45**, 5387–5398 (2017).
19. Taborska, E. et al. Restricted and non-essential redundancy of RNAi and piRNA pathways in mouse oocytes. *PLoS Genet.* **15**, e1008261 (2019).
20. Flemr, M. et al. A retrotransposon-driven Dicer isoform directs endogenous small interfering RNA production in mouse oocytes. *Cell* **155**, 807–816 (2013).
21. Roovers, E. F. et al. Piwi proteins and piRNAs in mammalian oocytes and early embryos. *Cell Rep.* **10**, 2069–2082 (2015).
22. Hirose, M. et al. Acrosin is essential for sperm penetration through the zona pellucida in hamsters. *Proc. Natl Acad. Sci. USA* **117**, 2513–2518 (2020).
23. Steppan, S., Adkins, R. & Anderson, J. Phylogeny and divergence-date estimates of rapid radiations in muroid rodents based on multiple nuclear genes. *Syst. Biol.* **53**, 533–553 (2004).
24. Seshagiri, P. B., McKenzie, D. I., Bavister, B. D., Williamson, J. L. & Aitken, J. M. Golden hamster embryonic genome activation occurs at the two-cell stage: correlation with major developmental changes. *Mol. Reprod. Dev.* **32**, 229–235 (1992).
25. Hirose, M. & Ogura, A. The golden (Syrian) hamster as a model for the study of reproductive biology: past, present, and future. *Reprod. Med Biol.* **18**, 34–39 (2019).
26. Abdel-Moneim, A. S. & Abdelwhab, E. M. Evidence for SARS-CoV-2 infection of animal hosts. *Pathogens* **9**, 529 (2020).
27. Franke, V. et al. Long terminal repeats power evolution of genes and gene expression programs in mammalian oocytes and zygotes. *Genome Res.* **27**, 1384–1394 (2017).
28. Miething, A. The establishment of spermatogenesis in the seminiferous epithelium of the pubertal golden hamster (*Mesocricetus auratus*). *Adv. Anat. Embryol. Cell Biol.* **140**, 1–92 (1998).
29. Ribet, D. et al. An infectious progenitor for the murine IAP retrotransposon: emergence of an intracellular genetic parasite from an ancient retrovirus. *Genome Res.* **18**, 597–609 (2008).
30. Magiorkinis, G., Gifford, R. J., Katzourakis, A., De Ranter, J. & Belshaw, R. Env-less endogenous retroviruses are genomic superspreaders. *Proc. Natl Acad. Sci. USA* **109**, 7385–7390 (2012).
31. Dewannieux, M., Dupressoir, A., Harper, F., Pierron, G. & Heidmann, T. Identification of autonomous IAP LTR retrotransposons mobile in mammalian cells. *Nat. Genet.* **36**, 534–539 (2004).
32. Ostertag, E. M. & Kazazian, H. H. Jr. Biology of mammalian L1 retrotransposons. *Annu. Rev. Genet* **35**, 501–538 (2001).
33. Penzkofer, T. et al. L1Base 2: more retrotransposition-active LINE-1s, more mammalian genomes. *Nucleic Acids Res.* **45**, D68–D73 (2017).
34. Hasuwa, H. et al. Production of functional oocytes requires maternally expressed PIWI genes and piRNAs in golden hamsters. *Nat. Cell Biol.* https://doi.org/10.1038/s41556-021-00745-3 (2021).
35. Gou, L. T. et al. Ubiquitination-deficient mutations in human *Piwil* cause male infertility by impairing histone-to-protamine exchange during spermiogenesis. *Cell* **169**, 1090–1104 (2017).
36. Svoboda, P., Franke, V. & Schultz, R. M. In *Maternal-to-Zygotic Transition* Vol. 113 (ed. Lipshitz, H. D.) 305–349 (2015).
37. Raz, E. The function and regulation of vasa-like genes in germ-cell development. *Genome Biol.* **1**, reviews1017.1 (2000).
38. Yuan, L. et al. The murine SCP3 gene is required for synaptonemal complex assembly, chromosome synapsis, and male fertility. *Mol. Cell* **5**, 73–83 (2000).
39. Costoya, J. A. et al. Essential role of Plzf in maintenance of spermatogonial stem cells. *Nat. Genet.* **36**, 653–659 (2004).
40. Ballow, D., Meistrich, M. L., Matzuk, M. & Rajkovic, A. Sohlh1 is essential for spermatogonial differentiation. *Dev. Biol.* **294**, 161–167 (2006).
41. Gutti, R. K., Tsai-Morris, C. H. & Dufau, M. L. Gonadotropin-regulated testicular helicase (DDX25), an essential regulator of spermatogenesis, prevents testicular germ cell apoptosis. *J. Biol. Chem.* **283**, 17055–17064 (2008).
42. Li, H. et al. DAZL is a master translational regulator of murine spermatogenesis. *Natl Sci. Rev.* **6**, 455–468 (2019).
43. Di Giacomo, M., Comazzetto, S., Sampath, S. C. & O'Carroll, D. G9a co-suppresses LINE1 elements in spermatogonia. *Epigenet. Chromatin* **7**, 24 (2014).
44. Zhang, H. et al. The piRNA pathway is essential for generating functional oocytes in golden hamsters. *Nat. Cell Biol.* https://doi.org/10.1038/s41556-021-00750-6 (2021).
45. Murchison, E. P. et al. Critical roles for Dicer in the female germline. *Genes Dev.* **21**, 682–693 (2007).
46. Tang, F. et al. Maternal microRNAs are essential for mouse zygotic development. *Genes Dev.* **21**, 644–648 (2007).
47. De Fazio, S. et al. The endonuclease activity of Mili fuels piRNA amplification that silences LINE1 elements. *Nature* **480**, 259–263 (2011).
48. Vasiliauskaite, L. et al. Defective germline reprogramming rewires the spermatogonial transcriptome. *Nat. Struct. Mol. Biol.* **25**, 394–404 (2018).
49. Watanabe, T., Cui, X., Yuan, Z., Qi, H. & Lin, H. MIWI2 targets RNAs transcribed from piRNA-dependent regions to drive DNA methylation in mouse prospermatogonia. *EMBO J.* **37**, e95329 (2018).
50. Di Giacomo, M. et al. Multiple epigenetic mechanisms and the piRNA pathway enforce LINE1 silencing during adult spermatogenesis. *Mol. Cell* **50**, 601–608 (2013).

Methods

Animals. Golden (Syrian) hamsters *M. auratus* were purchased from Japan SLC (for knockout production and initial breeding) and from Janvier Labs (subsequent breeding). Animals were housed under controlled lighting conditions (daily light period 7:00 to 21:00 and 6:00 to 18:00 in Japan and Czechia, respectively) and provided with water and food ad libitum. The animals used for experiments were euthanized by intraperitoneal injection of a lethal dose of Euthasol (Samohyl). All of the animal experiments were approved by the Animal Experimentation Committee at the RIKEN Tsukuba Institute (T2019-J004) and the Institutional Animal Use and Care Committee at the Institute of Molecular Genetics of the Czech Academy of Sciences (approval no. 42/2016 and 70/2018) and were performed in accordance with the law.

Production of *Mov10l1* mutants. The production of knockout hamsters was carried out using an in vivo electroporation CRISPR–Cas9 system as described previously[22,51]. Pairs of sgRNAs were designed to cleave the *Mov10l1* genomic sequence in intron 19 (sequence of DNA targets: 5′-GGGTATCACATGACTT GGGG-3′; 5′-GGTGTTGGGATCATAGTGGGG-3′) and in intron 20 (sequence of DNA targets: 5′-TCTCCACTCTTCCATGTGGGG-3′; 5′-TACCATTACATTTG TCAGGGG-3′) to delete exon 20 (Fig. 1f).

Five animals were born, of which one did not exhibit any deletion, two were homozygous for the deletion and were not used for breeding, and one male and one female showed modification of one allele (Extended Data Fig. 3a). Male 1 was fertile but did not transmit the allele, whereas female 4 transmitted the allele into progeny (number of progeny, 10; 3 males and 4 females carried the mutant allele) when bred with a wild-type animal. Subsequent breeding of heterozygotes for two generations with wild-type outbred animals was performed to minimize possible off-targeting and inbreeding effects when heterozygotes were mated to produce homozygotes. The allele bearing a 761 bp deletion comprising exon 20 (KB708136.1: 11,120,580–11,121,340) was confirmed by sequencing (Extended Data Fig. 3b). RNA-seq analysis showed a loss of signal over exon 20 and a strongly reduced transcript level of the mutant transcript (Extended Data Fig. 3c).

For genotyping, ear biopsies were lysed in PCR-friendly lysis buffer with 0.6 U per sample proteinase K (Thermo Fisher Scientific) at 55 °C, with shaking at 900 r.p.m. until dissolved (approximately 2.5 h). Samples were heat-inactivated 10 min at 90 °C and lysate was used for nested PCR reaction. Genotyping primers are provided in Supplementary Table 9.

Superovulation and zygote collection. Female golden hamsters were induced to superovulate by intraperitoneal injection of 15 IU or 25 IU pregnant mare's serum gonadotropin (PMSG, ProSpec Bio) at 10:00 on the day of post-oestrous vaginal discharge (day 1 of oestrous cycle). hCG (25 IU; Sigma-Aldrich) was injected 76 h later (14:00 on day 4 of the oestrous cycle) and females were mated with fertile males at 18:00 on the same day.

Zygotes were collected 40 h after mating and four-cell embryos 61 h after mating (without previous superovulation) by flushing oviducts with M199TE medium (M199 medium with HEPES, sodium bicarbonate and Eagle's salts, Gibco), supplemented with 5% fetal bovine serum (Sigma-Aldrich) inactivated for 30 min at 56 °C, 5 mM taurine, 25 µM EDTA and pre-equilibrated with 5% CO_2, 5% O_2 and 90% N_2 at 37 °C. Zygotes were isolated in a dark room with red filters on the microscope light source and were used immediately for experimental analysis as there was no highly efficient culture system for hamster zygotes and preimplantation embryos.

Oocyte collection. Preovulatory fully grown GV oocytes were collected from ovaries by puncturing antral follicles with a syringe needle in M2 medium (Sigma-Aldrich) containing 0.2 mM 3-isobutyl-1-methyl-xanthine (Sigma-Aldrich) to prevent resumption of meiosis. In the absence of a highly efficient culture system for meiotic maturation of hamster GV oocytes in vitro, ovulated unfertilized eggs arrested at MII were collected from the oviducts of superovulated females approximately 17 h after hCG injection. MII oocytes were released from cumulus cells after incubation with 0.1% bovine testes hyaluronidase (Sigma-Aldrich) in M199TE medium at 37 °C for 1 min and washed three times in equilibrated M199TE medium kept under paraffin oil.

Western blotting. Hamster and mouse tissues were homogenized mechanically in RIPA lysis buffer supplemented with 1× protease inhibitor cocktail set (Millipore) and loaded with SDS dye. Protein concentration was measured using the Bradford assay and 60 µg of protein was used per lane. Proteins were separated on 6% polyacrylamide gel and transferred onto a polyvinylidene difluoride membrane (Millipore) using semi-dry blotting. The membrane was blocked in 5% skim milk in TTBS, MOV10L1 was detected using anti-MOV10L1 primary antibodies[4] (gift from J. Wang) diluted 1:250 and incubated overnight at 4 °C. Anti-rabbit-HRP secondary antibodies (Thermo Fisher Scientific) were diluted 1:50,000 and the signal was detected using SuperSignal West Femto Substrate (Thermo Fisher Scientific). For TUBA4A detection, samples were run on 10% polyacrylamide gel and incubated with anti-tubulin (Sigma-Aldrich, T6074) mouse primary antibodies diluted to 1:10,000 and anti-mouse-HRP secondary antibodies (Thermo Fisher Scientific) diluted to 1:50,000.

RT–PCR analyses. For oocyte and embryo expression analysis, five to ten oocytes or embryos were collected per sample in 3 µl of PBS and snap-frozen in liquid nitrogen; the number of oocytes/embryos was kept constant in individual sample sets. Next, the samples were lysed by mixing an equal volume of the 2× lysis buffer[52]. Crude lysate was used for reverse transcription with SuperScript III (Thermo Fisher Scientific). An equal fraction of total RNA per oocyte/zygote was reverse transcribed using SuperScript III RT (Thermo Fisher Scientific) with random hexamers according to the manufacturer's recommendations. To avoid genomic DNA amplification, primers were designed to span multiple exons.

cDNA was amplified by ExTaqHS (TaKaRa) using the following program: 94 °C for 2 min; 35 cycles of 94 °C for 10 s, 60 °C for 30 s and 72 °C for 30 s; and a final extension at 72 °C for 3 min. The PCR products were resolved on 1.5% agarose gels and visualized using ethidium bromide. All PCR products were sequenced after cloning into pCR4 TOPO vector (TOPO-TA cloning kit for sequencing; Thermo Fisher Scientific). A list of the primers is provided in Supplementary Table 9.

For qPCR analyses, a 1 µg aliquot of total RNA used for NGS library preparation was reverse transcribed in a 30 µl volume using LunaScript RT SuperMix Kit (New England Biolabs) according to the manufacturer's instructions. A 0.5 µl cDNA aliquot and the Maxima SYBR Green qPCR master mix (Thermo Fisher Scientific) were used for the qPCR reaction. qPCR was performed on LightCycler 480 (Roche) in technical triplicates for each biological sample. Average C_t values of the technical replicates were normalized to the housekeeping genes Ma*HPRT* and Ma*B2MG* using the $\Delta\Delta C_t$ method[53]. A list of the primers used for qPCR is provided in Supplementary Table 9.

Histology and immunofluorescence analysis of histological sections. Ovaries and testes were fixed in Hartman's fixative (Sigma-Aldrich, H0290) or 4% paraformaldehyde in PBS for 1.5 h or overnight at 4 °C. Tissues were dehydrated in ethanol, embedded in paraffin, sectioned to a thickness of 2.5–6 µm and stained with H&E or used for immunofluorescence staining.

For immunofluorescence staining of testes, sections were deparaffinized and then boiled for 18 min in 10 mM pH 6 sodium citrate solution for antigen retrieval. After 45 min blocking with 5% normal donkey serum and 5% bovine serum albumin (BSA) in PBS, sections were incubated for 1 h at room temperature or overnight at 4 °C with the following primary antibodies used at 1:200 dilutions: anti-LINE1 ORF1p (provided by D. O'Carroll, University of Edinburgh), anti-SCP3 (Abcam, ab976672), anti-ZBTB16 (Atlas antibodies, HPA001499) and anti-γH2AX (Millipore, 05-636); and at 1:400 dilutions: anti-DDX4 (Abcam, ab27591 and ab13840) and anti-WT1 (Novus Biologicals, NB110-60011). Anti-IAP GAG antibodies (gift from B. R. Cullen) were used at a 1:500 dilution. Anti-mouse or anti-rabbit secondary antibodies conjugated with Alexa 488 or Alexa 594 (1:500; Thermo Fisher Scientific) were incubated for 1 h at room temperature. Nuclei were stained with 1 µg ml^{-1} DAPI for 10 min, slides were mounted in ProLong Diamond Antifade Mountant (Thermo Fisher Scientific) and images were acquired using the DM6000 or Leica SP8 confocal microscope.

Immunofluorescence staining of oocytes and zygotes. Oocytes and zygotes were fixed and permeabilized with 0.2% Triton X-100 in 4% paraformaldehyde for 30 min at room temperature followed by blocking in 2% BSA in PBS for 1 h or kept in blocking buffer overnight. To visualize the meiotic spindle, MII oocytes were stained with mouse anti-Tubulin (Abcam, ab7750) diluted 1:100 for 1 h at room temperature. To visualize H3K9me3 histone modification, rabbit anti-H3K9me3 (Upstate, 07-442) was used at 1:1,000 dilution overnight at 4 °C. MII oocytes and zygotes were incubated with secondary antibody conjugated with Alexa 488 or Alexa 594 (Thermo Fisher Scientific) diluted at 1:500 for 1 h at room temperature. DNA was stained with 1 µg ml^{-1} DAPI for 10 min. The Leica DM6000 microscope and SP8 confocal microscope were used for data collection, LAS AF LITE 3.3 software (Leica) was used for image processing, and Imaris v.9.6 (Bitplane) was used to determine the length and volume of the spindle and metaphase plate by three-dimensional reconstruction.

RNA sequencing: sequencing library preparation. For oocyte transcriptome analysis, total RNA was extracted from 6–12 fully-grown oocytes using the Arcturus Picopure RNA isolation kit (Thermo Fisher Scientific) according to the manufacturer's protocol. RNA-seq libraries were generated using the Ovation RNA-Seq system V2 (NuGEN) followed by the Ovation Ultralow Library system (DR Multiplex System, NuGEN) according to the manufacturer's protocol. cDNA fragmentation was performed on the Bioruptor sonication device (Diagenode) with 18 cycles of 30 s on and 30 s off at low intensity. Libraries were amplified by 9 cycles of PCR and sequenced by 100-nucleotide single-end reading using the Illumina NovaSeq6000 platform.

For small-RNA-seq analysis of oocytes, at least five oocytes were collected from each animal and were incubated at 75 °C for 3 min to release small RNAs. Small-RNA libraries were prepared using the NextFlex Small-RNA-seq v3 kit (Amplicon) according to the manufacturer's protocol; 3′ adapter ligation was performed overnight at 16 °C, 25 cycles were used for PCR amplification and gel purification was performed for size selection. For gel purification, libraries were

separated on a 2.5% agarose gel using 1× lithium borate buffer and visualized with ethidium bromide. The 140–170 bp fraction was cut off the gel and DNA was isolated using the MinElute Gel Extraction Kit (Qiagen). Final libraries were sequenced by 75-nucleotide single-end reading using the Illumina NextSeq500/550 platform.

For analysis of testicular transcriptomes, total RNA was extracted from adult, 21 d.p.p., 13 d.p.p., 9 d.p.p. and new-born (0 d.p.p.) hamster testes using the Sigma-Aldrich mirPremier microRNA isolation kit according to the manufacturer's protocol. Ribosomal RNA (rRNA) was depleted from RNA used for transcriptome analysis using the Ribo-Zero rRNA Removal Kit (Human/Mouse/Rat) (Epicentre) or the QIAseq FastSelect–rRNA HMR Kit (Qiagen) according to the manufacturer's protocols. rRNA depletion was confirmed using the 2100 Bioanalyzer (Agilent Technologies). RNA-seq libraries were generated using the NEBNext Ultra II directional RNA library Prep kit for Illumina (BioLabs, E7765S) according to the manufacturer's protocol. RNA-seq libraries from adult, 21 d.p.p. and 13 d.p.p. testes were sequenced by 150-nucleotide paired-end reading and RNA-seq libraries from 9 d.p.p. and new-born hamster testes were sequenced by 75-nucleotide single-end reading using the Illumina NextSeq500/550 platform.

For small-RNA-seq analysis of testes, total RNA isolated as described above was used with the NextFlex Small-RNA-seq v3 kit (Amplicon). Libraries were prepared according to the manufacturer's protocol with 3′ adapter ligation overnight at 16 °C, 15 cycles of PCR amplification and NextFlex beads or gel purification (described above) was used for size selection. RNA-seq libraries were sequenced by 75-nucleotide single-end reading using the Illumina NextSeq500/550 platform or 100-nucleotide single-end reading using NovaSeq6000 platform. A list of the analysed sequencing libraries is provided in Supplementary Table 10. Raw data were deposited at the Gene Expression Omnibus (GEO: GSE164658).

Bisulfite sequencing: library preparation. For bisulfite sequencing, ten fully grown GV oocytes (an equivalent of 40 haploid genomes and 80 single-stranded DNAs after bisulfite conversion) were directly subjected to EZ DNA Methylation-Direct kit (Zymo Research) for bisulfite conversion with the following modifications: samples were digested with proteinase K at 50 °C for 35 min and bisulfite conversion was performed as follows: 98 °C for 6 min, 64 °C for 30 min, 95 °C for 1 min, 64 °C for 90 min, 95 °C for 1 min and 64 °C for 90 min. DNA libraries were prepared using the EpiNext Post-Bisulfite DNA library Preparation kit according to the manufacturer's protocol, with 22 PCR cycles used for amplification. The final DNA libraries were sequenced by 250-nucleotide paired-end sequencing on the Illumina NovaSeq6000 platform.

Bioinformatics analyses. *RNA-seq and differential gene expression analysis.* Raw RNA-seq reads were mapped to mouse (mm10), human (hg38), cow (bosTau9), rat (rn6), golden hamster (mesAur1) and the newest golden hamster (PRJDB10770)[11] genomes using STAR v.2.7.3a[64] with following parameters:

```
STAR --readFilesIn $ {FILE}.fastq.gz --genomeDir
$ {GENOME_INDEX} --runThreadN 12 --genomeLoad
LoadAndRemove --limitBAMsortRAM 20000000000
--readFilesCommand unpigz -c --outFileNamePrefix
$ {FILENAME} --outSAMtype BAM SortedByCoordinate
--outReadsUnmapped Fastx --outFilterMultimapNmax
5000 --winAnchorMultimapNmax 5000
--seedSearchStartLmax 30 --alignTranscriptsPerReadNmax
30000 --alignWindowsPerReadNmax 30000
--alignTranscriptsPerWindowNmax 300 --seedPerReadNmax
3000 --seedPerWindowNmax 300 --seedNoneLociPerWindow
1000 --outFilterMultimapScoreRange 0
--outFilterMismatchNoverLmax 0.05 --sjdbScore 2
```

Those parameters were chosen to optimize mapping for quantification of transposable elements[65].

For analysis of expression of protein coding genes, reads were mapped with maximum of 20 multimapping alignments allowed. Reads mapped to mesAur1 were counted over exon features annotated by Ensembl (release 99) using featureCounts v.2.0.0 (ref. [66]):

```
featureCounts -a $ {FILE}.gtf -o $ {FILE}.counts.txt $
{FILE}.bam -T 12 -F GTF -M -O --fraction
```

For the paired-end libraries -p flag was added. For the stranded libraries, -s 2 flag was added. Statistical significance and fold changes in gene expression were computed in R (https://www.R-project.org/) using DESeq2 package[67]. Genes were considered to be significantly upregulated or downregulated if their corresponding adjusted *P* values were smaller than 0.01. Principal component analysis was computed on counts data that were transformed using the regularized logarithm (rlog) function.

For the heat map showing the expression of piRNA factors in testes and oocytes of four mammalian species (Fig. 1a), the following publicly available datasets were used: bovine oocyte GSE52415 (ref. [68]), bovine testis PRJNA471564 (ref. [69]), human oocyte GSE72379 (ref. [46]), human testis GSE74896 (ref. [45]), mouse oocyte GSE116771 (ref. [62]), mouse testis GSE49417 (ref. [63]), rat oocyte GSE137563 (ref. [64]) and rat testis GSE53960 (ref. [65]). Read mapping coverage was visualized in the UCSC Genome Browser by constructing bigWig tracks using the UCSC tools[66].

Small-RNA-seq analysis of testes. Small-RNA-seq reads were trimmed in two rounds using bbduk.sh v.38.87 (https://jgi.doe.gov/data-and-tools/bbtools/). First, the NEXTflex adapter was trimmed from the right end:

```
bbduk.sh -Xmx20G threads=6 in=$ {FILE}.fastq.gz out=$
{FILE}.atrim.fastq.gz literal= TGGAATTCTCGGGTGCCAAGG
stats=$ {FILE}.atrim.stats overwrite=t ktrim=r k=21
rcomp=f mink=10 hdist=1 minoverlap=8
```

Next, four random bases from both sides of the reads were trimmed:

```
bbduk.sh -Xmx20G threads=6 in=$ {FILE}.atrim.fastq.
gz out=$ {FILE}.trimmed.fastq.gz stats=$ {FILE}.ftrim.
stats overwrite=t forcetrimright2=4 forcetrimleft=4
minlength=18
```

Trimmed reads were mapped to the genomes using the following parameters:

```
STAR --readFilesIn $ {FILE}.fastq.gz
--genomeDir $ {GENOME_INDEX} --runThreadN 12
--genomeLoad LoadAndRemove --limitBAMsortRAM
20000000000 --readFilesCommand unpigz -c
--outFileNamePrefix $ {FILENAME} --outSAMtype
BAM SortedByCoordinate --outReadsUnmapped Fastx
--outFilterMismatchNmax 1 --outFilterMismatchNoverLmax
1 --outFilterMismatchNoverReadLmax 1
--outFilterMatchNmin 16 --outFilterMatchNminOverLread 0
--outFilterScoreMinOverLread 0 --outFilterMultimapNmax
5000 --winAnchorMultimapNmax 5000
--seedSearchStartLmax 30 --alignTranscriptsPerReadNmax
30000 --alignWindowsPerReadNmax 30000
--alignTranscriptsPerWindowNmax 300 --seedPerReadNmax
3000 --seedPerWindowNmax 300 --seedNoneLociPerWindow
1000 --outFilterMultimapScoreRange 0 --alignIntronMax 1
--alignSJDBoverhangMin 999999999999
```

Small-RNA-seq analysis of oocytes. Small-RNA-seq reads were trimmed using bbduk.sh v.38.87:

```
bbduk.sh -Xmx20G threads=6 in=$ {FILE}.fastq.gz out=$
{FILE}.atrim.fastq.gz literal= TGGAATTCTCGGGTGCCAAGG
stats=$ {FILE}.atrim.stats overwrite=t ktrim=r k=21
rcomp=f mink=10 hdist=1 minoverlap=8
```

Libraries were then deduplicated from PCR duplicates. First, using custom scripts (available at https://github.com/fhorval) both UMI sequences from the read (four random nucleotides from each end of the trimmed read) were added to the read header. UMI sequences were then removed from read sequence using Cutadapt v.2.10 (ref. [67]):

```
cutadapt -u 4 -o ${FILE}.trim_1.fastq -j 6 ${FILE}.umi.
fastq
cutadapt -m 18 -u -4 -o ${FILE}.trim_2.fastq -j 6
${FILE}.trim_1.fastq
Trimmed reads were then mapped to the new golden
hamster genome using STAR 2.7.3a:
STAR --readFilesIn $ {FILE}.dedup.fastq.
gz --genomeDir $ {GENOME_INDEX} --runThreadN 12
--genomeLoad LoadAndRemove --limitBAMsortRAM
20000000000 --readFilesCommand unpigz -c
--outFileNamePrefix $ {FILENAME} --outSAMtype
BAM SortedByCoordinate --outReadsUnmapped Fastx
--outFilterMismatchNmax 1 --outFilterMismatchNoverLmax
1 --outFilterMismatchNoverReadLmax 1
--outFilterMatchNmin 16 --outFilterMatchNminOverLread 0
--outFilterScoreMinOverLread 0 --outFilterMultimapNmax
5000 --winAnchorMultimapNmax 5000
--seedSearchStartLmax 30 --alignTranscriptsPerReadNmax
30000 --alignWindowsPerReadNmax 30000
--alignTranscriptsPerWindowNmax 300 --seedPerReadNmax
3000 --seedPerWindowNmax 300 --seedNoneLociPerWindow
1000 --outFilterMultimapScoreRange 0 --alignIntronMax 1
--alignSJDBoverhangMin 999999999999
```

Next, UMI tools v.1.1.1 (ref. [48]) was used on mapped .bam files to deduplicate them:

```
umi_tools dedup --method=directional
--multimapping-detection-method=NH -I ${FILE}.trim_1.
fastq --output-stats=${FILE}.dedup_stats --log=${FILE}.
dedup_log.txt -S ${FILE}.dedup.bam.
```

Final .fastq files were generated from deduplicated mapped reads .bam files using samtools v.1.10 (ref. [49]):

```
samtools fastq -@ 12 ${FILE}.dedup.bam > ${FILE}.dedup.
fastq
```

Those deduplicated reads were then mapped to the genomes using same STAR 2.7.3a with same parameters as above.

Definition of hamster piRNA clusters in testes and their analysis. Small-RNA-seq analysis of whole testes was used to distinguish pre-pachytene pre-meiotic piRNAs and meiotic pachytene piRNAs as 9 d.p.p. and 13 d.p.p. testes contain only pre-meiotic spermatogonia, whereas spermatogenesis in pubertal hamsters reaches the pachytene stage at 21 d.p.p. (ref. [28]). piRNA clusters in testes were defined using custom R scripts as follows:

1. The genome was divided into 1 kb windows and, for each window, alignments of 24–31-nucleotide reads were counted with fractional counts. Counts were normalized to the total number of 19–32-nucleotide reads in millions into RPM. RPMs were then normalized to the length of windows without counting gaps in assembly (N nucleotides) into RPKM values. Windows with RPKM < 1 were removed.
2. For pre-pachytene clusters, neighbouring tiles were merged into clusters if their $\log_2$-transformed fold changes of knockout/wild-type RPKMs at 9 d.p.p. and 13 d.p.p. were lower than −2. For pachytene clusters, neighbouring tiles were merged into clusters if their $\log_2$-transformed fold changes of knockout/wild-type RPKMs at 21 d.p.p. were lower than −2 and $\log_2$-transformed fold changes of knockout/wild-type RPKMs at 13 d.p.p. were higher than −2.
3. Next, clusters were merged into superclusters if they were at most 2 kb apart.
4. Clusters were manually curated and the final RPKM values were recalculated.

For further analysis, we selected loci with a piRNA density of greater than 10 RPM per kilobase for 9 d.p.p. and 13 d.p.p. pre-pachytene piRNAs and 100 RPM for 21 d.p.p. pachytene piRNAs (Extended Data Fig. 1a).

Definition of hamster piRNA clusters in oocytes and their analysis. For defining oocytic piRNA clusters, we took advantage of existing analysis of PIWIL1- and PIWIL3-associated small RNAs in the oocyte identified by Ishino et al.[11]. In brief, the genome was divided into 1 kb windows and, for each window, alignments of PIWIL1- and PIWIL3-associated reads were counted with fractional counts. Counts were normalized to the total number of reads in millions into RPM. Next, RPMs were normalized to the length of windows without counting gaps in assembly (N nucleotides) into RPKM values. Windows with RPKM < 1 were removed. Finally, clusters were merged into superclusters if they were at most 2 kb apart and expression of small-RNA-seq reads in oocyte samples was calculated using fractional counts.

Only clusters with a minimum of 10 RPMs in PIWIL1 or PIWIL3 IP samples and a minimum of 10 RPMs average for combined 18–20 and 24–32 reads (excluding the 21–23-nucleotide miRNA/siRNA-rich population) in WT oocyte samples were used for subsequent analysis.

Gene Ontology annotation analysis. Gene Ontology annotation analysis was performed using the clusterProfiler[70] R package.

piRNA sequence logos. The sequence logos (Extended Data Fig. 1e) were calculated from the primary alignments only. First, only the reads with aligned first nucleotide were selected (all reads with a clipped 5′ end were removed). Reads mapped within the piRNA clusters were then selected. The 25–31-nucleotide-long reads were used for drawing the sequence logo[71].

Annotation of transposable elements. Transposable elements in new golden hamster assembly were annotated using RepeatMasker (v.4.0.9)[72] using the mouse repeats database as the closest available annotated organism. In summarizing the expression of transposable element groups, each read was counted only once using a custom R script.

Bisulfite sequencing. Raw bisulfite sequencing reads were trimmed using the following parameters:

```
bbduk.sh -Xmx20G threads=12 in1=${FILE}_1.txt.gz
in2=${FILE}_2.txt.gz out1=${BASE}_1.trim.txt.gz
out2=${BASE}_2.trim.txt.gz outs=${BASE}_s.trim.txt.gz
stats=${BASE}.stats literal=AGATCGGAAGAGC overwrite=t
ktrim=r k=12 rcomp=t mink=8 hdist=1 minoverlap=8
minlength=25 minlength=50 tbo
```

Trimmed reads were mapped to the genome using Bismark[73]:

```
bismark --non_directional --parallel 4 --unmapped
--output_dir. --temp_dir.--genome_folder ${BISMARK_
INDEX} -1 ${FILE}_1.trim.txt.gz -2 ${FILE}_2.trim.
txt.gz ${FILE}_s.trim.txt.gz
```

Next, to remove alignments arising from excessive PCR amplification, alignments were deduplicated using the deduplicate_bismark script. Methylation information for individual cytosines was then extracted using bismark_methylation_extractor. For analysis of full-length intact consensus sequences, reads were first mapped to the genome. Next, reads mapping to individual full-length intact insertions were extracted and mapped again to full-length intact consensus sequences.

Statistics and reproducibility. All statistical analyses were performed in R software environment (https://www.R-project.org/). For transcriptome analyses, the DESeq2 package was used, which internally uses two-sided Wald test and corrects *P* values for multiple comparisons using the Benjamini–Hochberg method. DESeq2 $P < 0.01$ was considered to be significant. The χ^2 test from base R was used for analysis of the Mendelian distribution of genotypes after crossing heterozygotes and for comparison of germ cell numbers in seminiferous tubules. $P < 0.05$ was considered to be significant in all tests. For the box plots of the nucleotide exchange rate analyses, the median (box centre) and first and third quartiles (bounds of box) are shown, and the whiskers extend from the bounds to the values no lower (minimum) or higher (maximum) than 1.5× interquartile range. RT–qPCR analysis of expression changes used the $\Delta\Delta C_t$ method in the REST tool[52]. The error bars delineate the 95% confidence interval estimated by REST.

In general, experiments were performed with at least duplicate independent biological samples. The number of replicates was influenced by the limited availability of the biological material stemming from time-consuming and laborious hamster breeding. The sample sizes and numbers of replicates are provided in the figure captions and, for RNA-seq analyses, in Supplementary Table 10.

No statistical method was used to predetermine the sample sizes. Two RNA-seq libraries from hamster oocytes, which were outliers in PCA and had poor quality/low complexity (clearly because of a limited amount of starting material), were excluded from analysis. Furthermore, matings where fertilization did not occur (evidenced by the absence of pronucleus formation and a lack of the presence of paternal DNA in unfertilized eggs) were excluded from the preimplantation development analysis.

The experiments were not strictly randomized as they depended on a limited amount of available biological material. However, this also precluded any deliberate selection of samples. The investigators were not blinded to allocation during the experiments and outcome assessment because of integrated animal breeding, genotyping and phenotype analysis. All replications were successful.

Reporting Summary. Further information on research design is available in the Nature Research Reporting Summary linked to this article.

Data availability

All data are available in the main text or the Supplementary Information. High-throughput sequencing data have been deposited in the Gene Expression Omnibus (GEO) under the accession code GSE164658. Previously published data that were reanalysed here are available under accession codes GSE5241556, PRJNA471564, GSE7237958, GSE7489659, GSE11677160, GSE4941761, GSE13756362 and GSE5396063. All other data supporting the findings of this study are available from the corresponding authors on reasonable request. Inquiries concerning the hamster piRNA pathway analysis should be directed to P.S. (svobodap@img.cas.cz), inquiries concerning hamster animal model and its genome manipulation (iGONAD) should be directed to A.O. (ogura@rtc.riken.go.jp). Source data are provided with this paper.

Code availability

The code used for sequence data analysis is available at GitHub (https://github.com/fhorvat/bioinfo_repo/tree/master/papers/piRNA_2021).

References

51. Gurumurthy, C. B. et al. Creation of CRISPR-based germline-genome-engineered mice without ex vivo handling of zygotes by i-GONAD. *Nat. Protoc.* **14**, 2452–2482 (2019).
52. Shatzkes, K., Teferedegne, B. & Murata, H. A simple, inexpensive method for preparing cell lysates suitable for downstream reverse transcription quantitative PCR. *Sci. Rep.* **4**, 4659 (2014).

53. Pfaffl, M. W., Horgan, G. W. & Dempfle, L. Relative expression software tool (REST) for group-wise comparison and statistical analysis of relative expression results in real-time PCR. *Nucleic Acids Res.* **30**, e36 (2002).
54. Dobin, A. et al. STAR: ultrafast universal RNA-seq aligner. *Bioinformatics* **29**, 15–21 (2013).
55. Teissandier, A., Servant, N., Barillot, E. & Bourc'his, D. Tools and best practices for retrotransposon analysis using high-throughput sequencing data. *Mob. DNA* **10**, 52 (2019).
56. Liao, Y., Smyth, G. K. & Shi, W. featureCounts: an efficient general purpose program for assigning sequence reads to genomic features. *Bioinformatics* **30**, 923–930 (2014).
57. Love, M. I., Huber, W. & Anders, S. Moderated estimation of fold change and dispersion for RNA-seq data with DESeq2. *Genome Biol.* **15**, 550 (2014).
58. Graf, A. et al. Fine mapping of genome activation in bovine embryos by RNA sequencing. *Proc. Natl Acad. Sci. USA* **111**, 4139–4144 (2014).
59. Gao, Y. et al. Analysis of long non-coding RNA and mRNA expression profiling in immature and mature bovine (*Bos taurus*) testes. *Front. Genet* **10**, 646 (2019).
60. Hendrickson, P. G. et al. Conserved roles of mouse DUX and human DUX4 in activating cleavage-stage genes and MERVL/HERVL retrotransposons. *Nat. Genet.* **49**, 925–934 (2017).
61. Jegou, B., Sankararaman, S., Rolland, A. D., Reich, D. & Chalmel, F. Meiotic genes are enriched in regions of reduced archaic ancestry. *Mol. Biol. Evol.* **34**, 1974–1980 (2017).
62. Horvat, F. et al. Role of Cnot6l in maternal mRNA turnover. *Life Sci. Alliance* **1**, e201800084 (2018).
63. Yue, F. et al. A comparative encyclopedia of DNA elements in the mouse genome. *Nature* **515**, 355–364 (2014).
64. Ganesh, S. et al. The most abundant maternal lncRNA Strena1 acts post-transcriptionally and impacts mitochondrial distribution. *Nucleic Acids Res.* **48**, 3211–3227 (2020).
65. Yu, Y. et al. Comprehensive RNA-seq transcriptomic profiling across 11 organs, 4 ages, and 2 sexes of Fischer 344 rats. *Sci. Data* **1**, 140013 (2014).
66. Kent, W. J., Zweig, A. S., Barber, G., Hinrichs, A. S. & Karolchik, D. BigWig and BigBed: enabling browsing of large distributed datasets. *Bioinformatics* **26**, 2204–2207 (2010).
67. Martin, M. Cutadapt removes adapter sequences from high-throughput sequencing reads. *EMBnet J.* **17**, 10–12 (2011).
68. Smith, T., Heger, A. & Sudbery, I. UMI-tools: modeling sequencing errors in unique molecular identifiers to improve quantification accuracy. *Genome Res.* **27**, 491–499 (2017).
69. Li, H. et al. The Sequence Alignment/Map format and SAMtools. *Bioinformatics* **25**, 2078–2079 (2009).
70. Yu, G., Wang, L. G., Han, Y. & He, Q. Y. clusterProfiler: an R package for comparing biological themes among gene clusters. *OMICS* **16**, 284–287 (2012).
71. Wagih, O. ggseqlogo: a versatile R package for drawing sequence logos. *Bioinformatics* **33**, 3645–3647 (2017).
72. Smit, A. F. A., Hubley, R. & Green, P. RepeatMasker Open-4.0 (RepeatMasker, 2013–2015).
73. Krueger, F. & Andrews, S. R. Bismark: a flexible aligner and methylation caller for bisulfite-seq applications. *Bioinformatics* **27**, 1571–1572 (2011).

Acknowledgements

We thank H. Siomi for access to the refined golden hamster genome assembly; D. O'Carroll and C. Rodriquez for comments on the manuscript; R. Šustrová for taking care of hamsters; J. Valečka (Service Laboratory of Light Microscopy, IMG) for help with the Imaris system; and Š. Kocourková (Laboratory of Genomics and Bioinformatics, IMG) for assisting with RNA-seq. This work was funded by the European Research Council under the European Union's Horizon 2020 research and innovation programme (grant 647403 D-FENS awarded to P.S.). Additional support was provided to A.O. by KAKENHI grants JP19H03151 and JP19H05758. Financial support to Z.L. and F.H. was in part provided by Charles University in Prague in the form of a PhD student fellowship; this work will be in part used to fulfil the requirements for their PhD degrees. IMG institutional support included RVO: 68378050-KAV-NPUI and support from the Ministry of Education, Youth and Sports for the animal facility (Czech Centre for Phenogenomics) by LM2018126, and Light Microscopy Core Facility (Czech-Bioimaging) by LM2018129. Computational resources were supported by European Structural and Investment Funds grant (KK.01.1.1.01.0010), the Croatian National Centre of Research Excellence for Data Science and Advanced Cooperative Systems (KK.01.1.1.01.0009) and the project 'e-Infrastruktura CZ' (e-INFRA LM2018140).

Author contributions

Z.L., H.F., A.O. and P.S. designed the experiments. H.F., M.H. and A.O. generated mutant hamsters. Z.L. and H.F. analysed the phenotype. Z.L. conducted RNA-seq and bisulfite-seq experiments. F.H. and J.P. performed bioinformatics analyses. Z.L., H.F., F.H., J.P., R.M. and P.S. analysed phenotype data. P.S. led the project and drafted the first version of the manuscript, which all of the authors revised.

Competing interests

The authors declare no competing interests.

Additional information

Extended data is available for this paper at https://doi.org/10.1038/s41556-021-00746-2.

Supplementary information The online version contains supplementary material available at https://doi.org/10.1038/s41556-021-00746-2.

Correspondence and requests for materials should be addressed to Atsuo Ogura or Petr Svoboda.

Peer review information *Nature Cell Biology* thanks René Ketting, Jeremy Wang and the other, anonymous, reviewer(s) for their contribution to the peer review of this work. Peer reviewer reports are available.

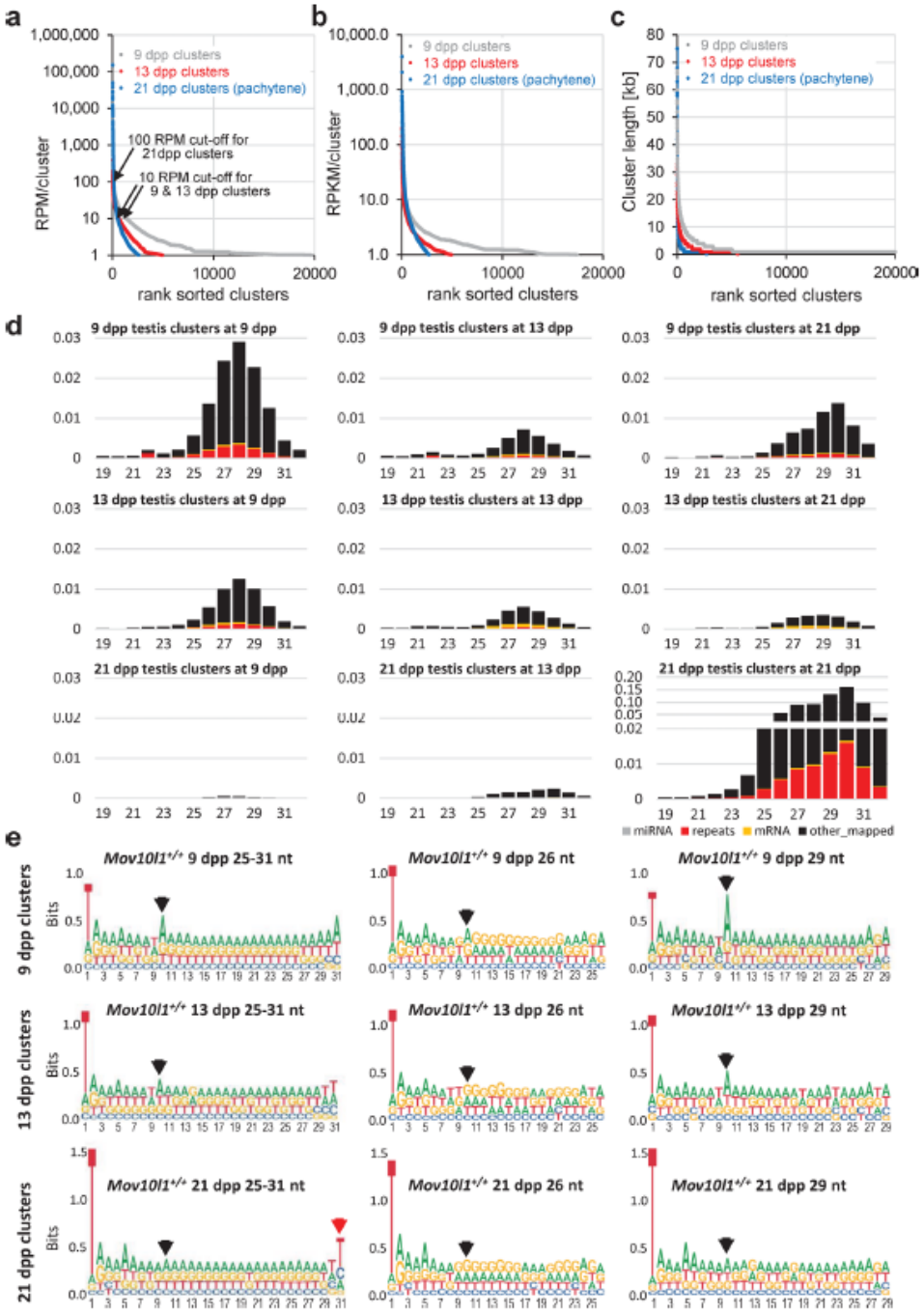

Extended Data Fig. 1 | See next page for caption.

Extended Data Fig. 1 | Analysis of golden hamster's testicular piRNA clusters. Analysis of golden hamster's testicular piRNA clusters. (a) Rank-sorted annotated pre-pachytene and pachytene clusters according to the amount of small RNAs per cluster (RPM). (b) Distribution of piRNA clusters according to average piRNA density (cluster per RPKM). (c) Distribution of piRNA cluster sizes. (d) Graphs depict frequencies of 19-32 nucleotides-long RNAs mapping to annotated pre-pachytene (9 d.p.p., 13 d.p.p.) and pachytene (21 d.p.p.) clusters (Supplementary Tables 1-3) at the three studied time points. Coloring of bars indicates proportions of miRNAs and small RNAs derived from repetitive sequences, mRNA, and other sequences. (e) Sequence logos for piRNA clusters from 9, 13, and 21 d.p.p. testes (Supplementary Tables 1-3). U at position 1 is a common piRNA feature[2], preference of A at the position 10 (black arrow) in the sequence logos of 29 nt long piRNA clusters from 9 and 13 d.p.p. testes is a "ping-pong" signature of secondary piRNAs[2]. 29 nt long piRNAs from 21 d.p.p. and shorter piRNA clusters from all three time points show little if any signs of the "ping-pong" signature. The red arrow points to apparent U-tailing of pachytene piRNAs. Three biological replicates of wild type 9 d.p.p. testes and two biological replicates of wild type 13 d.p.p. and 21 d.p.p. testes were used for small RNA analysis presented in this figure.

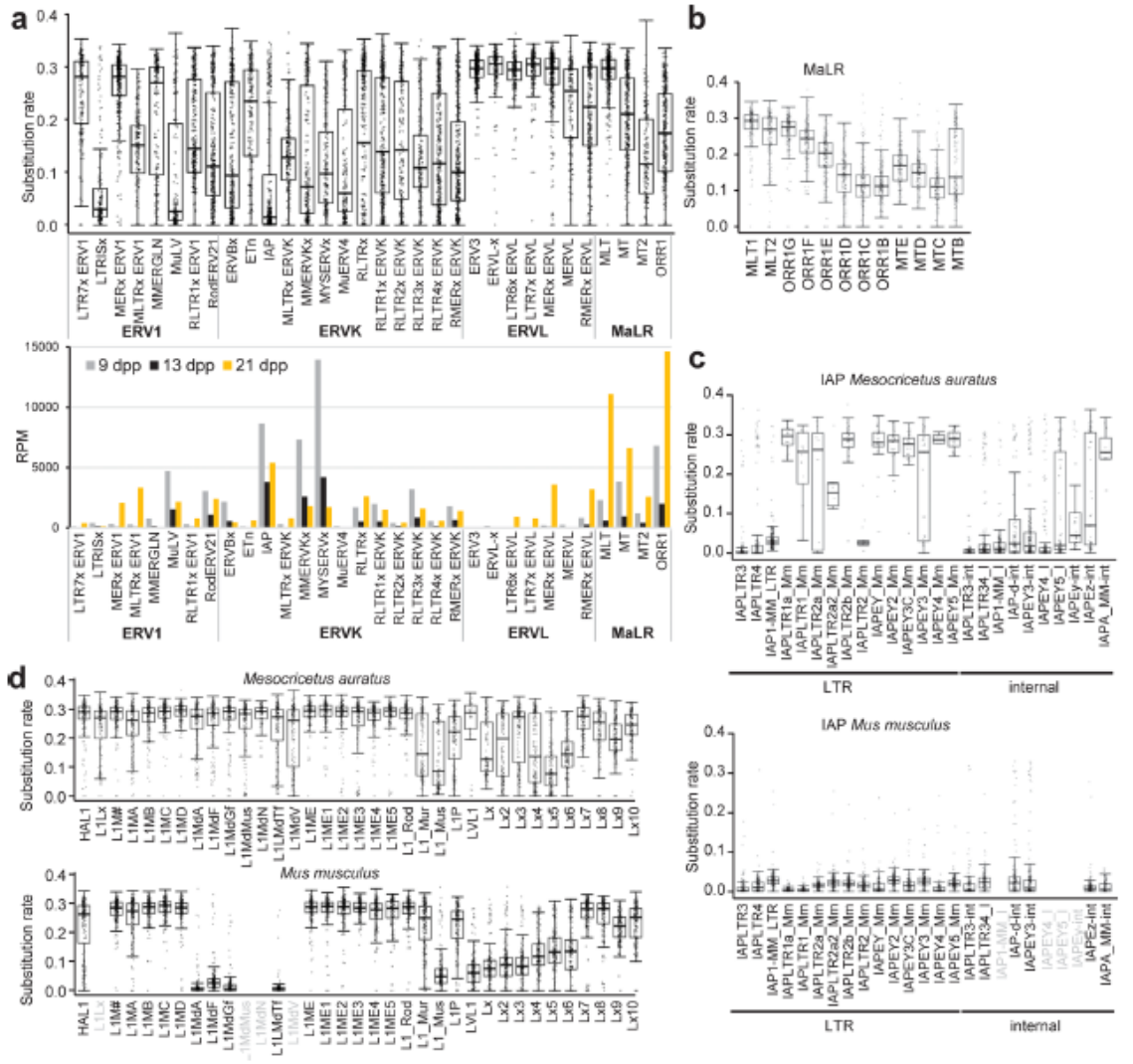

Extended Data Fig. 2 | Nucleotide substitution rates of retrotransposons sequences. Nucleotide substitution rates of retrotransposons sequences. (a) Boxplots show nucleotide substitution rates in selected LTR subgroups and abundance of 24-31 nt RNAs carrying depicted retrotransposon sequences. The lower graph depicts RPMs for 24-31 nt small RNAs per million of 19-32 nt reads from wild type 9 d.p.p., 13 d.p.p. and 21 d.p.p. whole testes small RNA sequencing. Sequencing was performed in three biological replicates from 9 d.p.p. and two biological replicates from 13 d.p.p. and 21 d.p.p. testes. (b) Nucleotide substitution rates in MaLR elements. (c, d) Nucleotide substitution rates in IAP and L1 subfamilies in golden hamster and mouse. Young IAP and L1 subfamilies, which supply most FLI elements show minimal nucleotide substitution rates. All boxplots were constructed from 200 randomly selected insertion sequences (or all insertions if there was less than 200 of them). The internal line in the boxplot represents median and bounds of box the 1st and the 3rd quartile; whiskers extends to values no lower (minima) or higher (maxima) than 1.5 * IQR (interquartile range).

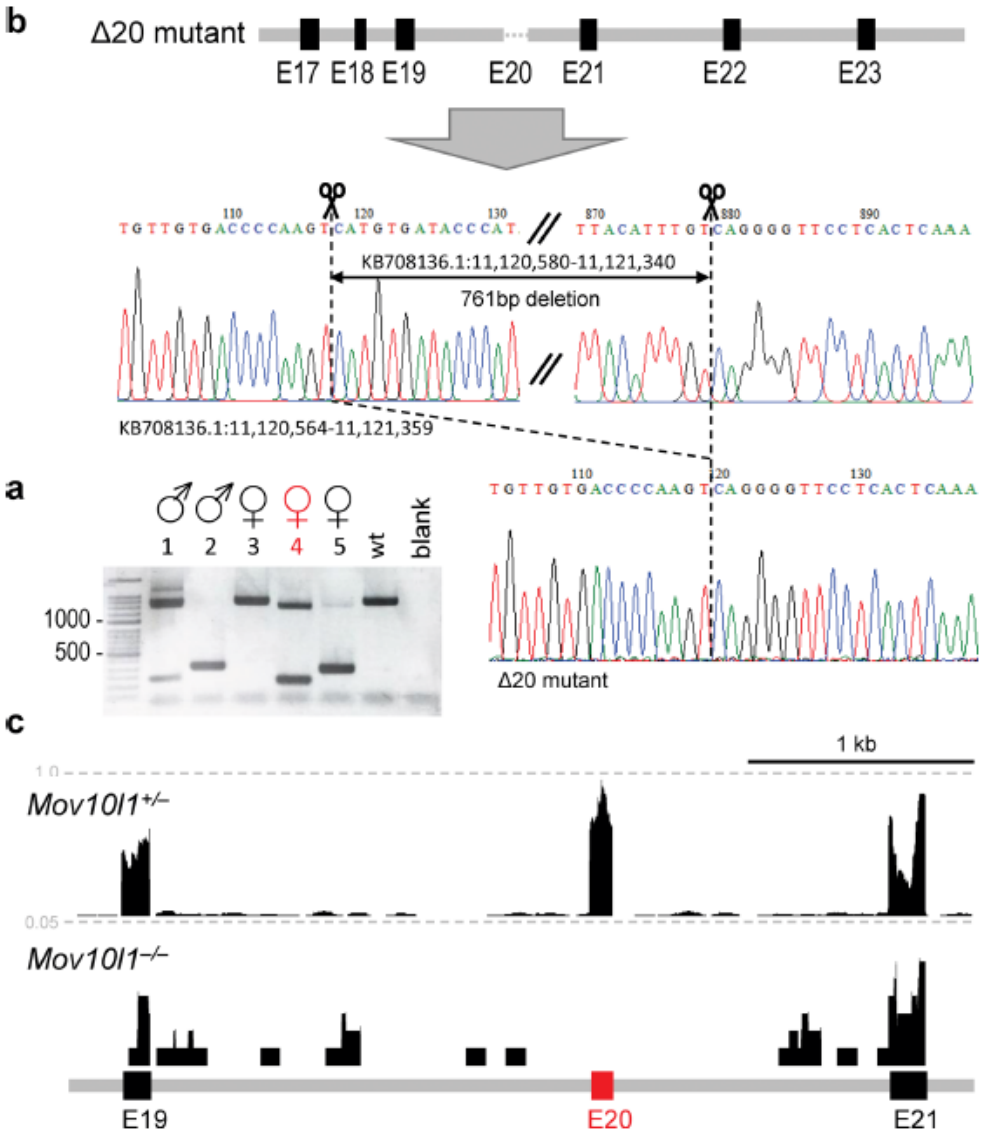

Extended Data Fig. 3 | Mov10l1$^{-/-}$ hamster model production. *Mov10l1*$^{-/-}$ hamster model production. (a) PCR genotyping of five F0 animals. The upper band >1 kb corresponds to the wild-type allele. 4/5 animals carried at least one mutated allele. Female #4 was heterozygous and transmitted the mutated allele into F1. (b) Schematic position of CRISPR-Cas9 cleavage sites and validation of the deletion induced in female #4 by Sanger sequencing. (c) A UCSC browser snapshot showing absence of *Mov10l1* sequences mapping to the removed exon 20 in RNA-sequencing data from 9 d.p.p. testes. Dashed lines depict counts per million (CPM) of normalized (per library size) expression data. Two biological replicates of 9 d.p.p. testes with each genotype were analyzed by RNA-seq, displayed tracks were constructed from merged RNA-seq data from each genotype.

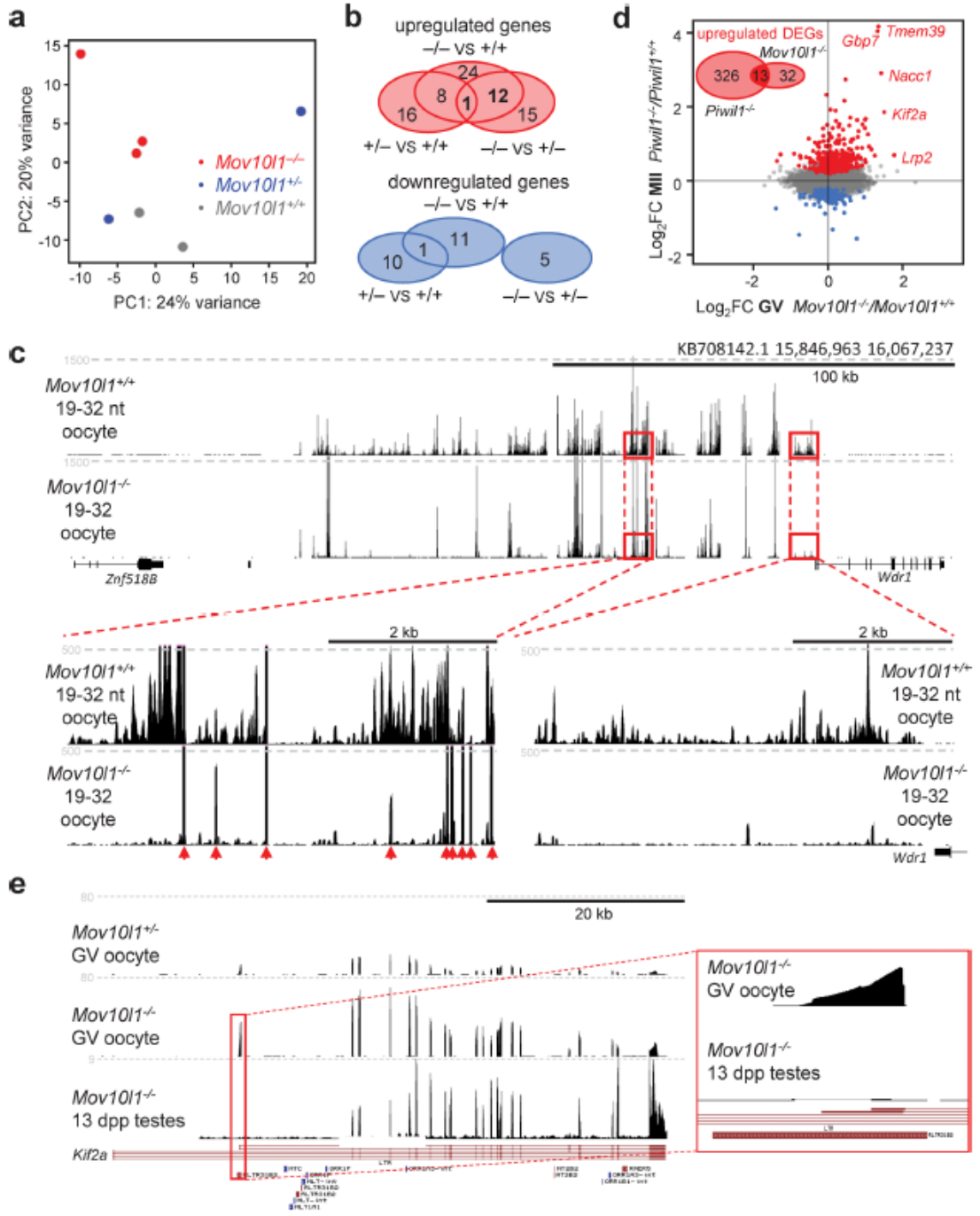

Extended Data Fig. 4 | See next page for caption.

Extended Data Fig. 4 | Transcriptome changes in Mov10l1$^{-/-}$ oocytes. Transcriptome changes in *Mov10l1*$^{-/-}$ oocytes. (a) Principal Component Analysis (PCA) depicting distribution of individual RNA sequencing libraries (produced as biological replicates) used for transcriptome analysis. (b) Venn diagrams show overlaps among transcripts with increased or decreased relative abundance when comparing different *Mov10l1* genotypes. (c) Snapshots from the UCSC genome browser depicting a female-specific piRNA cluster localized between *Wdr1* and *Znf518Bb* described previously[11]. While the majority of piRNAs along the cluster become strongly reduced in *Mov10l1*$^{-/-}$ oocytes, some specific piRNAs (red arrows) remain present. This contrasts with piRNA changes in male piRNA clusters at 9 d.p.p. (compare with Fig. 6c and Extended Data Fig. 7c). The *Mov10l1*$^{+/+}$ track is a "merged" track from two independent RNA-seq libraries, *Mov10l1*$^{-/-}$ track is derived from a single RNA-seq library. (d) Comparison of relative changes in *Mov10l1*$^{-/-}$ fully-grown oocytes and ovulated *Piwil1*$^{-/-}$ MII oocytes[34]. *Piwil1* analysis was done in triplicates, *Mov10l1* libraries are the same as in the panel a). Colored are genes differentially expressed in *Piwil1*$^{-/-}$ MII oocytes (DESeq2 p-value <0.01). Clustering of red points (significantly upregulated genes) in the upper right quadrant implies a common pool of upregulated genes. The Venn diagram shows overlap of upregulated DEGs (a single gene was common for downregulated DEGs). (e) A UCSC genome browser snapshot of RNA-seq data and genomic structure of *Kif2a* locus with an RLTR31B2 LTR-derived oocyte-specific promoter. The *Mov10l1*$^{-/-}$ track is a merged track from three independent RNA-seq libraries, the remaining two tracks were constructed from two independent RNA-seq libraries.

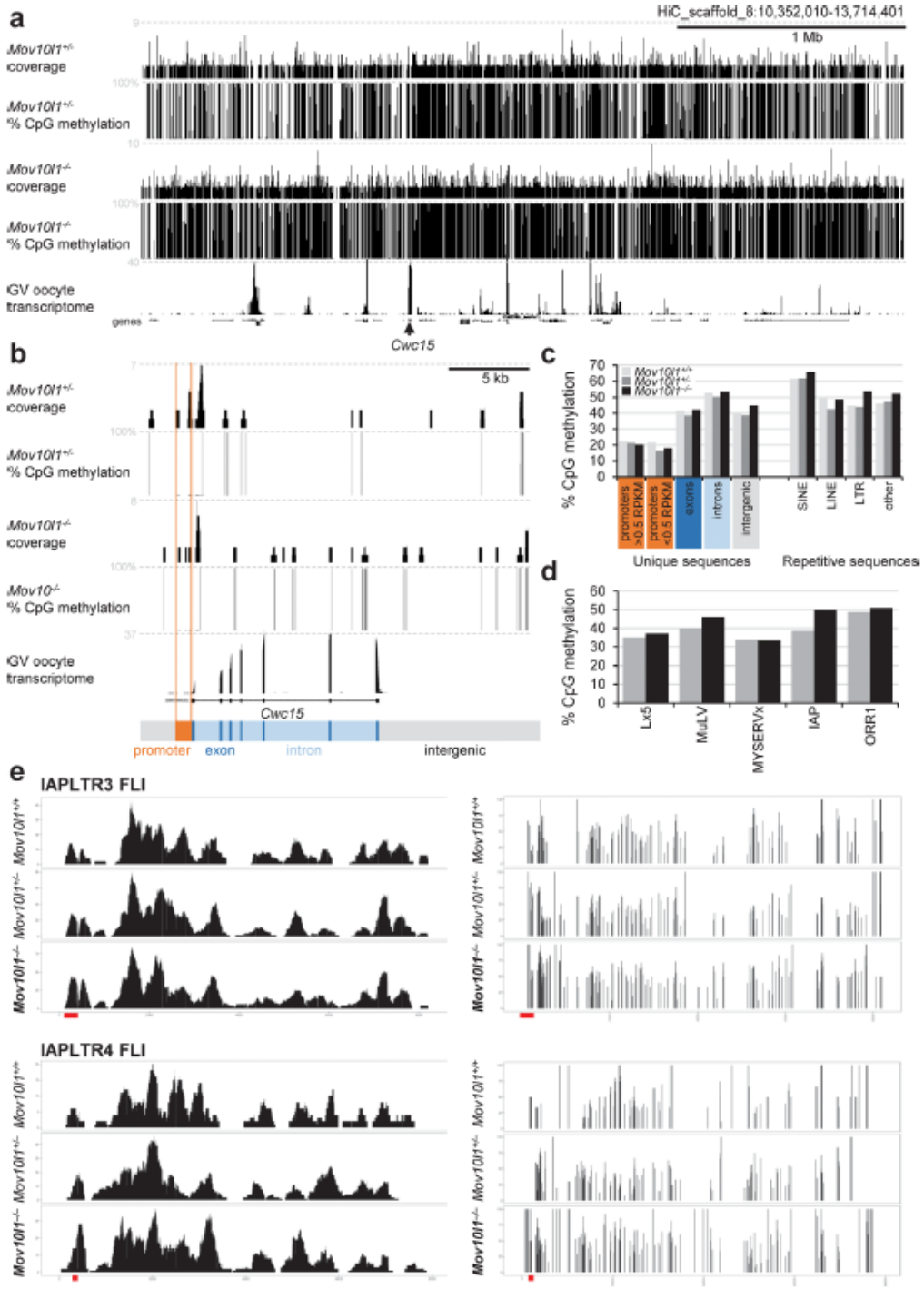

Extended Data Fig. 5 | See next page for caption.

Extended Data Fig. 5 | Bisulfite sequencing analysis of Mov10l1$^{-/-}$ oocytes. Bisulfite sequencing analysis of *Mov10l1*$^{-/-}$ oocytes. (a,b) Snapshots from the UCSC genome browser depicting coverage of the genome by bisulfite-sequenced fragments and CpG methylation frequency. For each genotype, one sequencing library was constructed from 10 oocytes. (b) A detailed UCSC genome browser snapshot depicts expressed *Cwc15* gene with apparent absence of DNA methylation in the promoter. (c) Quantification of distribution of CpG methylation in hamster oocytes in unique and selected repetitive sequences. Only regions covered by at least four fragments in *Mov10l1*$^{+/-}$ and *Mov10l1*$^{-/-}$ libraries were included in the analysis. Promoters were considered regions 1 kb upstream of an annotated transcription start sites and were divided into two groups according to their activity using an arbitrary expression threshold of 0.5 RPKM. (d) CpG methylation of selected retrotransposon subgroups in *Mov10l1*$^{+/-}$ and *Mov10l1*$^{-/-}$ libraries. (e) CpG methylation in IAP full-length intact retrotransposons. Panels on the left depict "coverage" of the retrotransposon genome (number of sequencing reads), panels on the right display methylation frequency at CpGs (vertical lines). Different coverage of 5′ and 3′ LTR sequences (which are identical) comes from the fact that sequencing was done as "paired-end sequencing", hence if one read mapped exclusively to an LTR, the second read typically allowed to distinguish between 3′ and 5′ LTRs. Red lines depict CpG positions shown in Fig. 3g.

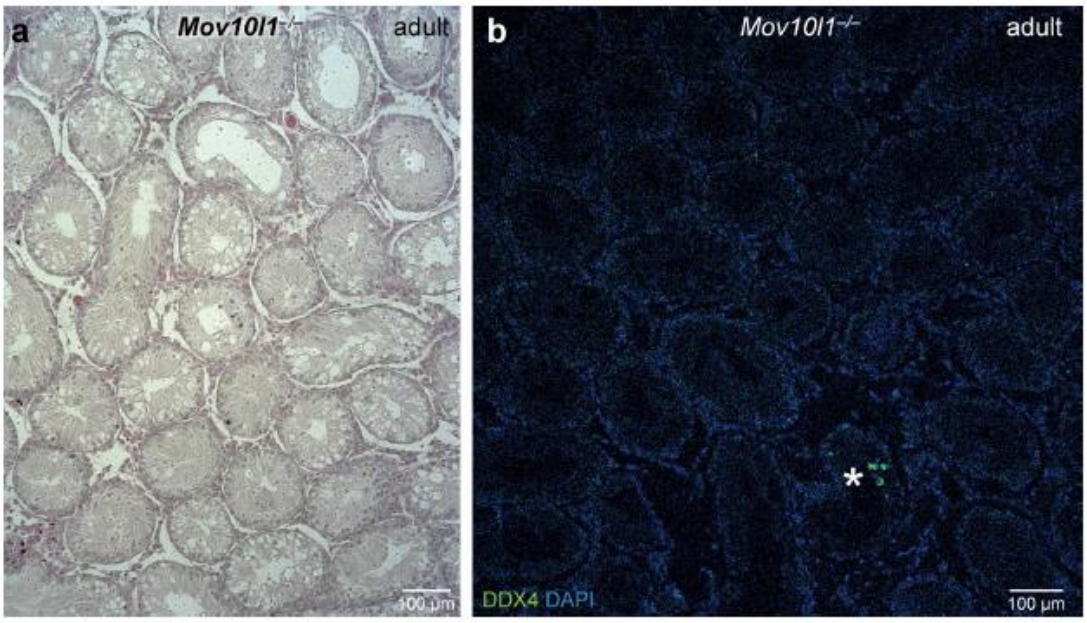

Extended Data Fig. 6 | Sterility in Mov10l1$^{-/-}$ males. Sterility in *Mov10l1*$^{-/-}$ males. (a) Most of the testicular seminiferous tubules in adult *Mov10l1*$^{-/-}$ testes (53 weeks) appear aspermatogenic in H&E staining. (b) Immunofluorescent staining with germ cell marker DDX4 (VASA) reveals rare clusters of spermatogenic cells (97% of tubules do not contain any germ cells). For both panels, testis sections from two adult males (three sections from each testis) were individually stained. Representative examples are shown.

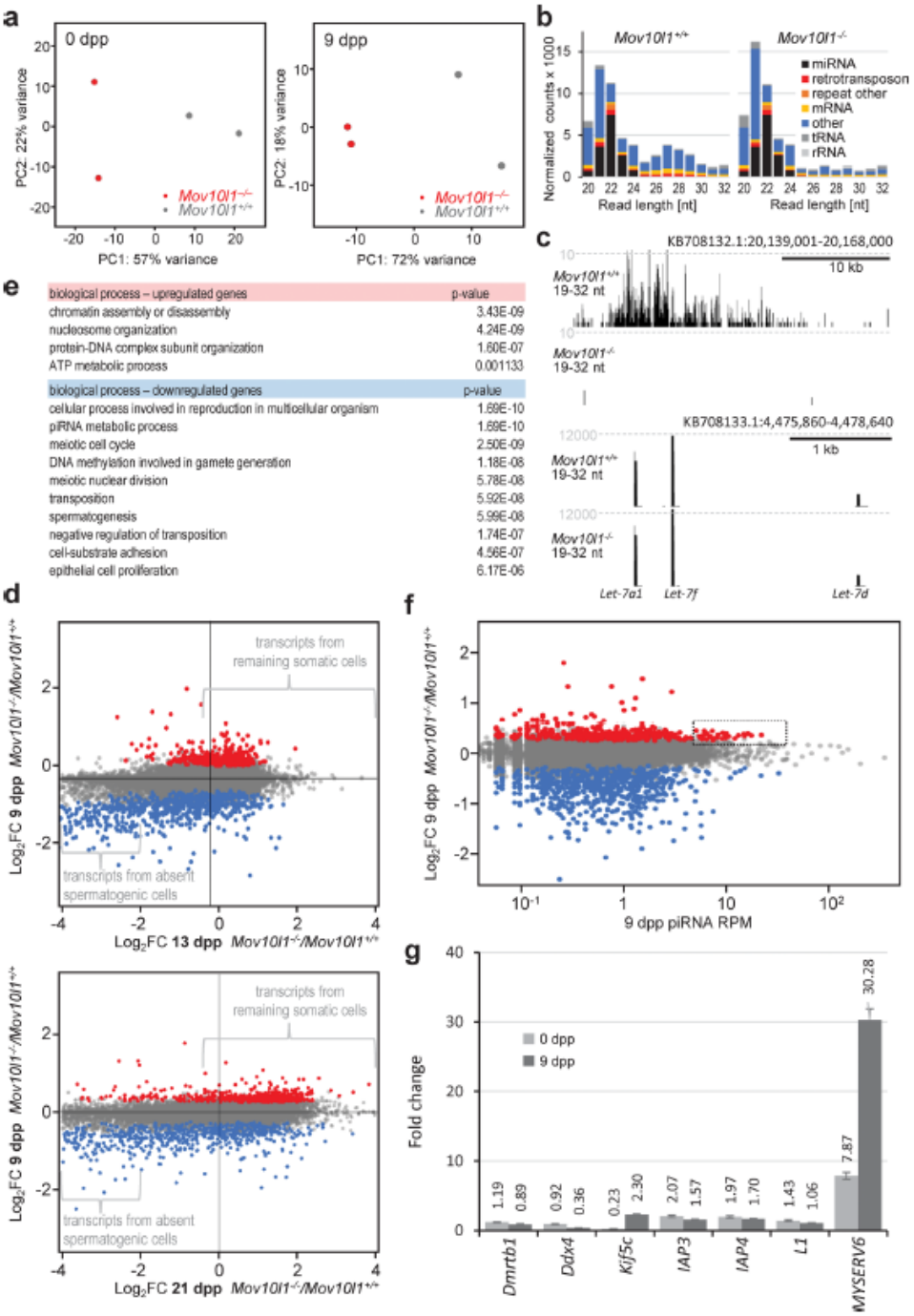

Extended Data Fig. 7 | See next page for caption.

Extended Data Fig. 7 | Transcriptome changes in Mov10l1$^{-/-}$ 9 d.p.p. testes. Transcriptome changes in *Mov10l1*$^{-/-}$ 9 d.p.p. testes. (a) PCA analyses of individual RNA-seq libraries produced in biological duplicates from newborn and 9 d.p.p. testes. (b) Composition of 20-32 nt RNA population in *Mov10l1*$^{+/+}$ and *Mov10l1*$^{-/-}$ 9 d.p.p. testes. Small RNA abundance in wild-type controls corresponds to reads per million of 18-32 nt reads. *Mov10l1*$^{-/-}$ libraries were normalized to the amount of testicular miRNAs. (c) Snapshots from the UCSC genome browser revealing loss of piRNAs in another top 9 d.p.p. cluster (in addition to the one shown in Fig. 6c) and the *Let-7* miRNA locus demonstrating intact miRNA expression. Three libraries from *Mov10l1*$^{+/+}$ and two from *Mov10l1*$^{-/-}$ testes were produced and used for analysis in b) and c). (d) Germ cell-specific genes are among downregulated DEGs at 9 d.p.p. Red and blue points depict significantly upregulated and downregulated DEGs in 9 d.p.p. testes (DESeq2 p-value <0.01). Gene expression changes in *Mov10l1*$^{-/-}$ 9 d.p.p. testes (y-axis) were plotted against gene expression changes in *Mov10l1*$^{-/-}$ 13 d.p.p. (upper graph) or 21 d.p.p. (lower graph) testes. Since 13 and 21 d.p.p. *Mov10l1*$^{-/-}$ testes lack most germ cells, germ cell-specific genes will be among strongly downregulated DEGs on the left side. (e) Gene Ontology analysis of enriched biological processes among DEGs in 9 d.p.p. testes. (f) Weak relationship between upregulated DEGs and piRNAs. Gene expression changes in *Mov10l1*$^{-/-}$ 9 d.p.p. testes (y-axis) were plotted against rank-sorted abundance of 24-31 nt reads mapping to exons of these genes (multimapping reads were weighted). The rectangle frames a small upregulated fraction of DEGs associated with more abundant piRNAs (> ~5 RPM). (g) Quantitative RT-PCR analysis of expression changes of selected genes and retrotransposons in *Mov10l1*$^{-/-}$ newborn and 9 d.p.p. testes. Numbers above each bar represent fold changes. One biological sample from each genotype was analyzed in a technical triplicate. Data are presented as relative fold changes of normalized median expression values in mutants and wild type controls calculated with the ΔΔCT method in the REST tool[53]. Error bars delineate 95% confidence interval estimated by REST.

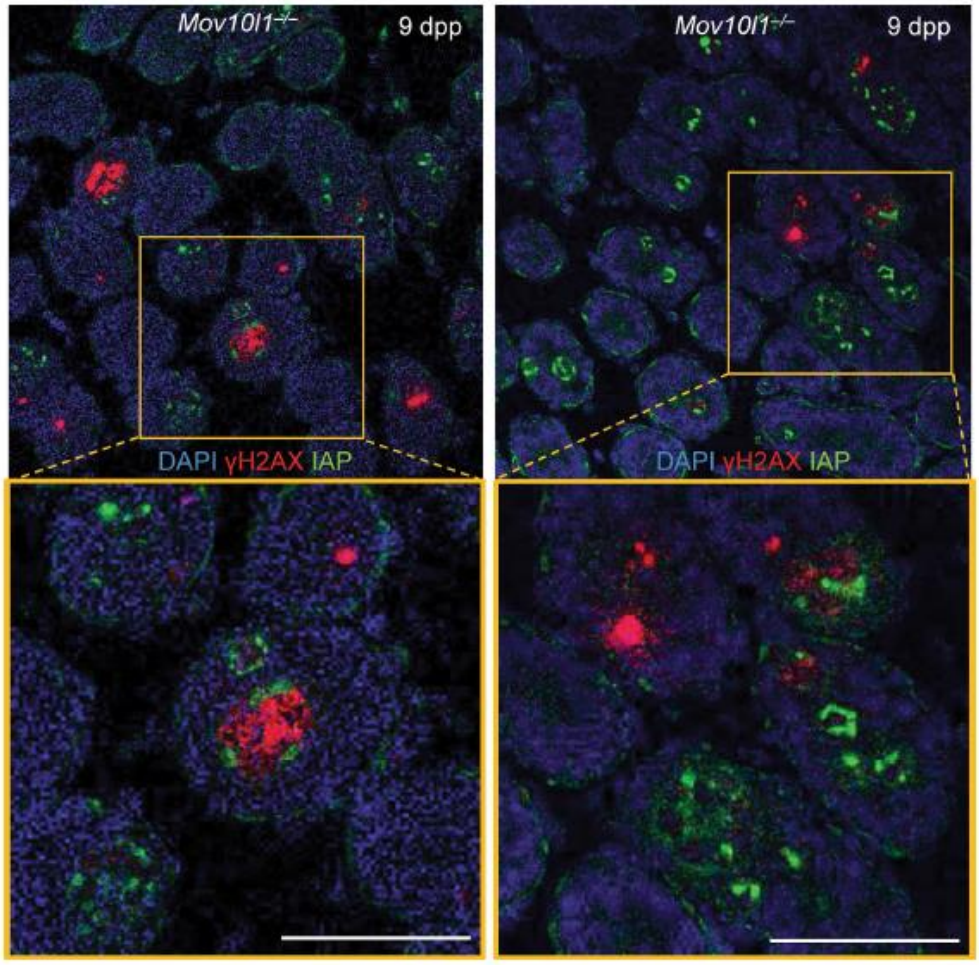

Extended Data Fig. 8 | Increased expression of IAP GAG protein in Mov10l1$^{-/-}$ 9 d.p.p. testes. Increased expression of IAP GAG protein in *Mov10l1*$^{-/-}$ 9 d.p.p. testes. Fluorescence staining of IAP GAG and γH2AX in two different stained histological sections show that increased IAP expression in germ cells in seminiferous tubules is not necessarily accompanied by immediate formation of γH2AX foci in the nucleus. Scale bars = 50 µm. Four sections from one testis were individually stained, two examples from two different sections are shown.

nature research

Corresponding author(s): Petr Svoboda

Last updated by author(s): Jul 25, 2021

Reporting Summary

Nature Research wishes to improve the reproducibility of the work that we publish. This form provides structure for consistency and transparency in reporting. For further information on Nature Research policies, see our Editorial Policies and the Editorial Policy Checklist.

Statistics

For all statistical analyses, confirm that the following items are present in the figure legend, table legend, main text, or Methods section.

n/a	Confirmed	
☐	☒	The exact sample size (*n*) for each experimental group/condition, given as a discrete number and unit of measurement
☒	☐	A statement on whether measurements were taken from distinct samples or whether the same sample was measured repeatedly
☐	☒	The statistical test(s) used AND whether they are one- or two-sided *Only common tests should be described solely by name; describe more complex techniques in the Methods section.*
☒	☐	A description of all covariates tested
☒	☐	A description of any assumptions or corrections, such as tests of normality and adjustment for multiple comparisons
☐	☒	A full description of the statistical parameters including central tendency (e.g. means) or other basic estimates (e.g. regression coefficient) AND variation (e.g. standard deviation) or associated estimates of uncertainty (e.g. confidence intervals)
☐	☒	For null hypothesis testing, the test statistic (e.g. *F*, *t*, *r*) with confidence intervals, effect sizes, degrees of freedom and *P* value noted *Give P values as exact values whenever suitable.*
☒	☐	For Bayesian analysis, information on the choice of priors and Markov chain Monte Carlo settings
☒	☐	For hierarchical and complex designs, identification of the appropriate level for tests and full reporting of outcomes
☒	☐	Estimates of effect sizes (e.g. Cohen's *d*, Pearson's *r*), indicating how they were calculated

Our web collection on statistics for biologists contains articles on many of the points above.

Software and code

Policy information about availability of computer code

Data collection	Microscopy images were obtained using Leica DM6000 and SP8 firmware.
Data analysis	Microscopy images were visualized and formatted in LAS AF LITE 3.3 (Leica), and quantitatively analyzed using the Imaris 9.6 software (Bitplane AG). Detailed description of software used for sequence data analyses, including original references, is provided in the subsection Bioinformatic analyses in the Methods section. Briefly, the following existing packages, algorithms, and scripts were used: STAR 2.7.3a aligner, featureCounts v2.0.0, DESeq2 package, UCSC tools, bbduk.sh 38.87, Cutadapt 2.10, UMI tools 1.1.1., clusterProfiler, RepeatMasker 4.0.9, Bismark (deduplicate_bismark, bismark_methylation_extractor), and samtools 1.10. The code used for bioinformatic data analysis is available here: https://github.com/fhorvat/bioinfo_repo/tree/master/papers/piRNA_2021.

For manuscripts utilizing custom algorithms or software that are central to the research but not yet described in published literature, software must be made available to editors and reviewers. We strongly encourage code deposition in a community repository (e.g. GitHub). See the Nature Research guidelines for submitting code & software for further information.

Data

Policy information about availability of data

All manuscripts must include a data availability statement. This statement should provide the following information, where applicable:

- Accession codes, unique identifiers, or web links for publicly available datasets
- A list of figures that have associated raw data
- A description of any restrictions on data availability

All data are available in the main text or the supplementary materials. High-throughput sequencing data access to original results in the manuscript: GSE164658. Previously published data that were re-analyzed: GSE5241556, PRJNA47156457, GSE7237958, GSE7489659, GSE11677160, GSE4941761, GSE13756362, and GSE5396053.

Field-specific reporting

Please select the one below that is the best fit for your research. If you are not sure, read the appropriate sections before making your selection.

☒ Life sciences ☐ Behavioural & social sciences ☐ Ecological, evolutionary & environmental sciences

For a reference copy of the document with all sections, see nature.com/documents/nr-reporting-summary-flat.pdf

Life sciences study design

All studies must disclose on these points even when the disclosure is negative.

Sample size	No sample size was calculated, the number of replicates was determined by availability of the limited material. All results were replicated at least twice or done in duplicates, except of the bisulfite sequencing of the genome, which was done once on a pool of oocytes because of the limited amount of material. Numbers of replicates in trancriptome analyses are apparent from the Supplementary Table 10.
Data exclusions	We excluded two RNA sequencing libraries produced from hamster oocyte transcriptome analysis. These two libraries were outliers in PCA and had poor quality/low complexity because of the limited amount of the starting material. In addition, we excluded from the preimplantation development analysis those matings where fertilization did not occur (evidenced by the absence of pronucleus formation and lack of paternal DNA presence in unfertilized eggs).
Replication	Key experiments were independently replicated using at least two biological replicates. Numbers of replicates are indicated in methods, figure legends or description of sequencing libraries. All attempts at replication were successful. Furthermore, post-zygotic sterile phenotype of Mov10l1 knock-out was independently replicated in a co-submitted manuscript from Haruhiko Siomi's group (Hasuwa et al. Production of functional oocytes requires maternally expressed PIWI genes and piRNAs in golden hamsters, 2021; https://doi.org/10.1101/2021.01.27.428354) and in a preprint from Jianmin Li's lab (Zhang H. et al., piRNA pathway is essential for generating functional oocytes in golden hamster; https://doi.org/10.1101/2021.03.21.434510).
Randomization	Planned sampling randomization was not implemented in this study because the project relied on genetically modified hamsters where the specific aspects of their breeding and supply of animals made limited sample availability. Accordingly, animals with required genotypes were used for experiments as they were produced, i.e. samples were not strictly randomized but were not deliberately chosen either.
Blinding	Blinding was not implemented. First, mutant phenotypes were expected to be of qualitative nature and their analysis should not be subconsciously biased. Particularly blinding sterile phenotype analyses where mutants have atrophic testes and obvious histological defects would not bring any benefit. Second, limited human resources did not allow separating management of the animal colony, mating & genotyping, and sample preparation from data acquisition and analysis.

Reporting for specific materials, systems and methods

We require information from authors about some types of materials, experimental systems and methods used in many studies. Here, indicate whether each material, system or method listed is relevant to your study. If you are not sure if a list item applies to your research, read the appropriate section before selecting a response.

Materials & experimental systems

n/a	Involved in the study
☐	☒ Antibodies
☒	☐ Eukaryotic cell lines
☒	☐ Palaeontology and archaeology
☐	☒ Animals and other organisms
☒	☐ Human research participants
☒	☐ Clinical data
☒	☐ Dual use research of concern

Methods

n/a	Involved in the study
☒	☐ ChIP-seq
☒	☐ Flow cytometry
☒	☐ MRI-based neuroimaging

Antibodies

Antibodies used

Antibody use including antibody origin (western blotting and immunofluorescence) is described in detail in methods. Here is just the list of used antibodies:

primary antibodies:
anti-DDX4 (Abcam, #ab27591 and #ab13840)
anti-γH2AX (Milipore, #05-636)
anti-H3K9me3 (Upstate (Merck-Millipore) #07-442)
anti-IAP GAG (non-commercial, a gift from B.R. Cullen, Duke University)
anti-LINE1 ORF1p (non-commercial, a gift from Dónal O´Carroll, University of Edinburgh)
anti-MOV10L1 (non-commercial, a gift from P. Jeremy Wang, University of Pennsylvania)
anti-SCP3 (Abcam, #ab976672)
anti-Tubulin (Sigma, #T6074)
anti-WT1 (Novus Biologicals, #NB110-60011)
anti-ZBTB16 (Atlas antibodies, #HPA001499)

secondary antibodies:
anti-Rabbit-HRP (Thermo Fisher Scientific, # G21234)
anti-mouse-HRP (Thermo Fisher Scientific, # G21040)
anti-mouse conjugated with Alexa 488 (Thermo Fisher, # A21202)
anti-mouse conjugated with Alexa 594 (Thermo Fisher, # A-21203)
anti-rabbit conjugated with Alexa 488 (Thermo Fisher, # A-21206)
anti-rabbit conjugated with Alexa 594 (Thermo Fisher, # A21207)

Validation

mouse anti-DDX4 (Abcam, cat# ab27591)
validation reference: https://www.abcam.com/ddx4--mvh-antibody-mabcam27591-ab27591.html

rabbit anti-DDX4 (Abcam, cat# ab13840)
validation reference: https://www.abcam.com/ddx4--mvh-antibody-ab13840.html

mouse anti-γH2AX (Milipore, cat# 05-636)
validation reference: https://www.merckmillipore.com/CZ/cs/product/Anti-phospho-Histone-H2A.X-Ser139-Antibody-clone-JBW301,MM_NF-05-636?ReferrerURL=https%3A%2F%2Fwww.google.com%2F

rabbit anti-H3K9-me3 (cat# 07-442)
validation reference: https://www.merckmillipore.com/CZ/cs/product/Anti-trimethyl-Histone-H3-Lys9-Antibody,MM_NF-07-442?ReferrerURL=https%3A%2F%2Fwww.google.com%2F&bd=1

rabbit anti-IAP GAG (gift from B.R. Cullen, Duke University Medical Center)
validation reference: doi: 10.1038/s41594-018-0058-0

rabbit anti-LINE1 ORF1p (gift from Dónal O´Carroll, University of Edinburgh)
validation reference: DOI:https://doi.org/10.1016/j.molcel.2013.04.026

rabbit anti-MOV10L1 (gift from P. Jeremy Wang, University of Pennsylvania)
validation reference: https://doi.org/10.1073/pnas.1003953107

mouse anti-SYCP3 (Abcam, cat# ab97672)
validation reference: https://www.abcam.com/scp3-antibody-cor-10g117-ab97672.html

mouse anti-Tubulin (Sigma cat# T6074)
validation reference: https://www.sigmaaldrich.com/catalog/product/sigma/t6074?lang=en&region=CZ

mouse anti-Tubulin (Abcam, cat# ab7750)
validation reference: https://www.abcam.com/alpha-tubulin-antibody-tu-01-ab7750.html

mouse anti-WT1 (Novus Biologicals, cat# NB110-60011)
validation reference: https://www.novusbio.com/products/wt1-antibody-6f-h2_nb110-60011

rabbit anti-ZBTB16 (Atlas antibodies, cat# HPA001499)
validation reference: https://www.atlasantibodies.com/products/antibodies/primary-antibodies/triple-a-polyclonals/zbtb16-antibody-hpa001499/

Animals and other organisms

Policy information about studies involving animals; ARRIVE guidelines recommended for reporting animal research

Laboratory animals

Golden (Syrian) hamsters Mesocricetus auratus, males 0 to 102 weeks and females 10 to 52 weeks old.

Wild animals

The study did not involve wild animals

Field-collected samples	The study did not involve samples collected in the field
Ethics oversight	Animal experiments were approved by the Animal Experimentation Committee at the RIKEN Tsukuba Institute (T2019-J004) and the Institutional Animal Use and Care Committee at the Institute of Molecular Genetics of the Czech Academy of Sciences (approvals no. 42/2016 and 70/2018).

Note that full information on the approval of the study protocol must also be provided in the manuscript.